Novel Organic Materials for Photovoltaic Devices

Thesis submitted in fulfillment of the requirements

For the degree of

Doctor of Philosophy

School of Chemistry College of Science and Engineering University of Glasgow

September 2014

Helen Smith

The School of Chemistry Joseph Black Building University of Glasgow Glasgow

G12 8QQ

ABSTRACT

Organic materials offer key advantages over their inorganic counterparts for photovoltaics due to the ability to easily tune the physical properties and develop cheaper, more flexible, photovoltaic devices. This thesis describes the synthesis and characterisation of a variety of compounds from small-molecule to supramolecular and polymeric systems with the potential to be used in organic electronics. Herein is described an optimised synthetic route for the synthesis of two flavins and the synthesis and characterisation of a novel flavin and fluorene polymer. Also described is the synthesis of two novel rotaxane structures with the potential for use in organic field effect transistors. The synthesis of a novel polymer incorporating the naphthalene diimide moiety and a P3HT functionality utilising click methodology is also described. Finally the synthesis of a thiophene based star shaped molecule as electron transporting material is also described along with a flavin based organic dye for use in dye-sensitised solar cells.

Table of Contents

Abstract **p.2**

List of Figures/Schemes/tables **p.7**

Acknowledgements **p.18**

Declaration **p.19**

Definitions and Abbreviations **p.20**

1.0 Photovoltaics **p.24**

1.1 Renewable Energy **p.24**

1.2 The principle of solar cells **p.26**

1.3 Current Market **p.27**

1.4 Organic Electronics **p.29**

1.4.1 Organic Field Effect Transistors **p.29**

1.4.2 Organic Photovoltaics **p.30**

1.4.2.1 Device architecture **p.30**

1.4.2.2 Mode of action **p.32**

1.4.2.3 Photovoltaic characterisation **p.33**

1.4.2.4 Acceptor/donor materials used in OPV **p.33**

1.4.3 Dye-sensitised solar cells **p.38**

1.5 Current Research **p.40**

1.5.1. Organic photovoltaics **p.40**

1.5.2 Dye-sensitised solar cells **p.47**

1.6 Summary **p.50**

2.0 Synthesis and characterisation of flavin functionalised conjugated polymers

2.1 Introduction **p.51**

2.1.1 Background **p.51**

2.1.2. Redox properties of flavins **p.53**

2.2 Project outline **p.59**

2.3 Results and Discussion **p.62**

2.3.1 Synthesis **p.62**

2.3.2 Analysis **p.73**

2.3.2.1 UV/Vis and Fluorescence Spectroscopy **p.73**

2.3.2.2 Cyclic Voltammetry (CV) **p.75**

2.4 Conclusions and Future Work **p.75**

3.0 Synthesis and characterisation of a series of rotaxanes

3.1 Rotaxanes incorporating donor and acceptor material **p.76**

3.1.1 Introduction **p.76**

3.1.1.1 Background **p.76**

3.1.1.2 Applications **p.81**

3.1.2 Project outline **p.86**

3.2 Results and Discussion **p.88**

3.2.1 Synthesis of naphthalene core and half unit **p.89**

3.2.2 Synthesis of rotaxane control compound **p.90**

3.2.3 Synthesis of donor and acceptor incorporating rotaxanes **p.91**

3.2.4 UV/Vis and Fluorescence Spectroscopy **p.96**

3.2.5 Cyclc Voltammetry **p.102**

3.2.6 OPV and OFET fabrication **p.104**

3.2.6.1 OPV **p.104**

3.2.6.2 OFETs **p.104**

3.3 Conclusions and Future Work **p.107**

3.3.1 Conclusions **p.107**

3.3.2 Future Work **p.108**

4.0 Synthesis of a Series of Block Co-Polymers and Conjugated Polymers

4.1 Introduction **p.109**

4.1.1 Synthesis and Applications of Block Co-Polymers **p.109**

4.1.1.1 Naphthalene Diimides **p.116**

4.1.1.2 Click Chemistry **p.117**

4.1.2 Conjugated Polymers **p.117**

4.2 Project Outline **p.122**

4.2.1 Donor-Acceptor and Donor-Donor Block Co-Polymers **p.122**

4.2.2 Conjugated Polymers Featuring Recognition Units **p.123**

4.3 Results and Discussion **p.124**

4.3.1 Donor-Acceptor Block Co-Polymer **p.124**

4.3.1.1 NDI monomer and polymerisation **p.124**

4.3.1.2 Donor monomers **p.127**

4.3.1.3 Block Co-Polymer Synthesis **p.129**

4.3.1.3.1 Click Methodology **p.130**

4.3.1.3.2 Synthesis of a clicked block acceptor-donor co-polymer **p.131**

4.3.1.3.3 UV/Vis and Fluorescence Spectroscopy **p.133**

4.3.1.3.4 Cyclc Voltammetry (CV) and Square Wave Voltammetry (SWV) **p.136**

4.3.1.3.5 AFM Imaging **p.138**

4.3.1.3.5.1 Sample preparation **p.138**

4.3.1.3.5.2 AFM characterisation **p.138**

4.3.2 Donor Block Polymers and Co-Polymers **p.141**

4.3.2.1 UV/Vis and fluorescence spectroscopy **p.143**

4.3.2.2 Cyclic voltammetry and Square Wave voltammetry **p.144**

4.3.3 Conjugated polymers featuring recognition groups **p.145**

4.4 Conclusions and Future Work **p.148**

5.0 Synthesis of thiophene based star-shaped molecules and dye-sensitised solar cells

5.1 Introduction **p.149**

5.1.1 Star-shaped structures **p.149**

5.1.2 Flavins as organic dyes for use in DSSCs **p.158**

5.2 Project Outlines **p.162**

5.2.1 Star-shaped molecules as electron transporting systems **p.162**

5.2.2 Flavin based material for DSSCs **p.163**

5.3 Results and Discussion **p.164**

5.3.1 Functionalised 1,3,5-tris (N-phenylbenzimidazol-2-yl) benzene **p.164**

5.3.2 Thiophene incorporated star shaped molecules **p.166**

5.3.3 Flavin incorporating material for DSSCs **p.167**

5.4 Conclusions and Future Work **p.168**

6.0 Experimental

6.1 Apparatus **p.169**

6.2 Chromatography **p.169**

6.3 Solvents and Reagents **p.169**

6.4 General Reaction Conditions **p.170**

6.5 Experimental Details **p.170**

7.0 References **p.210**

8.0 Appendices **p.218**

List of Figures/Schemes/tables

Figure 1 Share of global energy consumption in 2011 **p.25**

Figure 2 Share of global energy consumption in 2011 ** other includes geothermal, solar, wind **p.25**

Figure 3 Average annual growth rates or renewable energy capacity **p.26**

Figure 4 Solar spectrum **p.26**

Figure 5 Solar radiation versus wavelength **p.27**

Figure 6 Cell efficiencies for photovoltaic devices **p.28**

Figure 7 Three geometries of OFETs, from left to right: bottom gate, bottom contacts (BG-BC); bottom gate, top contacts (BG-TC); top gate, bottom contacts (TG-BC). S: Source, G: Gate, D: Drain **p.29**

Figure 8 Example of a regioregular P3HT and an OFET **p.30**

Figure 9 Cartoon representation of a bi-layer OPV **p.31**

Figure 10 Cartoon representation of a BHJ OPV **p.31**

Figure 11 Mode of action in a BHJ device **p.32**

Figure 12 Charge transfer between donor and acceptor **p.32**

Figure 13 Representation of a J-V curve **p.33**

Figure 14 Structures of **4** and **5** **p.34**

Figure 15 Structure of PCBM **p.34**

Figure 16 Structures of oligothiophenes **7** and **8** **p.35**

Figure 17 Structure of **9** **p.35**

Figure 18 Structure of **10** **p.36**

Figure 19 Structure of **11** **p.36**

Figure 20 Structures of **12** and **13** **p.37**

Figure 21 Structure of **14** **p.37**

Figure 22 Schematic representation of the operating principle of a DSSC **p.38**

Figure 23 Structure of **15** and **16** **p.39**

Figure 24 Structures of dyes **18** and **17** **p.40**

Figure 25 Structure of **19** **p.41**

Figure 26 Structures of **20-25** **p.41**

Figure 27 Cartoon showing the electron transfer process in dendron-rod-coil structures **p.42**

Figure 28 Structures of **26**, **27** and **28** **p.43**

Figure 29 Target dendron-rod-coil structures **29**, **30** and **31** **p.44**

Figure 30 Demonstration of the charge transfer of the dendron-rod-coil **p.45**

Figure 31 Structures of monomers **32**, **33**, **34** and **35** **p.46**

Figure 32 Structures of **36-39** with differing feed ratios of monomers **p.46**

Figure 33 Structures of indoline dyes **40** and **41** **p.48**

Table 1 Photovoltaic characteristics of DSSCs with the indoline dyes **40** and **41** Results obtained from three DSSCs **p.48**

Figure 34 Structures of **42** and **43** **p.49**

Figure 35 Riboflavin **44** also known as vitamin B2 **p.51**

Figure 36 Structure of **45** **p.52**

Figure 37 Structure of **46** and **47** **p.52**

Figure 38 Structures of the nine redox states of flavins **p.53**

Figure 39 Hydrogen bonding from model systems **48a-e** **p.54**

Figure 40 Hydrogen bonding from model systems **49a-c** **p.55**

Figure 41 Self assembly of a flavin incorporated molecule **50** **p.56**

Figure 42 Flavin functionalised polystyrene copolymer investigating flavin binding to DAP **p.57**

Figure 43 Binding of flavin **51** co-factors with **52** and **53** **p.58**

Figure 44 Structure of flavin **54** with substitution at C(7) and C(8) and binding with **55** **p.58**

Figure 45 Influence of π-stacking on the binding constant in flavins **p.59**

Figure 46 Structure of a flavin **56** featuring intramolecular H-bonding and π-stacking interactions **p.59**

Figure 47 Structure of **57** **p.60**

Figure 48 Structure of **58** **p.60**

Scheme 1 Proposed synthetic strategies for the synthesis of **57** and **58** **p.61**

Scheme 2 First attempt at the synthesis of **57** and **67** **p.62**

Scheme 3 Optimised synthetic route for the synthesis of **58** **p.63**

Scheme 4 Expected result of the alkylation with 2-ethylhexyl bromide **p.63**

Scheme 5 Result of the alkylation with 2-ethylhexyl bromide **p.63**

Scheme 6 Synthesis of compound **70** via a 2 day alkylation reaction **p.65**

Scheme 7 Proposed mechanism for the displacement of the ethyl group **p.65**

Scheme 8 Synthesis of **72** **p.66**

Scheme 9 Actual result from the alkylation with 2-ethylhexyl bromide **p.66**

Scheme 10 Methodology using differing alkyl groups **p.67**

Scheme 11 Second proposed mechanism explaining the replacement of the N10-alkyl group **p.67**

Scheme 12 Methylation of **72** **p.68**

Figure 49 X-ray structures of the two products **75** (right) and **76** (left) obtained from the methylation of **72** **p.69**

Figure 50 X-ray structure showing the π- π stacking in molecule **75** **p.69**

Scheme 13 Polymerisation of **69** using Suzuki conditions **p.70**

Figure 51 GPC data for the polymerisation of **69** and **77** **p.70**

Scheme 14 Polymerisation attempt using **75** **p.71**

Scheme 15 Optimised synthetic route for the synthesis of **57** **p.72**

Scheme 16 Alkylation of **57** **p.72**

Scheme 17 Alkylation of **57** **p.73**

Figure 52 UV/Vis spectrum of polymer **78** recorded at a concentration of 1 x 10^{-5}M in CH_2Cl_2 **p.74**

Figure 53 Resonance structure for the ICT in polymer **78** **p.74**

Figure 54 Emission spectrum of polymer **78** recorded at a concentration of 1 x 10^{-6}M in CH_2Cl_2 and excited at 453 nm **p.74**

Table 2 Optical and electrochemical properties of polymer **78** **p.75**

Figure 55 Schematic of a rotaxane **p.76**

Figure 56 Nomenclature for rotaxanes **p.77**

Figure 57 First synthesised rotaxane **82** **p.77**

Figure 58 Cartoon representing the three strategies rotaxane synthesis **p.78**

Scheme 18 Scheme showing and example of a slipping strategy for the synthesis of rotaxane **86** **p.79**

Scheme 19 Scheme showing the threading followed by stoppering strategy to give rotaxane **91** **p.80**

Scheme 20 Scheme showing an example of the clipping strategy for the synthesis of rotaxane **95** **p.81**

Figure 59 Example of polyrotaxanes used as molecular wires **p.82**

Figure 60 Chemically and electrochemically reversible molecular switch **p.83**

Figure 61 A molecular switch **97** controlled by counterions **98** and **99** **p.84**

Figure 62 Nanoscale molecular elevator **p.85**

Figure 63 Rotaxane mimicking the action of a muscle **p.86**

Scheme 21 Retrosynthetic analysis for the synthesis of rotaxanes **p.87**

Figure 64 Target structures **103**, **104** and **105** **p.88**

Scheme 22 General scheme for synthesis of a viologen **p.89**

Scheme 23 Synthesis of **106** **p.89**

Scheme 24 Synthesis of **102** **p.90**

Scheme 25 Synthesis of **92** **p.90**

Scheme 26 Synthesis of axle **109** **p.91**

Scheme 27 Synthesis of rotaxane **103** **p.91**

Scheme 28 Synthesis of **110** **p.92**

Scheme 29 Synthesis of **112** **p.92**

Scheme 30 Synthesis of axle **113** **p.92**

Scheme 31 Synthesis of rotaxane **104** **p.93**

Scheme 32 Synthesis of axle **115** **p.93**

Scheme 33 Synthesis of rotaxane **105** **p.94**

Scheme 34 Synthesis of compound **117** **p.94**

Scheme 35 Synthesis of compound **118** **p.95**

Scheme 36 Attempted coupling of **102** and **118** **p.95**

Scheme 37 Attempted synthesis of **121** **p.96**

Figure 65 UV/Vis spectra of **88** and **102** recorded at a concentration of 1 x 10^{-4}M in acetonitrile **p.97**

Figure 66 UV/Vis spectra of **113** and **115** recorded at a concentration of 1 x 10^{-4}M in acetonitrile **p.98**

Figure 67 UV/Vis spectrum of rotaxane **103** recorded at a concentration of 1 x 10^{-5} M (inset at 1 x 10^{-4}M) in acetonitrile **p.99**

Figure 68 Overlay of the emission spectra of **102** and rotaxane **103** recorded at concentrations of 1 x10^{-6}M in acetonitrile and excited at 297 nm **p.99**

Figure 69 UV/Vis spectra of rotaxane **104** recorded at a concentration of 1 x 10^{-5} M (inset at 1 x 10^{-4}M) in acetonitrile **p.100**

Figure 70 Overlay of the emission spectra of the axle **113** and rotaxane **104** recorded at a concentration 1 x 10^{-6}M in acetonitrile and excited at 297 nm **p.100**

Figure 71 UV/Vis spectrum of rotaxane **105** recorded at a concentration of 1 x 10^{-4}M in acetonitrile **p.101**

Figure 72 Overlay of the emission spectra of the axle **115** and rotaxane **105** recorded at a concentration of 1 x 10^{-6}M in acetonitrile and excited at 297 nm **p.101**

Table 3 Optical and electrochemical properties of **103**, **104** and **105** **p.102**

Figure 73 Cyclic voltammagram of rotaxane **103** recorded at a concentration of 1 x 10^{-4} M in acetonitrile, (0.1M TBA.PF_6, glassy carbon working electrode, platinum wire counter electrode and silver reference electrode, reference to Fc/Fc^+ = 0.0V) **p.103**

Figure 74 Cyclic voltammagram of rotaxane **104** recorded at a concentration of 1 x 10^{-4} M in acetonitrile, (0.1M TBA.PF_6, platinum working electrode, platinum wire counter electrode and silver reference electrode, reference to Fc/Fc^+ = 0.0V) **p.103**

Figure 75 Cyclic voltammagram of rotaxane **105** recorded at a concentration of 1 x 10^{-4} M in acetonitrile, (0.1M TBA.PF_6, platinum working electrode, platinum wire counter electrode and silver reference electrode, reference to Fc/Fc^+ = 0.0V) **p.104**

Figure 76 Output characteristics (left) and transfer characteristics (right) of rotaxane **103** using acetonitrile on PFBT treated Au/SiO_2 substrate **p.105**

Figure 77 Output characteristics (3a, left) and transfer characteristics (3b right) of Rotaxane **103** using acetonitrile on PFBT treated Au/SiO_2 substrate **p.105**

Table 4 OFET parameters for rotaxanes **103**, **104** and **105** **p.106**

Figure 78 AFM height images for rotaxanes **103**, **104** and **105** on silicon substrates annealed at 120°C **p.107**

Scheme 38 Synthesis of **124** **p.110**

Scheme 39 Synthesis of a dicolour fluorescent polymer **p.110**

Scheme 40 π- π stacking between monomer units **131** and **132** **p.111**

Scheme 41 π- π stacking between monomer units **131** and **132** **p.112**

Scheme 42 Investigation of π- π stacking on the rate of ATRP **p.112**

Figure 79 General structures of **134** and **135** **p.113**

Scheme 43 Synthesis of polymers **138** and **140** by RAFT polymerisation and deprotection **p.113**

Figure 80 Self assembly of block copolymers and their release of drugs **p.114**

Scheme 44 Synthesis of polymer–protein conjugates **p.114**

Scheme 45 Synthesis of macro-RAFT agent based upon **141** **p.115**

Scheme 46 Synthesis of a macro-RAFT agent based on **152** **p.115**

Scheme 47 Synthesis of **156** from **154** **p.116**

Scheme 48 Macro-RAFT agent synthesis from poly(3-hexylthiophene) RAFT polymerisation to form poly(3-hexylthiophene)-*block*-polystyrene (159) **p.116**

Scheme 49 Synthesis of **161** **p.116**

Figure 81 Mechanism of the Huisgen 1,3-dipolar cycloaddition **p.117**

Figure 82 Structures of **6** and **11** **p.118**

Figure 83 Controlled transition metal catalysed polymerisation **p.119**

Figure 84 Oxidative polymerisation giving 2,5-linked **167** and 2,4-linked **169** polymers **p.119**

Scheme 50 Synthesis of azo-dye substituted thiophene polymers **171**, **173** and **174** **p.120**

Scheme 51 Diblock polymer for FET characteristics **p.120**

Scheme 52 Synthesis of copolymers of carbazole and thiophene with acceptor end groups **p.121**

Scheme 53 Donor-Acceptor Block Co-Polymer targets **p.122**

Figure 85 Structure of polymer **188** **p.123**

Figure 86 Block Co-Polymer based upon **190** **p.123**

Figure 87 Proposed strategy for the synthesis of target polymer **193** **p.124**

Scheme 54 Synthesis of **182** **p.125**

Scheme 55 ATRP of **182** **p.125**

Scheme 56 First attempt at RAFT polymerisation of monomer **182** **p.126**

Table 5 RAFT polymerisation attempts using 2-cyano-2-propyl dodecyl trithiocarbonate **p.126**

Scheme 57 Successful RAFT polymerisation of monomer **182** **p.127**

Scheme 58 Synthesis of monomer **184** **p.127**

Scheme 59 Synthesis of monomer **185** **p.128**

Table 6 Reduction conditions for reducing nitro group to amine **p.129**

Scheme 60 Attempts at synthesis of a Donor-Acceptor block co-polymer **186** **p.130**

Scheme 61 Synthesis of compound **201** **p.130**

Scheme 62 Synthesis of compound **202** **p.131**

Scheme 63 Synthesis of **205** **p.131**

Scheme 64 Synthesis of **206** **p.132**

Table 7 Data obtained for RAFT polymerisation of **182** **p.132**

Scheme 65 Clicked polymerisation of **205** and **206** giving target polymer **188** **p.133**

Table 8 Data for the clicked polymerisations **p.133**

Figure 88 GPC monitoring the progress of the clicked polymerisation between polymer **205** and polymer **206** **p.133**

Figure 89 UV/Vis spectrum of **205** at concentration 10^{-4}M in CH_2Cl_2 **p.134**

Figure 90 UV/Vis spectrum of **206** at concentration 10^{-5}M in CH_2Cl_2 **p.135**

Figure 91 Emission spectrum of polymer **206** at concentration 10^{-7}M in CH_2Cl_2 when excited at 361 nm **p.135**

Figure 92 UV spectrum of polymer **188** at concentration 10^{-4}M in CH_2Cl_2 **p.136**

Figure 93 Emission spectrum of the polymer **188** when excited at 450 nm **p.136**

Figure 94 CV analysis of polymer **188** at 0.5 mM concentration in CH_2Cl_2, 0.1 M TBA.PF_6, platinum working electrode, platinum wire counter electrode and silver reference electrode, reference to Fc/Fc^+ **p.137**

Figure 95 Square wave voltammetry of polymer **188** at 0.5 mM concentration in CH_2Cl_2, 0.1 M TBA.PF_6, platinum working electrode, platinum wire counter electrode and silver reference electrode, reference to Fc/Fc^+ **p.137**

Figure 96 AFM imaging of polymer **188** **p.139**

Figure 97 AFM imaging of polymer **188** **p.140**

Figure 98 AFM imaging of polymer **188** **p.140**

Scheme 66 ATRP attempt with monomer **184** **p.141**

Scheme 67 First attempt at RAFT polymerisation of monomer **184** **p.141**

Scheme 68 RAFT polymerisation of monomer **184** **p.142**

Scheme 69 Synthesis of monomer **211** **p.142**

Scheme 70 ATRP of monomer **211** and monomer **212** **p.143**

Figure 99 UV/Vis spectrum of polymer **190** at a concentration of 10^{-4}M in CH_2Cl_2 **p.143**

Figure 100 CV of compound **190** at 0.5 mM concentration in CH_2Cl_2, 0.1 M $TBA.PF_6$, platinum working electrode, platinum wire counter electrode and silver reference electrode, reference to Fc/Fc^+ **p.144**

Figure 101 SW for compound **190** at 0.5 mM concentration in CH_2Cl_2, 0.1 M $TBA.PF_6$, platinum working electrode, platinum wire counter electrode and silver reference electrode, reference to Fc/Fc^+ **p.145**

Scheme 71 Synthesis of monomer **192** **p.145**

Table 9 Data for three polymers obtained from oxidative polymerisation **p.146**

Scheme 72 Oxidative polymerisation of monomer **192** and **191** **p.146**

Scheme 73 Synthesis of the second monomer **216** **p.147**

Scheme 74 Second oxidative polymerisation reaction with a 50:50 ratio of monomers **p.147**

Figure 102 Thiophene based oligomers with silicon centres **p.149**

Figure 103 Star-shaped thiophene based dendrimers with a silicon centre **p.150**

Figure 104 Structures of model structures **224** and **225** **p.151**

Figure 105 Structure of **226** **p.152**

Figure 106 Structures of **227** and **228** **p.153**

Figure 107 Structures of **229** and **230** **p.154**

Figure 108 Structure of **231** **p.155**

Figure 109 Structures of **232**, **233** and **234** **p.157**

Figure 110 Structures of indoline dye **235** and compound **236** **p.158**

Figure 111 Absorption properties of the TIO_2 electrode doped with dye **235** and ruthenium dye **16** **p.159**

Figure 112 Structure of dye **237** **p.159**

Figure 113 Structures of dyes **238** and **239** **p.160**

Figure 114 Structure of **240** **p.160**

Figure 115 Molecular recognition between **240** and DAP and the blocking of H-Bonding with methyl **p.161**

Figure 116 Neutral (left) and charge separated (right) forms of **240** **p.162**

Scheme 75 Synthetic strategy for the compound **242** **p.163**

Figure 117 Structure of target **249** **p.163**

Figure 118 Structure of flavin dye **250** **p.164**

Scheme 76 Proposed synthetic route for compound **250** **p.164**

Scheme 77 First attempt at synthesis of **245** **p.165**

Scheme 78 Synthesis of **246** **p.165**

Scheme 79 First attempts at coupling reaction **p.166**

Scheme 80 Addition of triethylamine to the coupling reaction **p.166**

Scheme 81 Synthesis of **249** **p.167**

Scheme 82 Coupling reaction between flavin **57** and 4-formylphenyl boronic acid **p.167**

Scheme 83 Synthesis of flavin dye **250** **p.168**

ACKNOWLEDGEMENTS

I would like to thank my husband Gordon Smith, I could not have made it this far without his constant support. I would also like to thank all my friends and family for their encouragement.

Special thanks go to Professor Graeme Cooke for the opportunity to work within his research group. All the members of the Cooke research group, past and present, in particular Dr. Brian Fitzpatrick for all of his advice and guidance, and Dr Alan Wiles for his friendship and support. I also would like to thank Dr Joanne Hewitt, Dr Anna Hansen and Miss Mhairi Matheson for their friendship, coffee and chats.

I would also like to thank Aaron Naden from the School of Physics for his work on the AFM imaging and Dr Sasikumar Arumugam and Dr Jesuraj Inigo from the University of Strathclyde for their work on the rotaxanes.

Further thanks needs to go to Mr Jim Tweedy and Mr Harry Jackson for the operation of the mass spectrometry facility, and to all of the technicians and staff at the School of Chemistry.

DECLARATION

I declare that, except where explicit reference is made to the contribution of others, that this dissertation is the result of my own work and has not been submitted for any other degree at the University of Glasgow or any other institution.

DEFINITIONS AND ABBREVIATIONS

IEO = International Energy Outlook

PV = Photovoltaic

CSP = Concentrating Solar thermal Power

UV = Ultra Violet

OFET = Organic Field Effect Transistor

P3AT = Poly-3-Alkylthiophene

P3HT = Poly-3-Hexylthiophene

HT = Head to Tail

HH = Head to Head

BHJ = Bulk hetero-junction

ITO = indium tin oxide

PEDOT:PSS = Poly(3,4-ethylenedioxythiophene):Poly(styrenesulfonate)

HOMO = Highest Occupied Molecular Orbital

LUMO = Lowest Unoccupied Molecular Orbital

PCE = Power Conversion Efficiency

$\mathbf{J_{sc}}$ = Short-Circuit Current Density

$\mathbf{V_{oc}}$ = Open Circuit Voltage

FF = Fill Factor

$\mathbf{P_i}$ = Light Power Incident

OPV = Organic Photovoltaics

PCBM = ([6,6]-phenyl-C_{61}-butyric acid methyl ester

***p*-DTS(FBTTh$_2$)$_2$** = 7′-(4,4-bis(2-ethylhexyl)-4H-silolo[3,2-b:4,5-b′] dithiophene-2,6-diyl)bis(6-fluoro-4-(5′-hexyl-[2,2′-bithiophen]- 5-yl)benzo[c][1,2,5] thiadiazole)

PDTP-DFBT = poly[2,7-(5,5-bis-(3,7-dimethyloctyl)-5H-dithieno[3,2-b:2′,3′-d]pyran)-alt-4,7-(5,6-difluoro-2,1,3-benzothia diazole)]

DSSC = Dye-sensitised Solar Cell

ICT = Intramolecular Charge Transfer

MBI = 2,2-dimethyl-*2H*-benzimidazole

PCPPDTMBI = poly[2,6-(4,4-bis(2-ethylhexyl)-*4H*-cyclopenta[def]phenanthrene)-*alt*-5,5-(4,7-di-2-thienyl-2,2-dimethyl-2H-benzimid azole)]

PCPPBBTMBI = poly[2,6-(4,4-bis(2-ethylhexyl)-*4H*-cyclopenta[def] phenanthrene)-alt-5,5-(4,7-bi-2-bithiophene-2,2-dimethyl-2H-benzimidazole]

ATRP = Atom Transfer Radical Polymerisation

D = Donor

A = Acceptor

PC = 6H-Phenanthro[1,10,9,8-cdefg]carbazole

DPP = Diketopyrrolopyrrole

T = Thiophene

TT = Thieno[3,2-b]thiophene

CDCA = Chenodeoxycholic acid

PTZ = Phenothiazine

PTZ1 = (2E)-2-cyano-3-(5-(5-((E)-2-(10-(2-ethylhexyl)-10H-pheno thiazin-7-yl)vinyl)thio-phene-2-yl)thiophen-2-yl)acrylic acid

PTZ2 = (2E)-3-(5-(5-(4,5-bis((E)-2-(10-(2-ethylhexyl)-10H-phenothiazin-3-yl)vinyl)thio-phen-2-yl)thio phen-2-yl)thiophen-2-yl)-2-cyanoacrylic acid

FMN = Flavin mononucleotide

FAD = Flavin adenine dinucleotide

DAP = Diaminopyridine

TPARF = Tetraphenylacetyl riboflavin

DMF = Dimethyl Formamide

DCM/CH_2Cl_2 = Dichloromethane

CV = Cyclic Voltammetry

CBPQT = Cyclobis (paraquat-*p*-phenylene)

LED = Light Emitting Diode

S_N^2 = Bimolecular nucleophilic substitution reaction

NMR = Nuclear Magnetic Resonance

C_{60} = Fullerene

PF_6 = Hexafluorophosphate

DMAP = Dimethylamino pyridine

DIC = Diisopropyl carbodiimide

SiO_2 = Silicon dioxide

PFBT = Pentafluorobenzenethiol

V_{DS} = Source drain voltage

I_{DS} = Drain current

V_{GS} = Gate voltage

AFM = Atomic force microscope

RAFT = Reversible addition fragment chain transfer

PMDETA = *N*,*N*,*N*′,*N*′,*N*′′-Pentamethyldiethylenetriamine

AGET = Activator generated by electron transfer

BPy = Bipyridine

PMMA = Poly(methyl methacrylate)

NAPH = 2-(2,3-dihydro-2-(4-methoxy-phenyl)-1,3-dioxo-1*H*-phenalen-7-ylamino)ethyl-2-chloroacetate

PNIPAM = Poly(*N*-isopropylacrylamide)

AIBN = Azobisisobutyronitrile

NDI = Naphthalene diimide

TTF = Tetrathiafulvalene

GPC = Gel permeation chromatography

M_n = Number average molecular weight

M_w = Weight average molecular weight

PDI = Poly dispersion index

SWV = Square wave voltammetry

TBA.PF_6 = Tetrabutylammonium hexafluorophosphate

F_c = Ferrocene

EBIB = Ethyl bromoisobutyrate

EDCI = 1-Ethyl-3-(3-dimethylaminopropyl)carbodiimide

HB = 5-hexyl-2,2'-bithiophene

HTMSB = 5-hexyl-5'-trimethylsilyl-2,2'-bithiophene

TPA = Triphenylamine

ABFL = 8-[[*p*-[bis(ethyl)amino]phenyl]azo]isobutylflavin

MABFL = Methyl-8-[[*p*-[bis(ethyl)amino]phenyl]azo]isobutylflavin

THF = Tetrahydrofuran

DBU = 1,8-Diazabicyclo[5.4.0]undec-7-ene

1.0 Photovoltaics

1.1 Renewable Energy

In the current economic weather, energy resources are a large concern. Conventional fossil fuels cause many problems with pollution and global warming as well as being a non-renewable energy source. Renewable energy and nuclear power have become the world's fastest growing energy sources, consumption of each increasing by 2.5% each year and the International Energy Outlook (IEO) has estimated that the world energy consumption will grow by 56 % between 2010 and 2040.[1]

Renewable energy is classed as energy which comes from natural resources and can be replenished, such as: sunlight, wind, rain, tides and geothermal heat. Global demand for renewable energy has continued to rise during 2011 and 2012, supplying an estimated 19% of global final energy consumption in 2011 (Figure 1)[2]. Almost half of this comes from traditional biomass. Modern renewable sources accounted for an estimated 9.7% of total energy use; hydropower made up approximately 3.7%; and an estimated 1.1% was provided by power from wind, solar, geothermal and biomass. Oil was the highest source of fuel, with over 30% of the total share (Figure 2).[3] In 2012, wind power accounted for about 39% of this renewable power capacity, followed by hydropower and solar photovoltaic (PV), each accounting for approximately 26%.[2]

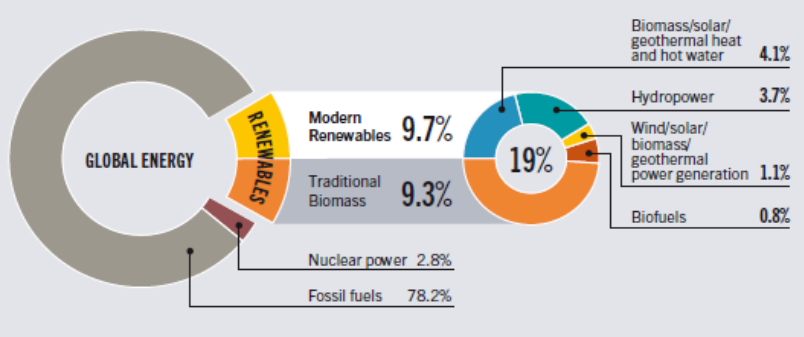

Figure 1 Share of global energy consumption in 2011[2]

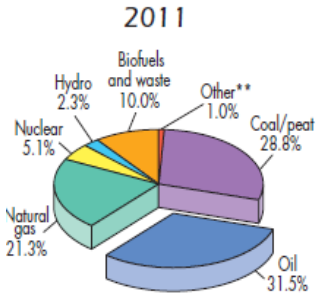

Figure 2 Share of global energy consumption in 2011 ** other includes geothermal, solar, wind[3]

Global primary energy consumption increased in 2013 by 2.5% with accelerated rates for oil, coal and nuclear power. However, the rate of increase for other sources of energy was below the average and oil is still the leading fuel with 32.9% of the global share. Natural gas increased to 23.7% of the global share, coal reached 30.1% of the global consumption, the highest it has been since 1970, nuclear power accounted for 4.4% and hydroelectric power accounted for 6.7%.[4]

During the five-year period, 2008–2012, renewable energy technologies grew very rapidly, showing the fastest growth within the power sector. Solar PV grew at rates averaging 60% annually. Concentrating solar thermal power (CSP) increased at more than 40% per year on average, growing from a small base, and wind power increased 25% annually over this period. Hydropower and geothermal power grew at much lower rates of 3-4% annually (Figure 3).[2] With the energy from the sun calculated as 120,000 TW which is thousands of times greater than the annual energy consumption required[5], solar energy is of great interest.

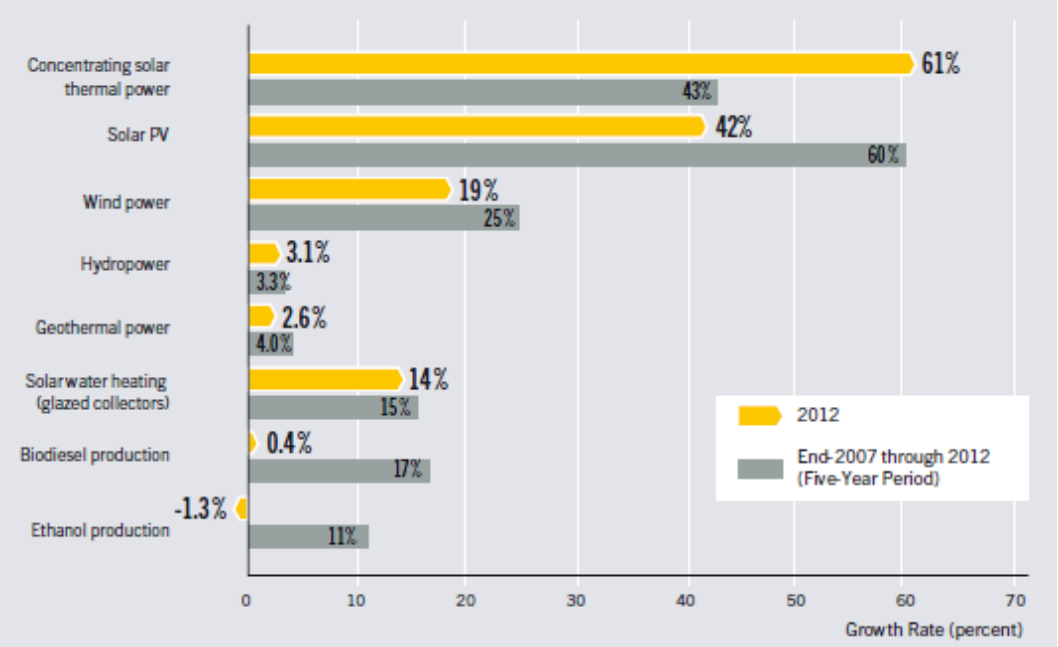

Figure 3 Average annual growth rates or renewable energy capacity[2]

1.2 The principle of solar cells

Converting solar radiation into electricity occurs by the photovoltaic effect. This is generally defined as the emergence of an electric voltage between two electrodes attached to a system (solid or liquid) by shining light onto the system. Typically a photovoltaic device consists of a pn-junction in a semiconductor, which must absorb a large part of the solar spectrum.[6] The solar spectrum spans from the UV region right through to infrared (Figure 4).

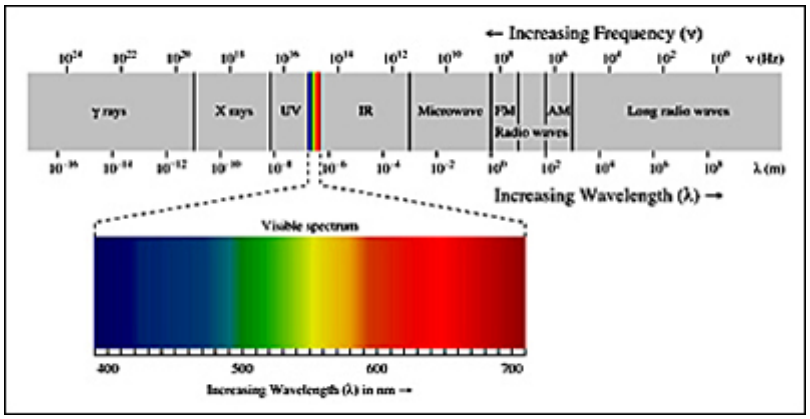

Figure 4 Solar spectrum[7]

In the designing of a new PV device the aim is to utilise as much of the energy from the solar spectrum as possible. In order to do this it is important to note that the majority of the energy arising from the solar spectrum actually comes from the

infrared region (Figure 5). In order to achieve high efficiencies for PV devices, the aim is to try and match the absorbance with this high photon region.

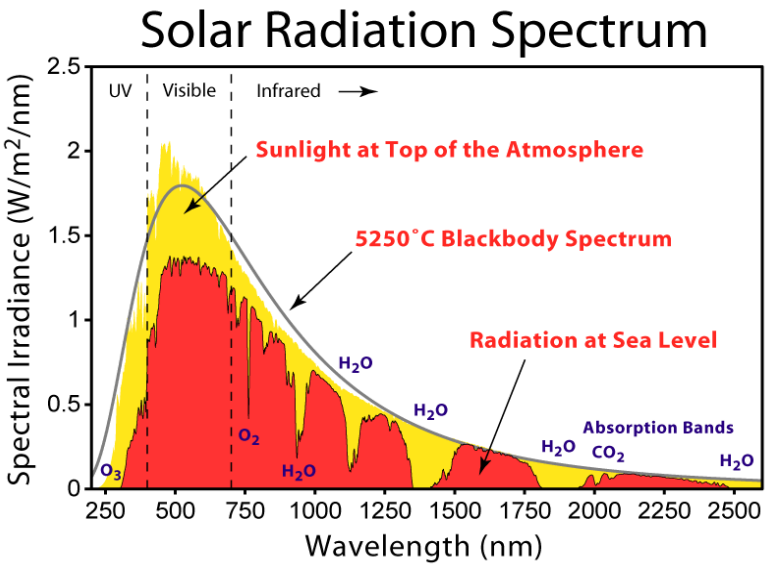

Figure 5 Solar radiation versus wavelength[8]

1.3 Current Market

The first silicon solar cell was developed in 1954 by Chapin et al.[9] Current photovoltaic devices are still dominated by inorganic materials, particularly silicon and multi-junction devices with the highest efficiency to date seen at 44.7% (Figure 6). Multi-junction devices consist of several p-n junctions in order to cover more of the solar spectrum. However, this increases the complexity and thus increases the cost. Due to the expense of these inorganic devices and the fragile nature of these inflexible devices, there has been more focus on organic photovoltaics.

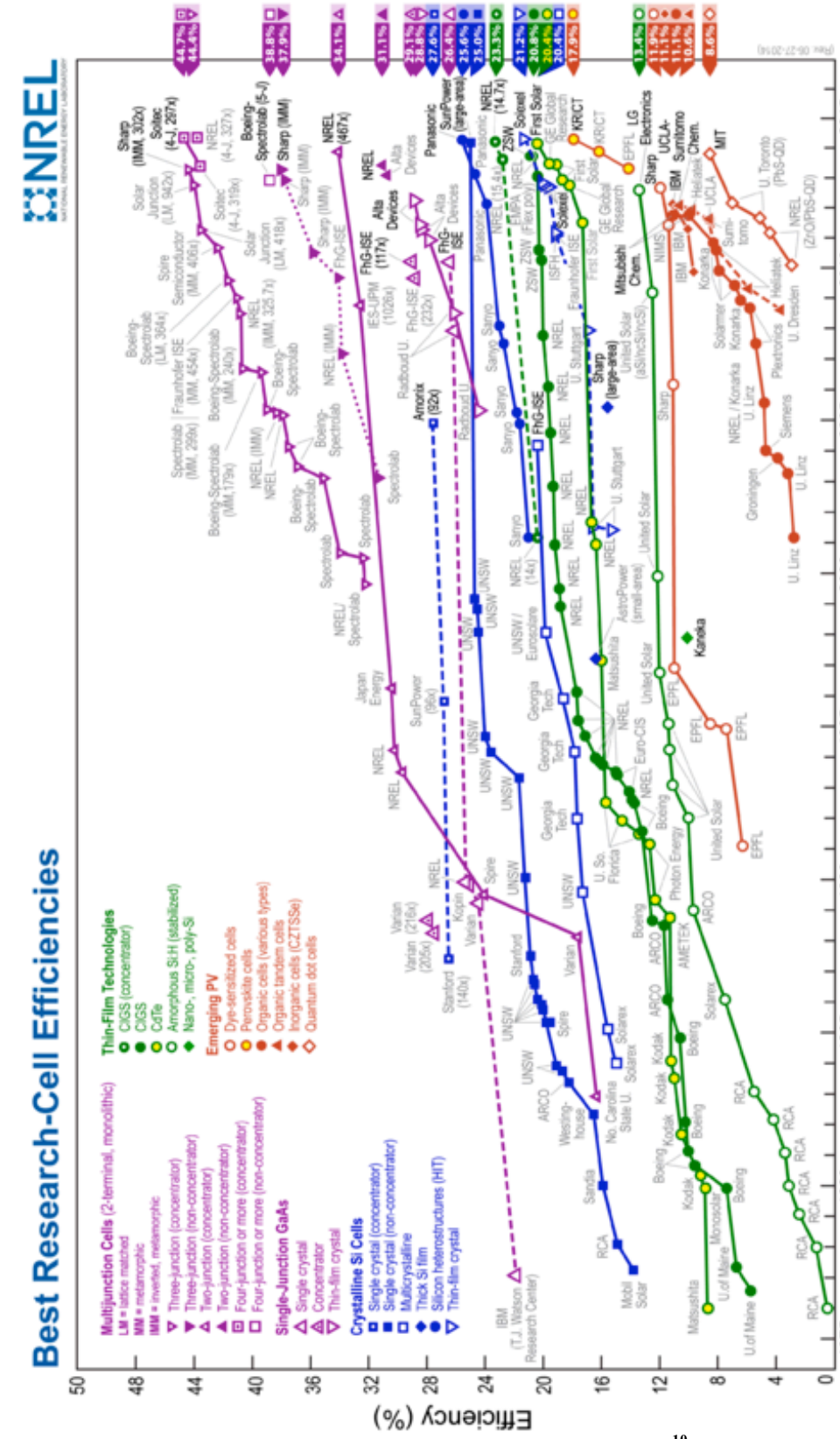

Figure 6 Cell efficiencies for photovoltaic devices[10]

1.4 Organic Electronics

1.4.1 Organic Field Effect Transistors

The beginning of the era of organic electronics can be traced to the mid eighties when the organic photovoltaic cells, light emitting diodes and field effect transistors were first introduced.[11] Organic field effect transistors (OFETs) have attracted a lot of attention due to the potential to promote low-cost and flexible circuitry. There are various geometries of OFETs, which can be seen in Figure 7. The main components of an OFET are an organic semiconducting layer, a dielectric layer and three conducting electrodes.[12]

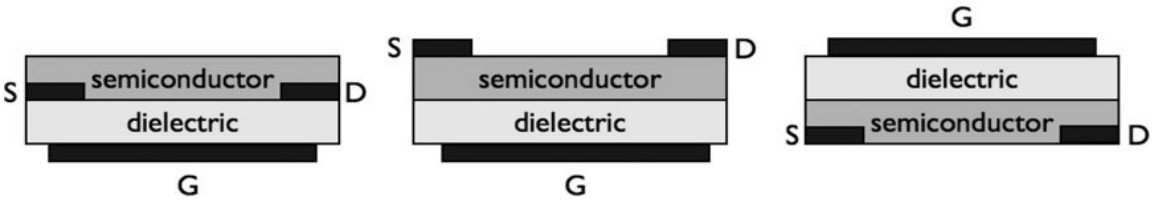

Figure 7 Three geometries of OFETs, from left to right: bottom gate, bottom contacts (BG-BC); bottom gate, top contacts (BG-TC); top gate, bottom contacts (TG-BC). S: Source, G: Gate, D: Drain

There are three methods for fabricating OFETs. One method for the fabrication of OFETs is to use electrochemical polymerisation to directly form a semiconducting polymer on to the surface of the electrodes. These electrodes are used subsequently as drain and source electrodes. The first ever OFET was fabricated in this manner in 1986 using polythiophene as the semiconducting polymer.[13] The second technique involves the use of either a conjugated polymer, such as poly-3-alkylthiophene (P3AT), or precursor materials that can undergo subsequent chemical reactions to give the desired compounds.[14] The third technique utilises vacuum deposition of oligomers and organic materials of low molecular weights in order to form highly ordered and self assembled films.[15]

One such study was by Bao et al., who investigated the use of regioregular poly-3-hexyl thiophene (P3HT) **3** in OFETs[15] Regiorandom P3HT contains both head to head **2** and head to tail **1** 3-alkylthiophenes whereas a regioregular P3HT contains only one kind (Figure 8).

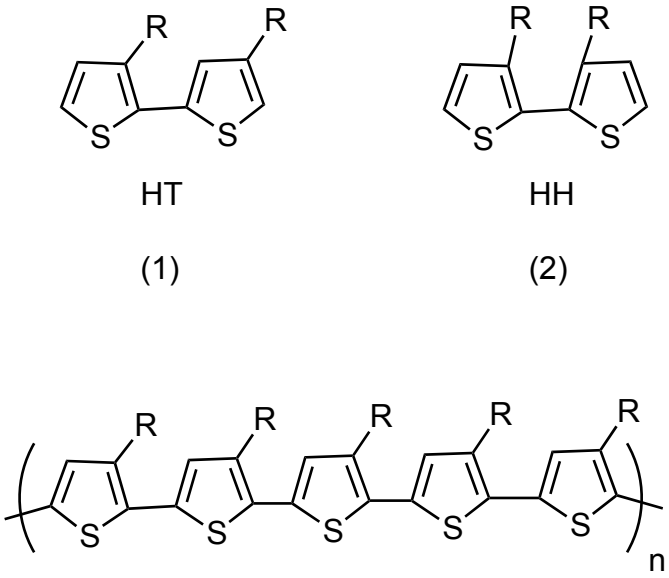

Figure 8 Example of a regioregular P3HT and an OFET.

They found that in utilising these regioregular P3ATs they could achieve high field effect mobilities in the order of 10^{-2} to 10^{-3} cm^2/Vs. The improvement over their regiorandom counterparts was attributed to the well-defined architectures resulting in higher crystallinity and a more ordered morphology. These polymers also proved to have good solubility and have easy processability, thus they concluded that they provided a promising alternative in organic electronics.

1.4.2 Organic Photovoltaics

1.4.2.1 Device architecture

Organic photovoltaics offer key advantages for photovoltaics such as the possibility to process directly from solution, which will thus afford lighter, cheaper and more flexible photovoltaic devices.[16]

Organic solar cells work on the same principles as inorganic solar cells in that they require semiconducting materials. However, in the case of organic solar cells these semiconductors are organic molecules made up of donor and acceptor compounds. There are typically two main types of device architecture, bi-layer and bulk heterojunction (BHJ). In a bi-layer architecture the device consists of two layers, one layer containing the donor material and one layer the acceptor material, sandwiched between two electrodes (Figure 9).

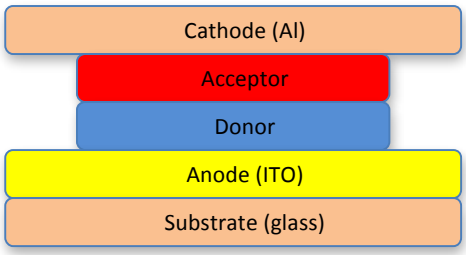

Figure 9 Cartoon representation of a bi-layer OPV

In a BHJ device, however, the donor and acceptor materials are blended together in one active layer (Figure 10). Aside from the active layers the device architectures remain the same. Typically, there is a transparent substrate coated with a conductive oxide, usually indium tin oxide (ITO) which acts as the anode. A layer of poly(3,4-ethylenedioxythiophene):poly(styrenesulfonate) (PEDOT:PSS) then follows, which acts as a hole transport layer. Following the PEDOT:PSS layer there is the active layer and the cathode (typically aluminium), respectively.

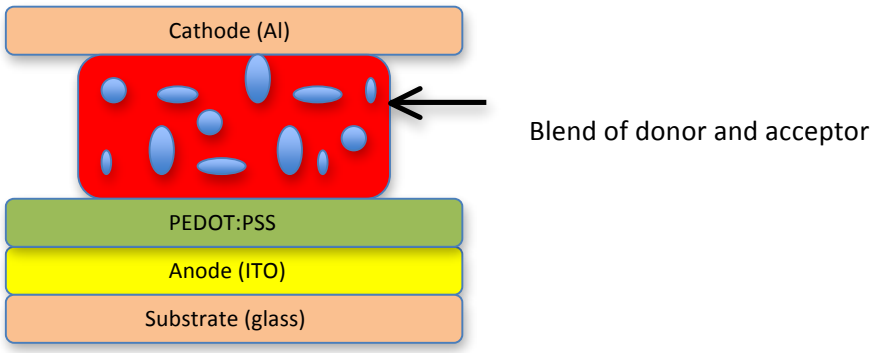

Figure 10 Cartoon representation of a BHJ OPV

BHJs increase the contact area between donor and acceptor materials which leads to a significant increase in the number of generated excitons as well as their dissociation into free charge carriers, which in turn leads to an increase in power conversion efficiency.[17] These architectures offer great advantages in that they can accommodate large scale production on flexible substrates by solution processing techniques such as ink-jet printing[18], brush painting[19] and roll to roll processing[20].

1.4.2.2 Mode of action

A BHJ works by photo-excitation of the donor to generate an exciton (electron-hole pair), this is then diffused to the donor-acceptor interface. This exciton then dissociates into a geminate pair, which then transfers to the electrodes (Figure 11).[21]

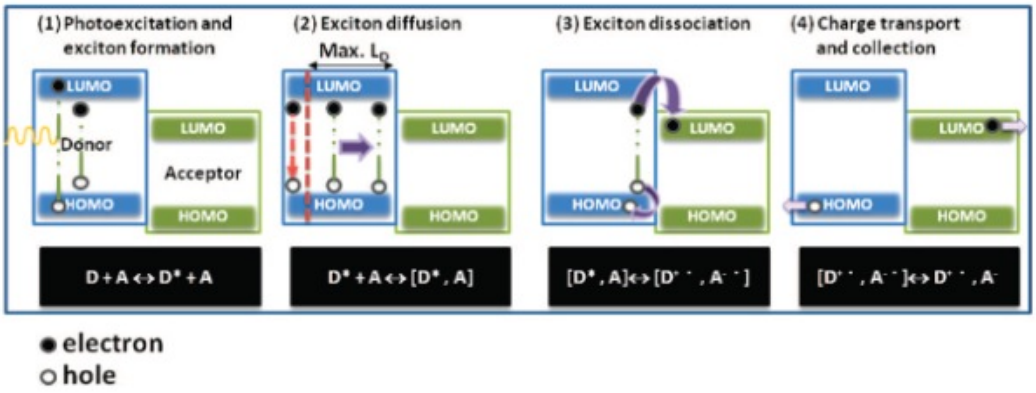

Figure 11 Mode of action in a BHJ device[21]

One of the most important factors to consider is the charge transfer between donor and acceptor. Upon excitation an electron is transferred from the highest occupied molecular orbital (HOMO) of the donor material to its lowest unoccupied molecular orbital (LUMO). This electron is then transferred to the LUMO of the acceptor material, which must occur rapidly in order to avoid recombination (Figure 12). Thus, it is important when considering donor and acceptor material that the HOMO/LUMO energy levels are well matched.

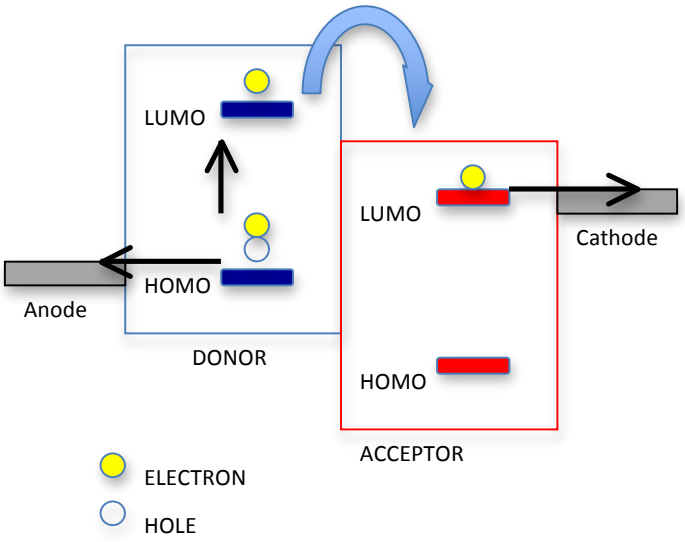

Figure 12 Charge transfer between donor and acceptor

1.4.2.3 Photovoltaic characterisation

Photovoltaic performance is characterised by the power conversion efficiency (PCE). The PCE is determined by three factors, short-circuit current density (J_{sc}), open circuit voltage (V_{oc}) and fill factor (FF). The PCE is calculated by the following formula[22]:

$$PCE = J_{sc} \times V_{oc} \times FF / P_i$$

Where P_i is the light power incident on the device. The FF is a characteristic, which defines the shape of the J-V curve, i.e. how "square" the curve is, and is an indicator of how difficult it is to extract the photogenerated carriers from the device. It is calculated by the following formula, where J_m and V_m are the current density and voltage taken directly from the J-V curve (Figure 13)[22]

$$FF = J_m \times V_m / J_{sc} \times V_{oc}$$

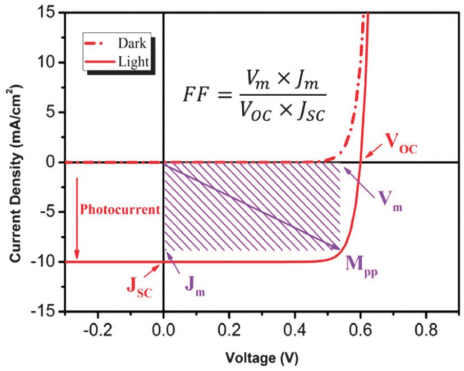

Figure 13 Representation of a J-V curve[22]

1.4.2.4 Acceptor/donor materials used in OPV

OPV materials can typically be divided into two sections, small molecules and polymers. [23] Small molecule OPVs were dominated by the use of copper phthalocyanine **4** as the donor material and fullerene C_{60} **5** as the acceptor material (Figure 14), with the highest efficiencies seen at 5% with these materials.[24]

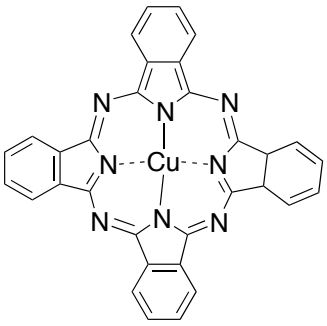

(4)

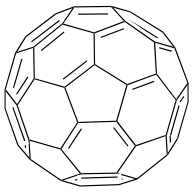

(5)

Figure 14 Structures of 4 and 5

There have been a variety of studies conducted to investigate non-fullerene based acceptor material. Perylene diimides[25], cyanopentacenes[26] and diketopyrrolopyrrole derivatives[27] have been among those compounds investigated, however, they have yet to match the PCE values achieved by fullerene based acceptor materials reaching 1.87%, 1.29% and 1% respectively. Thus, acceptor materials have remained primarily fullerene based with PCBM ([6,6]-phenyl-C_{61}-butyric acid methyl ester) **6**, a soluble C60 derivative, becoming the benchmark for acceptor materials in OPV (Figure 15).

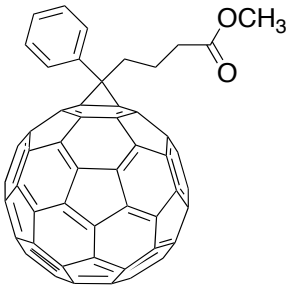

PCBM

(6)

Figure 15 Structure of 6

The main focus over recent years has been the development of new donor material, such as oligothiophenes. Li et al. looked at the use of oligothiophenes (Figure 16) with the use of $PC_{71}BM$ and $PC_{70}BM$ as the acceptor material and observed high efficiencies of 6.1% with oligothiophene **7** and $PC_{71}BM$ and 6.7% with oligothiophene **8** and $PC_{70}BM$, indicating the potential for achieving high efficiencies by investigating new donor materials.[28]

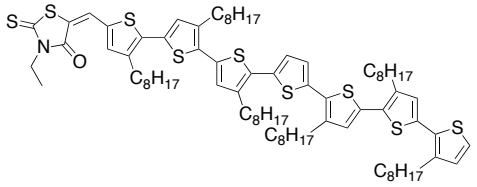

(7)

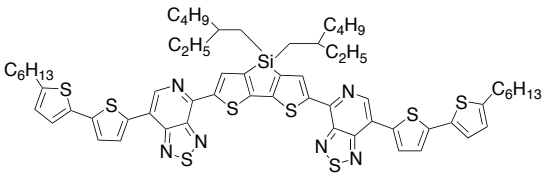

(8)

Figure 16 Structures of oligothiophenes 7 and 8

In 2013, Kyaw et al. developed a device with the high efficiency of 7.88%.[29] They utilised 7′-(4,4-bis(2-ethylhexyl)-4H-silolo[3,2-b:4,5-b′] dithiophene-2,6-diyl)bis(6-fluoro-4-(5′-hexyl-[2,2′-bithiophen]-5-yl)benzo[c][1,2,5]thiadiazole)(p-DTS(FBTTh$_2$)$_2$) **9** (Figure 17) and PC$_{70}$BM as the donor and the acceptor components, respectively.

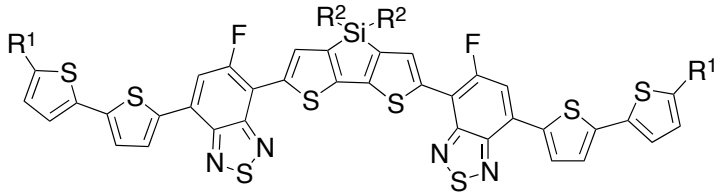

R^1 = hexyl
R^2 = 2-ethylhexyl

(9)

Figure 17 Structure of 9

In 2012, Zhou et al. achieved a power conversion efficiency of 8.12% using a device based upon an acceptor-donor-acceptor system with a benzodithiophene central building block, DR3TBDTT **10** (Figure 18). Rhodanine units were used as end units and the system was linked using alkyl-substituted terthiophene-based π-conjugated spacers. This provided good solubility and also formed a long conjugated acceptor−donor−acceptor (A−D−A) backbone structure with strong intramolecular charge transfer and broad absorption.[30]

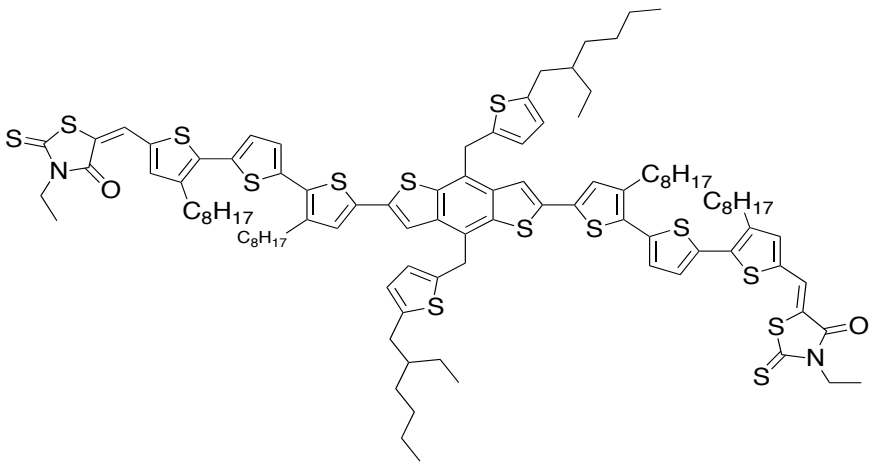

(10)

Figure 18 Structure of 10

A common characteristic of organic photovoltaic materials is a conjugated system and the most common organic materials used in photovoltaics are conjugated polymers blended with PCBM as the acceptor. It is well known that a greater extent of conjugation within a system results in an enhancement in absorbance maximum and a red-shift in the absorption spectra.[31] The most efficient polymer photovoltaic material is the polythiophene derivative P3HT **11** (Figure 19).

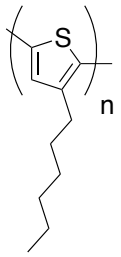

P3HT

(11)

Figure 19 Structure of 11

Efficiencies of above 8% have previously been recorded using **11**, in particular Dou et al. reached a high of 8.6% in 2012 with their tandem solar cell comprising of **11** and **12** as one active layer and a blend of **13** and **6** as the second active layer (Figure 20).[32]

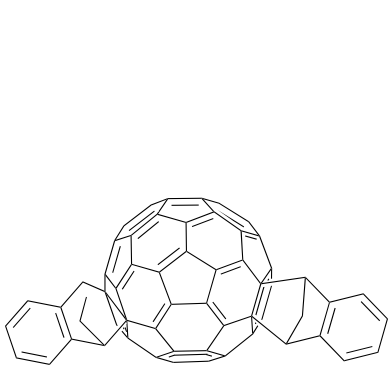

$IC_{60}BA$

(12)

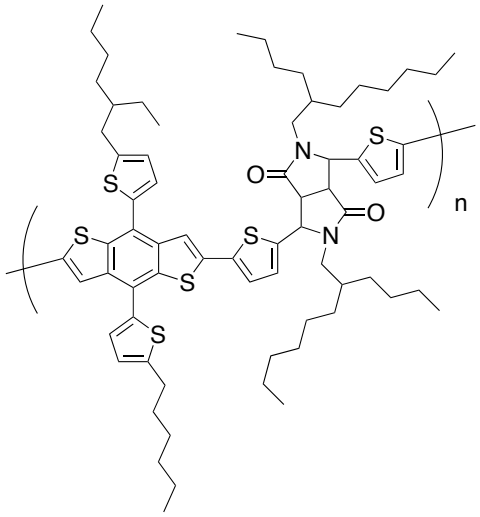

PBDTT-DPP

(13)

Figure 20 Structures of 12 and 13

However, more recently a solution processed tandem solar cell using poly[2,7-(5,5-bis-(3,7-dimethyloctyl)-5H-dithieno[3,2-b:2′,3′-d]pyran)-alt-4,7-(5,6-difluoro-2,1,3-benzothia diazole)] (PDTP-DFBT) **14** (Figure 21) has been developed by You et al. They developed a tandem solar cell with P3HT and $IC_{60}BA$ as one active layer and PDTP-DFBT **14** and $PC_{71}BM$ as the second active layer and reported an efficiency of 10.2%, however the replacement of $PC_{71}BM$ with $PC_{61}BM$ increased the efficiency to 10.6%, the highest reported to date for a polymer based solar cell.[33]

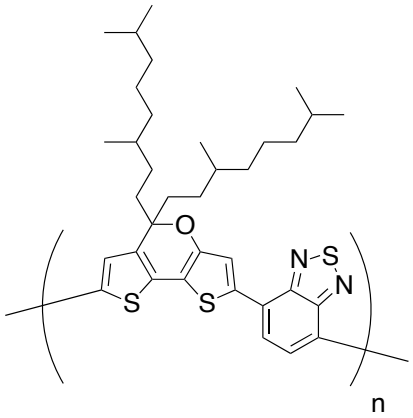

PDTP-DFBT

(14)

Figure 21 Structure of 14

1.4.3 Dye-sensitised solar cells

Dye-sensitised solar cells (DSSCs) have also attracted a lot of attention as a cost-effective alternative for photovoltaic devices. Typically, DSSCs are composed of a TiO_2 layer deposited on a conducting substrate, an anchored molecular sensitizer, a redox electrolyte and a platinum counter electrode. Improving the cost-efficiency of these DSSCs has focussed on developing new sensitizers. Ideally a DSSC should meet the following criteria: [34]

- An intense absorption in the visible and near-IR spectrum
- Preferred light absorption type is intramolecular charge transfer (ICT)
- Sufficiently high LUMO energy level for efficient electron injection into the TiO_2 conduction band
- Low HOMO energy level for efficient regeneration of the oxidised state
- Suitable anchoring group which ensures stable bonds with the TiO_2 surface

DSSCs typically work by photo-excitation of the charge transfer dye, which then injects and electron into the conductive oxide (TiO_2). The dye is then restored to its original state through electron donation from the electrolyte, which is typically an organic solvent containing a redox system such as the iodide/triiodide, this in turn prevents the recapture of the electron by the dye and thus closes the circuit (Figure 22).[35]

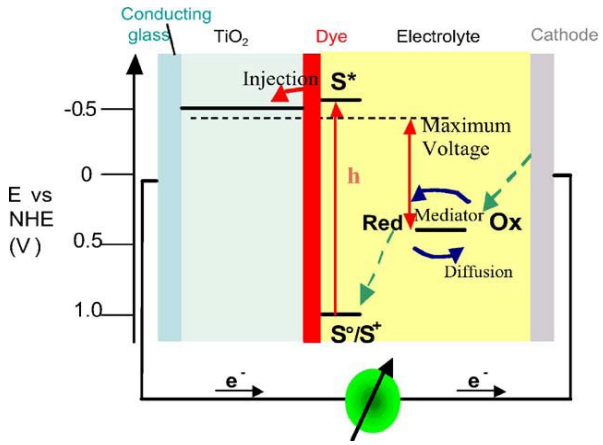

Figure 22 Schematic representation of the operating principle of a DSSC[35]

The first high efficiency DSSC device was reported by Grätzel and O'Regan in 1991, where they introduced the use of TiO_2 as a working electrode and utilised ruthenium based dyes and achieved a power conversion efficiency of 7.9%.[36] Ruthenium dyes are the most commonly used dyes in DSSCs with high efficiencies of over 10%

observed using "black dye" **15** and N719 **16** (Figure 23) [37]. Chiba et al. utilised **15** to achieve an efficiency of 11.1% [38] and Nazeeruddin et al. achieved an efficiency of 11.2% with a device based on **16**.[39]

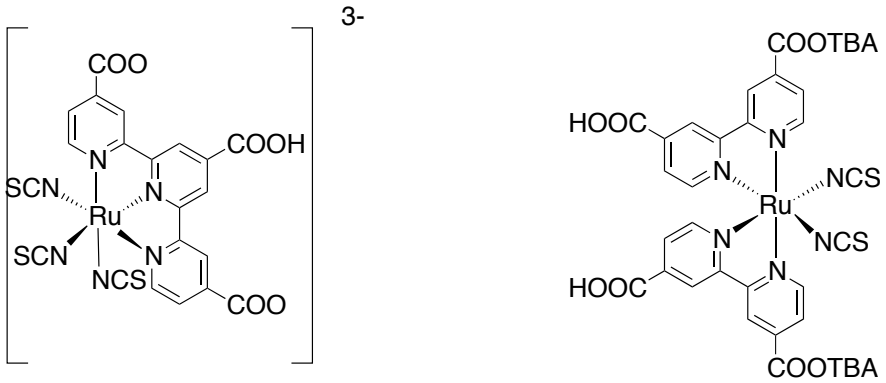

(15) (16)

Figure 23 Structures of 15 and 16

To date the highest efficiencies seen for DSSCs have been based upon dyes SM371 **17** and SM315 **18** (Figure 24) developed by Mathew et al., in which they achieved a power conversion efficiency greater than 12%, with SM315 **18** achieving the highest efficiency at 13%[40]

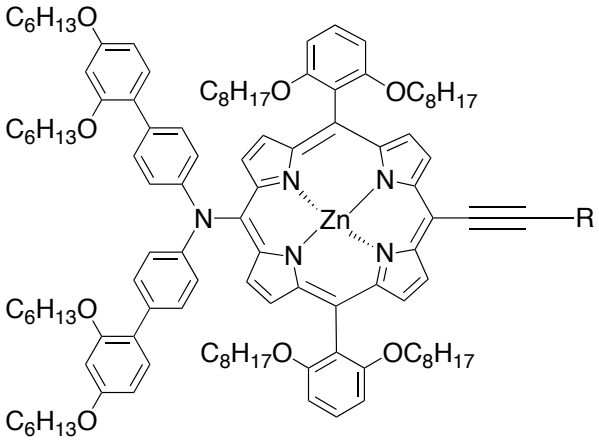

R = 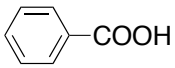

SM371

(17)

R = 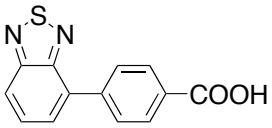

SM315

(18)

Figure 24 Structures of dyes 18 and 17

1.5 Current Research

1.5.1. Organic photovoltaics

Organic photovoltaics (OPV) have yet to reach the same power conversion efficiencies as inorganic materials with the highest being around 11%. Due to the potential for OPVs to replace existing energy sources, a vast amount of research has gone into developing these devices in order to increase the power conversion efficiencies. One way of doing this has been to look at developing low band gap conjugated polymers with low HOMO energy levels by synthesising polymers with electron-rich and electron-deficient moieties and utilising a "push-pull" architecture. Push-pull structures enhance the charge carrier mobility due to the π-π stacking distance being reduced.

Song et al. looked at using a new electron deficient group 2,2-dimethyl-*2H*-benzimidazole (MBI) **19** (Figure 25) as a replacement for 2,1,3-benzothiadiazole which has the disadvantage of having poor solubility in most organic solvents.[41] Their aim was to utilise the efficient intramolecular charge transfer effect of MBI to develop polymers with good solubility and low band gaps. They reported the synthesis of new conjugated polymers poly[2,6-(4,4-bis(2-ethylhexyl)-*4H*-cyclopenta[def] phenanthrene)-*alt*-5,5-(4,7-di-2-thienyl-2,2-dimethyl-2H-benzimidazole)] (PCPPDTMBI), **20**, **21** and **22**, and poly[2,6-(4,4-bis(2-ethylhexyl)-*4H* cyclopenta [def]phenanthrene)-alt-5,5-(4,7-bi-2-bithiophene-2,2-dimethyl-2Hbenzimidazole] (PCPPBBTMBI), **23**, **24** and **25**, (Figure 26).

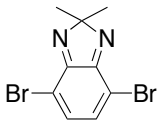

MBI

(19)

Figure 25 Structure of 19

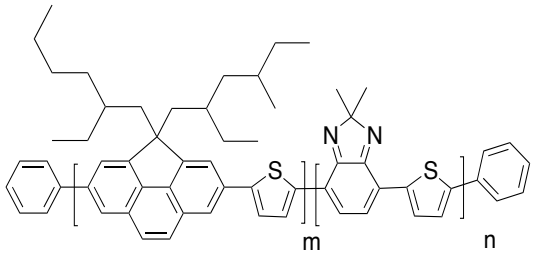

m:n = 7:3 PCPPDTMBI3 (20)
m:n = 5:5 PCPPDTMBI5 (21)
m:n = 3:7 PCPPDTMBI7 (22)

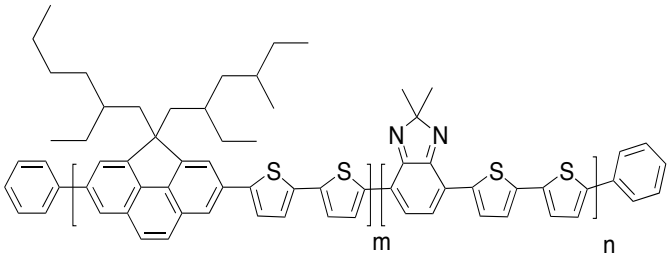

m:n = 7:3 PCPPBBTMBI3 (23)
m:n = 5:5 PCPPBBTMBI5 (24)
m:n = 3:7 PCPPBBTMBI7 (25)

Figure 26 Structures of 21-25

Focussing on the optical properties of these polymers, they found that the solid films of the PCPPDTMBIs displayed two absorption maxima at 408-417 nm and 613-640 nm and the PCPPBBTMBIs showed a red shift of around 5-30 nm with two absorption maxima at 440-444 nm and 627-650 nm, due to the introduction of the bithiophene units. Using cyclic voltammetry they observed that the HOMO energy levels were −5.52 to −5.70 eV and the LUMO energy levels were −3.59 to −3.73 eV, respectively. Although the efficiencies for the devices fabricated were low, 0.21-0.46%, the absorption maxima and band gaps indicate that these structures hold promise if they can be tuned further to increase the efficiencies.

In another study Nantalaksakul et al looked at mimicking the photo-induced charge transfer process seen in photosynthesis for photovoltaics.[42] They looked at creating a hybrid architecture combining the advantages of a dendritic structure in photo-induced charge transfer processes and the open nature of linear polymers for transporting the charges. The architecture they envisaged was a dendron-rod-coil triad with a rod chromophore, a dendron containing the electron rich moieties and a polymeric coil containing electron deficient moieties. This is demonstrated by the cartoon featured in Figure 27.

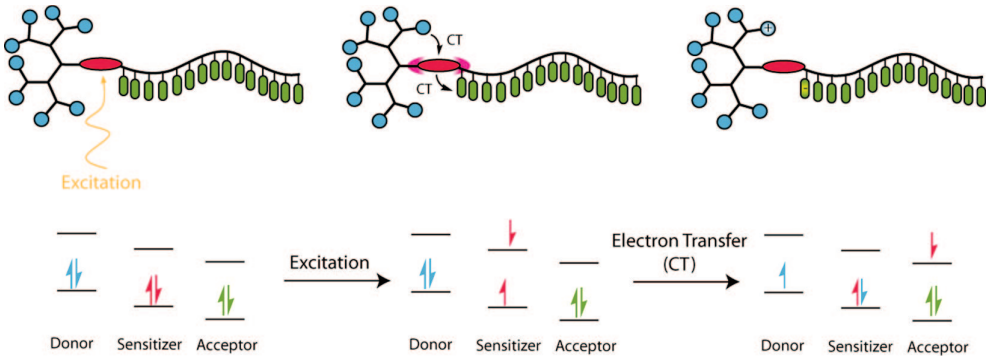

Figure 27 Cartoon showing the electron transfer process in dendron-rod-coil structures[42]

(Diarylamino)pyrene **26** was selected as the electron rich functionality on the dendron, where as naphthalenediimide **27** was the electron poor functionality in the polymer coil and a benzothiadiazole based compound **28** as the rod chromophore (Figure 28).

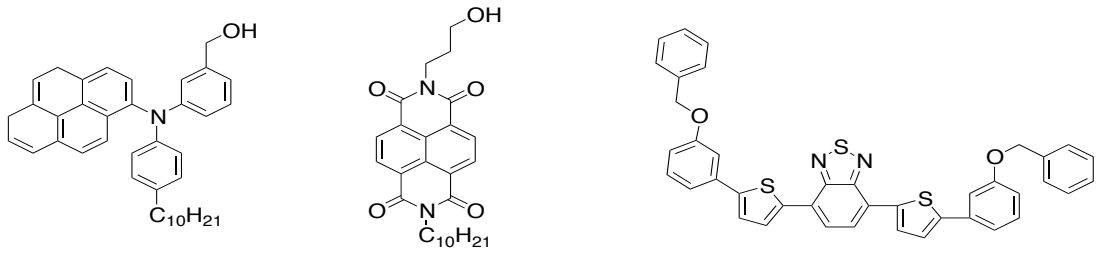

(26) (27) (28)

Figure 28 Structures of 26, 27 and 28

To synthesise the targets they opted for a modular approach, synthesising each individual component separately and then coupling them together at the end. They used atom transfer radical polymerisation (ATRP) to synthesise the naphthalenediimide polymer with an azide end group, they then synthesised the benzothiadiazole rod with an alkyne group at the end in order to utilize a 1,3-dipolar cycloaddition reaction to couple the two together. On the other side of the benzothiadiazole they used a phenol end group, which could couple with a bromomethyl dendron to create the whole structure (dendrons **26**, **27** and **28**) (Figure 29).

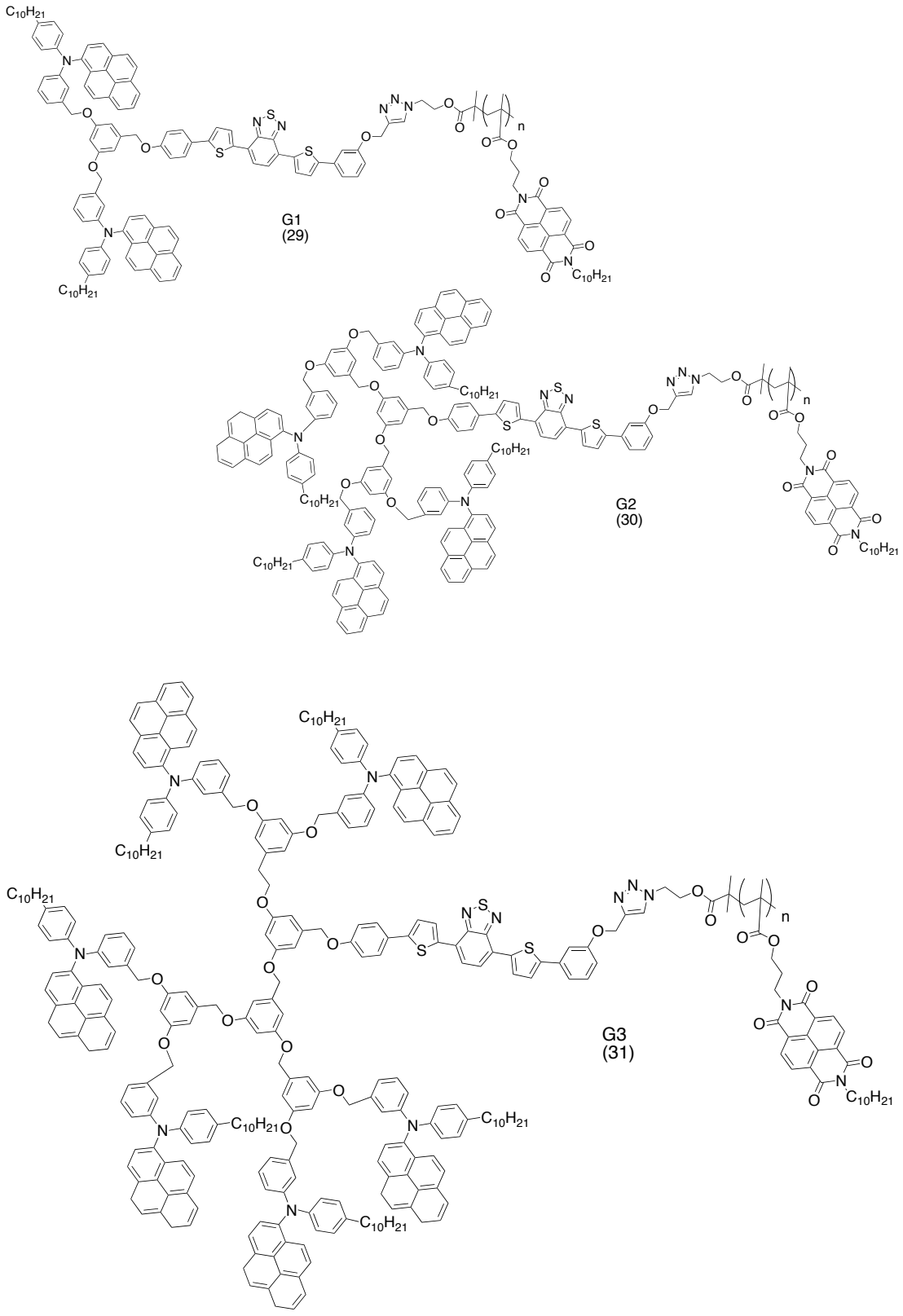

Figure 29 Target dendron-rod-coil structures 29, 30 and 31

They found that these dendron-rod-coil triads were indeed advantageous in the photo-induced charge transfer (Figure 30), which indicates that the excited state of the chromophore can be reduced by the diarylaminopyrene **26** or oxidised by the

naphthalenediimide **27**, thus showing it is feasible that the excitation of the chromophore results in a photo-induced charge transfer state. They also showed that these structures displayed higher efficiencies comparative to their diad counterparts and thus show great promise in terms of organic photovoltaics.

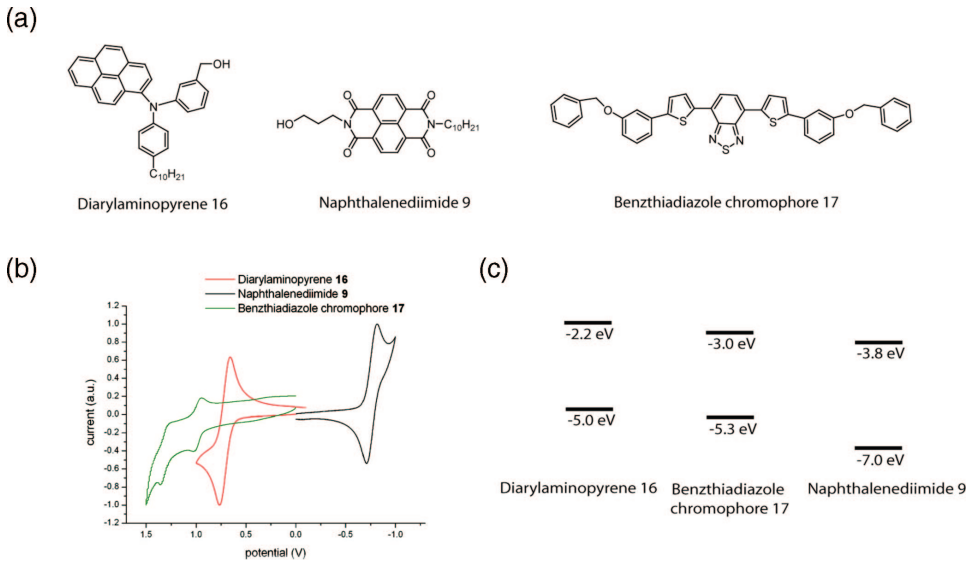

Figure 30 Demonstration of the charge transfer of the dendron-rod-coil[42]

A common feature of organic solar cells is the use of conjugated polymers. In order to achieve high power conversion efficiencies with these types of organic solar cells it is necessary to develop p-type conjugated polymers that possess both a narrow band gap for matching the high photon region of the solar spectrum and high hole mobility for efficient charge transport. One way of doing this is to develop donor-acceptor (D-A) conjugated polymers with strong π-stacking structures in their solid-state films. Deng et al[43] utilised the donor advantages of 6H-phenanthro[1,10,9,8-cdefg]carbazole (PC) **32** and an electron deficient diketopyrrolopyrrole (DPP) **33** in order to create novel condensed aromatic D-A random conjugated copolymers. In order to adjust the conjugated backbone packing and the photoelectric properties they used thiophene (T) **34** and thieno[3,2-b]thiophene (TT) **35** (Figure 31) as a bridge between the donor and acceptor functionalities to develop a series of copolymers as shown in Figure 32.

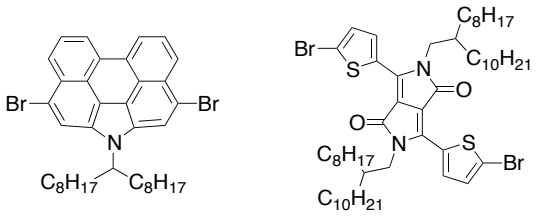

PC (32)

DPP (33)

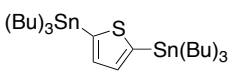

T (34)

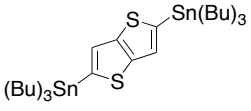

TT (35)

Figure 31 Structures of monomers 32, 33, 34 and 35

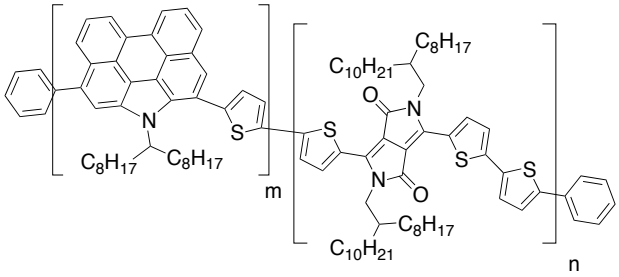

PCC-T-DPP_2/1 molar ratio: PC:T:DPP = 2:3:1 (36)
PCC-T-DPP_1/1 molar ratio: PC:T:DPP = 1:2:1 (37)
PCC-T-DPP_1/2 molar ratio: PC:T:DPP = 1:3:2 (38)

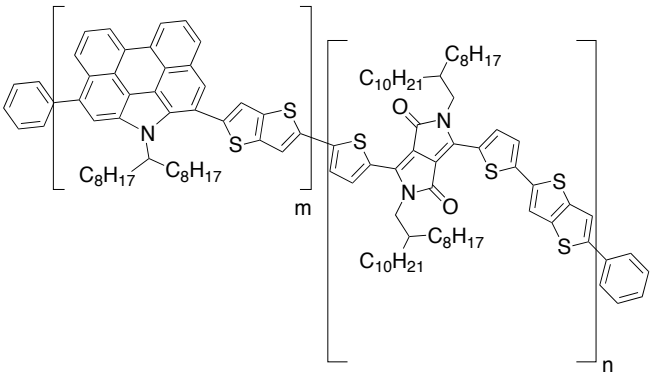

PCC-TT-DPP_1/2 molar ratio: PC:TT:DPP = 1:3:2 (39)

Figure 32 Structures of 36, 37, 38 and 39 with differing feed ratios of monomers

On investigating the thermal properties of the polymers they found that they exhibited sufficient thermal stability for polymer solar cell applications with 5% weight loss between 400 ºC and 420 ºC. They also found that in differing the feed molar ratios of

the monomers had little effect on their thermal stability. Studying the optical properties, they found that all of the polymers displayed broad absorption bands with distinct peaks at 400-550 nm and 600-850 nm. This was attributed to the strong push-pull interaction between PC **32** donor and DPP **33** acceptor unit, with the 400-550 nm corresponding to the localized π-π* transition from the PC **32** segment and the 600-850 nm corresponding to the intramolecular charge transfer between the DPP **33** acceptor and the PC **32** donor unit. When fabricated into films, they observed a bathochromic shift of ca 5-28 nm, indicating stronger intermolecular interactions in the solid state. The optical band gaps for the polymers were found to be 1.39 eV, 1.42 eV, 1.46 eV and 1.57 eV for PPC-T-DPP_2/1 **36**, PPC-TT-DPP_1/2 **39**, PPC-T-DPP_1/1 **37** and PPC-T-DPP_1/2 **38** respectively. These figures match well with the solar spectrum, which show that they have great potential for photon-harvesting. Cyclic voltammetry showed that the copolymers have a low-lying HOMO level which would offer a relatively high open circuit voltage and a suitable LUMO level for effective charge transfer from the polymer to PCBM. The photovoltaic properties also showed the promise of these structures with the highest efficiency of 2.0% for PPC-T-DPP_1/2 **38** and by switching to the TT **35** this increased to 2.2% due to the better charge mobility of the planar TT **35** moiety.

1.5.2 Dye-sensitised solar cells

Dye-sensitised solar cells (DSSCs) have incurred a lot of interest for use as renewable energy systems.[44] Currently, photoenergy conversions of 11% can be achieved using ruthenium complexes; however these ruthenium dyes are not effective for photovoltaic systems due to the high cost of the ruthenium and the fact that they are environmentally unfriendly. Thus, investigations into metal –free organic dyes have attracted a lot of interest.[38]

A study by Ito et al. looked at the use of an indoline dye in DSSCs.[45] Their aim was to control the dye-aggregation by designing a new indoline dye by introducing an *n*-octyl solubilising group onto the rhodanine ring of the existing dye D149 **40** giving a new dye D205 **41** (Figure 33)

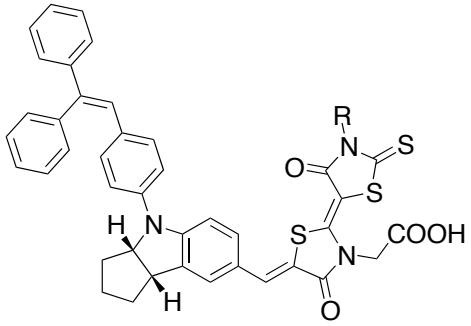

R = -C_2H_5 D149 (40)

R = -C_8H_{17}-n D205 (41)

Figure 33 Structures of indoline dyes 40 and 41

They fabricated DSSCs using both indoline dyes and also added a co-absorbent, chenodeoxycholic acid (CDCA), which had previously been shown to be an anti-aggregation reagent, which improved photovoltaic effect. They found that by adding this *n*-octyl group along with the CDCA the DSSC with **41** gave a conversion efficiency of 9.52%, one of the highest observed for metal-free organic dyes rivalling that of the standard ruthenium dye **16** at 11%. The addition of the CDCA improved the efficiency from ~8.43%. Comparison between the two dyes showed that **41** showed a higher efficiency both alone and when combined with CDCA as can be seen in Table 1.

Table 1 Photovoltaic characteristics of DSSCs with the indoline dyes 40 and 41. Results obtained from three DSSCs

Photovoltaic Characteristics	**Without CDCA**	**Without CDCA**	**With CDCA**	**With CDCA**
	D149	**D205**	**D149**	**D205**
J_{sc} / mA cm^{-2}	19.08 ± 0.26	18.99 ± 0.19	19.86 ± 0.10	18.68 ± 0.08
V_{oc} / V	0.638 ± 0.05	0.656 ± 0.11	0.644 ± 0.13	0.710 ± 0.07
FF	0.682 ± 0.06	0.678 ± 0.09	0.694 ± 0.06	0.707 ± 0.09
Efficiency / %	8.26 ± 0.09	8.43 ± 0.16	8.85 ± 0.18	9.40 ± 0.12

They concluded that these results indicated that the control of the dye aggregation using the *n*-octyl and CDCA was a key factor in achieving the high conversion efficiency. They also summarised that these results indicated that the use of organic photosensitizers in DSSCs were highly promising in regard to high solar cell performance and low cost production.

In another study, Xie et al. looked at developing novel organic dye sensitizers.[34] They utilised the phenothiazine (PTZ) moiety in order to synthesise two unsymmetrical dyes (2E)-2-cyano-3-(5-(5-((E)-2-(10-(2-ethylhexyl)-10H-phenothiazin-7-yl)vinyl) thio-phene-2-yl)thiophen-2-yl)acrylic acid (PTZ1) **42** and (2E)-3-(5- (5-(4,5-bis((E)-2-(10-(2-ethylhexyl)-10H-phenothiazin-3-yl)vinyl)thio-phen-2-yl)thiophen-2-yl)thio phen-2-yl)-2-cyanoacrylic acid (PTZ2) **43** (Figure 34). They employed the PTZ moiety as the electron donor functionality due to the electron rich sulphur and nitrogen heteroatoms, the 2-ethylhexyl group was introduced in order to increase the solubility of the dyes and they used the cyanoacrylic acid functionality to act as an acceptor and anchoring group. Using bithiophene-vinylene as the connecting groups also proved to extend the π-conjugation and in PTZ2 **43** they included a second PTZ unit in order to study the effects of the substituted donor on the optical, electrochemical and PV properties.

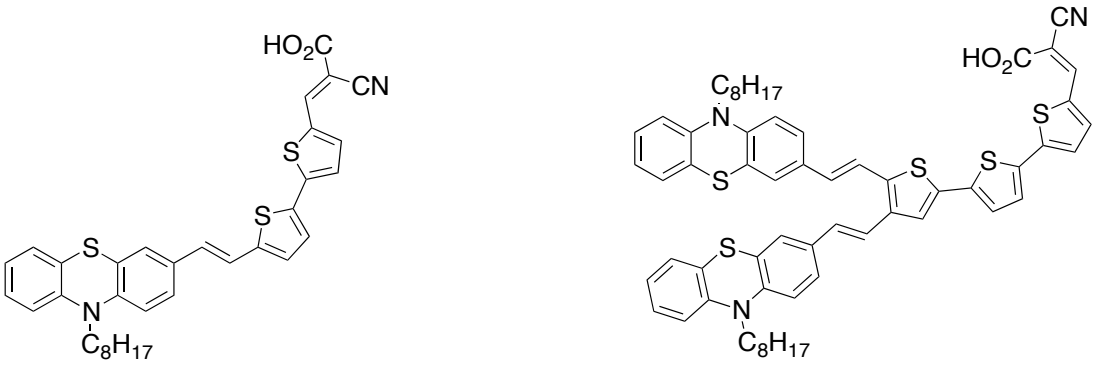

PTZ-1 **(42)** **PTZ-2** **(43)**

Figure 34 Structures of 42 and 43

A study of the optical properties showed that PTZ1 **42** and PTZ2 **43** displayed strong absorption bands at 496 nm and 508 nm respectively due to the intramolecular charge transfer from the PTZ donor to the cyanoacrylic acceptor. The slightly red shifted band for **43** was attributed to the additional donor moiety and the longer conjugation.

It was also noted that the absorption coefficients for these dyes, 30300 $M^{-1}cm^{-1}$ for **42** and 31700 $M^{-1}cm^{-1}$ for **43**, were also considerably larger than the standard ruthenium dye **16**, 13000 $M^{-1}cm^{-1}$. This suggests that the dyes can absorb visible light more readily than the ruthenium dye **16** using the same device architecture. The photovoltaic performance of these dyes also proved to be very promising with efficiencies of 6.17% achieved for **42** and 2.8% for **43**. However, when combined with a coadsorbent, chenodeoxy cholic acid (CDCA) the efficiency for **43** increased to 4.34%, although still lower than for **42**. They concluded from this study that the introduction of further donor moieties has a detrimental effect on the PV performance likely due to dye aggregation. Although the efficiencies achieved are not yet reaching the high values of 12-13% currently observed, they do show a lot of promise and thus with further optimisation could be potential replacements for existing dyes.

1.6 Summary

Greater focus towards organic electronics, and particularly organic photovoltaics, has occurred over the last few decades, and with the need for new energy sources, the interest is great. Although the efficiencies seen are lower than their inorganic counterparts, there is a lot of potential in utilising organic materials. The key aims appear to be to develop structures that absorb as much of the solar spectrum as possible, particularly pushing into the near-IR to IR region, a sufficiently high LUMO energy level and low HOMO energy level and good solubility of the compounds to enable device fabrication. These are the aims I set out to achieve in the research outlined in this thesis.

2.0 Synthesis and characterisation of flavin functionalised conjugated polymers

2.1 Introduction

2.1.1 Background

Since flavins were discovered, they have been recognised as being capable of both one and two electron transfer.[46] In addition to this, they are also known as being capable of functioning as both electrophiles and nucleophiles.[48] However, before they were recognised and chemically characterised, they were drawing attention in other ways. In 1874 HMS Challenger recorded seeing a "brilliant crest of clear white light" in the ripples of the ocean. This white light was the result of the bioluminescence in the marine bacteria from the enzyme luciferase, which acted on reduced flavin and oxygen. Interest in flavins flourished in the late 1920's and early 1930's when yellow, highly fluorescent pigments were isolated from a variety of sources. The interest peaked once it was realised that they were constituents of vitamin B2 and that the activity was correlated with the intensity of the fluorescence. This vitamin B2 complex is also known as riboflavin **44** (Figure 35).[47]

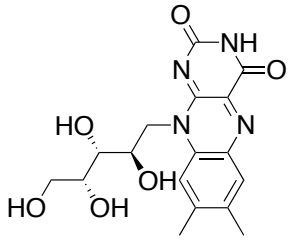

(44)

Figure 35 Riboflavin 44 also known as vitamin B2

The term flavin comes from a class of enzymes called flavoproteins, which are found in many plants and animals. They are based upon the nitrogen heterocycle 7,8-dimethylisoalloxazine **45** (Figure 36). They catalyse redox reactions using many important pathways including photosynthesis, DNA repair, electron transport and bacterial cell-wall biosynthesis. The redox chemistry occurs at the three-ringed, highly electron-deficient, aromatic core of the flavins. Flavins can be tuned by functionalising at the N3 and N10 position and also by changing the functionality at the 7 and 8 position.[48]

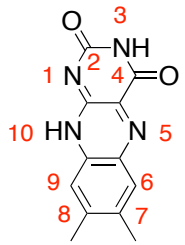

(45)

Figure 36. Structure of 45

Flavin mononucleotide (FMN, **46**) and flavin adenine dinucleotide (FAD, **47**) (Figure 37) are the biologically active forms of riboflavin. It is the flavoenzymes containing these groups that are responsible for catalysing one and two electron oxidation and reduction reactions critical in the energy metabolism systems. Flavoenzymes are also capable of catalysing oxygenation reactions such as the Baeyer-Villiger oxidation and aromatic hydroxylations, which are involved in soil detoxification processes.[49] Flavin dependent halogenases are also required for the biosynthesis of halogenated natural products. Flavins are also involved in the photo-repair of DNA damage.[50]

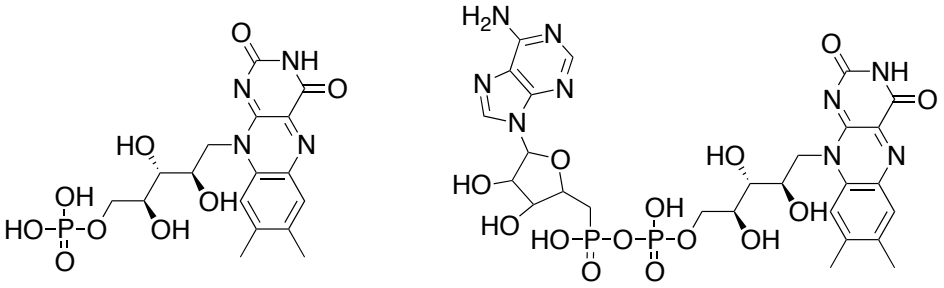

FMN (46)

FAD (47)

Figure 37 Structures of 46 and 47

Flavins have an array of attributes that explain their widespread occurrence in nature. This includes photostability, reversible electrochemistry and the tunability of their optical, electronic and redox properties. Alongside their importance in the biological world these properties are also key features for organic electronics and optoelectronic devices.

2.1.2. Redox properties of flavins

Flavins can exist in three different redox states, fully oxidised, one electron reduced giving the semiquinone and, finally, the two electron reduced flavin. Heelis proposed that flavins can exist in nine different redox and protonation states dependent upon the pH and potential of the solution.[47]

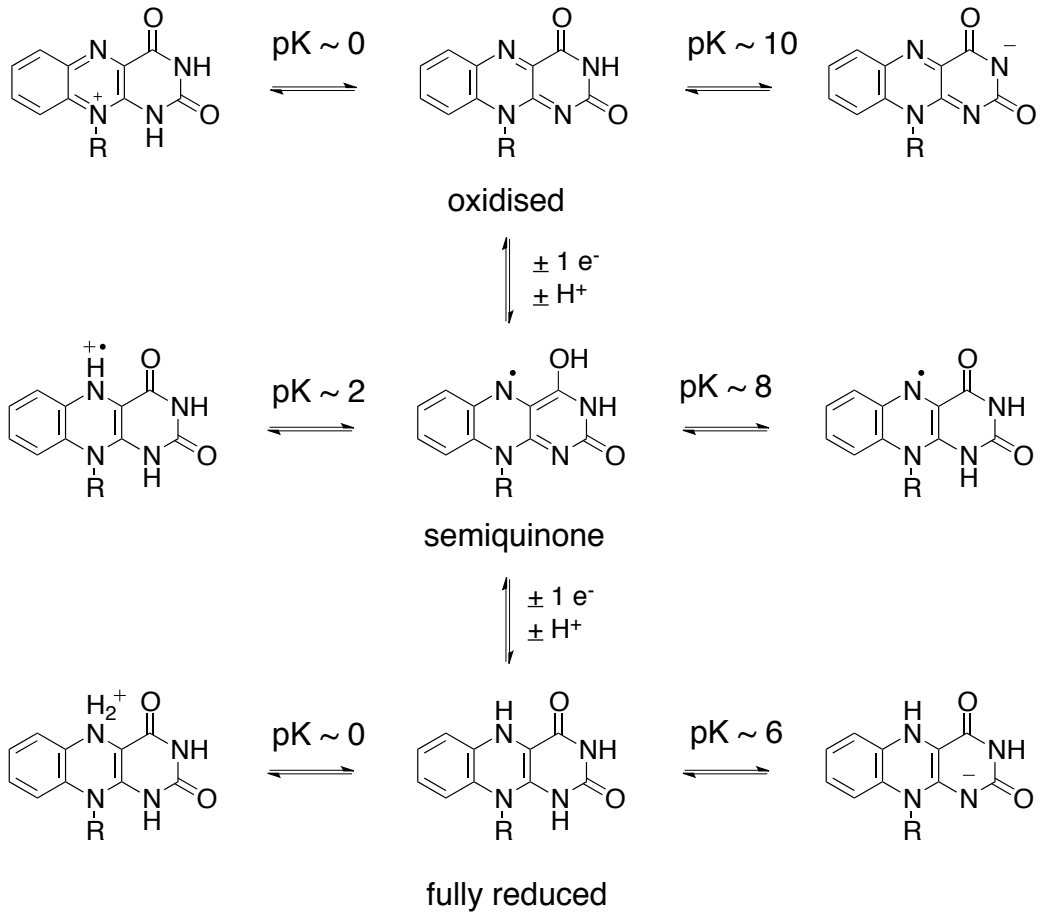

Figure 38 Structures of the nine redox states of flavins

Riboflavin **44** has a redox potential of ~200 mV, this can be influenced, however, by intermolecular interactions[51] or via substitution on the riboflavin core.[52] Hydrogen bonding, π-stacking and cation-π interactions are three fundamental non-covalent interactions in molecular recognition. There have been many model systems that have been devised for the investigation of these forces and their role in a variety of areas such as protein structure, ligand binding and host-guest chemistry. Host-guest interactions have been used to investigate the role of recognition on the redox chemistry of flavoenzymes.

The flavin cofactors riboflavin, **46** and **47** usually bind to the active site of the apoenzyme via non-covalent interactions that modulate the redox properties and thus control the overall catalytic activity of the enzyme. Nandwana et al. developed a xanthene-based model system to study π-stacking in flavoenzymes.[53] They carried out a variety of investigations on π-stacking and H-bonding interactions. In the hydrogen bonding versus π-stacking investigations the xanthene based model systems contained a diaminotriazine moiety **48** which, through hydrogen bonding, would orientate the flavin over an aromatic surface (Figure 39).

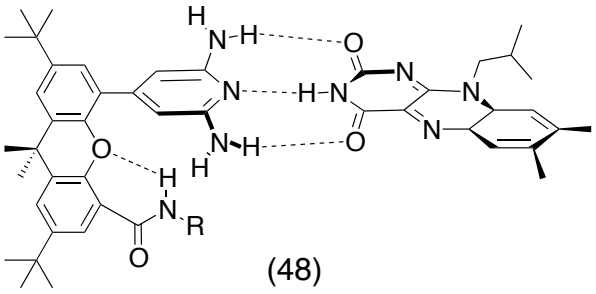

(48)

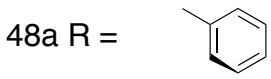

48a R = $K_a = 394\ M^{-1}$

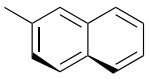

48b R = $K_a = 1080\ M^{-1}$

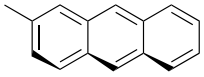

48c R = $K_a = 11520\ M^{-1}$

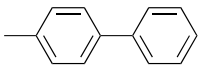

48d R = $K_a = 2800\ M^{-1}$

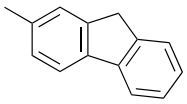

48e R = $K_a = 17600\ M^{-1}$

Figure 39 Hydrogen bonding from model systems (48a-e) orienting the flavin

This allowed the aromatic surface to be varied whilst maintaining the hydrogen bonding interactions thus allowing the effect of different aromatic moieties on the flavin redox properties to be investigated. When investigating the donor-π interactions the receptors seen in Figure 40 showed that varying the donor moiety resulted in

significant changes in the association constant. They also showed that incorporating a diaminopyridine (DAP) moiety into the model system **49**, in place of the diaminotriazine, increased the binding of the flavin to a greater extent.

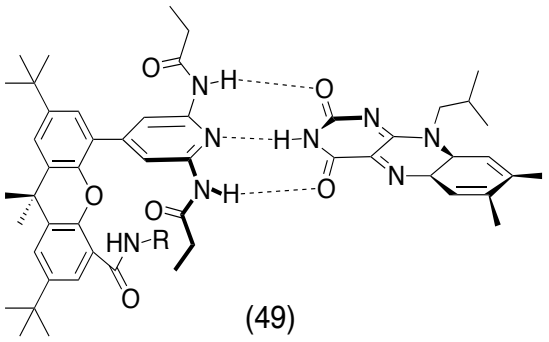

(49)

49a R = 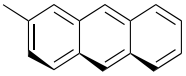

49b R = 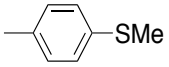

49c R = 

Figure 40 DAP moiety and changing the donor substituent

Along with intermolecular interactions they also showed that there can be intramolecular interactions whereby the flavin can self-assemble as seen in Figure 41. Here they developed a molecule containing a flavin moiety, diaminopyridine (DAP) moiety and a naphthalene moiety **50**. It showed that the structure formed an intramolecular complex with hydrogen bonding between the diaminopyridine and the flavin and aromatic stacking with the naphthalene unit.

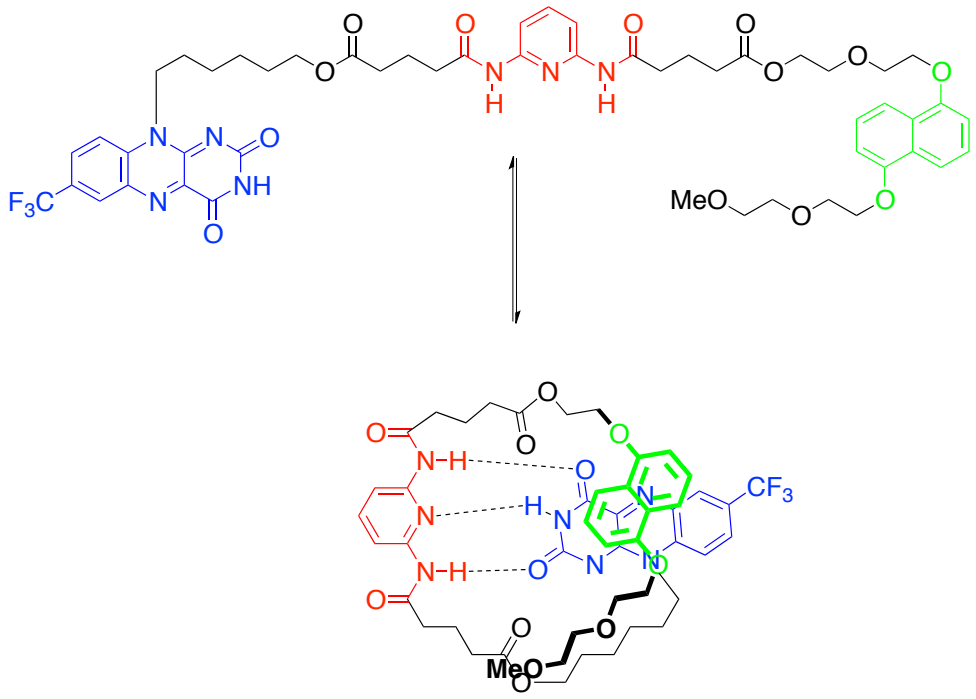

(50)

Figure 41 Self assembly of a flavin incorporated molecule 50

They concluded that the properties of flavins are not only relevant in a biological sense but that they could also be relevant to organic electronic and optoelectronic devices. Flavins are electron deficient and this could make them ideal candidates for electron-transporting materials for devices such as organic light-emitting diodes, organic field effect transistors, and organic solar cells. Additional advantages include their photo-stability, their reversible electrochemistry, and the scope for tuning their optical, electronic, and redox properties[54].

Research was also carried out into incorporating flavins into co-polymers as a recognition site to investigate flavin binding in polymeric structures. A polystyrene co-polymer was developed with an azide functionality. This was coupled using the Huisgen 1,3-dipolar "click" cycloaddition with an alkyne-functionalised flavin creating a new polymer with a flavin recognition site. It was illustrated that the N3-H flavin functionalised polymer demonstrated 3-point hydrogen bonding with diaminopyridine. However, alkylating the N3 position with a methyl group prevented this interaction from occurring (Figure 42).[55]

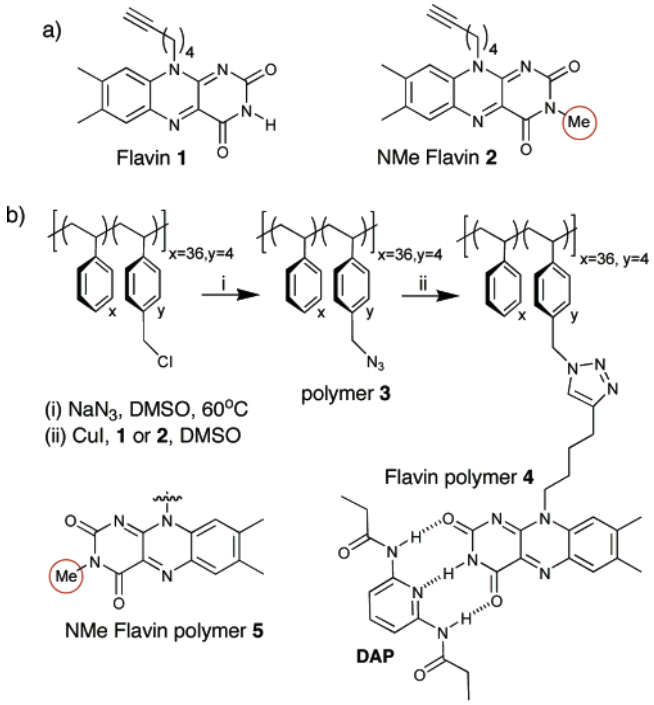

Figure 42 Flavin functionalised polystyrene copolymer investigating flavin binding to DAP[55]

Interactions between host and guest are something that have proved difficult to quantify, mainly due to the complexity of the protein environment as well as the aqueous medium making it almost impossible to isolate specific physiologically relevant flavin-protein interactions. One way to overcome this has been to construct models that are soluble in aprotic solvents. One study into developing these models was carried out by Cerda et al.[56] They looked at transforming riboflavin, which is insoluble in benzene, into tetraphenylacetyl riboflavin (TPARF) **51**, which is soluble. They studied the electrochemical properties of both the flavin alone and in complexes with DBAP **52** and MBAP **53** (Figure 43), this showed that this model system performed similarly to other model systems that had been soluble in only polar solvents such as dichloromethane. In looking at the binding titrations of these models in both benzene and dichloromethane they saw that the association constants for TPARF with an associated ligand was over an order of magnitude higher in benzene than in dichloromethane. They attributed this to the fact that benzene does not compete for H-bonds where dichloromethane does. They successfully showed that in order to analyse the effects of H-bonding on a host-guest model system a non-polar solvent is required and they developed a system that was soluble in an aprotic solvent to perform this.

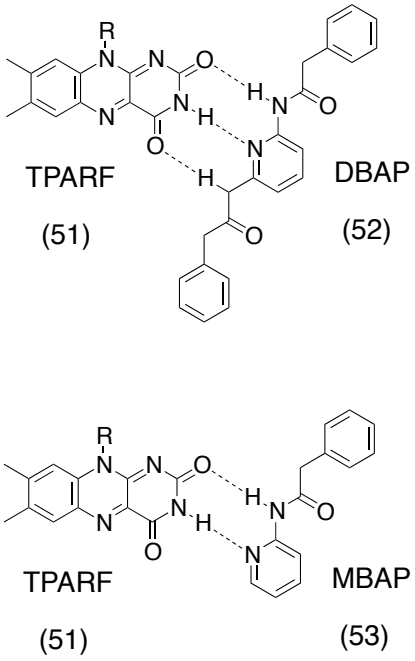

Figure 43 Binding of flavin 51 co-factors with 52 and 53 through H-bonding

Some of the leading research in this field has been through the collaboration between Cooke and Rotello, who in their research have focussed on synthesising model systems in order to study flavoenzymes further. In one study they looked at substitution at the C(7) and C(8) positions on the flavin core (Figure 44) and the effect this had on the redox potential and H-bonding affinity.[57] With this study, they demonstrated that the binding of the flavin **54** to a diaminopyridine (DAP) **55** moiety shifts the redox potential by ~80-90 mV, suggesting that the reduced flavin radical anion is stabilised by intermolecular interactions. They also noted that, with substitution at the C(7) and C(8), it was possible to modulate the redox potential by approximately +400 mV and increase the H-bonding affinity by 618 M^{-1}.

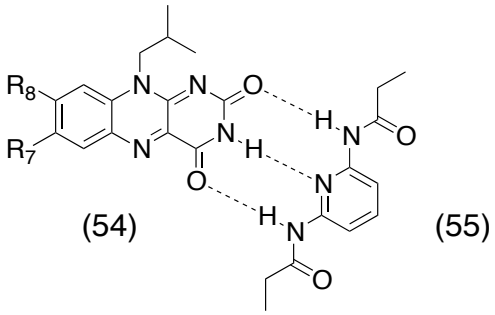

Figure 44 Structure of flavin 54 with substitution at C(7) and C(8) and binding with DAP 55

In another study, they investigated the influence of π-stacking on H-bonding

affinities.[58] From this study they concluded that π-stacking interactions increase the binding constant by 14 times when in the oxidised form and 2.5 times when in the reduced form (Figure 45).

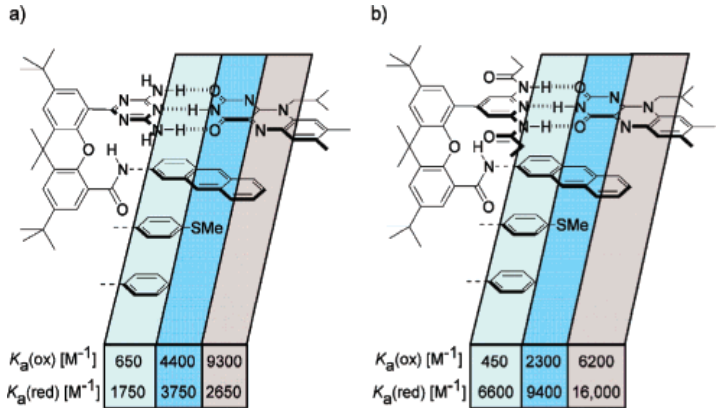

Figure 45 Influence of π-stacking on the binding constant in flavins[58]

Similarly, they found that π-stacking and binding through H-Bonding in an intramolecular system **56** (Figure 46) demonstrated the same effects. Through this study, they concluded that these interactions shifted the redox potential by ~ 10-30 mV, again indicating the stabilisation of the reduced flavin by the π-interactions.[59]

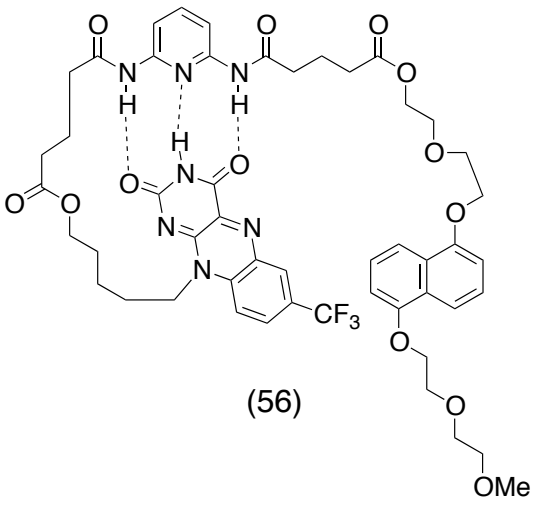

(56)

Figure 46 Structure of a flavin 56 featuring intramolecular H-bonding and π-stacking interactions

2.2 Project outline

Flavins are highly fluorescent, redox active molecules with tuneable acceptor properties. These properties can be tuned by altering the functionality at the C(7) and C(8) positions and also by adding functionality at the N3 and N10 positions. The main issue associated with flavins is the solubility of the compounds. Thus by introducing a

range of alkyl groups at the N3 and N10 positions, the solubility of the flavins could be improved. These newly functionalised flavins could then be used to synthesise a range of flavin functionalised conjugated polymers in order to exploit the acceptor ability of the flavin for photovoltaic materials.

With this information in mind, the aim for this project was to synthesise functionalised flavins to incorporate into conjugated polymers. The first target was 10-ethyl-6,9-*bis*-thiophene-benzopteridine-2,4-(3*H*,10*H*)-dione **57**, which had previously been developed within the research group (Figure 47). It was believed that the introduction of the thiophene donor groups at C(6) and C(9) would enhance the electrochemical and optical properties of the flavin and further alkylation at N(3) would increase the solubility of the compound which could then be polymerised to give a conjugated polymer to be used in photovoltaic applications.

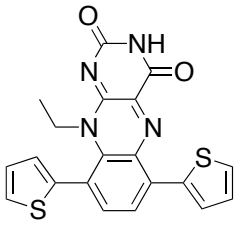

(57)

Figure 47 Structure of 57

In order to optimise the synthetic route for **57** a comparative, simpler target was chosen, 6,9-dibromo-10-ethylbenzo[*g*]pteridine-2,4(3*H*,10*H*)-dione **58** (Figure 48). This compound could also be further functionalised and polymerised to act as a comparison with compound **57** to determine if the addition of the thiophenes would have any impact on the properties of the final conjugated polymer.

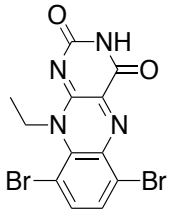

(58)

Figure 48 Structure of 58

The proposed synthetic routes for the synthesis of compounds **57** and **58** are seen in Scheme 1. Both start with a bromination of 2,1,3-benzothiadiazole **59** to give 4,7-dibromo-2,1,3-benzothiadiazole **60**. A Stille coupling would be used to add the thiophenes giving 4,7-dithienyl-2,1,3-benzothiadiazole **61**. The un-optimised route for the synthesis of target **57** involved reduction of compound **61** to give 1,2-diamino-3,6-dithienyl-benzene **62** followed by an acylation reaction to give **63**, further reduction would give **64** and then final reaction with alloxan monohydrate would give the final target **57**. The plan for optimisation of the route using target **58** would involve reduction of **60** to give the 1,2-diamino-3,6-dibromo-benzene **65**, this would then be directly alkylated to give **66** and the final reaction with alloxan monohydrate to give the target **58**. This optimised route of direct alkylation would then be used on the dithiophene compound **62**.

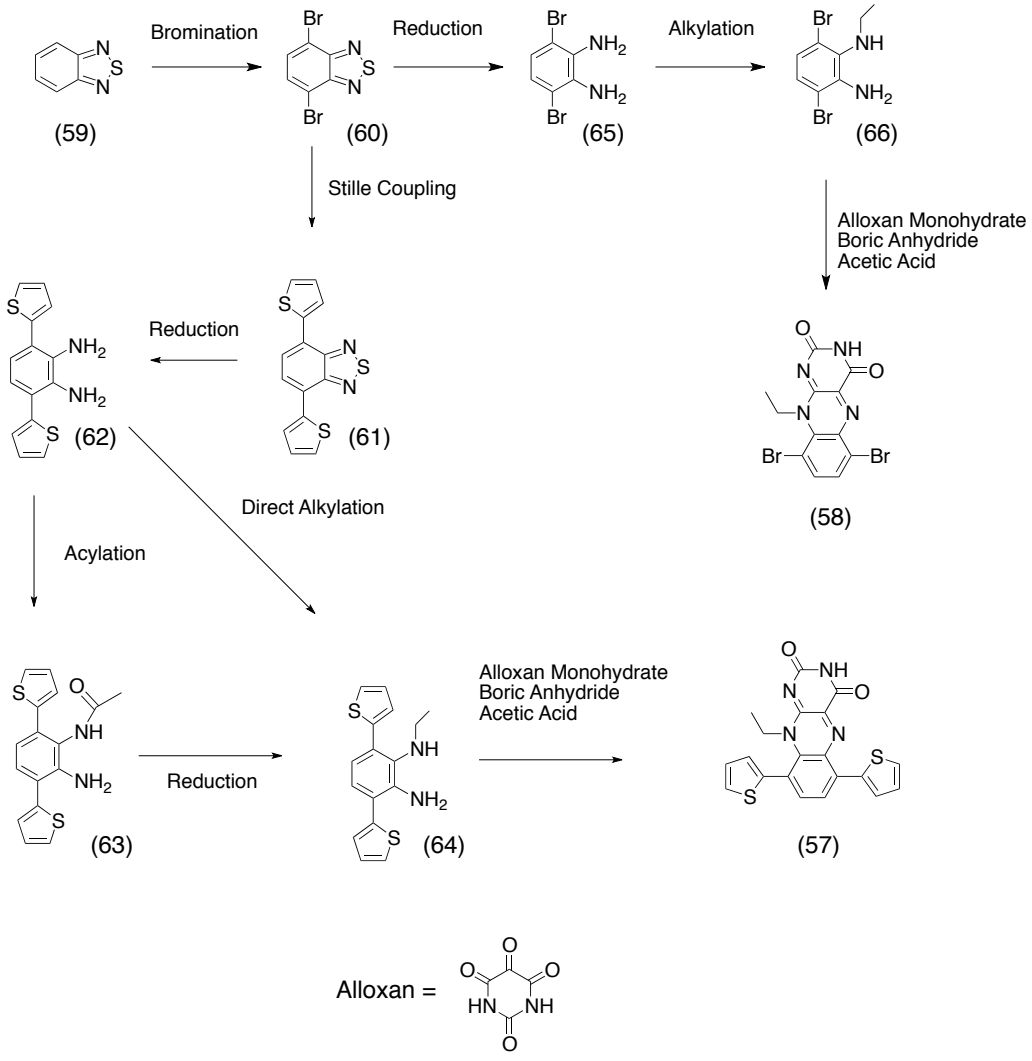

Scheme 1 Proposed synthetic strategies for the synthesis of flavins 57 and 58

2.3 Results and Discussion

2.3.1 Synthesis

The first attempt at the synthesis of a flavin featured a dithienyl moiety using methodology previously used within the group. The synthesis began with a Stille coupling of 4,7-dibromo-2,1,3-benzothiadiazole **60**, this gave the 4,7-dithienyl-2,1,3-benzothiadiazole **61** in an excellent yield. This compound was then reduced using lithium aluminium hydride to give compound **62** followed by acylation with acetyl chloride giving compound **63**. The carbonyl was then reduced, again using lithium aluminium hydride to give compound **64**. The final stage was the reaction with alloxan monohydrate to give the final compound **57** in a poor yield over 4 steps (Scheme 2). Due to the poor yield this strategy needed further development in order to achieve optimum results. Alkylation of this flavin using iodoheptane gave compound **67**, also in a poor yield thus the alkylation conditions also required optimisation.

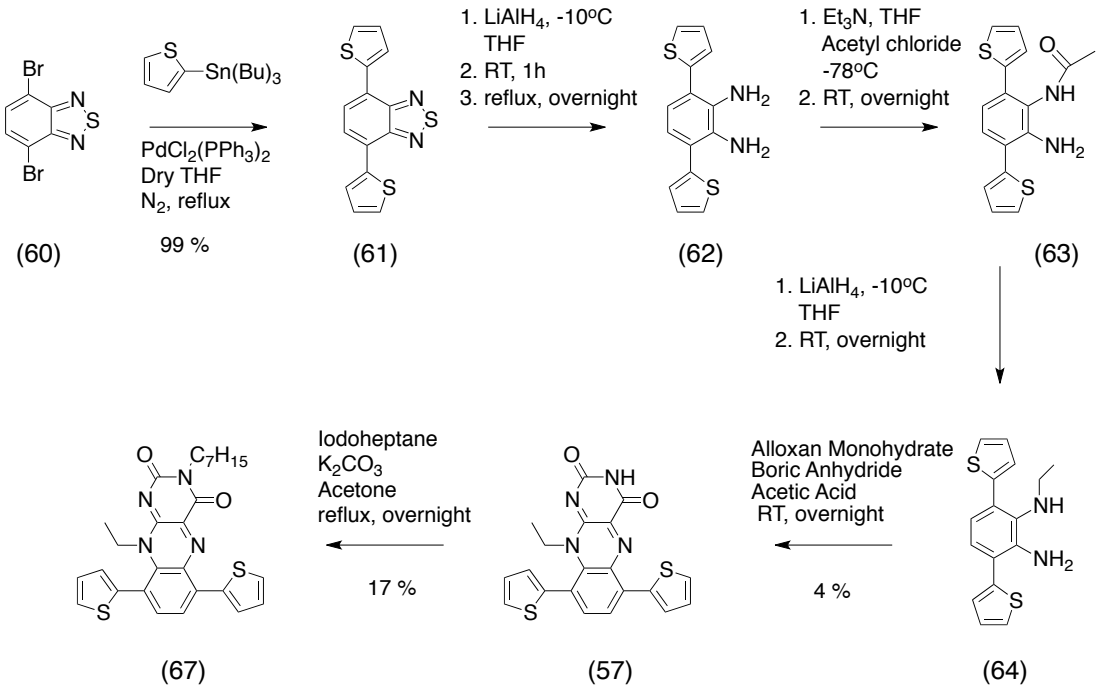

Scheme 2 First attempt at the synthesis of flavin 57 and alkylated flavin 67

In order to optimise the synthetic route for the synthesis of the flavin, **58** was chosen in order to develop the core synthetic steps prior to introducing the thiophene moieties. This compound would also act as a good comparison with flavin **57** following polymerisation due to there being less conjugation along the backbone. The synthesis started with a bromination reaction of 2,1,3-benzothiadiazole. Compound **59**

was dissolved in dry THF with bromine and bromic acid heated under reflux for 6 hours. After quenching with sodium bisulfite, **61** was achieved in good yield. The following two steps were carried out without purification and involved, first, a reduction reaction using sodium borohydride in ethanol to give compound **65** followed by alkylation using ethyl triflate and potassium carbonate in diethyl ether to give compound **66**. The final stage of the synthesis was the reaction of **66** with alloxan monohydrate and boric anhydride. The crude product from the alkylation was dissolved in acetic acid and cooled to -10ºC before the addition of boric anhydride and alloxan monohydrate. The solution was then slowly warmed to room temperature and left to stir overnight to give **58** in high yield over the 3 steps (Scheme 3).

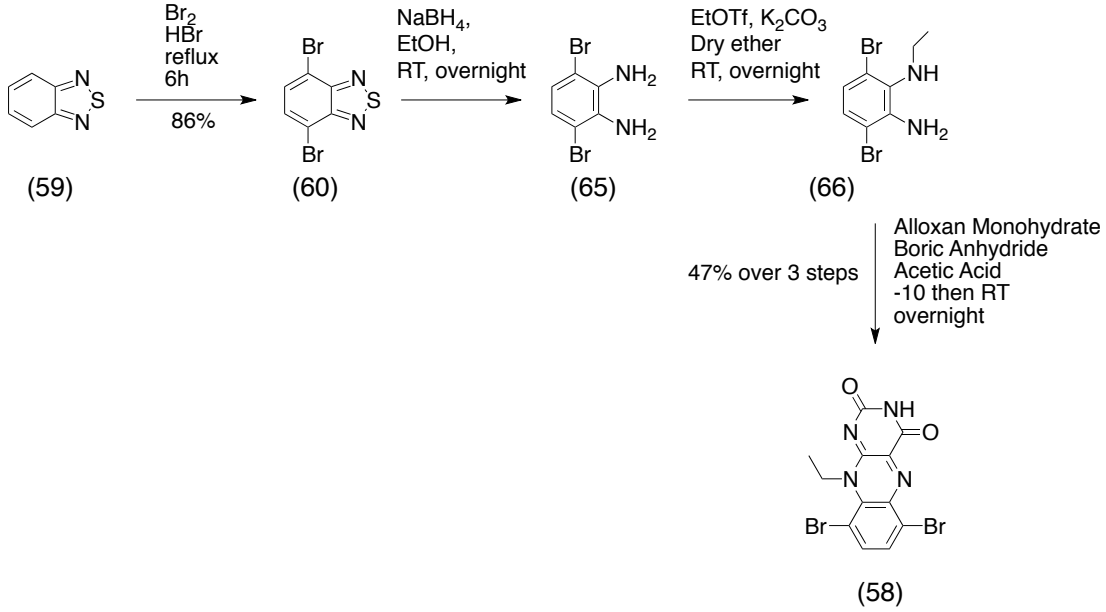

Scheme 3 Optimised synthetic route for the synthesis of the 58

Following the synthesis of the core flavin **58**, the next stage was to alkylate at the N3 position using 2-ethylhexyl bromide to give the alkylated flavin **68** (Scheme 4).

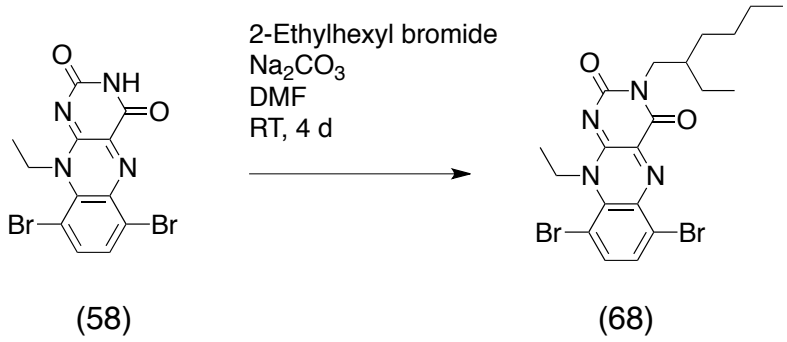

Scheme 4 Expected result of the alkylation with 2-ethylhexyl bromide

Upon examination of the ^{1}H NMR data of the product from the above reaction, it was clear that compound **68** was not what was produced. Two peaks corresponding to the alkyl single C-H proton at the branched chain of the 2-ethylhexyl group were present and the integration of all alkyl signals corresponded to two of the 2-ethylhexyl groups being present (see Appendix 1). This led to the identification of compound **69** (Scheme 5), which was further confirmed by mass spectrometry. This was the only product from the reaction along with recovered starting material **58** while none of the expected compound **68** was isolated.

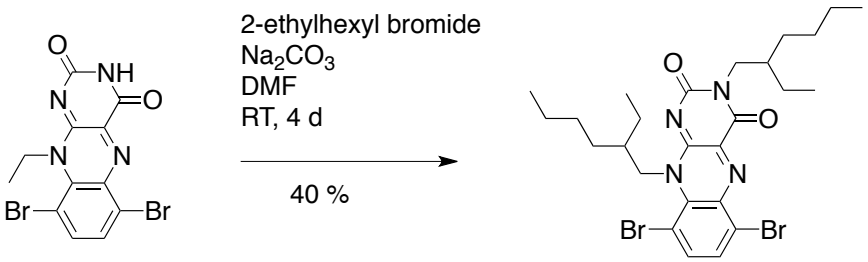

(58) (69)

Scheme 5 Result of the alkylation with 2-ethylhexyl bromide

Although it was an unexpected product, having the 2-ethylhexyl in both the N3 and N10 position actually worked in favour of what was to be achieved, which was increased solubility of the flavin unit. This product was then taken forward and polymerised with a fluorene moiety, to be discussed later. However, due to the interesting results from this reaction, this was investigated further. Initial thoughts were that the alkylation had been left for too long. Therefore the alkylation was attempted again leaving the reaction to stir for 2 days instead of 4 days, in an attempt to prevent the substitution of the ethyl chain. However, as shown in Scheme 6, this resulted in the substitution of the N10 ethyl group by the 2-ethylhexyl group, while the N3 position remained un-substituted giving compound **70**, with trace amounts of the di-2-ethylhexyl flavin **69** as well as recovered starting material **58**.

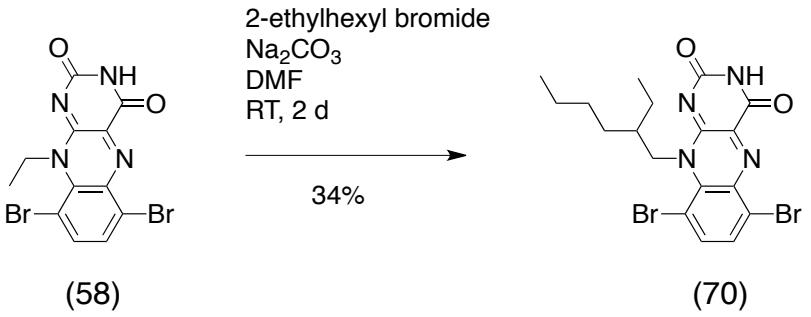

Scheme 6 Synthesis of compound 70 via a 2 day alkylation reaction

The substitution at the N10 position could be the result of deprotonation of the ethyl group by the base, resulting in the loss of one molecule of ethene and producing the N^- ion **58a** which would then undergo S_N^2 substitution with 2-ethylhexyl bromide as shown in Scheme 7.

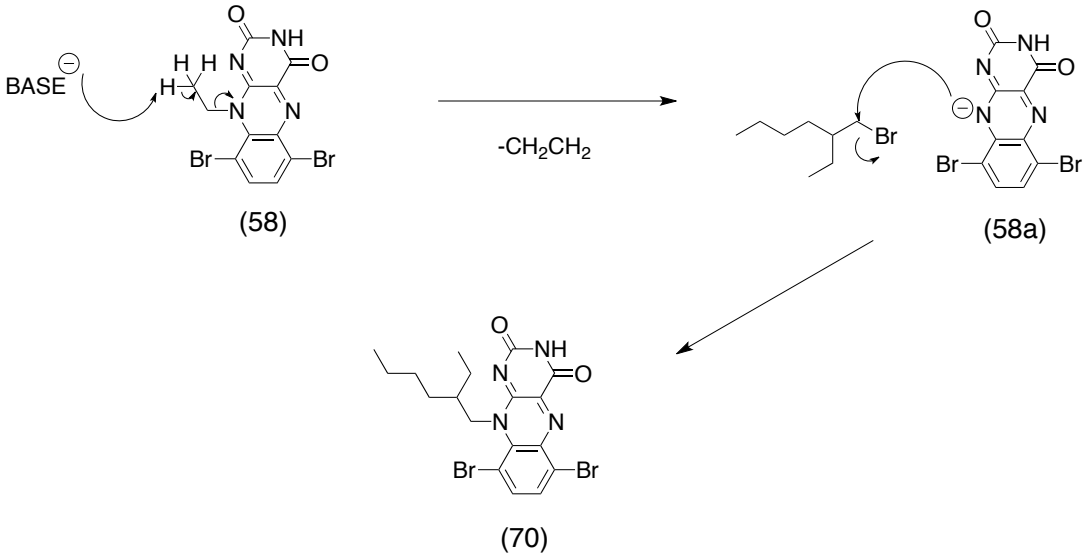

Scheme 7 Proposed mechanism for the displacement of the ethyl group

The synthesis of the flavin was then repeated to incorporate a methyl group rather than an ethyl group to avoid the loss of ethene and promote the desired N3 substitution. The initial steps remained the same and the alkylation of **62** occurred using methyl triflate rather than the ethyl triflate, giving compound **71**. Following the final reaction with alloxan monohydrate, the final flavin **72** with N10-methyl group was isolated in high yield (Scheme 8)

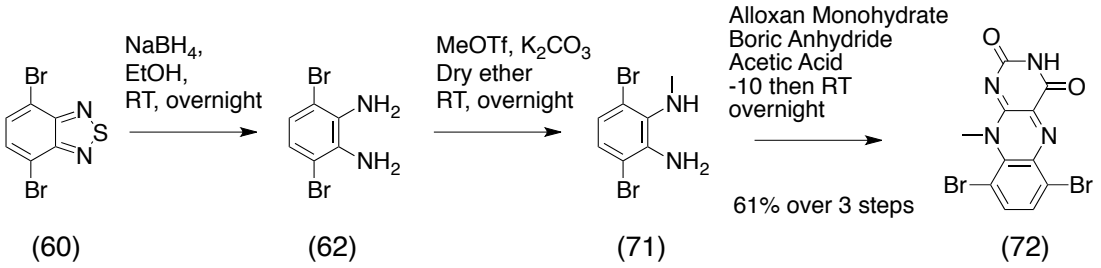

Scheme 8 Synthesis of the N10-methyl flavin

The N10-methyl flavin **72** was then carried forward to the alkylation with 2-ethylhexyl. However, as shown in Scheme 9, the same N10 substitution (compound **69**) was observed. Therefore the first proposal of this substitution resulting from a loss of ethene cannot be correct.

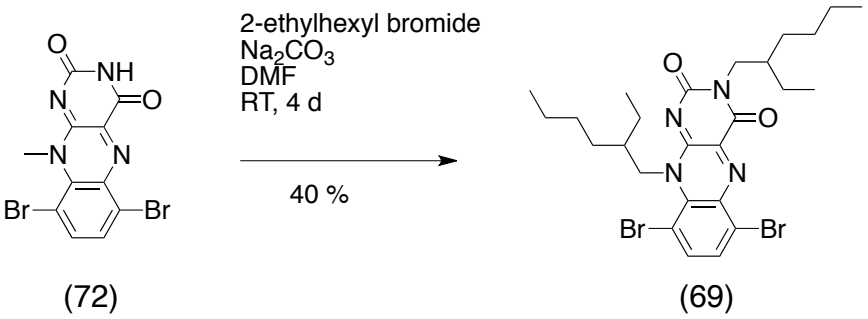

Scheme 9 Actual result from the alkylation with 2-ethylhexyl bromide

Previous attempts at changing the duration of the reaction and changing the alkyl group on the flavin proved to have no effect on whether this replacement was taking place. Therefore, to investigate this further, two further alkylations were carried out using different alkyl groups. In one reaction there was a decrease in the sterics by removing the branched ethyl group and using just hexyl bromide. The second reaction increased the sterics with a benzyl group. The results of these two reactions showed the same substitution that was observed with the 2-ethylhexyl and afforded compound **73** and **74** respectively (Scheme 10).

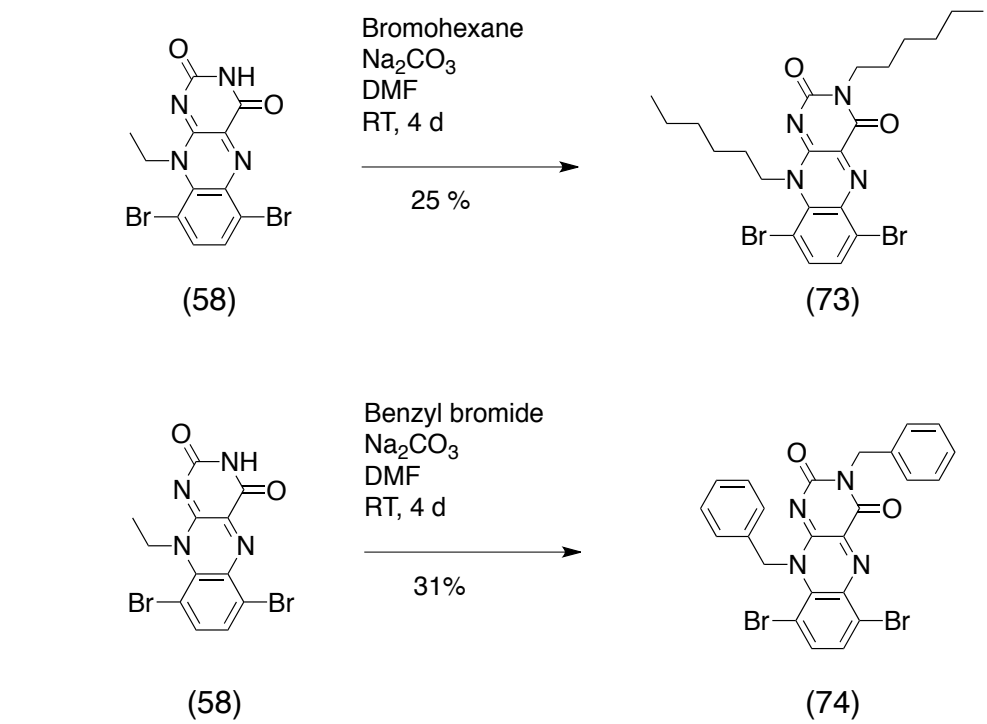

Scheme 10 Methodology using differing alkyl groups

Upon review of the results and the reagents involved in the reaction, a new mechanism was proposed. A nucleophilic substitution could occur at the N10 position breaking the carbon-nitrogen bond (Scheme 11) and pushing the electrons through the system up to the oxygen **58b**.

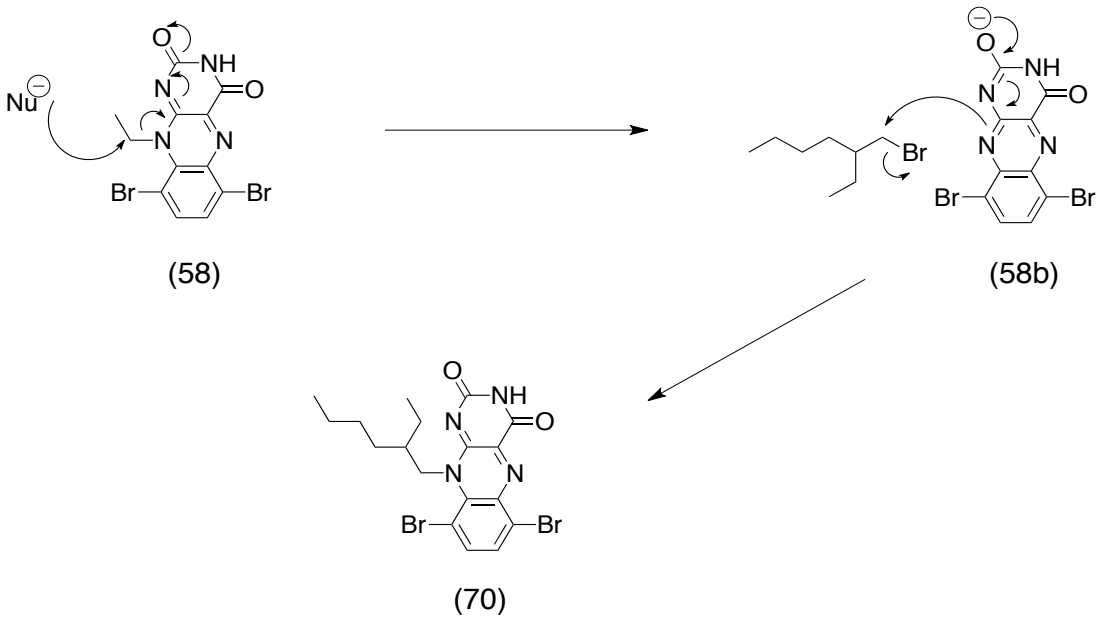

Scheme 11 Second proposed mechanism explaining the replacement of the N10-alkyl group

As a comparison, the N10-methyl flavin **72** was alkylated with another methyl group in order to give a good comparison for the polymerisations due to the shorter chain with the methyl group and the differing solubilities associated with the compounds. Thus, the N10-methyl flavin **72** was alkylated using iodomethane to give compound **75** (Scheme 12). It was anticipated that, with the introduction of the same alkyl group the yield for this reaction would be a lot higher than had been observed for the previous alkylations described earlier. However, the yield was only 30% and thin layer chromatography showed that another compound was present. ^{1}H NMR of both compounds proved to be almost identical, however, on close examination it was observed that the N-CH_3 peaks were seen at different chemical shifts for the two products. Integration of these peaks showed that in both cases these peaks equated to a CH_3 unit and mass spectrometry confirmed that the mass of the two products obtained was identical. To investigate this further, X-ray crystallography was performed.[60] The X-ray structures produced can be seen in Figure 49 and showed that the second product was an N1, N3-methylated flavin **76**, also shown in Scheme 12, which was obtained with a yield of 30%. This methyl migration provided further evidence for the proposed mechanism in Scheme 11. X-ray crystallography also showed how the molecules interact through π- π interactions (Figure 50).

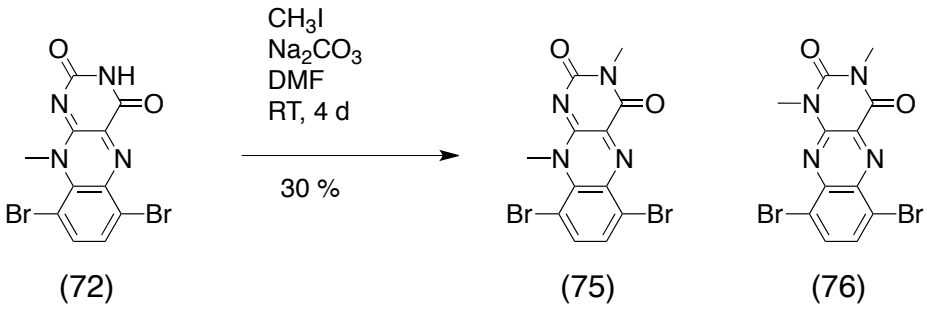

Scheme 12 Methylation of 72

Figure 49 X-ray structures of the two products 75 (right) and 76 (left) obtained from the methylation of 72

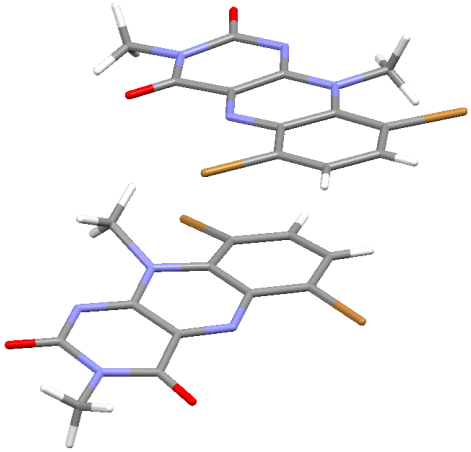

Figure 50 X-ray structure showing the π- π stacking in molecule 75

The final stage of this project was to perform the polymerisation, using a fluorene compound as the co-monomer. This was done using Suzuki conditions. Di-2-ethylhexyl flavin **69** and fluorene boronic ester **77** were dissolved in toluene with aqueous potassium carbonate and placed in darkness. $Pd(PPh_3)_4$ was then added and the solution degassed before heating under reflux and stirring for 48 hours. After this, an end-capping procedure was performed upon the addition of the phenyl boronic acid, subsequent stirring for 12 hours followed by the addition of the bromobenzene and a further 12 hours of stirring to produce polymer **78** (Scheme 13). The GPC data showed a non-homogeneous polymer in terms of molecular weight (Figure 51).

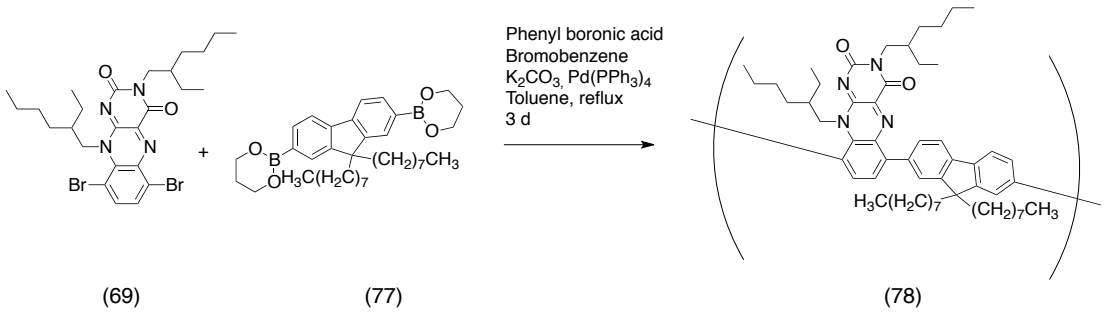

(69) (77) (78)

Scheme 13 Polymerisation of 69 using Suzuki conditions

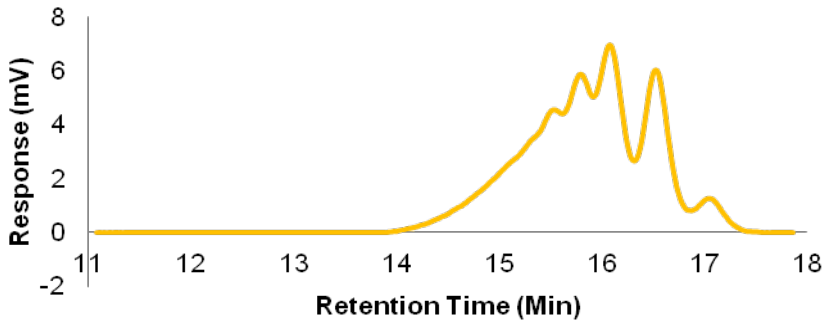

Figure 51 GPC data for the polymerisation of flavin 69 and fluorene 77

Due to producing the non-homogeneous polymer shown above, a second polymerisation was performed. The reaction was performed using the same general conditions with the exception of the end-capping procedure. After 48 hours, the first end-capping group was added and the reaction stirred for one hour before the second end-capping group was added and the reaction stirred overnight. This resulted in a slight improvement in the number of peaks seen on the GPC, however, a non-homogenous polymer was produced.

Due to the successful synthesis of a polymer using di-2-ethyl hexyl flavin **69**, the same polymerisation method was used with dimethyl flavin **75**. Dimethyl flavin **75** and fluorene boronic ester **77** were dissolved in toluene with aqueous potassium carbonate and placed in darkness. The $Pd(PPh_3)_4$ was then added and the solution degassed before heating under reflux and stirring for 48 hours. After 48 hours an end-capping procedure took place. This involved the addition of the phenyl boronic acid

(stirring for 12 hours) and then the addition of the bromobenzene (stirring for 12 hours) producing the polymer **79** (Scheme 14). The GPC results, however, showed that the polymerisation had not occurred and instead indicated that the reaction had instead produced oligomers. This is most likely due to the solubility issues associated with the dimethyl flavin **75** as it was observed during the reaction that the flavin would precipitate out of solution during the reaction.

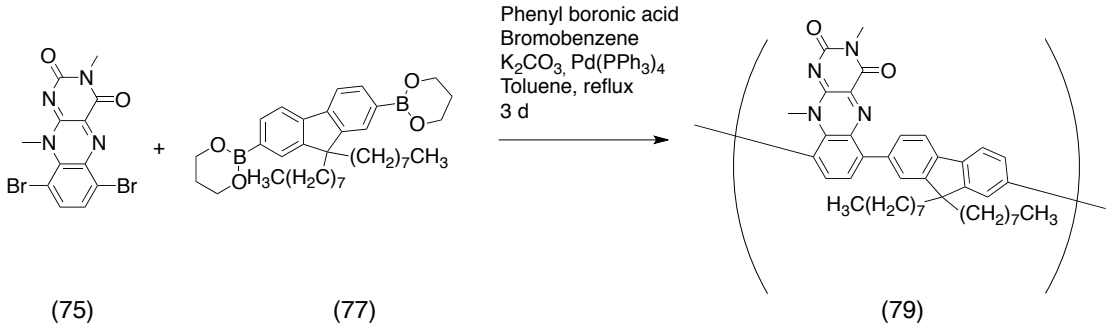

Scheme 14 Polymerisation attempt using flavin 75

Further investigations were also carried out into the alkyl replacement reaction to see if the same result would take place when the bromine atoms at positions C(6) and C(9) were replaced with thiophenes. The optimised synthetic strategy again started with the Stille coupling with 4,7-dibromo-2,1,3-benzothiadiazole **60** to give **61**. The reduction was then performed using sodium borohydride and cobalt chloride, taking only 2 hours for completion, giving compound **62**. The ethylation was then performed using the same conditions seen for the dibromo compound **65**, which gave compound **64**, followed by a reaction with the alloxan monohydrate giving flavin **57** in reasonable yield over the 3 steps.

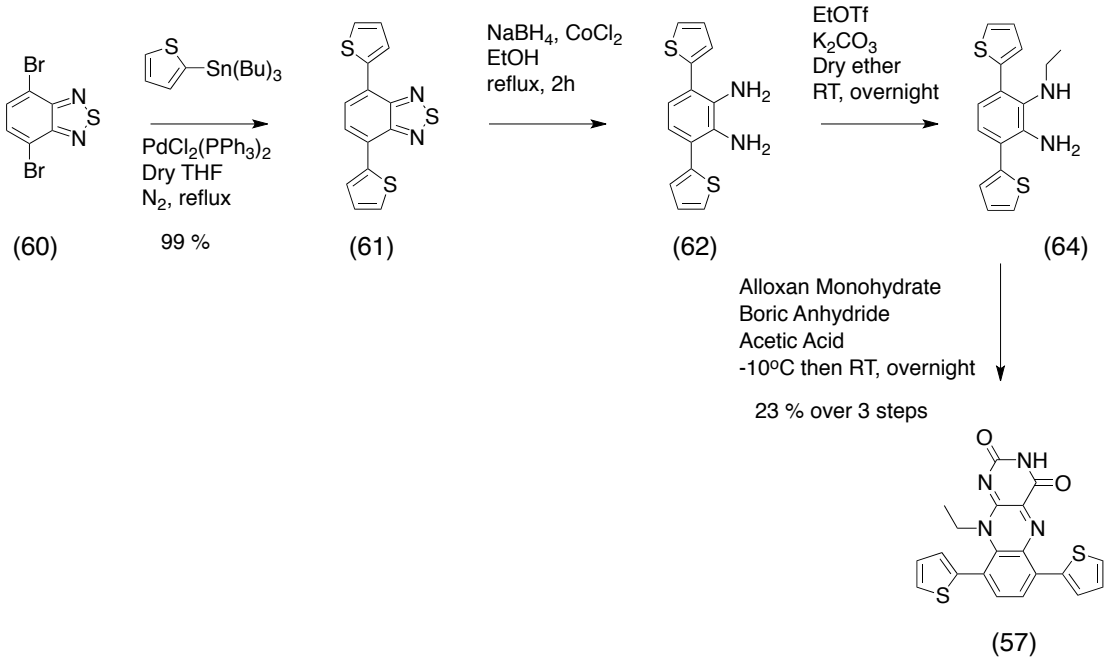

Scheme 15 Optimised synthetic route for the synthesis of 57

Following the synthesis of the core flavin **57** the next stage was to investigate the alkylation reaction to determine whether there would be a replacement of the ethyl group as seen with the dibromo compound **58**. The first reaction was to use iodoheptane, which had been used previously with this compound producing a poor yield of compound **67**. The reaction was performed using the conditions used with the dibromo flavin **58**. Compound **57** was dissolved in dry DMF with sodium carbonate. Iodoheptane was then added and the reaction stirred at room temperature for 4 days. The result was very interesting. As observed with the dibromoflavin **58** the replacement of the ethyl did occur producing compound **80** in a 30 % yield (Scheme 16).

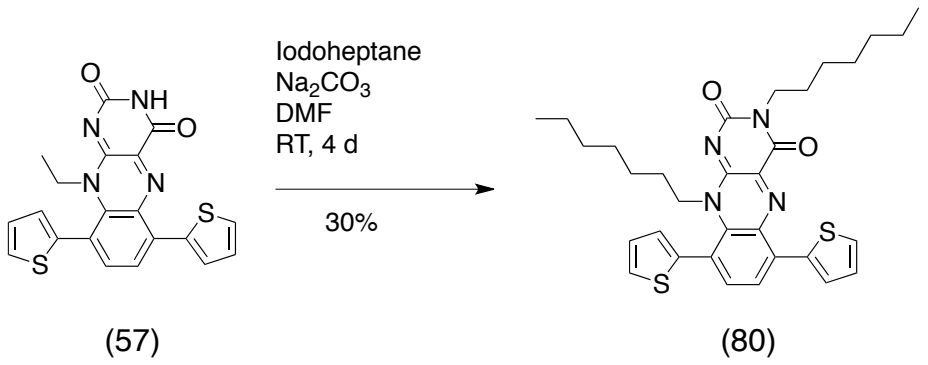

Scheme 16 Alkylation of 57

However, in this instance trace amounts of the desired product were also observed. This indicated that perhaps thiophenes play a steric role in controlling product formation. This theory was investigated by repeating the reaction with 2-ethyl hexyl bromide. The reaction was performed using the same conditions as previously shown (Scheme 17). Spectroscopy again confirmed that there was substitution of the ethyl group by the di-2-ethyl hexyl group and flavin **81** was produced in a slightly lower yield. Thus, the steric size of the thiophene groups, does not significantly hinder the displacement reaction and just reduce the yield slightly.

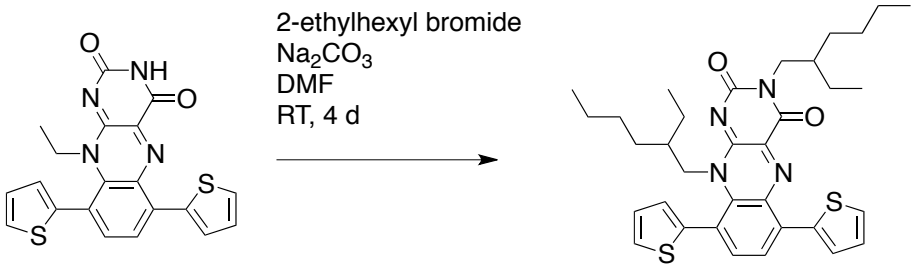

(57) (81)

Scheme 17 Alkylation of 57

2.3.2 Analysis

2.3.2.1 UV/Vis and Fluorescence Spectroscopy

UV/Vis spectroscopy and fluorescence spectroscopy was performed on polymer **78**. The UV/Vis spectrum shows a λ_{max} at 328 nm and a broad absorbance at 453 nm (Figure 52) presumably due to an intramolecular charge transfer interaction (Figure 53). This broad absorbance at 453 nm was used as the excitation wavelength for the fluorescence spectroscopy. The emission spectrum for the polymer **78** shows that it is a highly fluorescent polymer with an emission peak seen at 566 nm when excited at 453 nm (Figure 54).

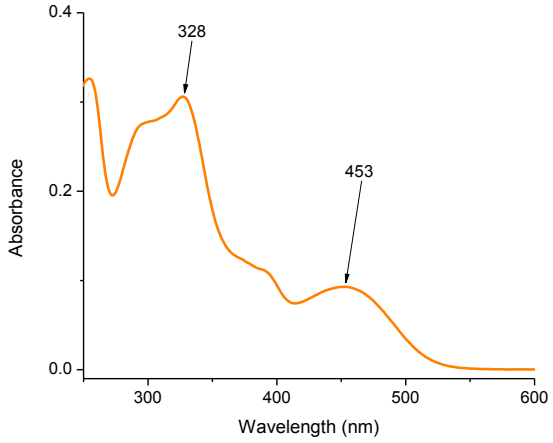

Figure 52 UV/Vis spectrum of polymer 78 recorded at a concentration of 1 x 10^{-5}M in CH_2Cl_2

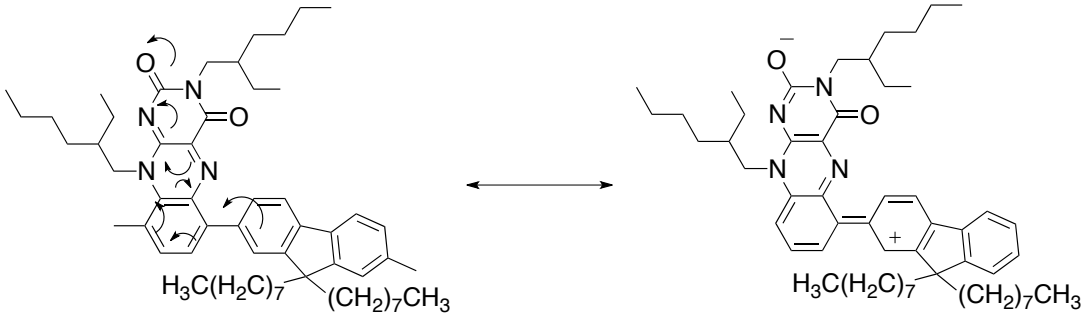

(78) (78)

Figure 53 Resonance structure for the intramolecular charge transfer in polymer 78

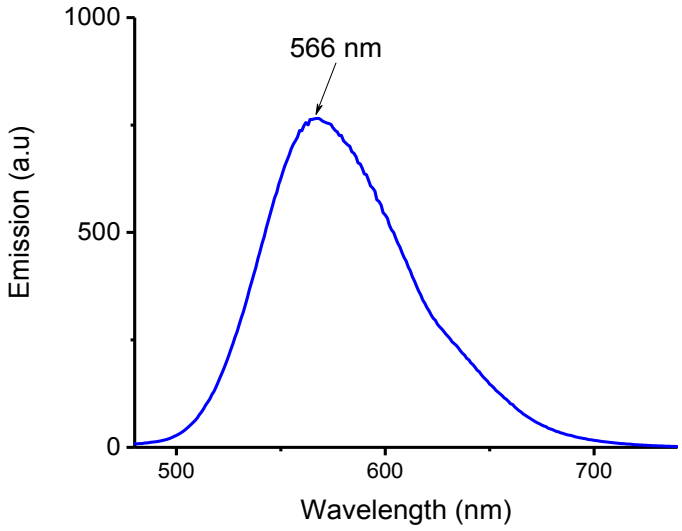

Figure 54 Emission spectrum of polymer 78 recorded at a concentration of 1 x 10^{-6}M in CH_2Cl_2 and excited at 453 nm

2.3.2.2 Cyclic Voltammetry (CV)

CV was performed at 10^{-4} M concentrations using 0.1M TBA.PF_6 as the electrolyte. The HOMO level energy for the 2-ethylhexyl flavin polymer **78** was calculated using the formula $-[4.8 - (E_{1/2})_{ox}]$[61] where $(E_{1/2})_{ox}$ is the onset of the oxidation wave seen for the compound and the LUMO level energy was calculated using the formula $-[4.8 - (E_{1/2})_{red}]$ where $(E_{1/2})_{red}$ is the onset of the reduction wave observed for the compound. The LUMO values calculated from CV data and UV data can be seen in table 2.

Table 2 Optical and electrochemical properties of polymer 78

Compound	$\ddot{e}_{max}$ (nm)	$E_{1/2}$ (eV)	E_{LUMO} (eV)	E_{HOMO} (eV)	E_g^{opt} (eV)[a]	E_g^{el} (eV)[b]
78	328	-2.34	-2.46	-	2.3	-

[a] determined from the onset of UV-vis absorption spectrum ($1240/\lambda_{abs}$)

[b] determined from cyclic voltammetry

2.4 Conclusions and Future Work

A series of flavins were successfully synthesised and a new optimised synthetic strategy devised for the synthesis of flavins **57** and **58**. Methodology of the alkylation indicated an interesting nucleophilic substitution reaction that had previously not been investigated. Another interesting discovery was that of the alkyl migration with the alkyl group appearing on the N1 position rather than the N3 position which had not previously been seen. This migration has not previously been reported and has also not been reported when positions C(7) and C(8) are functionalised[62] A flavin incorporating conjugated polymer **78** was also successfully synthesised using the 2-ethyl hexyl flavin **69** under Suzuki conditions. Attempts to synthesise a polymer using the same conditions and the dimethyl flavin **75** proved unsuccessful, most likely due to the low solubility of the flavin. The 2-ethyl hexyl flavin polymer **78** will be sent to Prof I. Samuel's group at the University of St Andrews for investigation into the photovoltaic properties of this polymer. Future work would be to optimise the conditions of the polymerisation and to synthesise a polymer using the dithiophene-functionalised flavins such as **73** in order to extend the conjugation of the system further.

3.0 Synthesis and characterisation of a series of rotaxanes

3.1 Rotaxanes incorporating donor and acceptor material

3.1.1 Introduction

3.1.1.1 Background

Rotaxanes are what are known as interlocked structures held together by mechanical bonds as opposed to the typical covalent bonds. The interactions that typically give rise to these interlocked structures are H-bonding, π-stacking and donor/acceptor interactions. Rotaxane comes from the latin word “rota” meaning wheel and “axis” meaning axle due to the distinctive shape (Figure 55) consisting of a ring threaded onto an axle and two bulky stopper groups attached at each end to keep the ring from slipping off.

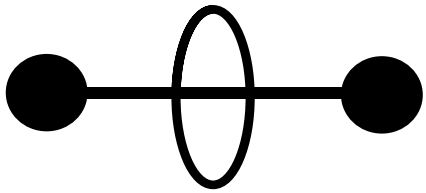

Figure 55 Schematic of a rotaxane

These types of molecules are rather complex and thus naming them can be complex. Each individual rotaxane is not only named chemically but is defined in terms of the number of rings involved to the one axle. For example, one ring gives rise to a [2]-rotaxane, two rings a [3]-rotaxane or where there are no stoppering groups, a pseudorotaxane is formed (Figure 56).

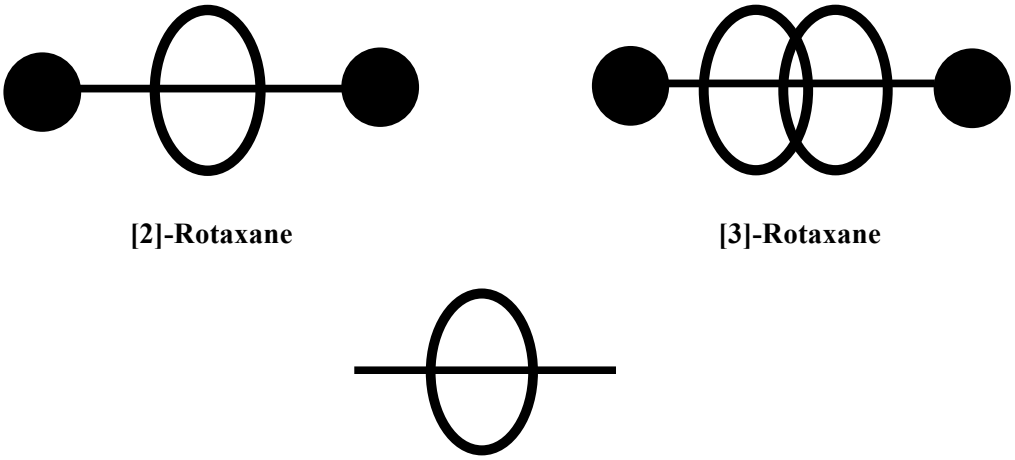

[2]-Rotaxane **[3]-Rotaxane**

Pseudorotaxane

Figure 56 Nomenclature for rotaxanes

The first reported synthesis of a rotaxane came in the 1960's by Schill and Zollenkopf[63] who reported the synthesis of **82** (Figure 57) and since then there have been a range of rotaxane molecules synthesised via a range of strategies. These strategies can be seen in Figure 58.

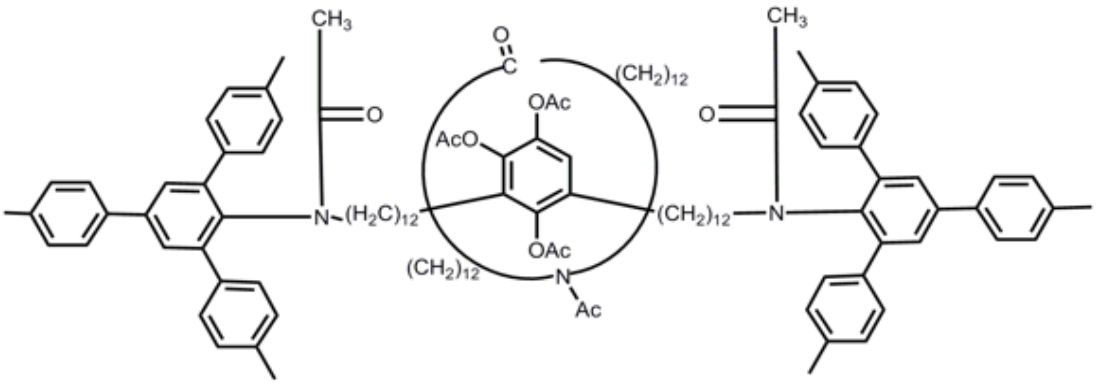

(82)

Figure 57 First synthesised rotaxane 82

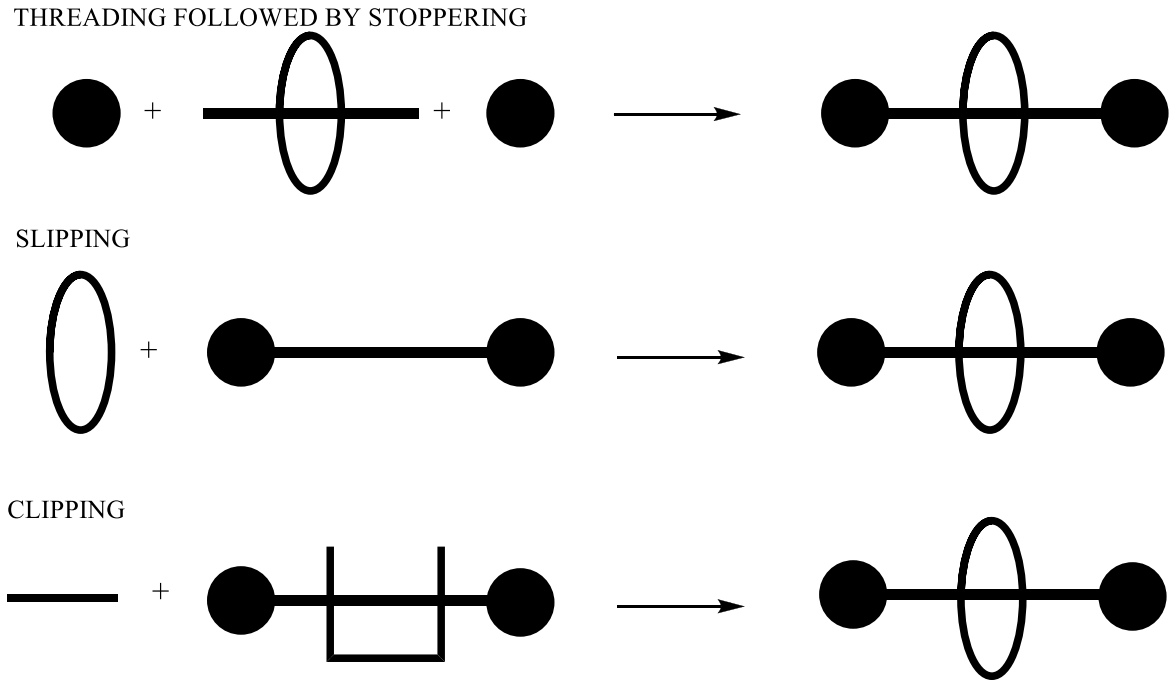

Figure 58 Cartoon representing the three strategies for the synthesis of rotaxanes

The least common method used for the synthesis of rotaxanes is the slipping reaction. Here the axle already has the bulky stopper groups and the ring system is slipped over the stoppers and interactions hold the ring in the place. Although classed as a slipping method, the method usually involves a cleavage and reforming of a bond for the slipping to occur. This methodology was utilised by Furusho et al[64] in the synthesis of their rotaxane **86** based on an ammonium salt axle **84** with a trityl thioether and a di-t-butylphenyl group as stoppers (Scheme 18). Here, they slip on the dibenzo-24-crown-8-ether **85** by utilising the reversible cleavage and reforming of the trityl thioether linkage.

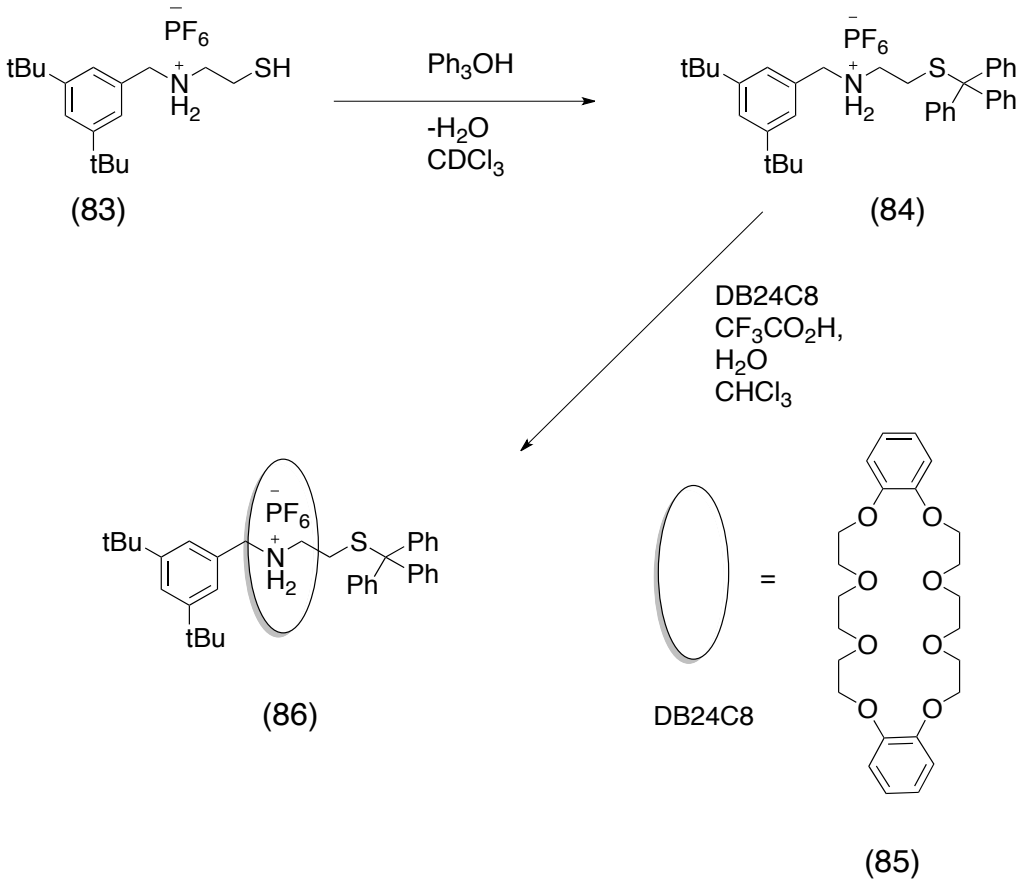

Scheme 18 Scheme showing and example of a slipping strategy for the synthesis of a rotaxane 86

One of the most common methods for the synthesis is the threading followed by stoppering approach. Here, the ring is threaded onto the axle and interactions between the axle and the ring hold the ring in place, giving a pseudorotaxane structure. The final step is to add two bulky stopper groups to give the rotaxane. This method was used by Stoddart et al.[65] Here, they used a naphthalene triethylene glycol with an azide unit as the axle **87** and threaded the ring cyclobis (paraquat-*p*-phenylene) (CBPQT) **88**. π–interactions between the benzene rings hold the ring in place **89**. Finally, stopper groups **90** are added using a click reaction, specifically, the azide-alkyne Huisgen cycloaddition, which involves the reaction of an azide and an alkyne to give a triazole unit in the final rotaxane **91** (Scheme 19)

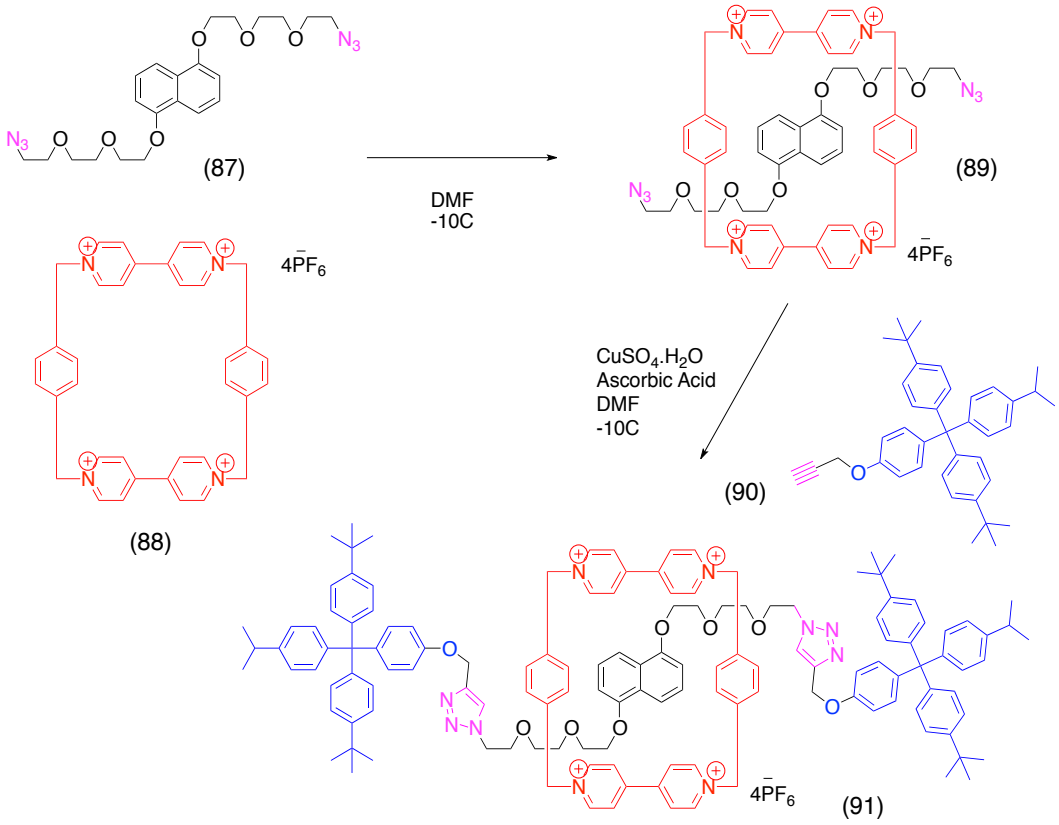

Scheme 19 Scheme showing the threading followed by stoppering strategy to give rotaxane 91

However, by far the most common strategy for the synthesis of rotaxanes is the clipping reaction. In this reaction the axle and stoppers are formed and the ring system is clipped around the axle. Stoddart et al[66] used the clipping reaction in the formation of a [2] rotaxane **95** (Scheme 20). In this synthesis, the axle **94** is mixed with a half unit of CBPQT **92** and bis-(bromomethyl) benzene **93** which clips together around the axle to give the [2] rotaxane **95**.

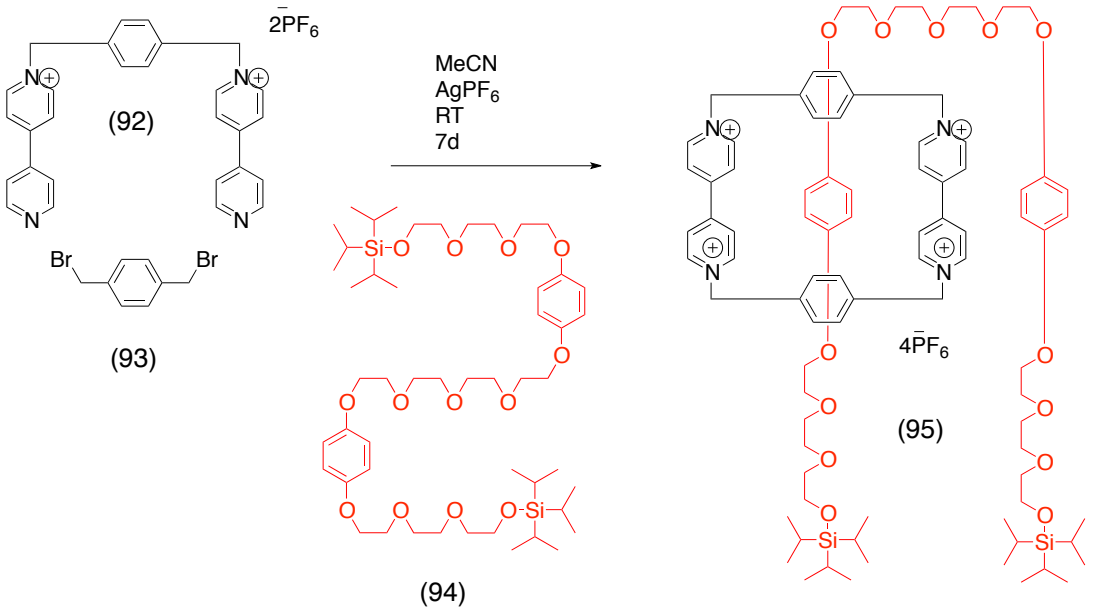

Scheme 20 Scheme showing an example of the clipping strategy for the synthesis of rotaxane 95

3.1.1.2 Applications

These compounds have attracted a lot of interest for use in molecular devices and machines due to the motion around the rings and the axis.[67] A device is defined as something invented or constructed for a specific purpose and a machine is any combination of mechanisms for utilising, modifying, applying or transmitting energy, whether simple or complex.[68]At the molecular level, devices and machines are usually multi-component systems in which the components can be linked by chemical bonds of various nature.[69]

Rotaxanes have been used in many different molecular devices, both at the chemical and electrochemical level, and also in biological purposes. Cacialli et al showed that cyclodextrin threaded conjugated polyrotaxanes can be used as molecular wires (Figure 59). They demonstrated that the use of polyrotaxane architectures offered better control over the design compared with the polymer substituents. They threaded the luminescent conjugated cores into non-conjugated isolated rings resulting in insulated molecular wires that displayed basic semiconducting and optical properties that could be used as molecular materials. Such materials included LED and more generally nanoscience and nanotechnology.[70]

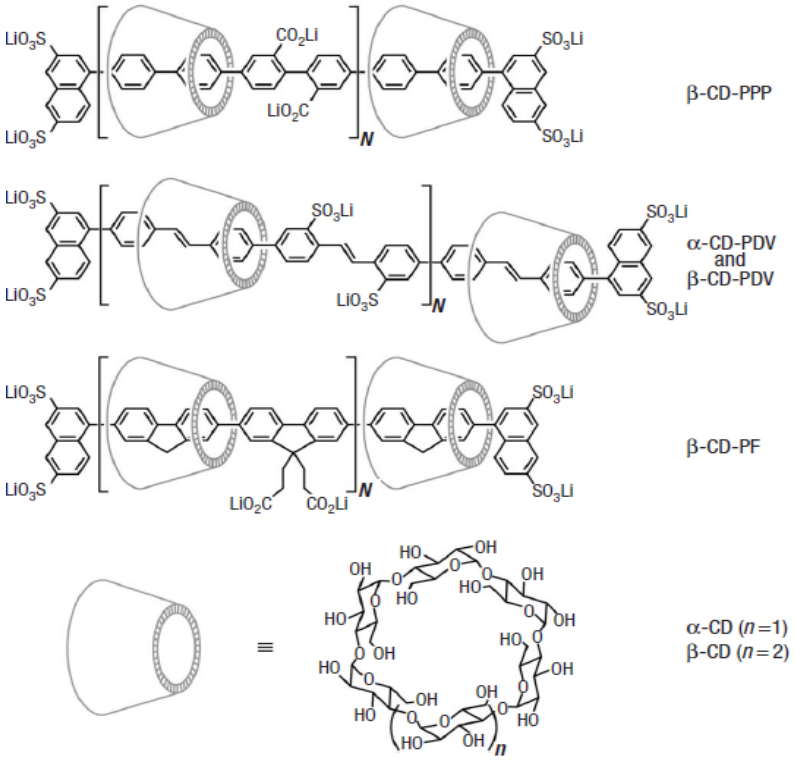

Figure 59 Example of polyrotaxanes used as molecular wires[69]

Stoddart demonstrated with the rotaxane seen previously in Scheme 20 that rotaxanes can be used as molecular shuttles. Using ^{1}H NMR they showed that the tetracationic ring moves back and forth between the two hydroquinol stations.[66] Bissell et al realised that nanoscale switching devices could have great implications in computing and biomimetic engineering.[71] They demonstrated the ability to synthesise a rotaxane **96** that could be used as a chemically and electrochemically reversible switch as seen in Figure 60.

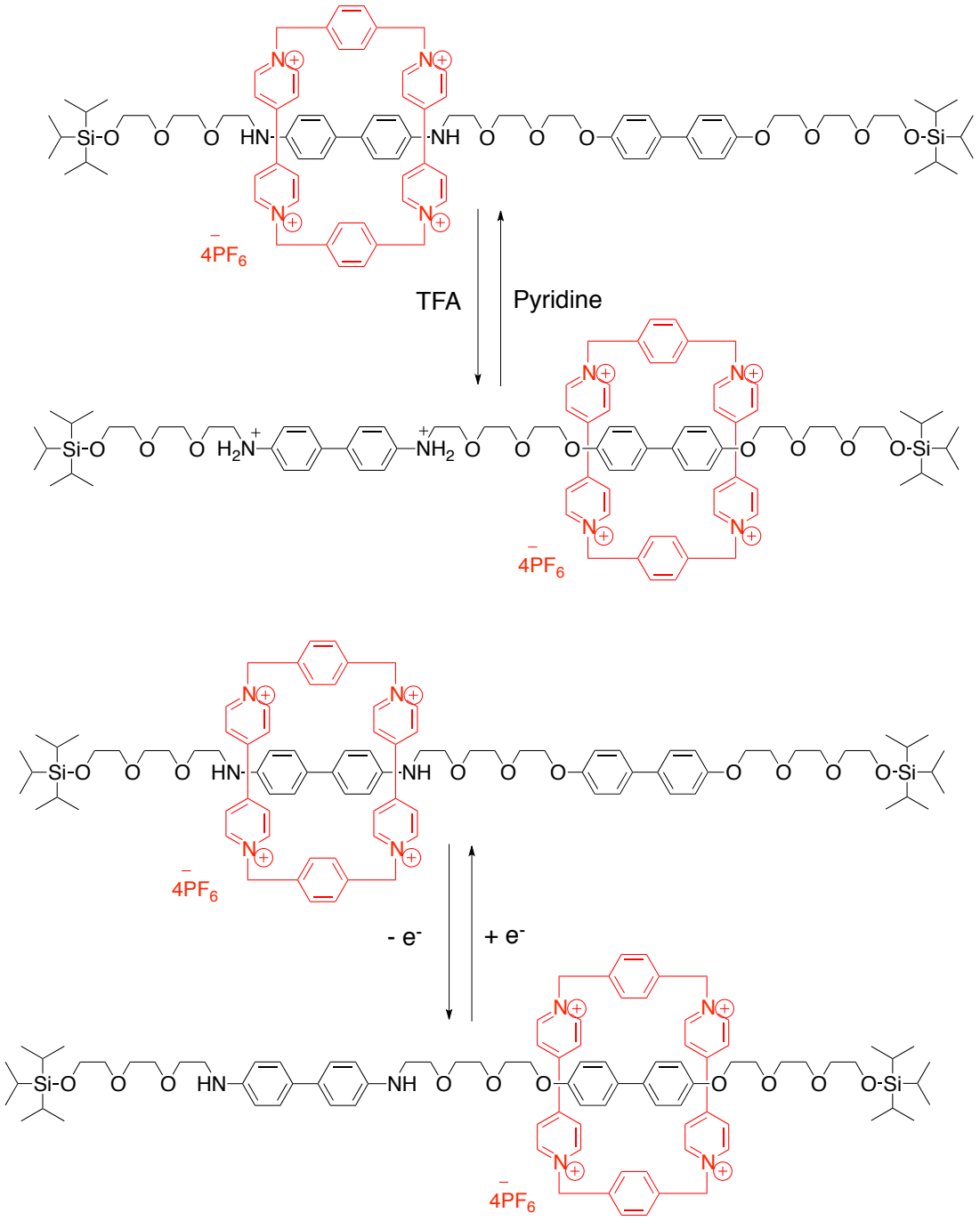

(96)

Figure 60 Chemically and electrochemically reversible molecular switch 96

Figure 61 shows a [2]-rotaxane incorporating a tetrathiafulvalene and a dioxynaphthalene **97**. Here it was shown that the interactions between the cationic CBPQT ring and the counter ion such as PF_6^- **98** and $TRISPHAT^-$ **99** have a great impact on the shuttling properties of the molecule. This exchange between the two isomers can be seen by the naked eye through a colour change between red and green.[72]

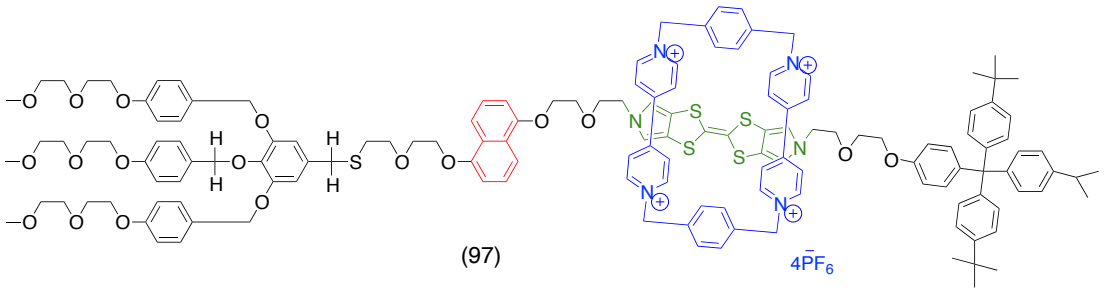

(97)

$4PF_6^-$

COUNTERIONS =

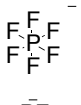

PF_6^-

(98)

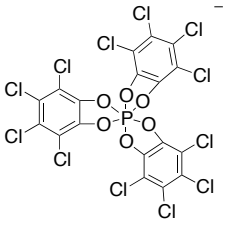

TRISPHAT $^-$

(99)

Figure 61 A molecular switch 97 with counter ions 98 and 99

It has been greatly demonstrated that these structures can be used as molecular shuttles with the ring moving back and forth along the axle. This motion can be taken further, as demonstrated by Bajić et al where they describe a two component molecular machine that behaves as a nanometre scale elevator.[73] The structure seen in Figure 62 comprised of a platform made up of three macrocycles fused to a central core with three legs that each contain two stations where the macrocycles can move between acting as an elevator.

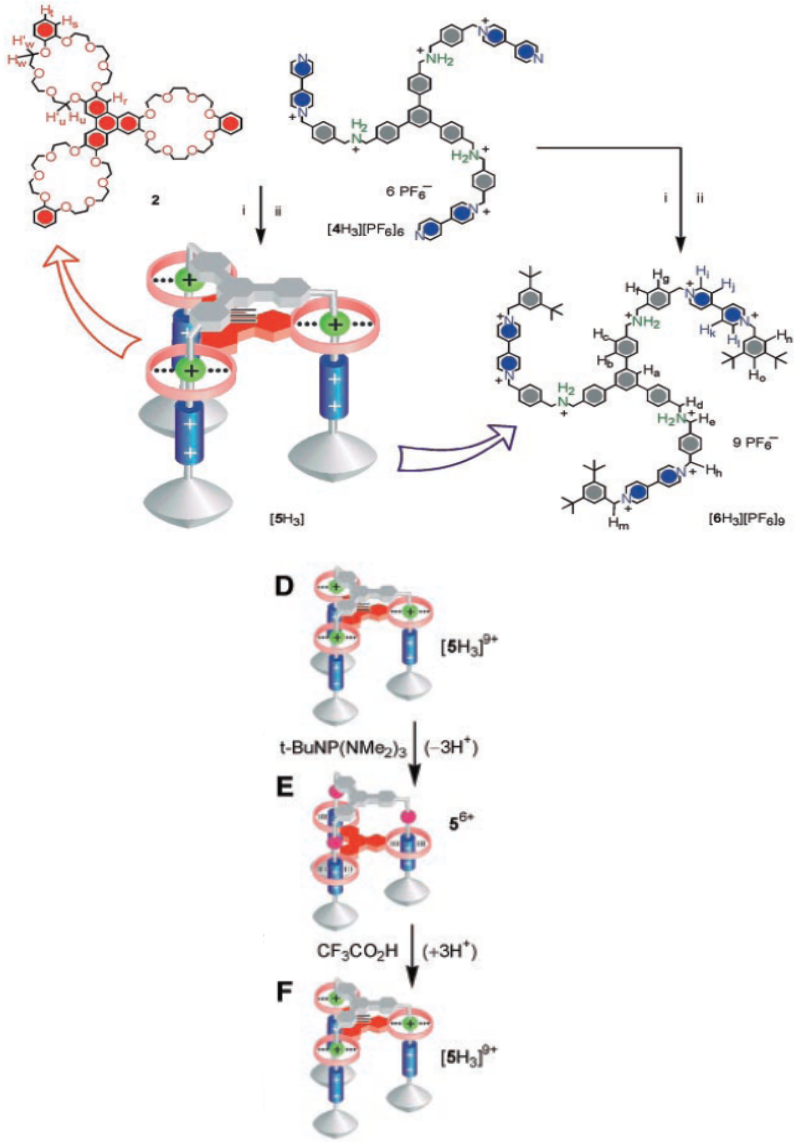

Figure 62 Nanoscale molecular elevator[72]

Not only are molecular machines and devices important in electronics and engineering, it has been shown that they play an essential role in biology. Collins et al showed that the shuttle ability of rotaxanes can be used to mimic the stretching and contraction ability of muscles. Figure 63 shows a schematic representation of a rotaxane that mimics the action of muscles by changing the coordinating metal.[74]

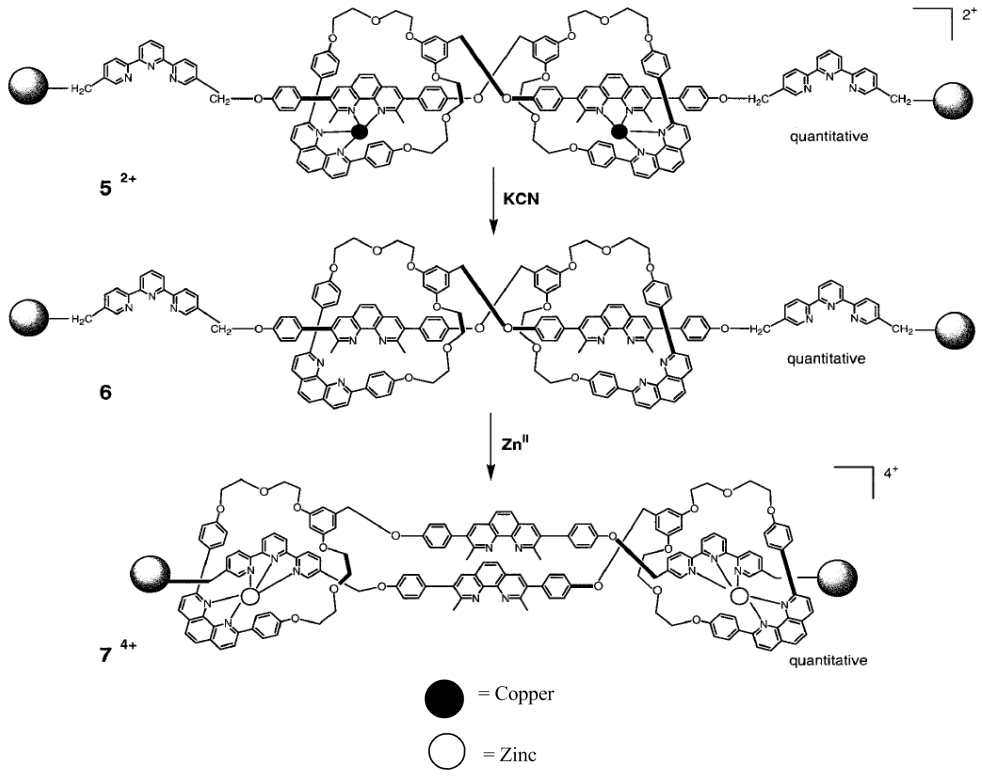

Figure 63 Rotaxane mimicking the actions of a muscle[74]

By tuning the components of the molecules, rotaxanes have been shown to be able to be used as molecular machines and as devices such as LEDs in electronics. This knowledge was the basis of the attraction of these molecules during my research into organic materials for photovoltaics. If by changing the functionality of these structures they can be used in a variety of applications, it could be possible to tune them towards use in a range of devices including photovoltaics and OFETs.

3.1.2 Project outline

Current organic photovoltaics use a bulk heterojunction of a blend of acceptor and donor material. These compounds are currently two separate molecules. The aim of this project was to synthesise a series of rotaxanes incorporating both donor and acceptor material creating a single molecular structure that can be used without requiring a second compound. CBPQT is well known for its acceptor ability thus the synthetic strategy was to use this as the ring structure and alter the donor groups within the axle.

The synthetic strategy for the synthesis of the rotaxanes was devised using the retrosynthetic analysis in Scheme 21. Using the most common method of synthesis, the clipping reaction, the rotaxane could be synthesised from an axle structure **102a**

with stopper groups attached, labelled X in the Scheme, and a CBPQT half unit **92**. This half unit could be synthesised from the 4,4'-bipyridine **100**. The axle could be taken back to the naphthalene core **102**, which in turn could be synthesised from the naphthalene diol **101**.

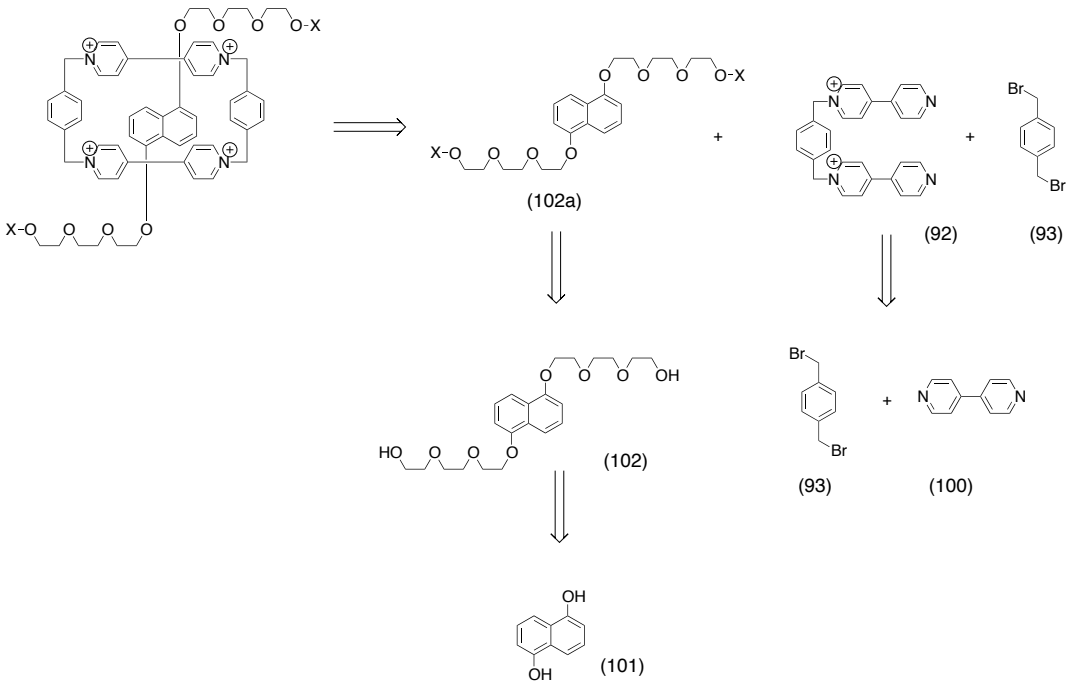

Scheme 21 Retrosynthetic analysis for the synthesis of rotaxanes

The structures of the target compounds can be seen in Figure 64, compound **103** incorporates a triisopropyl silyl stopper group. This is an established rotaxane synthesised previously by Stoddart.[75] This rotaxane has only the acceptor moiety in the CBPQT **88** with no donor ability in the core axle **109**, thus this would be used as a control compound for comparison. The idea of using this as a control was to check that any activity would be due to the interaction between donor and acceptor. Targets **104** and **105** have included a donor moiety in the axle in order to establish if these structures could act as a donor-acceptor single molecule with interaction occurring between the donor groups and the acceptor ring structure. The idea was that this interaction could give rise to intrinsic photovoltaic properties thus negating the need to blend with a second molecule. As carbazole and thiophene molecules are established donor structures, these were chosen to be used in the stopper groups.

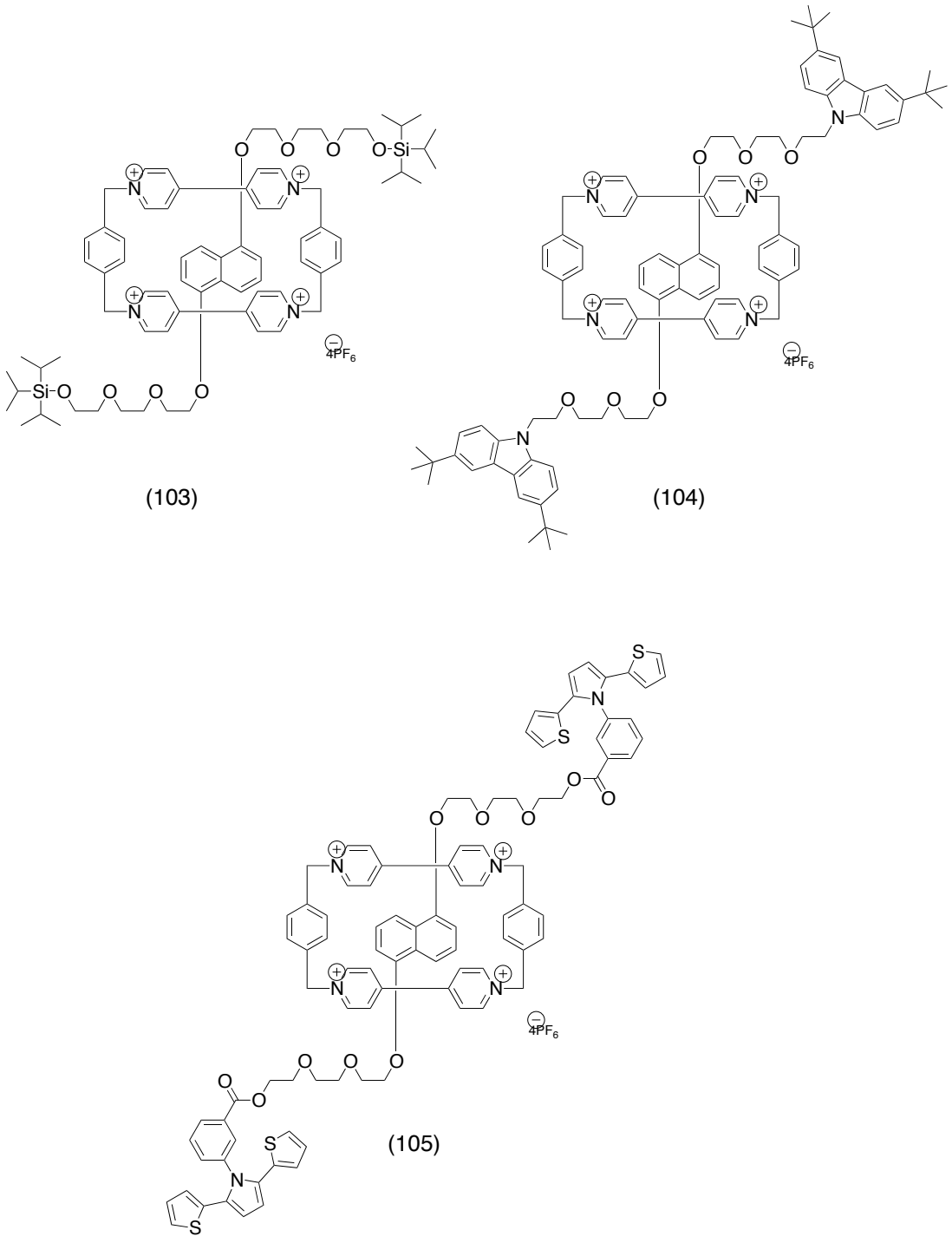

Figure 64 Target structures 103, 104 and 105

3.2 Results and Discussion

Due to the use of CBPQT **88**, a tetracationic ammonium salt, a test reaction was performed using a closely related structure, dibenzyl viologen **106**. Viologens are formed from the diquaternizing of 4,4'-bipyridine to form 1,1'-disubstituent-4,4'-bipyridinium salts (Scheme 22).[76] The name viologen came from Michaelis[77] who

noted the violet colour formed when 1,1'-dimethyl-4,4'-bipyridilium underwent a one electron reduction. Viologens are synthesised by an S_N^2reaction of 4,4'-bipyridine **100** with an R-X compound to give the viologen **100a**.

Scheme 22 General Scheme for synthesis of a viologen

Dibenzyl viologen **106** had previously been synthesised by Kamogawa and Suzuki in 1987.[78] The synthesis involved the reaction of 4,4'-bipyridine **100** with two equivalents of benzyl bromide **93** heated to reflux in dry acetonitrile. The reaction was complete after 6 hours when the compound was observed as a yellow precipitate, which was obtained in good yield (Scheme 23). The reaction was performed several times, all achieving good yields.

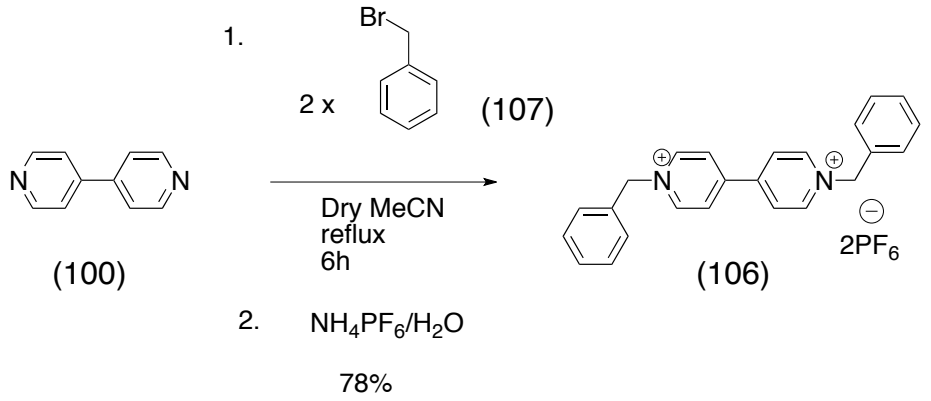

Scheme 23 Synthesis of 106

3.2.1 Synthesis of naphthalene core 102 and half unit 92

The naphthalene core was synthesised according to a procedure by M. J. Gunter and co-workers.[79] This involved the reaction of 1,5-dihydroxynaphthalene **101** with 2-(2'-(2''-chloroethoxy) ethoxy)-ethanol **108** in dry acetonitrile with potassium carbonate. The reaction was heated to reflux and stirred for 7 days producing the product **102** in good yield, on a large scale (10 g) (Scheme 24). This naphthalene core **102** was used in each of the subsequent axles.

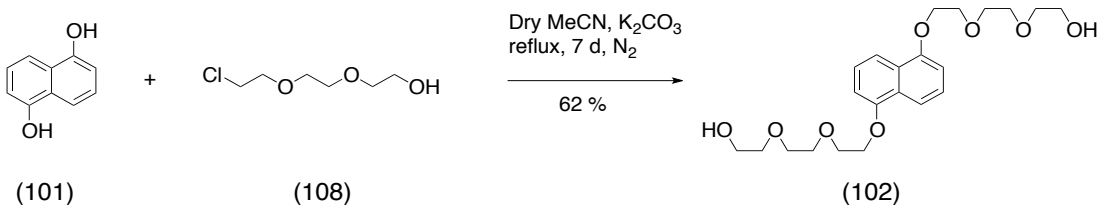

(101) (108) (102)

Scheme 24 Synthesis of naphthalene core 102

Another key feature of the rotaxanes is the CBPQT ring structure **100**. This is incorporated into the structure via a clipping reaction, which will be detailed later. The half unit, 1,1''-1,4-phenylene-bis(methylene) bis-4,4'-bipyridinium **92**, was synthesised by reacting two equivalents of 4,4'-bipyridine **100** with 1,4-bis-bromomethylbenzene **93** in dry acetonitrile, at reflux, overnight.[80] This was followed by conversion to the PF_6 salt, giving the compound in very high yield (Scheme 25). Compound **92** will be used in each rotaxane reaction.

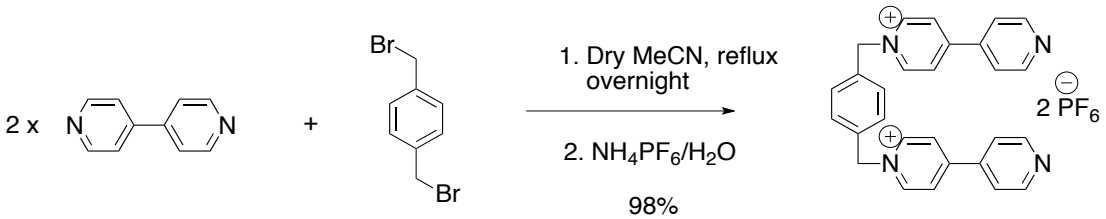

(100) (93) (92)

Scheme 25 Synthesis of 92

3.2.2 Synthesis of rotaxane control compound

The first target in the series was to synthesise a rotaxane with triisopropyl stopper groups, previously synthesised by Stoddart.[74] The first step was to synthesise the axle **109**. This involved reacting compound **102** with two equivalents of triisopropyl triflate in dry CH_2Cl_2 and 2,6-lutidine. This reaction was carried out at room temperature for 1 hour producing the axle **109** in high yield (Scheme 26).

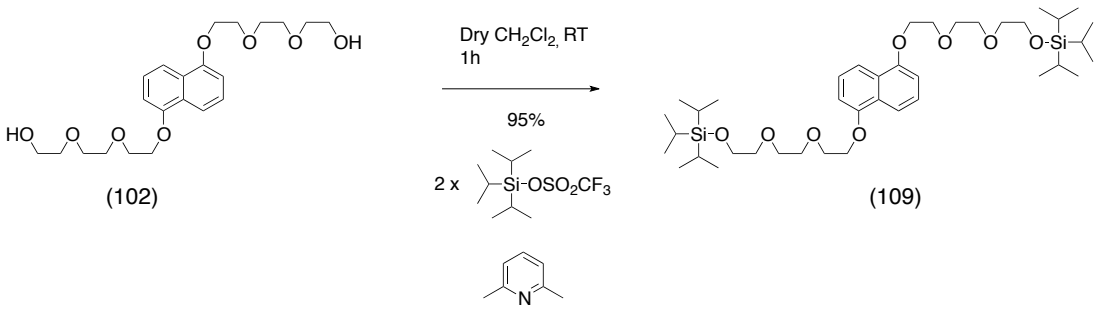

Scheme 26 Synthesis of axle 109

Synthesis of the rotaxane was performed using a "clipping" reaction methodology outlined by Stoddart.[74] Compound **109** was stirred in dry acetonitrile with **92** and **93** at room temperature for 3 weeks. This produced the final rotaxane **103** in an 11 % yield (Scheme 27).

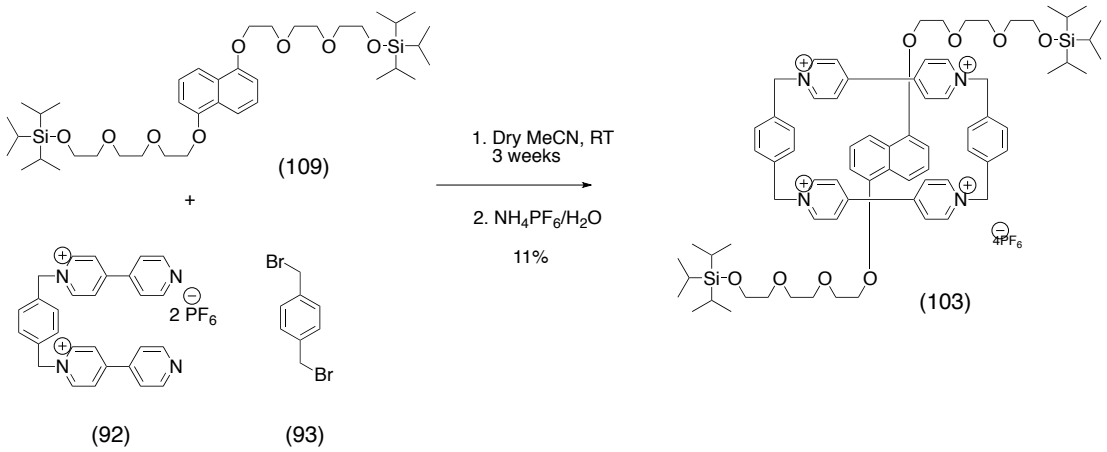

Scheme 27 Synthesis of rotaxane 103

3.2.3 Synthesis of donor and acceptor incorporating rotaxanes

The synthesis of the donor-incorporating axle started with the conversion of compound **102** ıinto 1,5-bis(2-(2-(2-bromoethoxy)ethoxy)ethoxy)naphthalene **110** by reacting it with carbon tetrabromide in dry acetonitrile with triphenyl phosphine. The reaction took 24 hours at room temperature and gave a 67% yield of the desired compound **110** (Scheme 28).

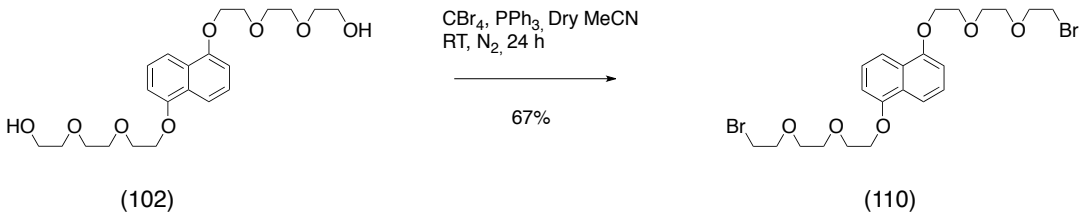

(102) (110)

Scheme 28 Synthesis of 110

The second step of the synthesis was to synthesise the donor stopper groups. This was done by reacting carbazole **111** with *tert*-butyl chloride in CH_2Cl_2 with aluminium chloride as catalyst.[81] The reaction occurred over 24 hours at room temperature and produced the compound **112** in a moderate yield, 41% (Scheme 29).

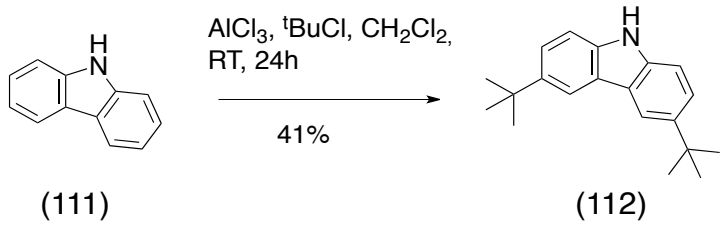

(111) (112)

Scheme 29 Synthesis of 112

This *tert*-butyl carbazole stopper group **112** was coupled with the dibrominated naphthalene core **110** using potassium hydroxide and sodium iodide. The reaction took place in acetone at room temperature for 48 hours and produced the axle in a moderate yield, 39% (Scheme 30).

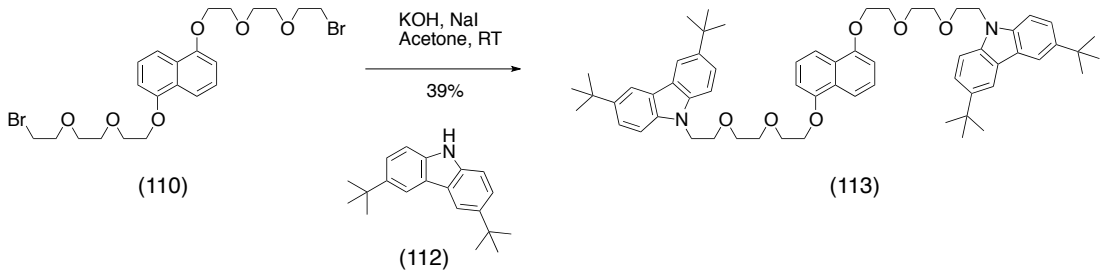

(110) (112) (113)

Scheme 30 Synthesis of axle 113

The final stage of the synthesis was to perform the same clipping reaction as had been used for rotaxane **103**. Axle **113** was stirred with **92** and **93** in dry acetonitrile for 10 days. After conversion to the PF_6 salt, the rotaxane **104** was obtained in a 20% yield (Scheme 31).

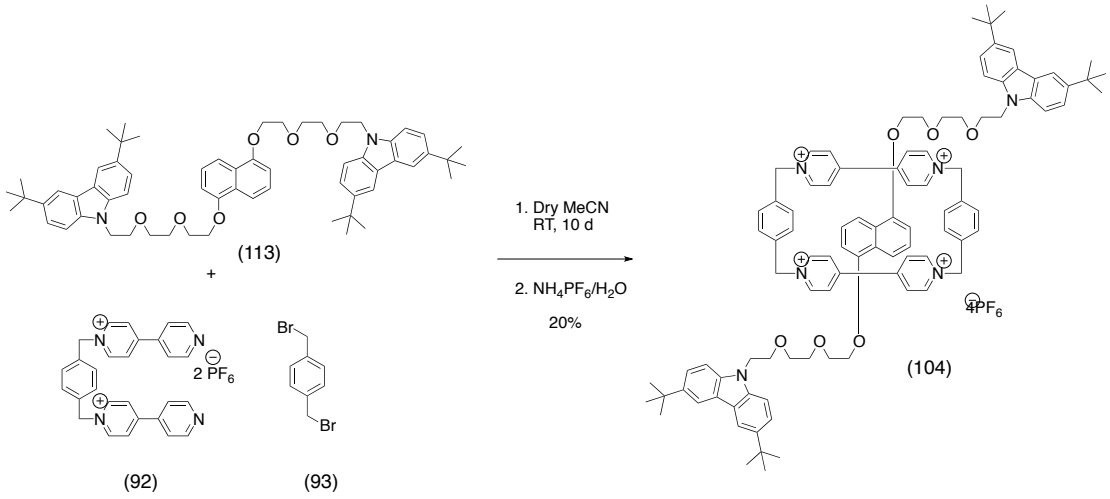

Scheme 31 Synthesis of rotaxane 104

The second donor-incorporating rotaxane started with an esterification reaction between the naphthalene core **102** and bis-4,4'-[(2,2'-bithienyl)-*N*-pyrrolyl]-3-carboxybenzene **114** using DMAP and DIC in CH_2Cl_2. The reaction took 6 days to complete and produced the axle **115** in a moderate yield of 56% (Scheme 32).

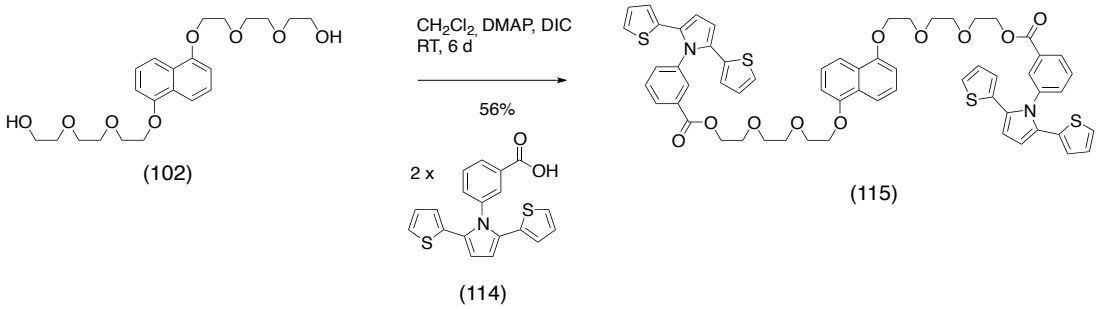

Scheme 32 Synthesis of axle 115

The final rotaxane **105** was synthesised using the conditions previously outlined for the two rotaxanes mentioned earlier. The reaction took 10 days to complete and after conversion to the PF_6 salt, gave the final rotaxane **105** in a 28% yield (Scheme 33).

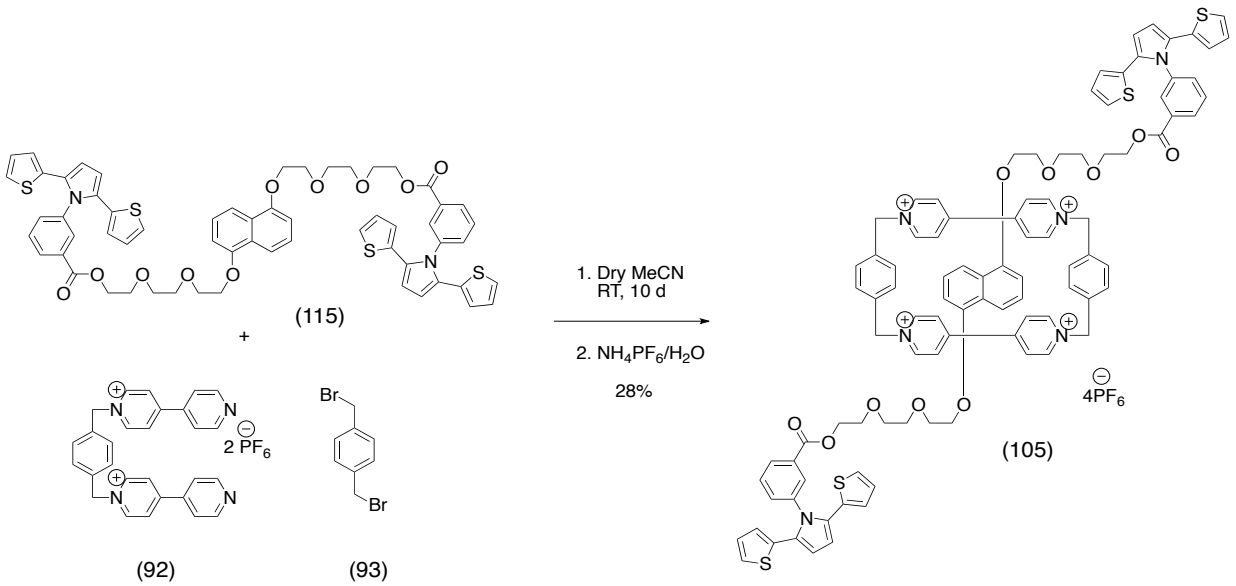

Scheme 33 Synthesis of rotaxane 105

Another rotaxane was attempted with the aim of incorporating a 3,5-(benzyloxy)-benzyl stopper group to the structure. This started with the conversion of 3,5-(benzyloxy)-benzyl alcohol **116**, which had previously been synthesised within the group, to 3,5-(benzyloxy)-benzyl chloride **117** using thionyl chloride in toluene with triethylamine.[82] This product was obtained after 3 hours in a poor yield for this reaction (Scheme 34). It was thought that the problem lay with the quality of the thionyl chloride and thus another route was adopted.

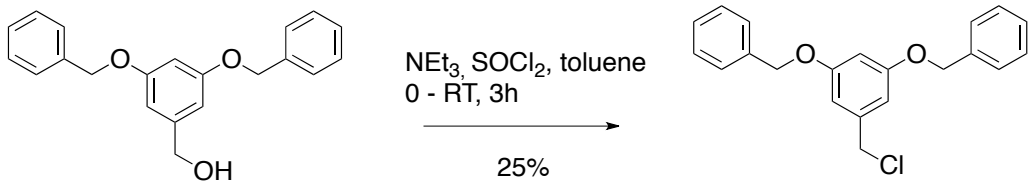

(116) (117)

Scheme 34 Synthesis of compound 117

The new route involved conversion of **116** to the mesylate **118** using methane sulfonyl chloride in CH_2Cl_2 with triethylamine.[83] This product was obtained after 2 hours in a good yield (Scheme 35). Due to the success of this conversion this compound was used in the second step and the formation of the axle.

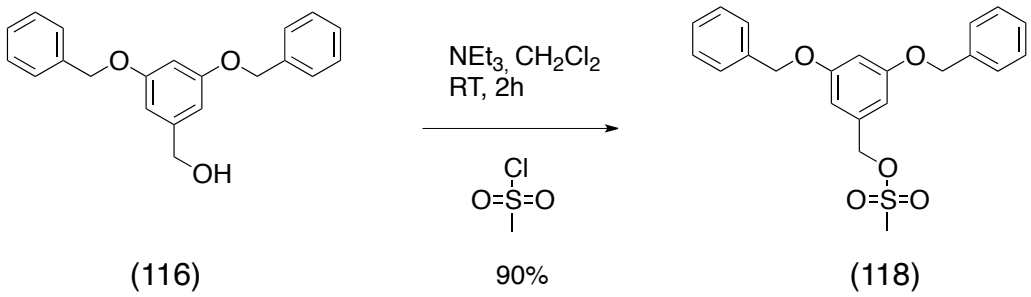

(116) 90% (118)

Scheme 35 Synthesis of compound 118

A coupling of the naphthalene core **102** with the mesylate **118** was attempted using potassium carbonate and 18-crown-6 in acetone (Scheme 36). The reaction stirred at reflux overnight, however, ^{1}H NMR analysis and mass spectrometry showed that no product was formed and only starting material remained. Due to time constraints and lack of starting material, this reaction was not investigated further and the coupling conditions could not be optimised.

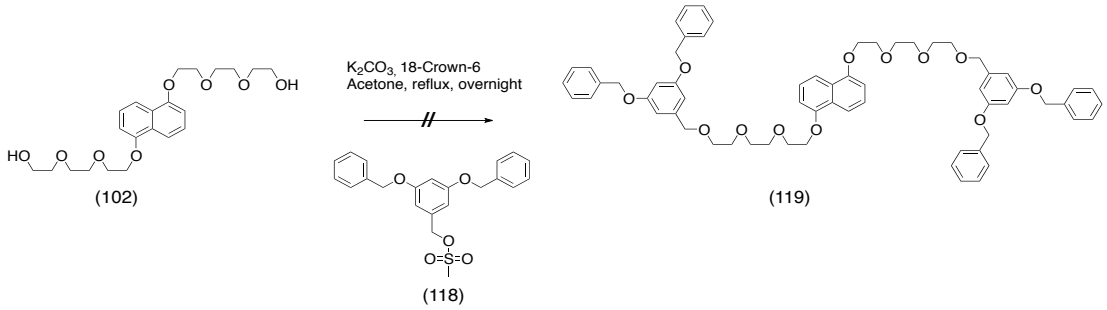

Scheme 36 Attempted coupling of 102 and 118

The synthesis of a rotaxane incorporating a C_{60} moiety was also attempted. The first step was to end-cap the naphthalene core **102**, with a C_{60} stopper group, which had been synthesised by a colleague within the group, giving axle **120**.[84] The capping conditions used were those previously used in the synthesis of rotaxane **103** (Scheme 37). ^{1}H NMR indicated that the reaction had occurred, however, purification proved problematic and compound **121** was not isolated. Many attempts at purification were to prove unsuccessful and thus this project was not continued.

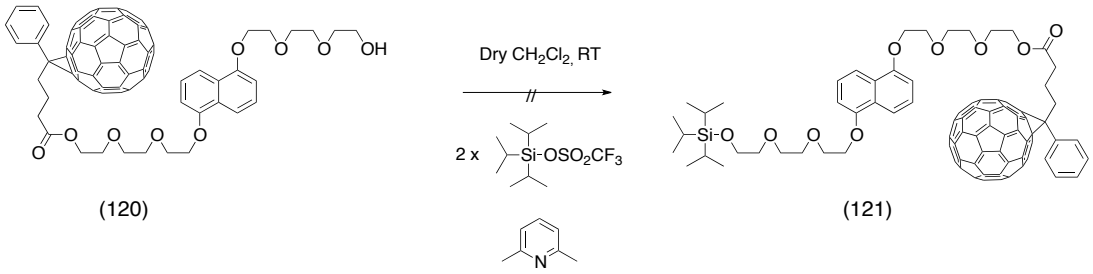

Scheme 37 Attempted synthesis of 121

3.2.4 UV/Vis and Fluorescence Spectroscopy

UV/Vis and fluorescence spectroscopy were performed on each of the rotaxane compounds **103**, **104** and **105** as well as a sample of CBPQT **88**, the naphthalene core **102** and the two novel axles **113** and **115** to allow for comparison. The samples were run at concentrations of 10^{-4}M and fluorescence at concentrations of 10^{-5} M in acetonitrile. Figure 65 shows the UV/Vis spectrum of **88** and the core **102**. It can be seen that there is an absorption at 272 nm in the spectrum of **88** and at 294 nm in the spectrum for **102**. When comparing with the two donor-incorporating axles **113** and **115** seen in Figure 66, it can be seen that the addition of the donor moieties to the naphthalene core **102** has limited effect on the absorption from the naphthalene.

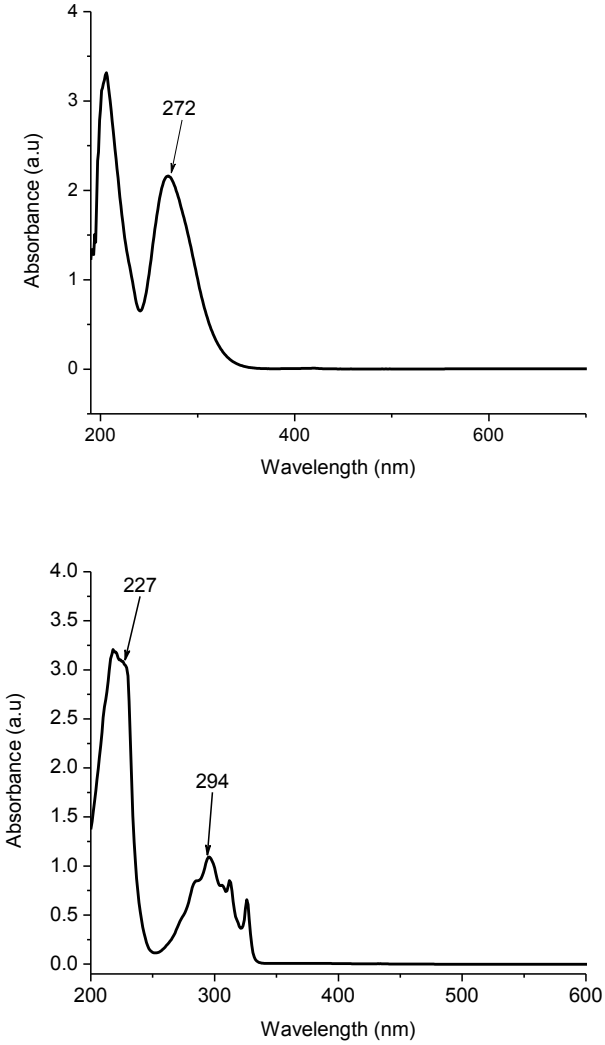

Figure 65 UV/Vis spectra of 88 (top) and 102 (bottom) recorded at a concentration of 1 x 10^{-4}M in acetonitrile

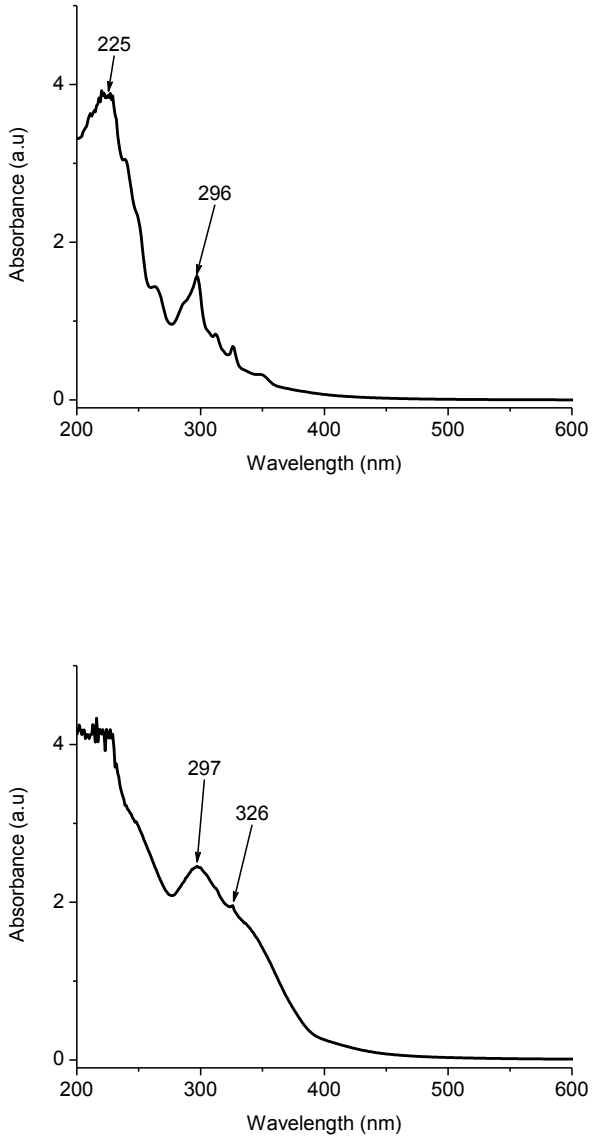

Figure 66 UV/Vis spectra of 113 and 115 recorded at a concentration of 1 x 10^{-4}M in acetonitrile

The UV/Vis spectrum of rotaxane **103** (Figure 67) shows a λ_{max} at 279 nm most likely arising from the CBPQT **88** ring. A new broad absorption can be seen at 540 nm. Due to the lack of this in both the **88** and core **102** spectra, it indicates π-π interactions between the naphthalene in the axle and the aromatic rings in **88**[85]. The UV/Vis analysis indicates that the naphthalene absorption is quenched by **88**, which is shown further by the fluorescence analysis. Figure 68 shows an overlay of the emission spectra for the naphthalene core **102** and rotaxane **103**. It can be seen that there are two emission peaks at 331 nm and 346 nm when excited at 279 nm. On coordination with **88**, the emission is quenched indicating a definite interaction between the axle and the ring.

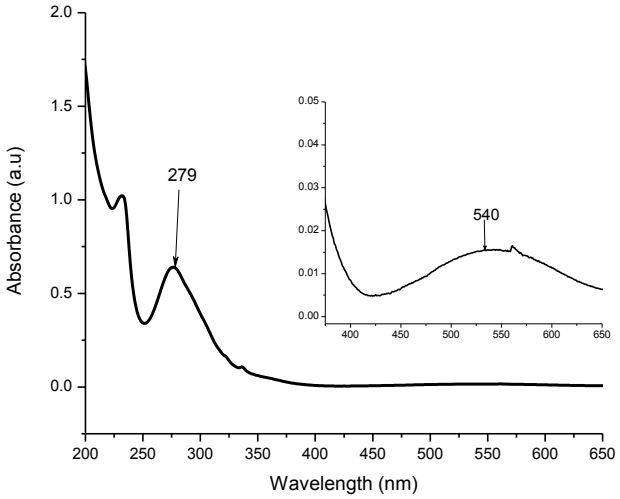

Figure 67 UV/Vis spectrum of rotaxane 103 recorded at a concentration of 1 x 10^{-5} M (inset at 1 x 10^{-4}M) in acetonitrile

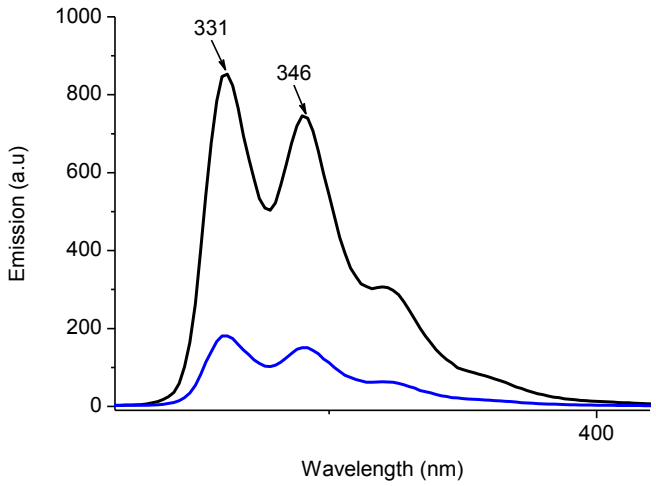

Figure 68 Overlay of the emission spectra of the naphthalene core (black) and rotaxane 103 (blue) recorded at concentrations of 1 x10^{-6}M in acetonitrile and excited at 297 nm

UV/Vis spectroscopy of rotaxane **104** (Figure 69) shows a λ_{max} at 271 nm and an absorption at around 297 nm. Again, it is seen that a new broad absorbance has appeared at 516 nm. Comparison to the spectra for **88** and the control compound **103** shows that there is no change in absorption from **88**. The new absorbance band again indicates that there is an interaction between the axle **113** and the ring **88**. Overlay of the emission spectra Figure 70 shows emission peaks at 329, 360 and 376 nm when excited at 297 nm. Comparison with the spectra of the core **102** shows that the carbazole moiety produces a change in the emission spectra with the appearance of

the peak at 376 nm. Figure 70 also shows that on complexation to the CBPQT **88** the fluorescence from the axle **113** is quenched providing further evidence of interaction between axle **113** and ring **88**.

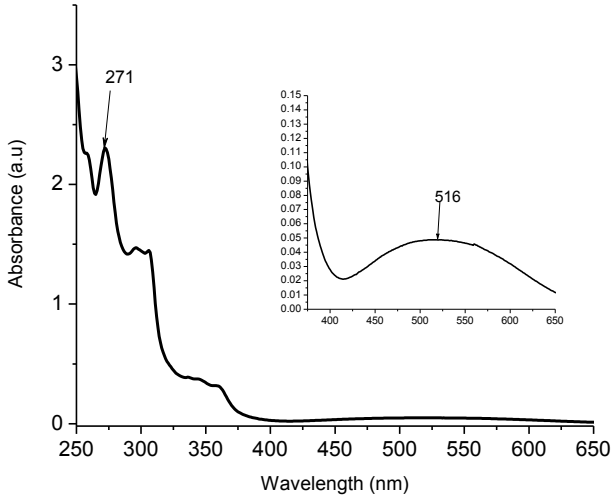

Figure 69 UV/Vis spectrum of rotaxane 104 recorded at a concentration of 1 x 10^{-5} M (inset at 1 x 10^{-4}M) in acetonitrile

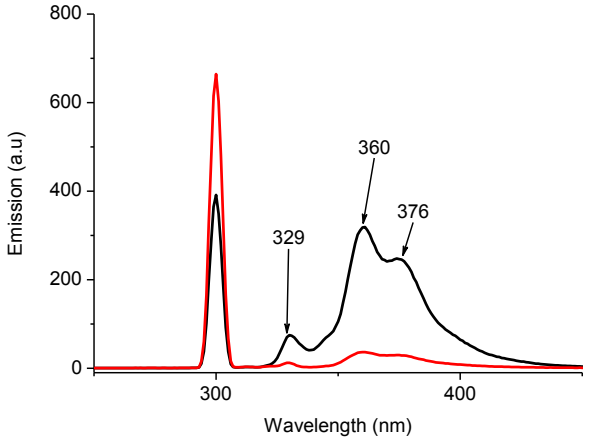

Figure 70 Overlay of the emission spectra of the axle 113 (black) and rotaxane 104 (red) recorded at a concentration 1 x 10^{-6}M in acetonitrile and excited at 297 nm

UV/Vis spectroscopy of rotaxane **105** (Figure 72) shows a λ_{max} at 326 nm and a broad absorbance at 522 nm. This rotaxane showed the biggest change in terms of the absorbance observed. The absorption at around 270 nm resulting from the CBPQT ring structure **88** has significantly reduced. The absorption of the naphthalene core

102 can also be seen to have shifted to 326 nm. The change in UV could be due to a sandwich effect whereby the axle folds upon itself and the conjugated stopper groups interact with the naphthalene causing a shift. This is also supported by the fluorescence analysis as fluorescence is completely quenched both for this compound **105** and for the axle **115** alone when excited at 297 nm (Figure 73).

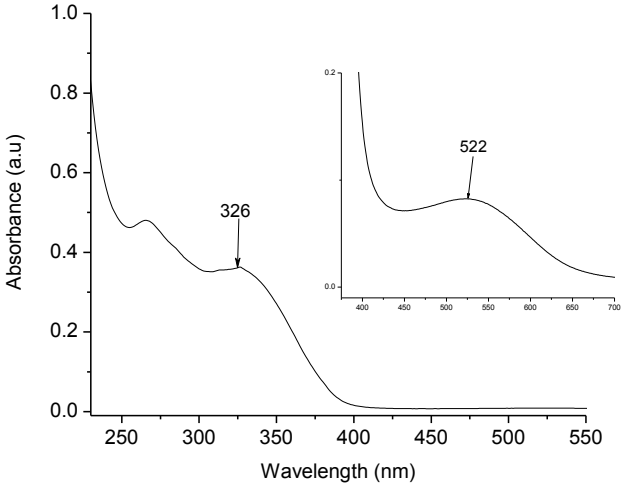

Figure 71 UV/Vis spectrum of rotaxane 105 recorded at a concentration of 1 x 10^{-4}M in acetonitrile

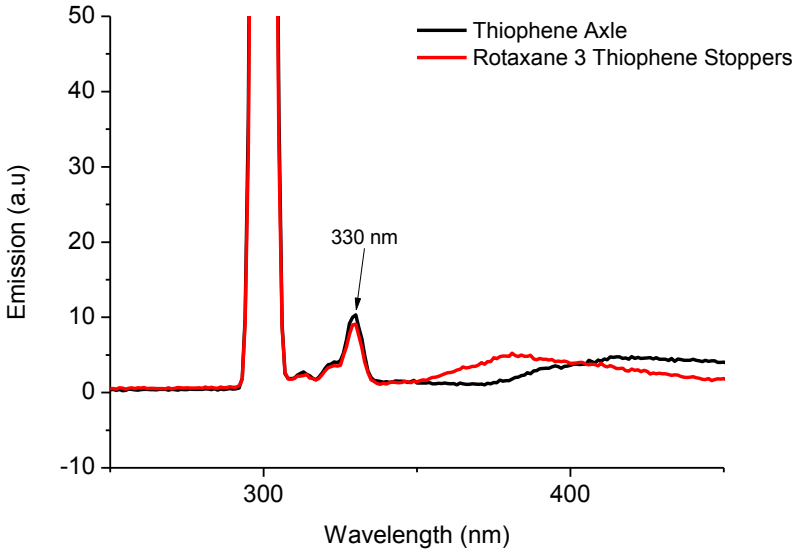

Figure 72 Overlay of the emission spectra of the axle 115 and rotaxane 105 recorded at a concentration of 1 x 10^{-6}M in acetonitrile and excited at 297 nm

3.2.5 Cyclic Voltammetry

CV was performed at 1 x 10^{-4} M concentrations using 0.1M TBA.PF_6 as the electrolyte. The HOMO level energy for rotaxane **105** was calculated using the formula –[4.8 – $(E_{1/2})_{ox}$], where $(E_{1/2})_{ox}$ is the onset of the oxidation wave observed for the compound and the LUMO level energy was calculated using the formula –[4.8 – $(E_{1/2})_{red}$] where $(E_{1/2})_{red,}$ is the onset of the reduction wave seen for the compound. A summary of the CV analysis of all 3 rotaxanes can be seen in Table 3.

Table 3 Optical and electrochemical properties of rotaxanes 1, 2 and 3.

Compound	$\ddot{e}_{max}$ (nm)	$E_{1/2}$ (eV)	E_{LUMO} (eV)	E_{HOMO} (eV)	E_g^{opt} (eV)[a]	E_g^{el} (eV)[b]
103	279	-0.73	-4.07	-	1.98	-
104	271	-0.74	-4.06	-	1.90	-
105	326	-0.71	-4.09	-5.20	1.85	1.11

[a] determined from the onset of UV-vis absorption spectrum (1240/ λ_{abs})

[b] determined from cyclic voltammetry

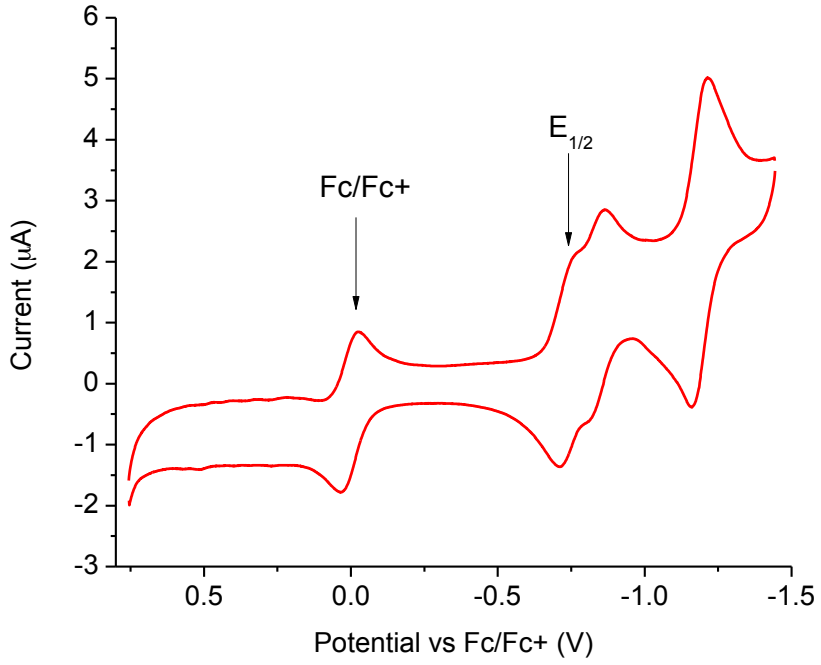

Figure 73 Cyclic voltammagram of rotaxane 103 recorded at a concentration of 1 x 10^{-4} M in acetonitrile, (0.1M TBA.PF_6, glassy carbon working electrode, platinum wire counter electrode and silver reference electrode, reference to Fc/Fc^+ = 0.0V)

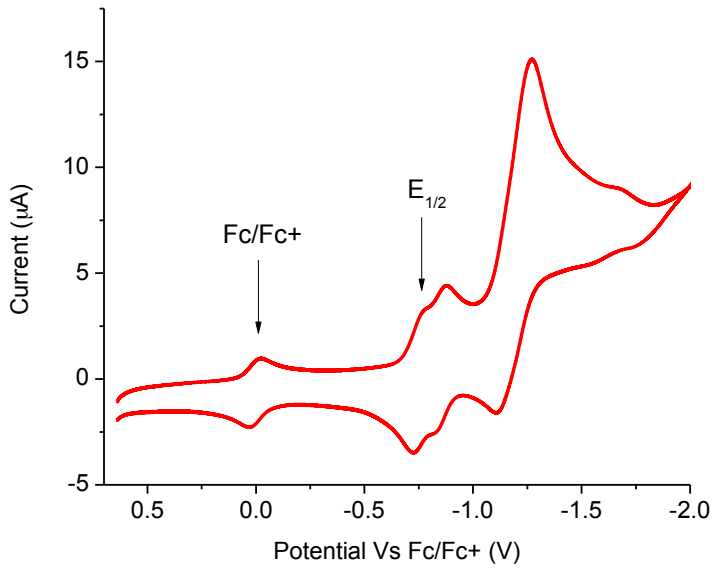

Figure 74 Cyclic voltammagram of rotaxane 104 recorded at a concentration of 1 x 10^{-4} M in acetonitrile, (0.1M TBA.PF_6, platinum working electrode, platinum wire counter electrode and silver reference electrode, reference to Fc/Fc^+ = 0.0V)

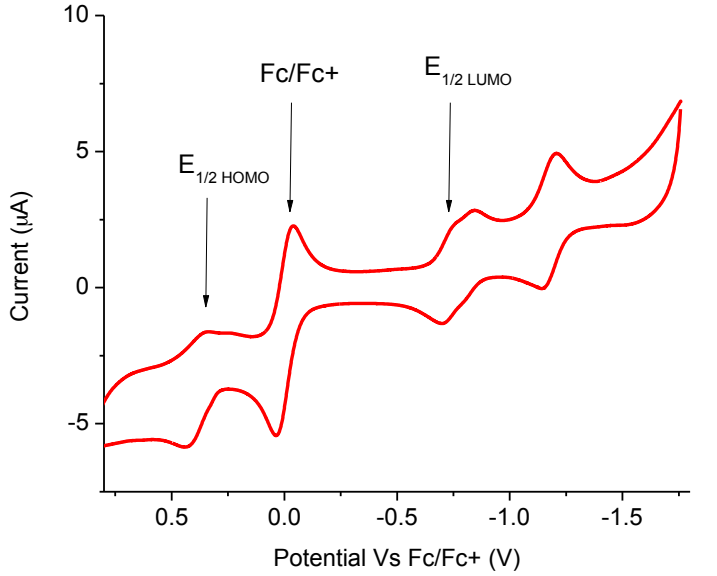

Figure 75 Cyclic voltammagram of rotaxane 105 recorded at a concentration of 1 x 10^{-4} M in acetonitrile, (0.1M TBA.PF_6, platinum working electrode, platinum wire counter electrode and silver reference electrode, reference to Fc/Fc^+ = 0.0V)

3.2.6 OPV and OFET fabrication

3.2.6.1 OPV

Solution-processed, bulk-heterojunction, photovoltaic cells were fabricated with rotaxanes **103**, **104** and **105**. However, the results showed that there is no photovoltaic response under illumination of light. This is likely due to the poor film quality and the solubility issue. Several attempts were made to improve the film formation using solvents like DMF and acetonitrile but nothing worked. The different ratios of active layers with varying solvents are mentioned with respect to the Figures.

3.2.6.2 OFETs

Three rotaxanes were analysed at the University of Strathclyde by members of Prof. Peter Skabara's group for use as organic photovoltaics (OPV) and organic field effect transistors (OFETs). Thin-film FETs were fabricated in bottom gate, source and drain geometry on highly doped silicon substrates with a 240 nm thick, thermally grown, silicon oxide (SiO_2) insulating layer and an interdigitated gold source and drain electrodes with channel length (L) and width (W) of 10 μm and 10 mm respectively. These pre-fabricated substrates were carefully cleaned using several rounds of acetone and methanol. After drying in a flow of nitrogen, these substrates were treated with pentafluorobenzenethiol (PFBT) (7 mM in propanol). The processed substrates were then transferred to a nitrogen-filled glove box where nitrogen and oxygen levels were maintained below 0.1 ppm. Rotaxane solutions from acetonitrile were then deposited by spin-coating. The coated films were baked on a hotplate for one hour at 120° C. The film thickness was observed around 40-50nm for each device. The concentration of rotaxanes was 10 mg of the compound dissolved in 0.5 ml of acetonitrile**.** The output characteristics of rotaxane **103** (Figure 76) show the drain current (I_{DS}) as a function of source drain voltage (V_{DS}) for different values of gate voltage (V_{GS}). The output characteristics have fewer amounts of hysteresis, a linear and saturation region. The transfer characteristics are measured at V_{DS} = -50 V also show fewer hysteresis, but not negligible. However, the mobility of this device obtained a value of $1.0x10^{-7} cm^2/Vs$ exhibited as p-type (hole transport) behaviour. Also, the on/off ratio ($I_{on}/I_{off} = 10^2$) and a threshold voltage of 27 V was observed. The output and transfer characteristics (V_{DS} = -50 V) of rotaxane **104** can be seen in Figure 77 with the mobility calculated as $1.3x10^{-6} cm^2/Vs$.

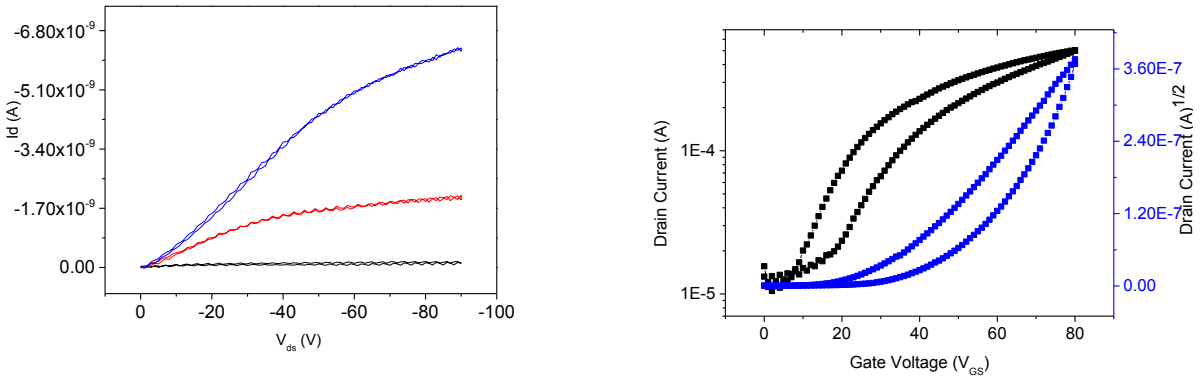

Figure 76 Output characteristics (left) and transfer characteristics (right) of rotaxane 103 using acetonitrile on PFBT treated Au/SiO_2 substrate.

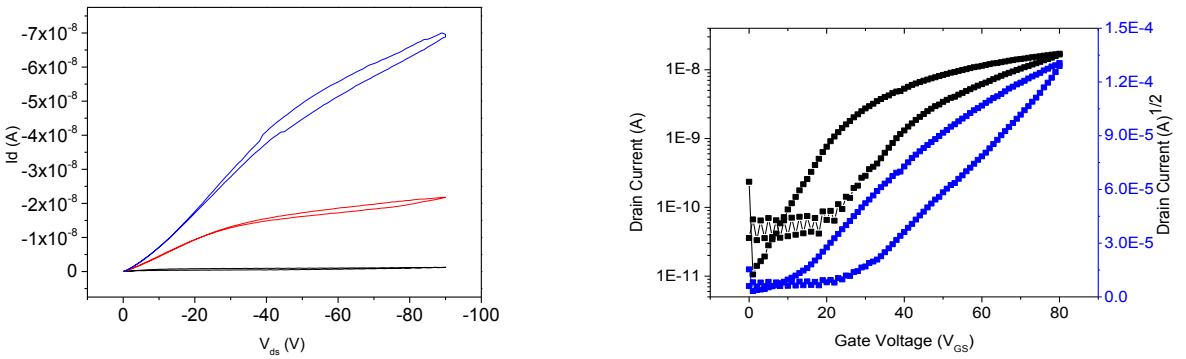

Figure 77 Output characteristics (3a, left) and transfer characteristics (3b right) of rotaxane 103using acetonitrile on PFBT treated Au/SiO_2 substrate.

As previously mentioned, rotaxanes have the potential ability to self assemble by hydrogen bonding and π-π interactions. This self-assembly results in charge-transfer interactions between donor and acceptor units, which enable the charge transport properties, particularly, one order higher magnitude of mobility in rotaxane **104** than rotaxane **103**. This is likely to be a result of the presence of carbazole donor units at both ends which can interact with naphthalene core **102** through π-stacking and H-bonding from the glycol chain. Both rotaxanes **103** and **104** exhibit p-type behaviour, but in the case of rotaxane **105** there is no field effect mobility observed. It is most likely due to the poor solubility and hence poor thin film on the substrate.

Table 4 OFET parameters for Rotaxanes 103, 104 and 105

Rotaxanes	Mobility, (μ) Cm^2/Vs	I_{on}/I_{off} ratio	Threshold Voltage, (V_T) V
103	$1.0x10^{-7}$	10^4	27
104	$1.1x10^{-6}$	10^6	30
105	---	---	---

The low mobilities observed could be explained by the AFM images shown in Figure 78. The discontinuous films with very rough structures might explain much lower mobility in rotaxanes **103** and **104**. Upon closer examination, rotaxane **104** appears to have more uniformly sized larger particulate structures than that of rotaxane **103**. The bigger size cluster in rotaxane **103** might also be the cause for lower mobilities. The AFM image of rotaxane **105** has a bigger particulate structure similar to rotaxane **104**, it also has an underlying branched fibre-like structures. It is possible that these branched fibres are not well connected and lack the favourable orientation to facilitate charge transport across them.

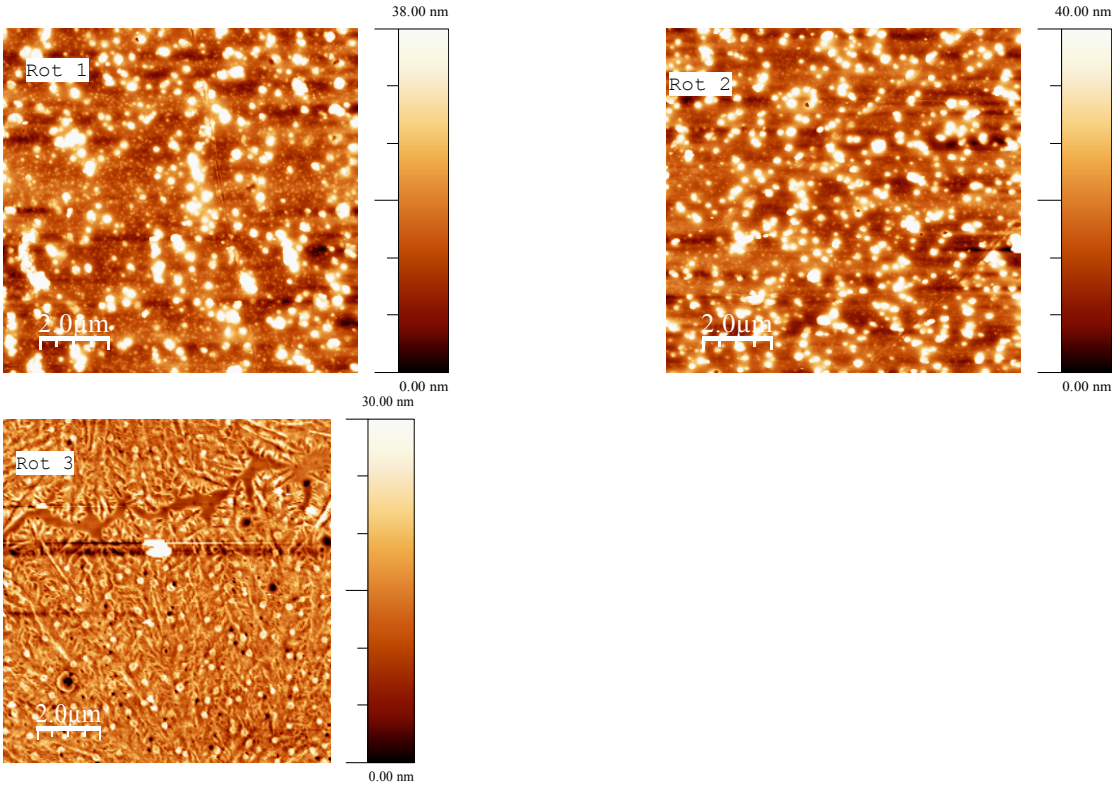

Figure 78 AFM height images for rotaxanes 103, 104 and 105 on silicon substrates annealed at 120°C

3.3 Conclusions and Future Work

3.3.1 Conclusions

In conclusion, 3 rotaxanes were successfully synthesised including two novel compounds with a carbazole moiety **104** and thiophene moiety **105** in the axle. The UV/Vis and fluorescence experiments showed an interaction between the axle and the CBPQT.

The compounds were tested at the University of Strathclyde within Prof. Peter Skabara's group. They were analysed for use as both OPVs and OFETs. The OPV tests showed that the lack of solubility and poor film quality resulted in no photovoltaic effect observed on illumination of the devices. However, OFET results were more promising showing that the self assembly of the compounds caused an increase in charge mobility and increasing the functionalisation in the axle also caused an improvement in charge mobility.

3.3.2 Future Work

Two target compounds were unfortunately not synthesised due to insufficient time and purification issues. Further investigations could be done on the coupling reaction between the naphthalene diol and the benzyl mesylate in order to complete the synthesis of the novel rotaxane target and investigating if the presence of the three aromatic rings of the stopper group could further increase the field effect ability. Further work could also be done to improve the purification method of the C_{60} axle to complete the synthesis of the double acceptor compound to see if this could improve on the current widely used PCBM acceptor. Due to the success of the methodology for the synthesis of the rotaxanes, further investigations could be carried out to further tune the structures to further improve the UV/Vis properties and hopefully improve both the OPV and OFET results.

4.0 Synthesis of a Series of Block Co-Polymers and Conjugated Polymers

4.1 Introduction

4.1.1 Synthesis and Applications of Block Co-Polymers

Block copolymers have been of particular interest due to the possibility to tune the polymeric building blocks to alter the physical properties of the polymer. They are also interesting due to the ability to synthesise large molecular weight polymers from small molecules with the ability to self assemble, creating highly ordered polymers.[86] Supramolecular polymerisations have incurred a lot of interest due to the self-assembly of small monomeric units through non-covalent interactions. A supramolecular polymer is described simply as a system characterised by non-bonded interactions between repeating units.[87] These types of systems also allow for self-assembly of functional units within a polymeric structure, which can exhibit optical and electronic properties.[88]

Radical polymerisation is commonly used for the synthesis of high molecular weight polymers. The advantages of radical polymerisations are that the techniques can be used on a wide range or monomers, it can be used in the presence of a wide range of functional groups and conditions and it is relatively easy and cheap in comparison to other techniques.[89] There are many types of radical polymerisations, but here I will discuss two, atom transfer radical polymerisation (ATRP) and reversible addition fragmentation chain transfer (RAFT).

ATRP is an example of a controlled radical polymerisation. It is one of the most widely used methods for the synthesis of block copolymers with narrow molecular weight distributions. ATRP involves activation of R-X by Cu(I) aided by a ligand, often PMDETA, giving Cu(II) and a radical which starts the polymerisation.[90]

Since it was first proposed in 1995 ATRP has been rapidly developed as a polymerisation technique. This well developed method has become a very simple way to synthesise well-defined polymers with control over molecular weight, however, it does have limitations including sensitivity to air and the fact that transition metal complexes need to be removed from the reaction mixture. One way of improving this technique has been to develop a new method known as activator generated by electron transfer for atom transfer radical polymerisation (AGET ATRP). This technique uses

a reducing agent to reduce the oxidation state of the transition metal into an active lower state transition metal as demonstrated by Zhao et al in the synthesis of a fluorescent poly(methyl methacrylate) **124** (Scheme 38). Here they use a simple methyl methacrylate monomer **122**, Cu(II)Cl_2/BPy complex as a catalyst, tin(II) 2-ethylhexanoate as a reducing agent and naphthalene-1,5-diyl-bis(2-bromo-2-methylpropanoate) **123** as an initiator to give the fluorescent polymer PMMA **124**.[91]

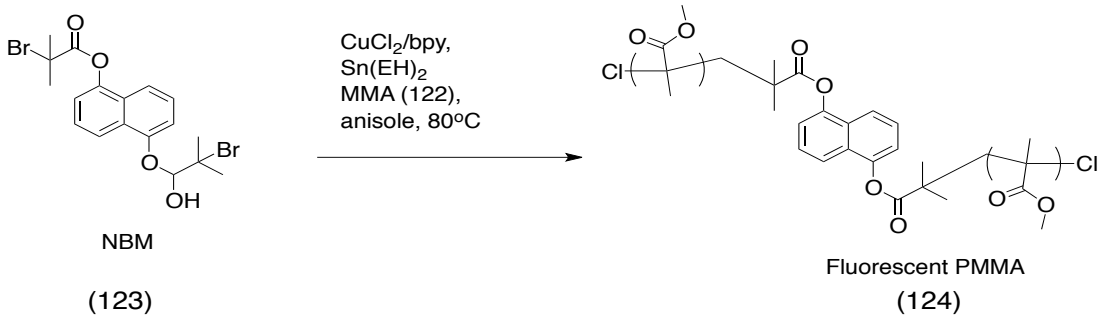

Scheme 38 Synthesis of 124

Along with the synthesis of fluorescent polymers with a single colour emission, ATRP can also be used to synthesise block co-polymers with di-colour emission using two different fluorescent monomers as demonstrated by Lu et al. They used a blue-emitting stilbene derivative, 1-(4-vinylstyryl) naphthalene **125** as the monomer and a green-emitting 1,8-naphthalimide derivative, 2-(2,3-dihydro-2-(4-methoxy-phenyl)-1,3-dioxo-1*H*-phenalen-7-ylamino)ethyl-2-chloroacetate (NAPH) as the initiator **126** to synthesise the di-colour fluorescent polymer **127** (Scheme 39).[92]

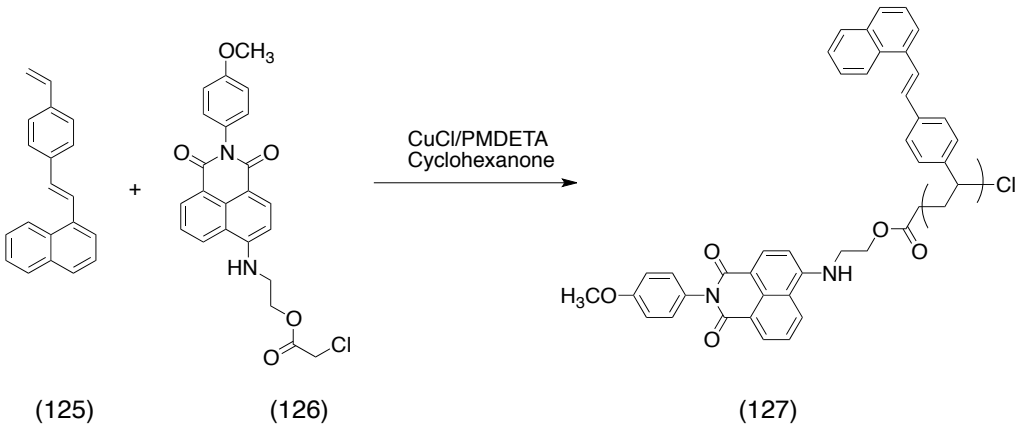

Scheme 39 Synthesis of a fluorescent polymer

ATRP has also been used to enable advancements in water-based applications synthesising high molecular weight polyacrylamides. Poly(*N*-isopropylacrylamide)

(PNIPAM) is a very important acrylamide polymer which has attracted a lot of attention due to its temperature-dependent solubility in water arising from a temperature-triggered coil to globule conformational transition which has been exploited in many applications such as drug delivery.[93] ATRP was employed by Ifuku et al to develop a co-polymer **130** with NIPAM **128** and chitosan **129** for use in biomedical activities (Scheme 40).[94]

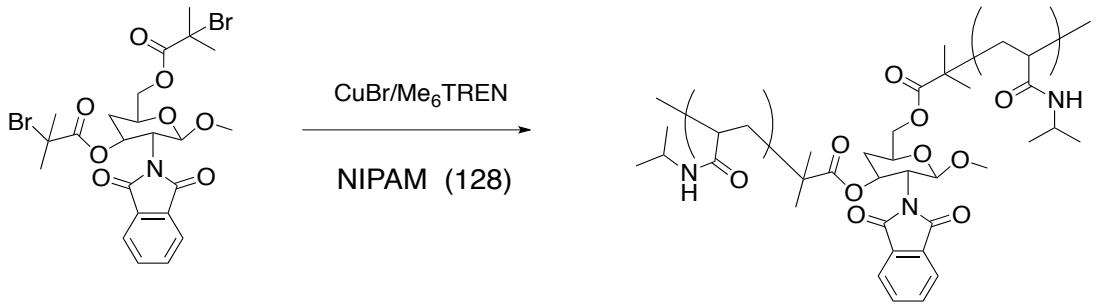

(129) (130)

Scheme 40 Synthesis of 130

The ability to tune the monomeric units of the polymer in order to tune the polymeric properties has been readily investigated. Such investigations include the investigation on the π- π stacking which can be found in polymers with an electron deficient face. Along with the exploitation of the π- π stacking to synthesise copolymers **133** of fluorinated **131** and non-fluorinated styrene **132** units (Scheme 41)[95] However, Pickett et al also showed how the rate of ATRP can also be dependent on the π- π stacking interactions. They studied the ATRP of styrene **132** in the presence of hexaflurobenzene and octafluorotoluene (Scheme 42).[96]

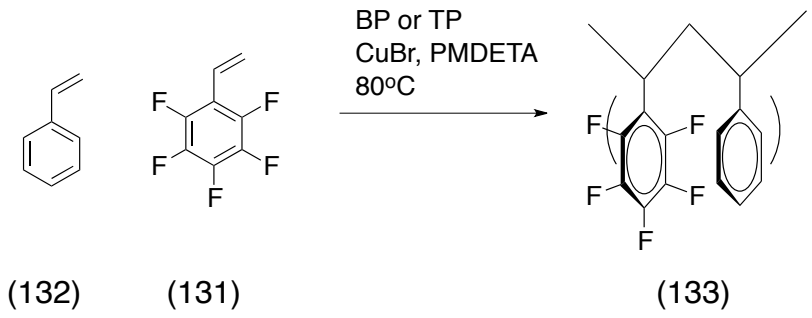

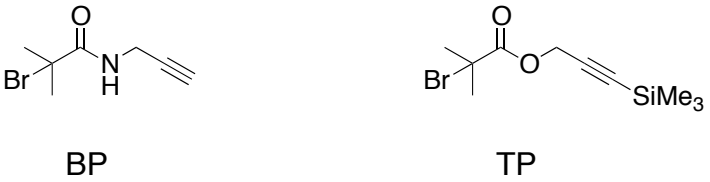

Scheme 41 π- π stacking between 131 and 132 monomer units

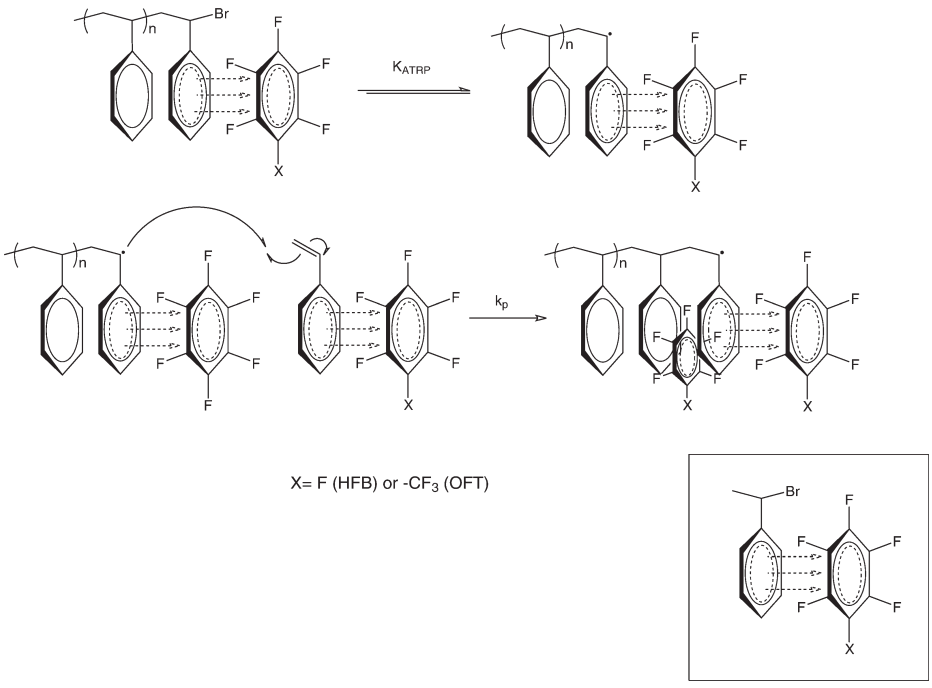

Scheme 42 Investigation of π- π stacking on the rate of ATRP[95]

RAFT polymerisation is another example of a controlled radical polymerisation and can also be used on a wide range of monomers. The process involves the use of a thiocarbonylthio compound known as a RAFT agent **134**. The mechanism involves insertion of the monomer into the C-S bond of the RAFT agent **135** with an initiator such as AIBN **134** (Figure 79).[97]

RAFT AGENT (134)

AIBN (135)

Figure 79 General structures of 134 and 135

RAFT polymerisation has been used to investigate the use of amino acid-based functional monomers in order to synthesise non-biological macromolecules with properties for various biomedical applications. Kumar et al applied this method in order to synthesise a polymer incorporating a C-terminus modified amino acid **136**, which had previously not been possible. They achieved this via protection of the C-terminus with a boc-protecting group, which was removed post polymerisation (Scheme 43).[98]

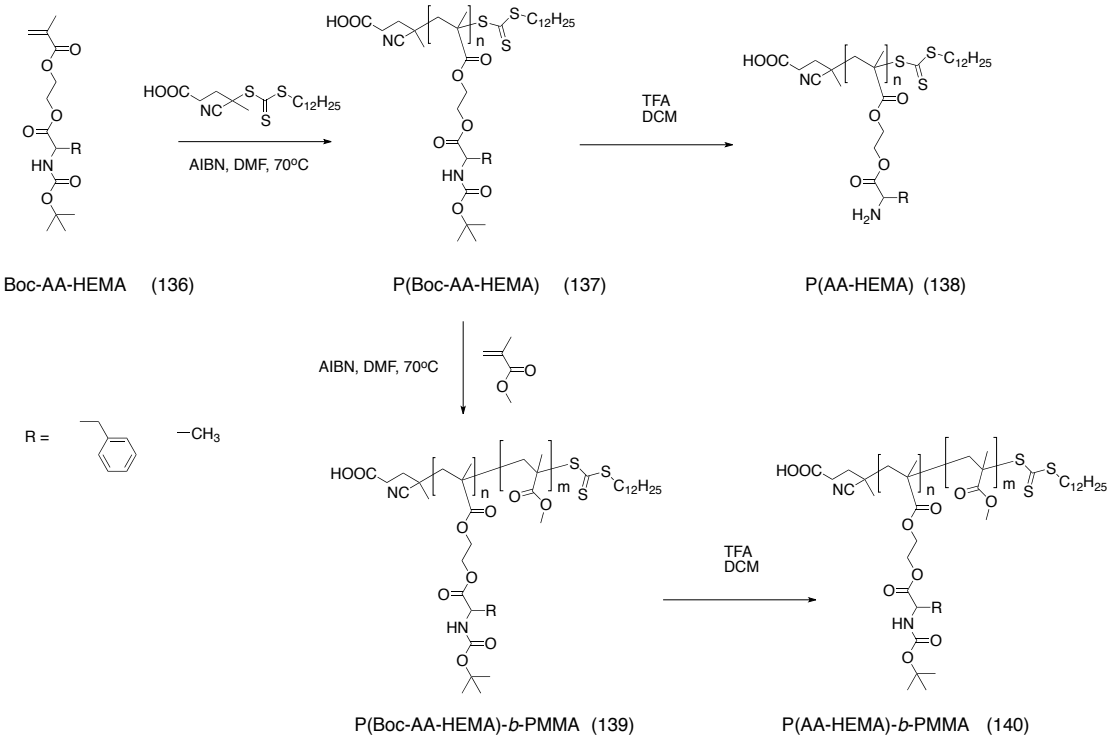

Scheme 43 Synthesis of amino acid polymers 138 and 140 by RAFT polymerisation and deprotection

Polymers are also widely investigated as a carrier system for drugs within the body. The advantage of using polymers is the increased circulation time in the body. Highly promising carriers are self-assembled structures of amphiphilic block copolymers typically micelles (Figure 80). RAFT polymerisation has been used to synthesise

functional polymeric micelles. Investigations into RAFT polymerisation have shown that the RAFT process is a versatile tool for obtaining functional block copolymers to generate micelles for drug delivery purposes. It was also shown that the incorporation of biological moieties such as sugars, proteins or peptides can also be achieved (Scheme 44). The process has been shown to be stable in the presence of most functional groups and can be employed to control monomers such as vinyl acetate or N-vinyl pyrrolidone, which can now potentially take on a role in biomedical applications similar to polyethylene glycol.[99]

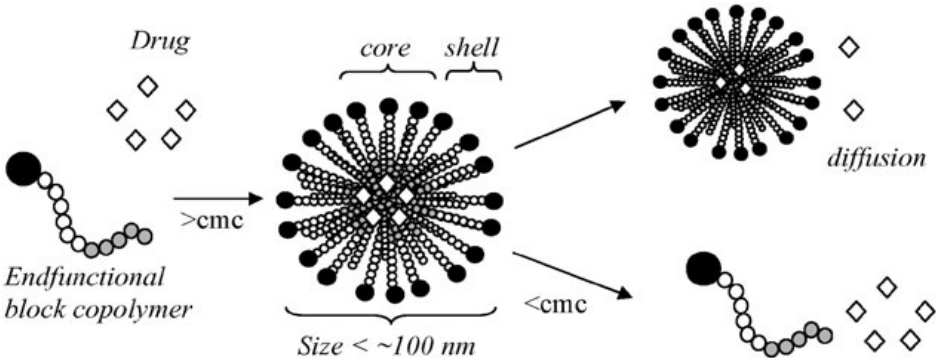

Figure 80 Self assembly of block copolymers and their release of drugs[98]

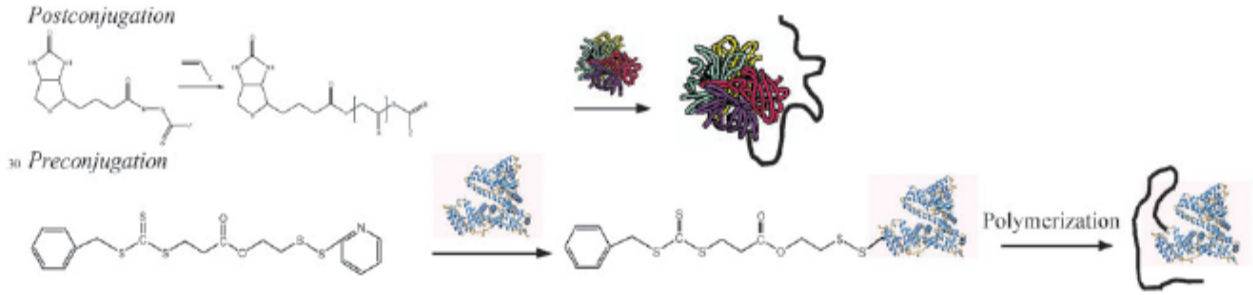

Scheme 44 Synthesis of polymer–protein conjugates via RAFT polymerisation[98]

Along with the uses in biomedical applications, RAFT polymerisation has also been investigated for use in organic electronics. Chen et al looked at the possibility of using the RAFT polymerisation technique to synthesise a block copolymer with organic semiconductor segments.[100] They prepared a range of macro-RAFT agents, I will mention two here; one based upon a tetrathiophene **141** (Scheme 45) and one based on P3HT **152** (Scheme 46)

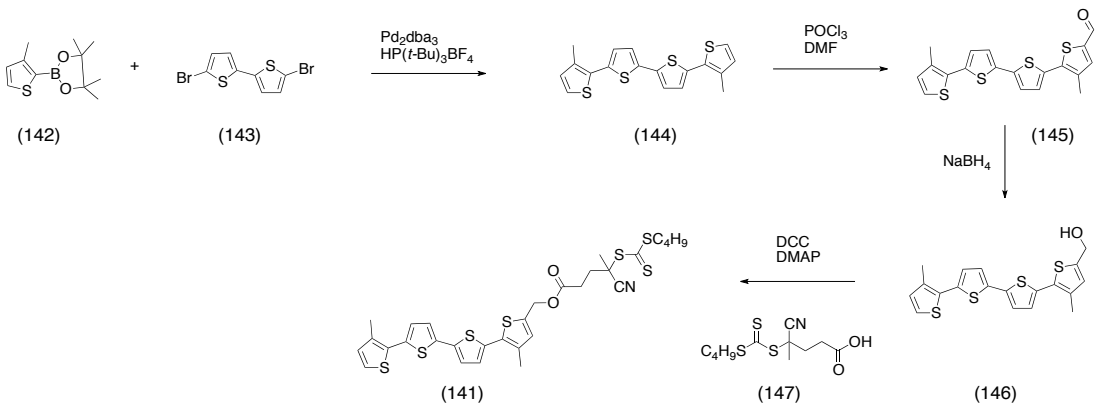

Scheme 45 Synthesis of macro-RAFT agent based upon tetrathiophene 141

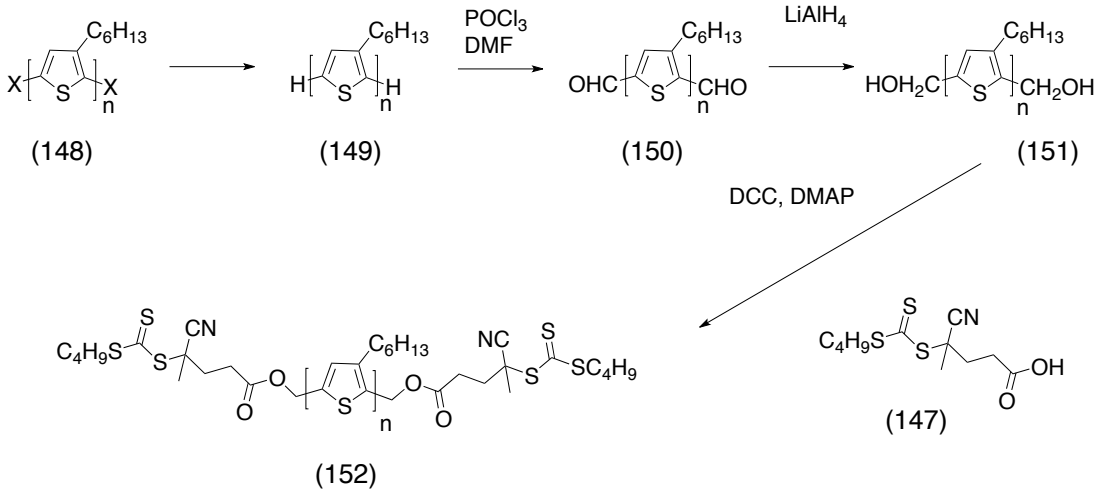

Scheme 46 Synthesis of a macro-RAFT agent based on P3HT 152

From their investigations, they found that RAFT polymerisation was a useful method for synthesising a range of block copolymers. During their investigations, the results highlighted the reactivity of thiophene in radical reactions and the importance to block the 2- and 5- positions on the thiophene. They also showed that this method could be used to synthesise polymers from vinylthiophene **154** giving **156** (Scheme 47) and styrene **132** (Scheme 48) giving **159**, which resulted in block copolymers with organic semiconducting segments.

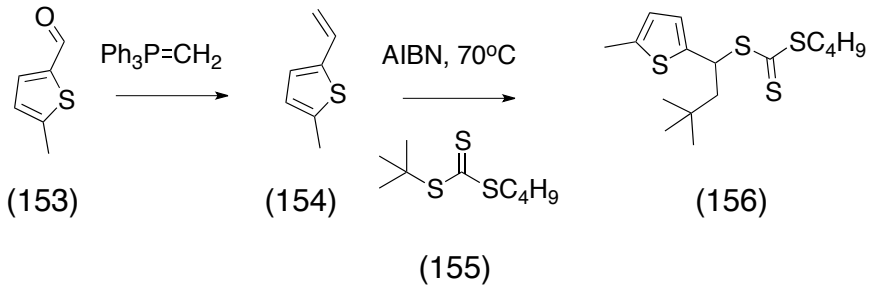

Scheme 47 Synthesis of macro-RAFT agent 156 from vinylthiophene 154

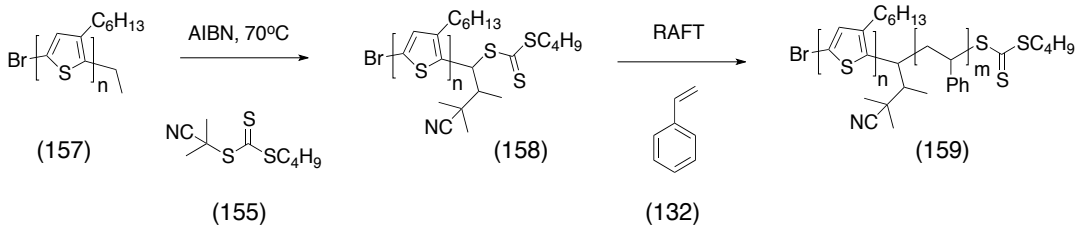

Scheme 48 Macro-RAFT agent synthesis from poly(3-hexylthiophene) RAFT polymerisation to form poly(3-hexylthiophene)-*block*-polystyrene 159

4.1.1.1 Naphthalene Diimides

Naphthalene diimide (NDI) **161** is formed from 1,4,5,8-naphthalenetetracarboxylic dianhydride **160** and an appropriate amine (Scheme 49).

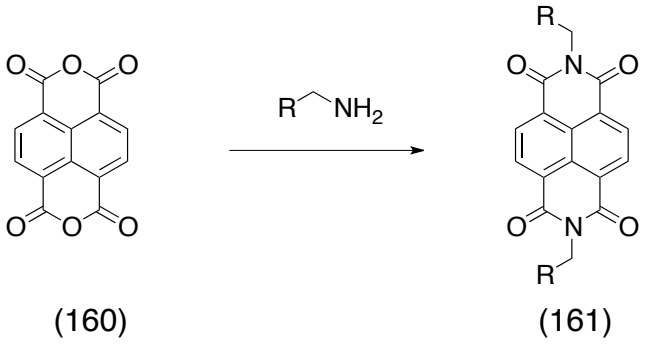

Scheme 49 Synthesis of 161

Naphthalene diimides are compact electron-deficient compounds[101] and are currently used as acceptor materials in photovoltaics. These molecules are also useful as they can be functionalised at the diimide nitrogens, or on the aromatic framework in order to vary the absorption and emission properties.[102]

4.1.1.2 Click Chemistry

The term "click chemistry" was initially used by Sharpless[103] and is used to describe reactions that are easy to perform, require a little or simple work-up, produce high yields and are stable to water and oxygen. However, over the years one reaction has come to be known as the "click reaction" and that is the Huisgen 1,3-dipolar cycloadditions of terminal alkynes **162** and azides **163** to give 1,2,3-triazoles **164** and **165** (Figure 81) The use of copper not only makes the reaction faster but also makes it regio-specific.[104]

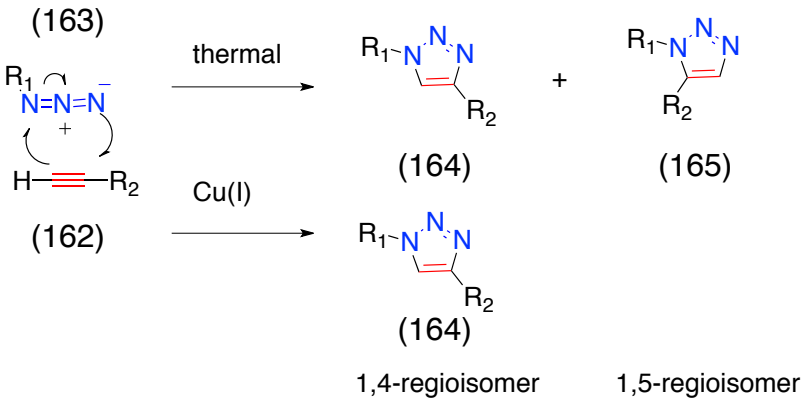

Figure 81 Mechanism of the Huisgen 1,3-dipolar cycloaddition

4.1.2 Conjugated Polymers

Conjugated polymers have encountered a lot of interest in recent years with potential applications in electronics and optoelectronics.[105] P3HT **11** is considered one of the most promising materials for organic photovoltaics (OPVs) due to high carrier mobility and solution processibilty.[106] The structure of the polymer can be easily tuned to alter its properties and achieve polymers with a high electron affinity for improved electron transport or for low ionization potential for improved hole transport.[107]

One of the most promising OPV devices is based on a bulk heterojunction (BHJ) consisting of **11** as the electron donating polymer and using **6** as an electron acceptor. However, optimisation of the processing conditions has only managed to reach a power conversion efficiency of 5% which is still very low compared to the inorganic counterparts of >40%. The main issues in terms of these compounds are to match the

absorption with the solar spectrum and decreasing the band gap in the polymers could be a way to solve this issue.[108]

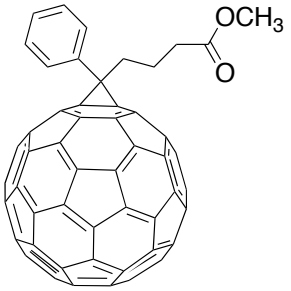

PCBM

(6)

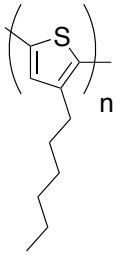

P3HT

(11)

Figure 82 Structures of 6 and 11

Polythiophenes are commonly synthesised by chemical polymerisations. There are two main classes of chemical polymerisation, transition metal catalysed polymerisation and oxidative polymerisation. Transition metal catalysed polymerisation commonly starts from a 2,5-dihalogenated thiophene. The classical metal-catalysed reaction starts by preparation of a mono-Grignard monomer after treatment of the dihalogenated thiophene **166** with magnesium. This is then followed by the addition of the transition metal catalyst such as Ni(II) or Pd(II). This is what is commonly known as a controlled polymerisation, giving a regiocontrolled polymer **167**. Oxidative polymerisation simply consists of polymerisation of thiophene or 3-substituted thiophenes **168** in the presence of $FeCl_3$. This method, however, is not a controlled polymerisation. There is the possibility of a 2,4- linkage of thiophenes in the polymer **169** chain, thus limiting the π-electron system whereas in the controlled method of a transition metal catalysed reaction the polymer chain tends to be 2,5-linked **167**.[109]

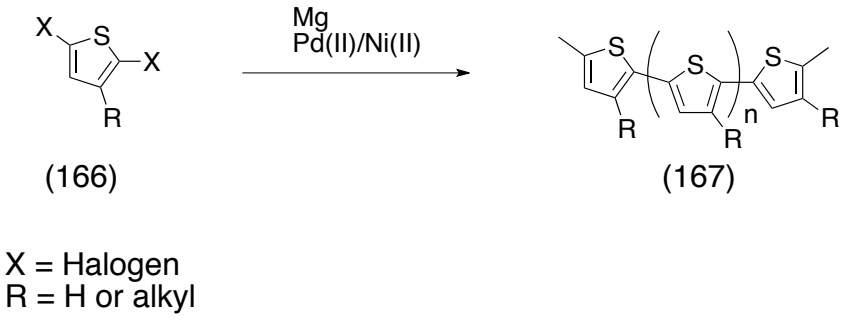

Figure 83 Controlled transition metal catalysed polymerisation

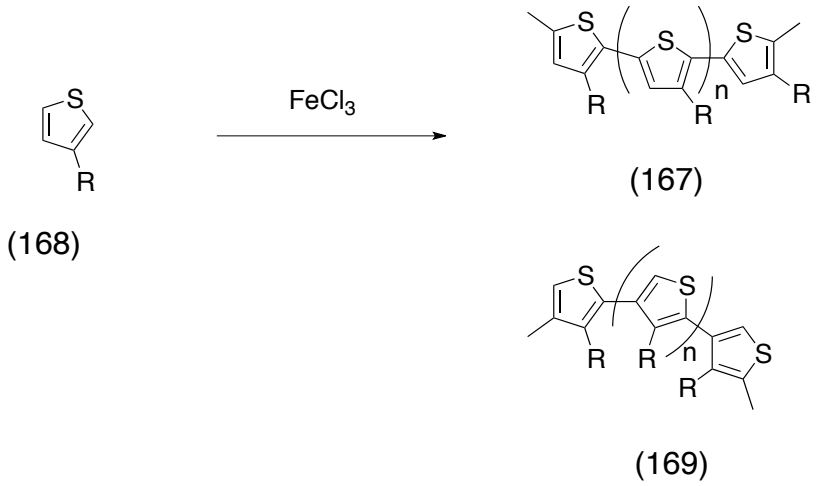

Figure 84 Oxidative polymerisation giving 167 and 169 polymers

Oxidative polymerisation was utilised by Fraleoni-Morgera et al in the synthesis of soluble azo-dye substituted thiophene copolymers **171**, **173** and **174**.[110] Here, they studied the co-polymerisation of **11** and two acceptor-donor azo dye thiophene monomers **170** and **172**. They showed that it is possible to prepare soluble thiophene based copolymers by using molecular design and the oxidative polymerisation technique (Scheme 50).

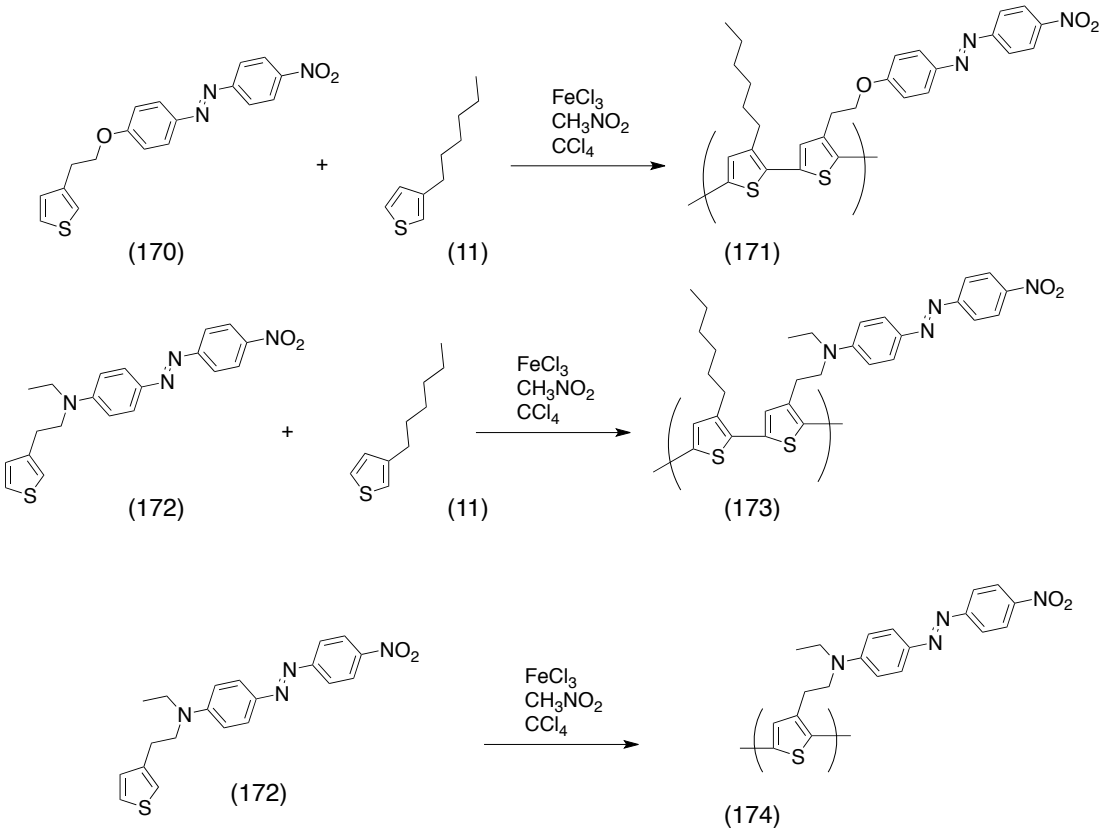

Scheme 50 Synthesis of azo-dye substituted thiophene polymers 171, 173 and 174

As previously mentioned **11**, is considered the standard for donor material in organic electronics. One study investigated the field effect transistor characteristics of crystalline diblock copolymers with **11** and syndiotactic polypropylene. Here, they synthesised an alkynyl end-capped P3HT **175** and azide end-capped polypropylene **176** and used "click" chemistry to construct the diblock polymer **177** in order to investigate the relationship between the molecular packing structures, morphologies and their field-effect transistor characteristics (Scheme 51).[105]

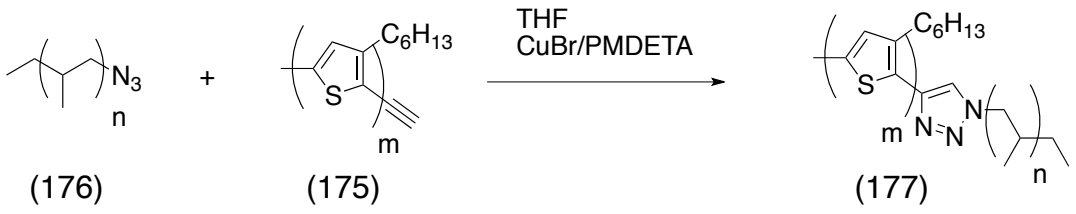

Scheme 51 Diblock polymer for FET characteristics

One of the main issues associated with OPVs are the power conversion efficiencies (PCEs) achieved. One way to improve on this has been to develop donor-acceptor polymers in order to broaden the visible absorption and tune the energy levels. One

investigation has been to synthesise alternating copolymers of 2,6-carbazole, thiophene and thienylene-vinylene conjugated side chains containing various acceptor end groups such as aldehyde **178**, mono-cyano **179**, dicyano **180** and 1,3-diethyl-2-thiobarbituric acid **181** (Scheme 52). This study showed that through manipulation of the acceptor groups attached to the conjugated side chain the photophysical and electronic properties as well as the absorption spectra could be tuned.[111]

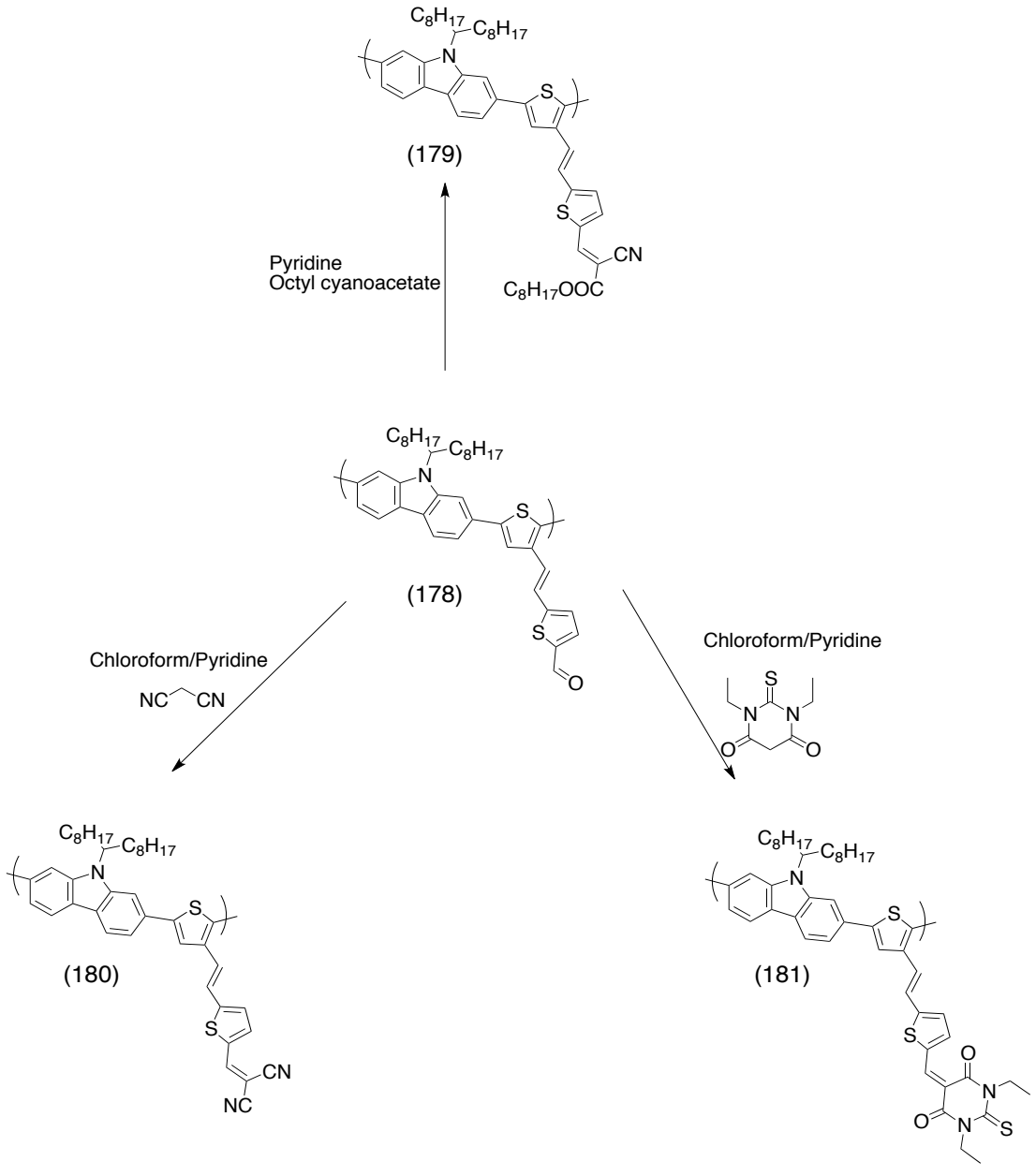

Scheme 52 Synthesis of copolymers of carbazole and thiophene with acceptor end groups

4.2 Project Outline

4.2.1 Donor-Acceptor and Donor-Donor Block Co-Polymers

Naphthalene diimides are already commonly used as acceptor material in photovoltaics. Due to their ability to be easily functionalised, the aim was to synthesise a series of donor-acceptor block co-polymers which would incorporate the functionalised NDI group as the acceptor and a range of donor groups using radical polymerisation techniques and use the Huisgen 1,3-dipolar cycloaddition "click" reaction to connect the polymeric species. The ability to tune the polymeric building blocks provides great scope for synthesising materials that can be tuned to meet specific requirements. Synthesis of donor-donor block co-polymers are also of interest as a potential replacement for the existing **11**.

The aim was to synthesise a polymer **183** from an NDI monomer **182** using the ATRP technique. This polymer **183** would then be used as a macroinitiator in a polymerisation with a terthiophene monomer **184** and a carbazole monomer **185** giving the donor-acceptor block co-polymers **186** and **187** (Scheme 53). A second target was a donor-acceptor polymer based on P3HT **11** and NDI monomer **182** coupled together using the click reaction to give the polymer **188** (Figure 85).

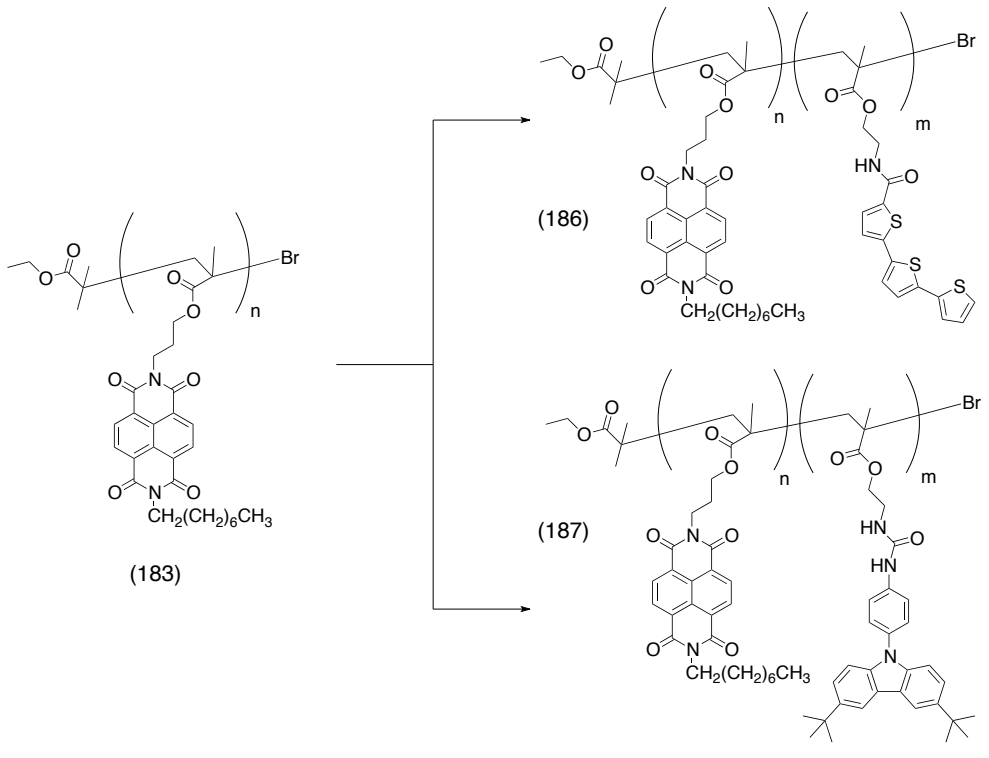

Scheme 53 Donor-Acceptor Block Co-Polymer targets

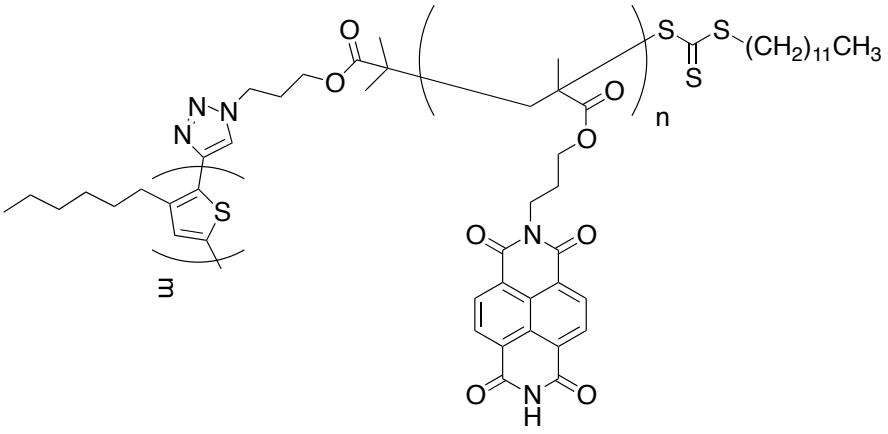

(188)

Figure 85 Structure of polymer 188

A final target involved a donor-donor block co-polymer **190** based on tetrathiafulvalene (TTF) **189**, a donor group (Figure 86). However, TTF **189** has never been used in a polymer using the ATRP technique. The aim was to show that the ATRP technique could be used with this monomer and the unreacted monomer could be recovered from the reactions.

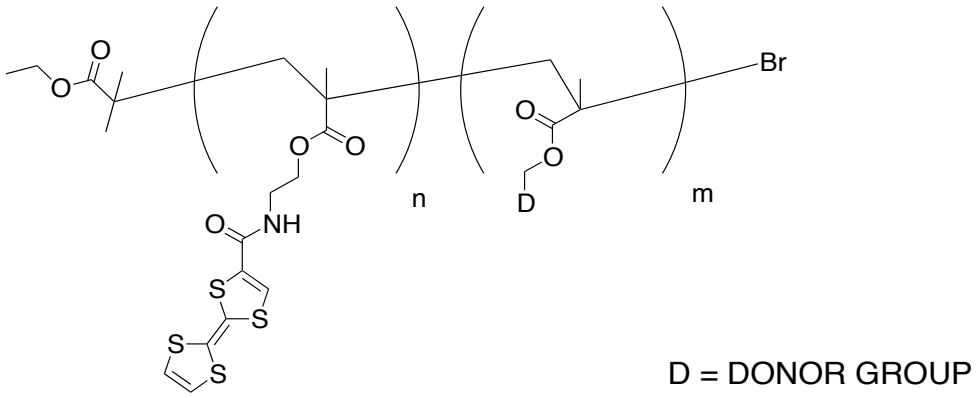

Figure 86 Block Co-Polymer based upon 190

4.2.2 Conjugated Polymers Featuring Recognition Units

Polythiophene is already a well documented compound for use in polymer solar cells. The aim of this project was to synthesise a new range of polythiophenes, which would incorporate a diaminopyridine group as a recognition site for interaction with another polythiophene through H-bonding and π- π interactions in order to devise a structure with the ability to self assemble. The target structure for this conjugated polymer can be seen in Figure 87, the aim was to synthesise a polymer **193** consisting of two

monomers, 3-hexylthiophene **191** and a second DAP functionalised thiophene **192** and use a controlled polymerisation technique to couple the two together.

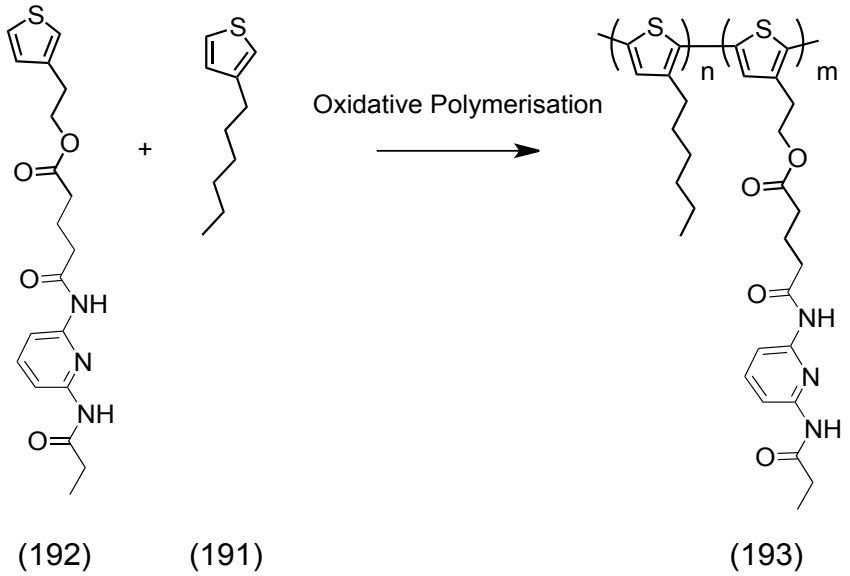

Figure 87 Proposed strategy for the synthesis of target polymer 193

4.3 Results and Discussion

4.3.1 Synthesis of Donor-Acceptor Block Co-Polymer

4.3.1.1 Synthesis of NDI monomer and polymerisation

The first stage of the synthesis was to synthesise the monomers. The NDI incorporating monomer **182** was synthesised from 1,4,5,8-naphthalene tetracarboxylic dianhydride **160** and in a one-pot reaction with octylamine and 1-amino-3-propanol to yield the N-(propanol)-N'-(octyl) naphthalene diimide **194** in poor yield. Due to the poor yield, and problems with this reaction, NDI-alcohol from a colleague in the group was used. This was then converted to the methacrylate monomer **182** in good yield using methacrolyl chloride (Scheme 54)

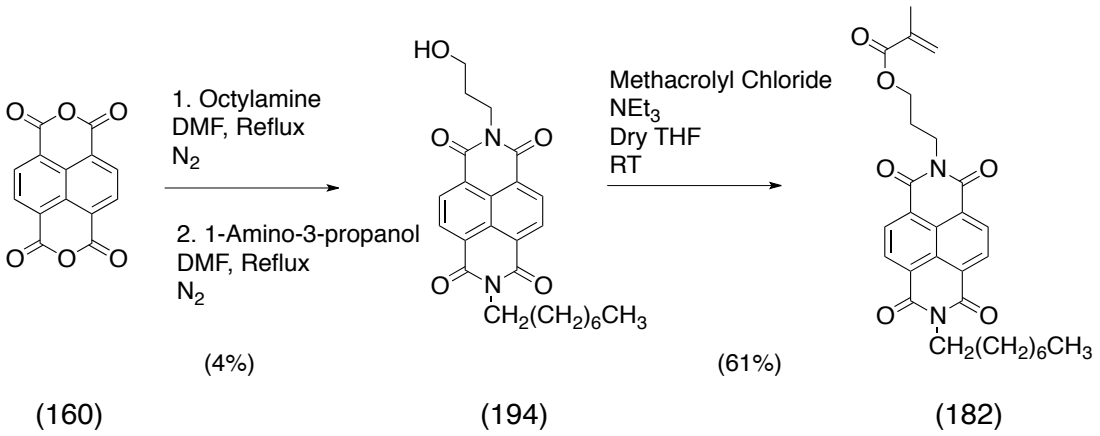

Scheme 54 Synthesis of 182

The first attempts at polymerisation were carried out using the ATRP technique. NDI-methacrylate, Cu(I)Cl, Cu(II)Br_2 and PMDETA in anisole were subjected to three cycles of degassing through the freeze-pump-thaw method. The flask was then transferred to a pre-heated oil bath set at 70°C and the ethyl bromoisobutyrate initiator added (Scheme 55). The polymerisation was monitored every 30 minutes using GPC. Unfortunately, the polymerisation was not occurring and the solvent was changed. ATRP was then attempted using DMF as a solvent. After two hours, the polymerisation did not appear to be proceeding and copper powder was added in an attempt to assist in the reaction. After an hour, the polymerisation had reached a 73% conversion and was precipitated into methanol. However, following purification using column chromatography, the recovery was very low at only 55 milligrams (11% yield) of polymer **183** (Scheme 55).

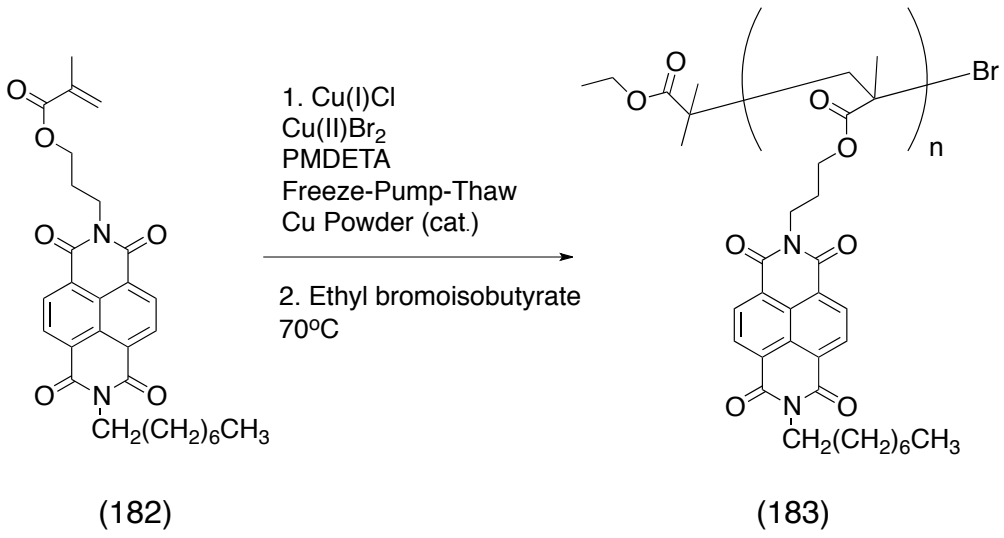

Scheme 55 ATRP of 182

A final attempt to polymerise monomer **182** using ATRP was carried out using only a catalytic amount of copper powder with PMDETA in DMF. However, the conversion was very low at only 12%. After precipitation, purification was attempted using a soxhlet method. However, this proved unsuccessful with only starting material recovered.

Due to the unsuccessful attempts using ATRP, the method was switched to the RAFT polymerisation technique. Monomer **182**, AIBN and 2-cyano-2-propyldodecyl trithiocarbonate as the RAFT agent were dissolved in toluene and subjected to three cycles of freeze-pump-thaw degassing before transfer to a pre-heated oil bath (Scheme 56). These conditions were attempted several times and the results are included in Table 5.

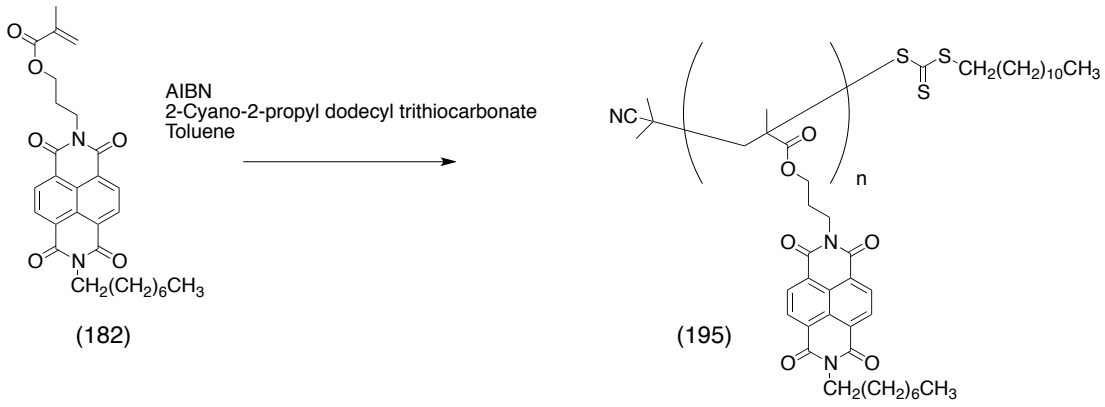

Scheme 56 First attempt at RAFT polymerisation of monomer 182

Table 5 RAFT polymerisation attempts using 2-cyano-2-propyl dodecyl trithiocarbonate

Amount 182 (g)	Time (hr)	Purification	Recovery (g)	M_n & PDI
0.5	3	Soxhlet	0.0182	7396, 1.74
0.5	5	Soxhlet & Column	0.0138	22616, 3.62
0.5	2	Soxhlet	0.016	9550, 2.54
1.0	3	Soxhlet &Column	0.0326	42956, 1.27

These attempts showed both poor recovery of material after purification and inconsistent results in terms of the M_n and PDI values. It was thought that this could be due to incompatibility with the RAFT agent chosen. Therefore, a new RAFT agent

was used, 2-cyano-2-propyl benzodithioate. Investigations also showed that 1,2-dichlorobenzene proved a better solvent in terms of solubility of the NDI monomer **182** over toluene. The polymerisation was performed in dark conditions and took 3.5 hours, giving a conversion of 55%, M_n of 8168, M_w of 9038 and a PDI of 1.1 and after purification, using soxhlet conditions, gave polymer **196** in good yield (Scheme 57). After the successful synthesis of polymer **196**, the focus was switched to the donor polymers.

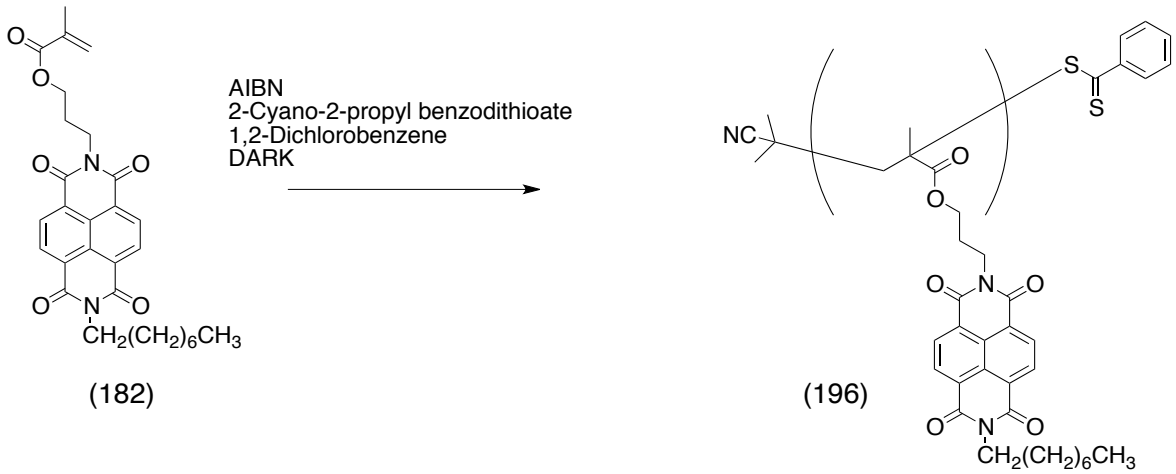

Scheme 57 Successful RAFT polymerisation of monomer 182

4.3.1.2 Donor monomers

The first of the donor monomers to be synthesised was a terthiophene monomer **184**. The synthesis started from 2,2′:5′,2″-terthiophene **197** which was deprotonated using *n*-butyl lithium followed by reaction with 2-isocyanatoethyl methacrylate to give the monomer **184** in moderate yield (Scheme 58)

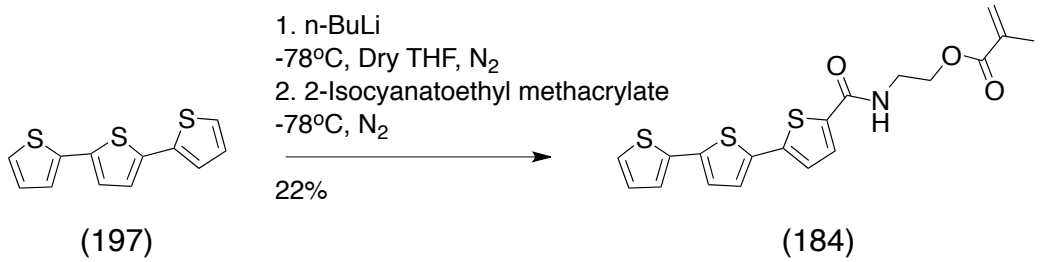

Scheme 58 Synthesis of monomer 184

The second donor monomer was a carbazole monomer **185**. The synthesis started with the Friedel-Crafts alkylation of carbazole **111** with tertiarybutylchloride and aluminium trichloride giving the alkylated carbazole **112** in good yield for the reaction. The next step was to couple at the N position with 1-iodo-4-nitrobenzene

199 using rubidium carbonate, palladium acetate and tri-tertiarybutylphosphine giving the *N*-(nitrobenzene)-3,6-di-^{t}Bu-carbazole **198** in high yield. The final two steps involved reduction of the nitro group using palladium on carbon and ammonium formate to give the amine **200**, which was used without purification in the reaction with 2-isocyanatoethyl methacrylate, which appeared to give monomer **185** in good yield.

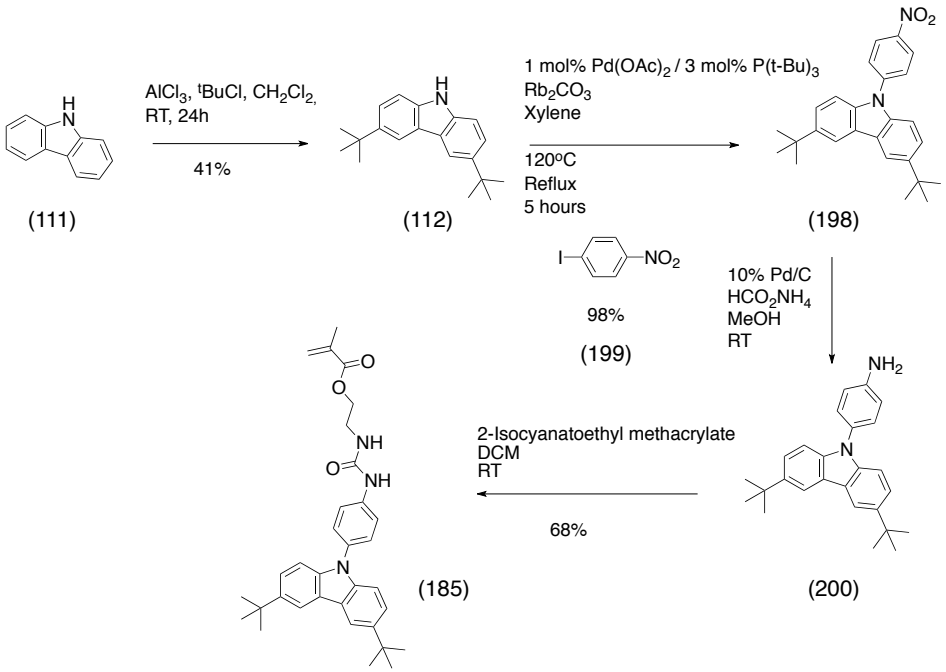

Scheme 59 Synthesis of monomer 185

However, although the ^{1}H NMR was very clean and showed all the expected peaks analysis by mass spectrometry indicated that in fact the final compound was not achieved. The final two steps were repeated using the same reduction conditions and used without purification in the methacrylate reaction and again the ^{1}H NMR and the mass spectrometry analysis showed a discrepancy. It was thought that perhaps the reduction step was the problem and a new method was attempted to reduce the nitro group using $SnCl_2$ with sonication. Thin layer chromatography indicated that the reduction had occurred and the final step was carried out. However, this did not solve the problem. A full summary of the reduction conditions attempted can be found in Table 6. In each instance, thin layer chromatography indicated that reduction had occurred, however, when the final methacrylate reaction was carried out, although the ^{1}H NMR looked promising, the mass spectrometry analysis showed no evidence of the final product.

Table 6 Reduction conditions for reducing nitro group to amine

Conditions	Equivalents	Solvent	Time
10% Pd/C, HCO_2NH_4, Acetic Acid	0.1, 10, one drop	MeOH	3 days
10% Pd/C, Hydrazine	0.1, 10	MeOH	Overnight
10% Pd/C, HCO_2NH_4, Acetic Acid, Hydrazine	0.1, 10, one drop, 1.0 mL	MeOH	Overnight
10% Pd/C, HCO_2NH_4, Acetic Acid	0.1, 10, 1.0 mL	MeOH	Overnight
10% Pd/C, HCO_2NH_4	0.1, 20	MeOH	Overnight
$SnCl_2$	20	EtOH	2hr
10% Pd/C, Hydrazine, 40ºC	0.1, 10	MeOH	Overnight
10% Pd/C, HCO_2NH_4	0.1, 20	DMF	Overnight

On examination of the mass spectrometry analysis, there was no evidence of the ion for compound **198** or the reduced aniline **200**. There is, however, a molecular ion peak present for the carbazole **112** alone. This could indicate that there was a cleaving of the N-aryl bond occurring. Due to the problems with producing this monomer, focus was directed towards the terthiophene monomer **184** and the polymerisation from this monomer.

4.3.1.3 Block Co-Polymer Synthesis

With the terthiophene monomer **184** synthesised, an attempt at a block co-polymer synthesis was attempted using polymer **196** as a macroinitiator. Monomer **184** was dissolved in 1,2-dichlorobenzene with the RAFT agent, 2-cyano-2-propyl benzodithioate and polymer **196** with AIBN (Scheme 60). After degassing with three cycles of the freeze-pump-thaw method, the mixture was transferred to a pre-heated oil bath and monitored every 30 minutes. After 4 hours, there was no evidence of the co-polymer **186** forming and thus the polymerisation was terminated.

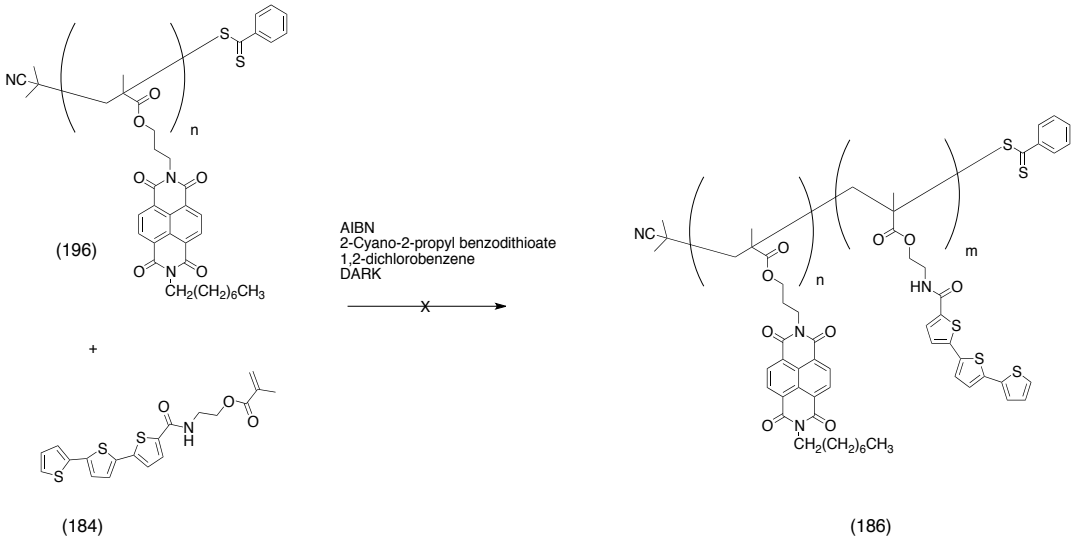

Scheme 60 Attempts at synthesis of a Donor-Acceptor block co-polymer 186

4.3.1.3.1 Click Methodology

The new strategy devised was to use click chemistry to join two polymers together. To begin with, initial investigations were carried out using click chemistry. This started with the synthesis of *N*,*N*'-(di-propy-1-nyl)-naphthalene diimide **201**. 1,4,5,8-Naphthalenetetracarboxylicdianhydride **160** was reacted with propargyl amine in DMF to give compound **201** in good yield (Scheme 61).

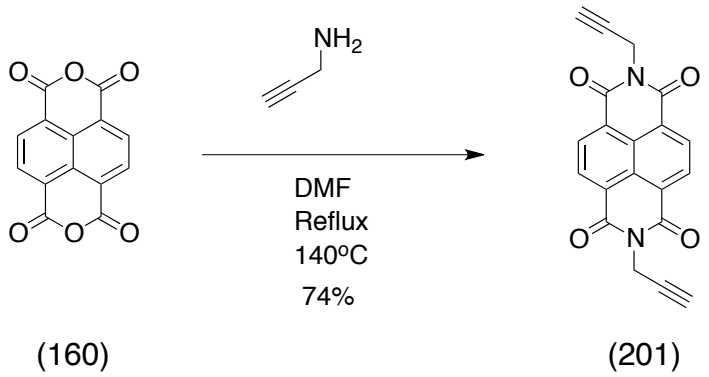

Scheme 61 Synthesis of compound 201

Compound **201** was then reacted with benzyl azide to produce the triazole linker (Scheme 62). ^{1}H NMR confirmed the presence of the triazole, however, purification of this compound was problematic due to the insolubility of the structure.

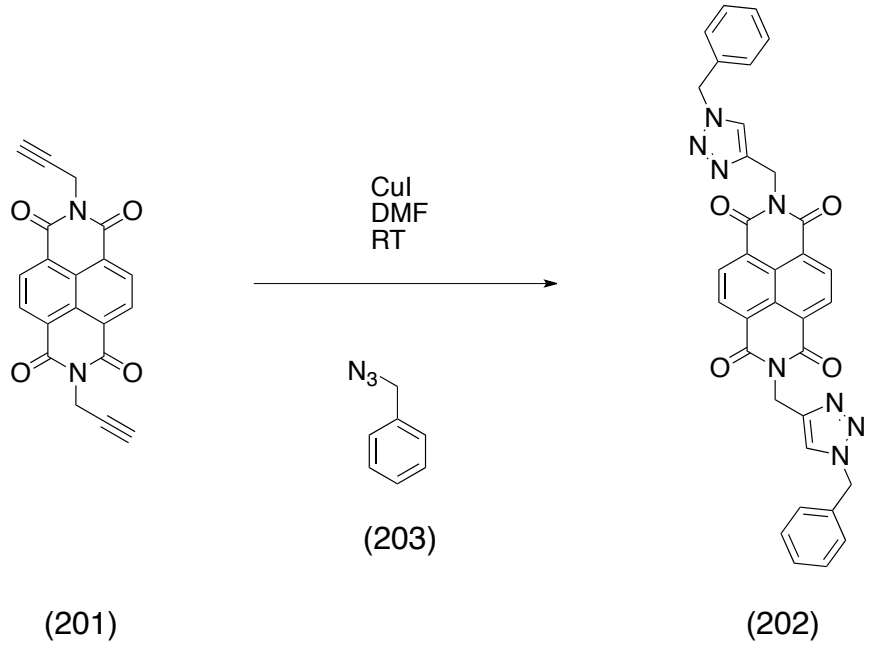

Scheme 62 Synthesis of compound 202

4.3.1.3.2 Synthesis of a clicked block acceptor-donor co-polymer

The synthesis of the clicked block co-polymer began by first synthesising a donor polymer incorporating an alkyne moiety using the Grignard metathesis method.[105] The polymerisation occurred using 2,5-dibromo-3-hexylthiophene **204**, isopropylmagnesium chloride, Ni(dppp)Cl_2 and ethynylmagnesium bromide to give a poly-hexyl thiophene with an alkyne end group (polymer **205**) (Scheme 63). The P3HT was chosen as the donor half as it is already well-known as donor material for photovoltaics, it is highlighted below in red for distinction when coupled with an acceptor compound, discussed later.

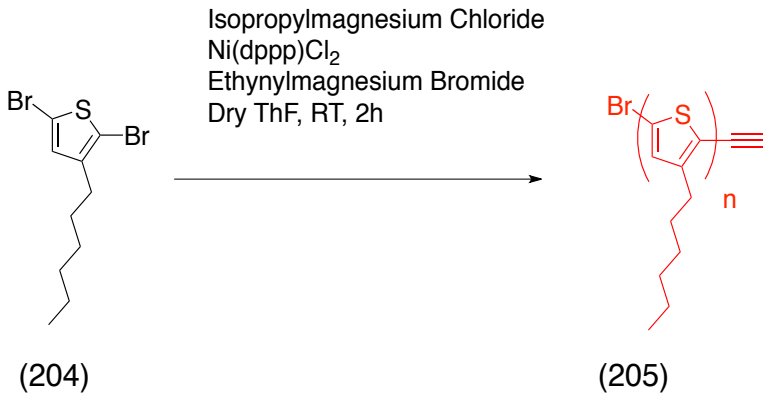

Scheme 63 Synthesis of alkyne-end capped P3HT 205

With the donor polymer **205** synthesised, the next step was to synthesise an acceptor incorporating polymer with an azide end group **206**. The polymerisation involved the use of AIBN as an initiator and 2-(dodecylthiocarbonothioylthio)-2-methyl propionic acid 3-azido-1-propanol ester as the RAFT agent **207** (Scheme 64). This reaction was performed twice and produced two novel NDI polymers **206**, the data of which can be found in Table 7. This polymer has been highlighted blue in order to distinguish the acceptor moiety when later coupled with a donor group.

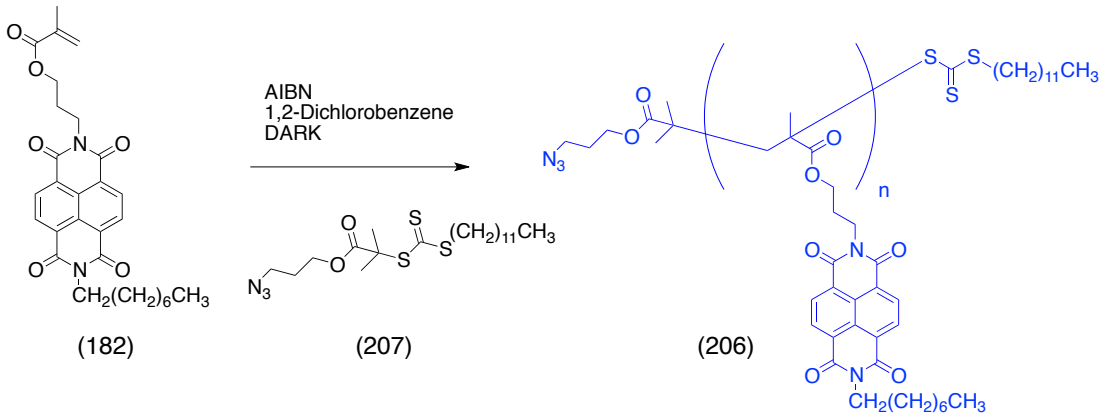

Scheme 64 Synthesis of polymer 206

Table 7 Data obtained for RAFT polymerisation of 182

Polymer	Reaction time (hrs)	Conversion	M_n	M_w	PDI
206a	2.5	53%	21135	28059	1.3
206b	1.5	56%	59503	86623	1.4

The final step was to couple the two polymers together using a Huisgen 1,3-dipolar cycloaddition "click" reaction. Polymers **206** and **205** were mixed with Cu(I)Br and PMDETA in dry THF for 3 days (Scheme 65). The reaction was monitored by GPC where the decrease from the original polymer and the emergence of a new polymer peak is evident (Figure 88). This polymerisation was performed twice using the two different NDI polymers (polymer **206a** and polymer **206b**) and polymer **205** and gave good recovery of polymer **188** after purification using column chromatography with aluminium oxide with a narrow PDI. The results from the two reactions are summarised in Table 8.

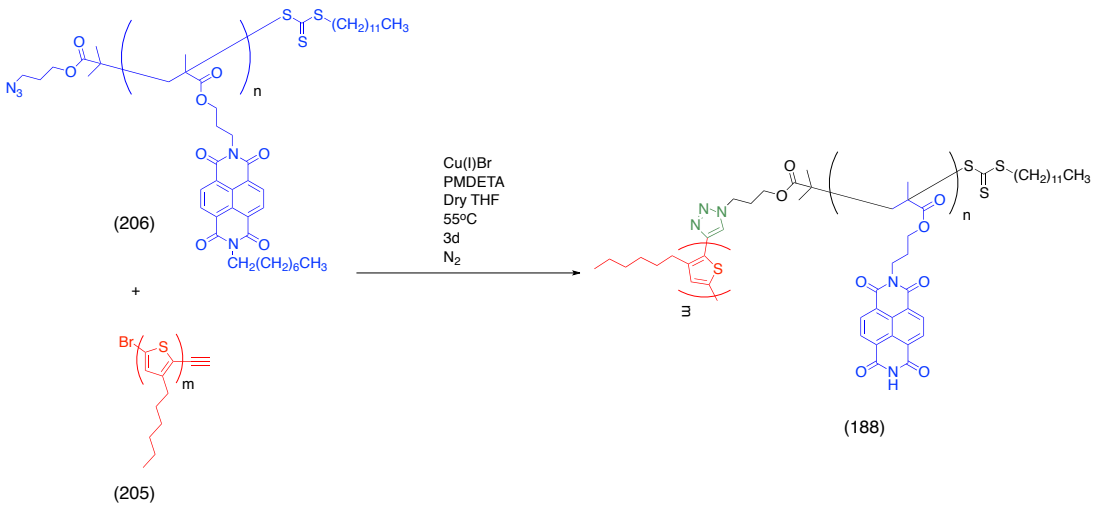

Scheme 65 Clicked polymerisation of 205 and 206 giving target polymer 188

Table 8 Data for the clicked polymerisations

Reaction	206 M_n	205 M_n	Clicked M_n	Clicked M_w	PDI
1	21135	6021	24029	30100	1.2
2	59503	6021	79828	104469	1.3

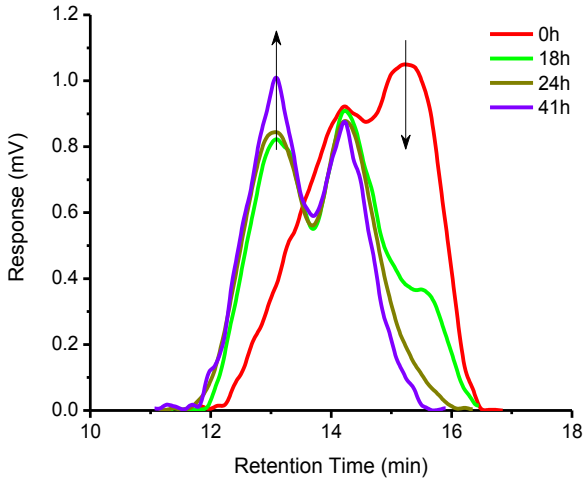

Figure 88 GPC monitoring the progress of the clicked polymerisation between polymer 205 and polymer 206

4.3.1.3.3 UV/Vis and Fluorescence Spectroscopy

UV/Vis and fluorescence spectroscopy were performed on each of the clicked polymers along with the individual polymers used for the click reaction. The samples were run at concentrations of 10^{-4}M and fluorescence at concentrations of 10^{-5}M in

CH_2Cl_2. The NDI polymer **206**, however, was highly UV active and highly fluorescent, thus concentrations of 10^{-5}M and 10^{-7}M were used respectively. Figure 89 shows the UV/Visspectrum of polymer **205**, here it can be seen that there is a broad absorbance at 446 nm, which is typical for polythiophene compounds. Fluorescence spectroscopy experiments on the polymer **205** compound showed limited fluorescence.

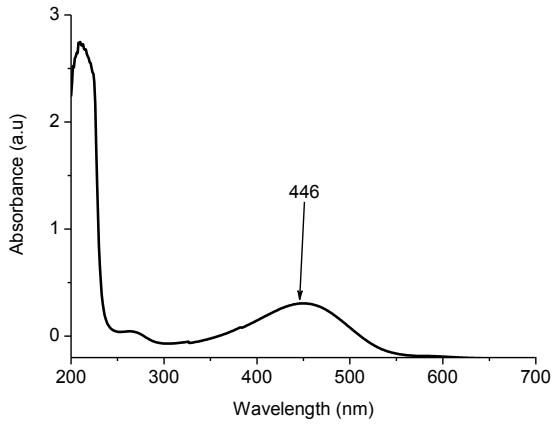

Figure 89 UV/Vis spectrum of 205 at concentration 10^{-4}M in CH_2Cl_2

The UV/Vis and fluorescene spectra for polymer **206** can be seen in Figures 90 and 91. The polymer was highly UV active and highly fluorescent thus the sample needed to be diluted to a greater extent than that of polymer **205**. From the UV/Vis spectrum, it can be seen that there are three main absorbances observed at 235, 361 and 382 nm. It can be seen from the fluorescence spectrum that there is a very strong emission at 497 nm when excited at 360 nm. The two different NDI polymers **206** synthesised gave identical UV/Vis and fluorescence spectra.

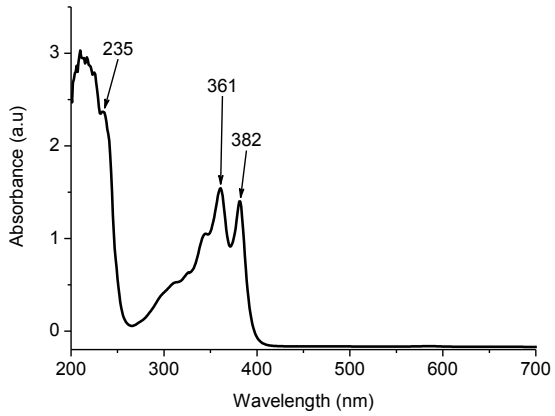

Figure 90 UV/Vis spectrum of polymer 206 at concentration 10^{-5}M in CH_2Cl_2

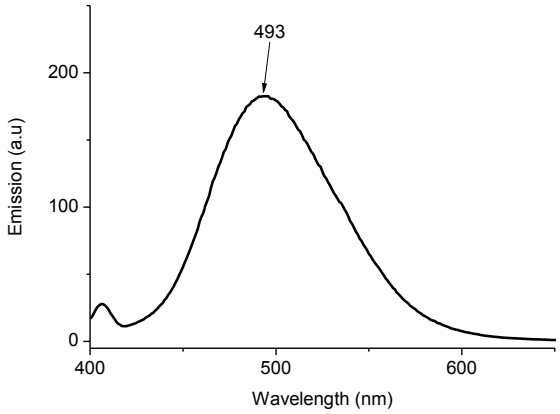

Figure 91 Emission spectrum of polymer 206 at concentration 10^{-7}M in CH_2Cl_2 when excited at 361 nm

Following the clicked polymerisation, the UV/Vis activity is retained with all four absorbances seen at 236, 361, 382 and 459 nm (Figure 92). The fluorescence spectrum gave the most interesting observation. The fluorescence, from the NDI moiety, is quenched by the P3HT moiety. The spectrum (Figure 93) was obtained with a sample at a higher concentration, 10^{-5}M, and yet it shows the same level of emission. This quenching is most likely due to π-π interactions between the two halves of the polymer. This is also a good indicator that the polymer does indeed self assemble.

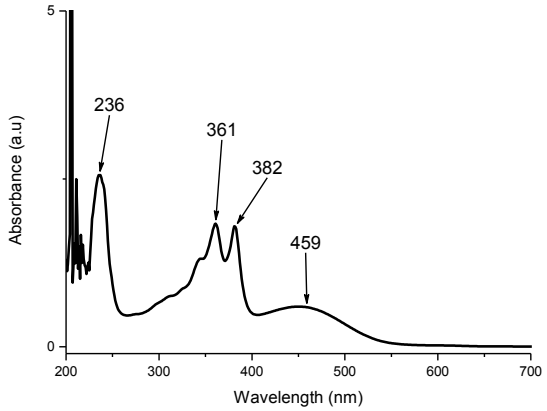

Figure 92 UV spectrum of polymer 188 at concentration 10^{-4}M in CH_2Cl_2

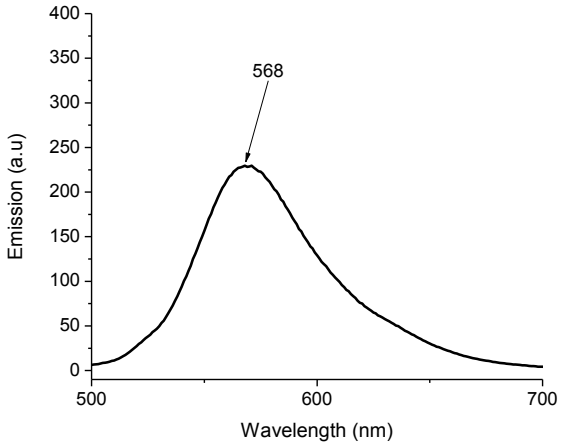

Figure 93 Emission spectrum of the polymer 188 when excited at 450 nm

4.3.1.3.4 Cyclc Voltammetry (CV) and Square Wave Voltammetry (SWV)

CV and SWV were performed at 0.5 mM concentrations using 0.1M TBA.PF_6 as the electrolyte. The LUMO level energy was calculated using the formula –[4.8 – $(E_{1/2})_{red}$], where $(E_{1/2})_{red}$ is the onset of the reduction wave observed for the compound. The CV for polymer **188** can be observed in Figure 94. A redox wave can be observed with an $E_{1/2}$ of -1.14 eV corresponding to a LUMO energy value of -3.66 eV.

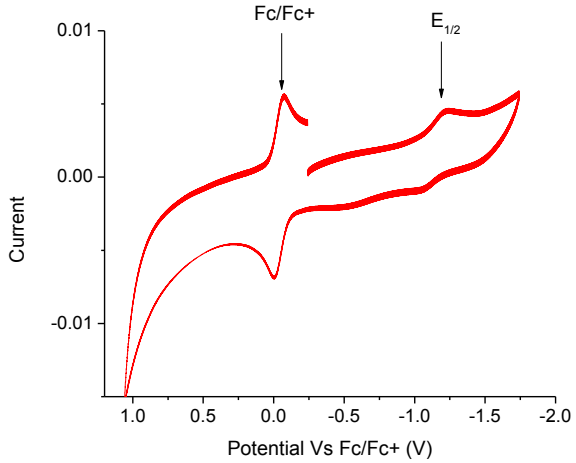

Figure 94 CV of polymer 188 recorded at a concentration of 0.5 mM in CH_2Cl_2, (0.1 M TBA.PF_6, platinum working electrode, platinum wire counter electrode and silver reference electrode, reference to Fc/Fc^+ = 0.0eV)

Along with cyclic voltammetry, square wave voltammetry was also performed in order to better see the redox activity of the polymer. The SWV for the polymer **188** can be observed in Figure 95. Here, two redox waves can be seen with $E_{1/2}$ values of -1.07 eV and -1.48 eV corresponding to LUMO energy values of -3.73 eV and -3.32 eV respectively.

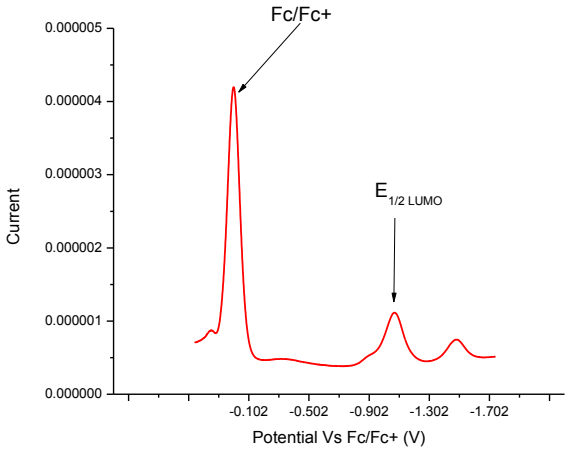

Figure 95 Square wave voltammetry of polymer 188 recorded at a concentration of 0.5 mM in CH_2Cl_2, (0.1 M TBA.PF_6, platinum working electrode, platinum wire counter electrode and silver reference electrode, reference to Fc/Fc^+ = 0.0eV)

4.3.1.3.5 AFM Imaging

4.3.1.3.5.1 Sample preparation

AFM imaging was carried out by colleagues in the School of Physics at the University of Glasgow[112]. The polymer was prepared in THF solution at 5 mg/mL. The images shown in Figure 96 were achieved using the drop casting techique where the solution was drop casted onto cleaned Si/SiOx substrate heated to 80°C using a Linkam hot stage. After drying, the sample was annealed at 80°C for a further five minutes. The images shown in Figure 97 were achieved from a sample which had been drop casted onto substrate at room temperature without annealing. The image in Figure 98 was achieved from a sample drop casted onto substrate at room temperature then after drying baked at 80 - 150°C in increments of 5°C, held at each temperature for 30s.

4.3.1.3.5.2 AFM characterisation

AFM characterisation was performed using an NT-MDT Solver Next in tapping mode with CSG10/Au and FMG01 probes purchased from NT-MDT. Figure 96a shows a typical region of the sample. Across the image, a predominantly amorphous film can be seen with an apparent network of 'spaghetti-like' crystallites in the centre. Figures 96(b) and (c) show higher resolution scans of the region in (a), indicated by the blue box. The phase image in (c) clearly shows a marked phase difference of approximately 10° between the crystallites and the bulk film, strongly suggesting that the two have different chemical or mechanical properties[113].

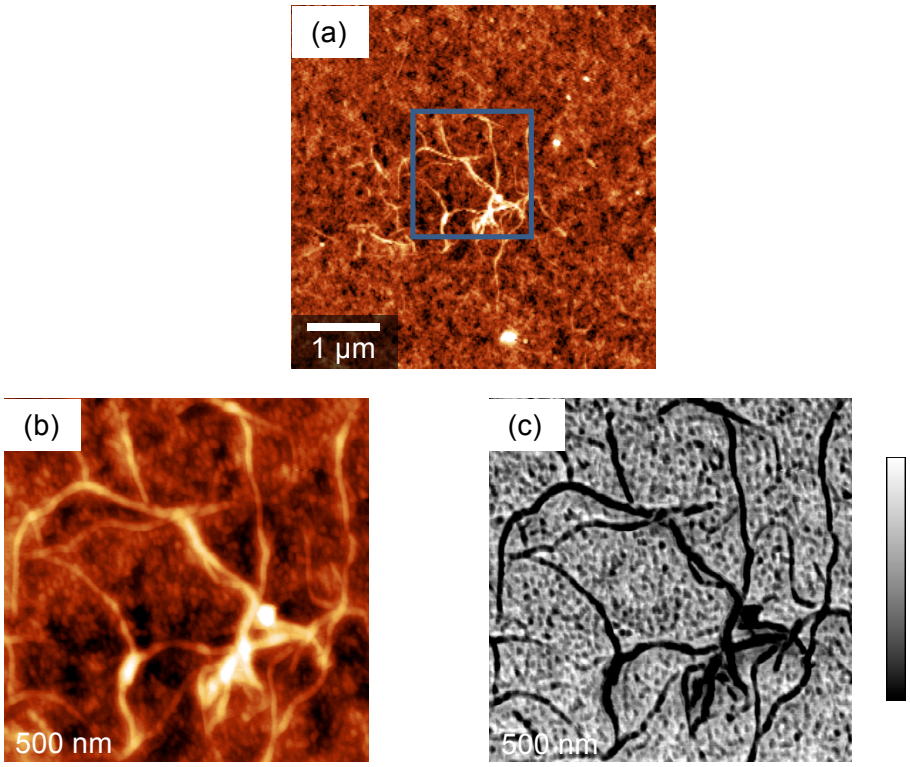

Figure 96 AFM imaging of polymer 188

In the absence of an annealing step, a surface layer was observed and the presence of 'spaghetti' crystallites was diminished with much straighter, more rod-like, crystallites being prevalent, as can be observed in Figure 98. It seems likely that this surface layer arises due to residual solvent which was subsequently driven off by annealing. This is supported by the AFM phase image in Figure 97(b) which shows a notable phase difference between this layer and the underlying film. It is noted that there is little or no discernable difference in height between the two layers from the topography in Figure 97(a) and so a height influence of the phase can be excluded. The change in morphology between the unannealed and annealed samples is interesting as it appears that there is significant reorganisation. The discrete rod-like crystallites of Figures 97(c and d) appear to curl up and form a network of 'spaghetti-like' crystallites as in Figure 98. We can discount the faster drying time due to the substrate being held at 80°C as being the sole reason for this change as we see similar 'spaghetti-like' morphologies when the material is allowed to dry at room temperature before being heated from 80 to 150°C in increments of 5°C.

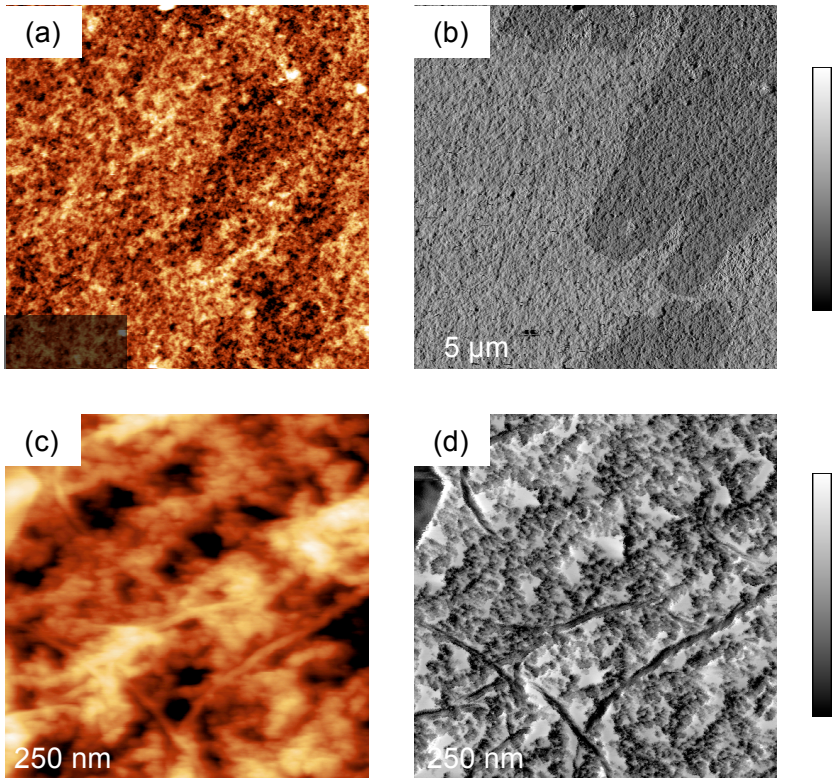

Figure 97 AFM imaging of polymer 188

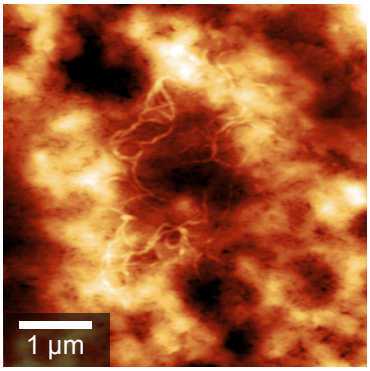

Figure 98 AFM imaging of polymer 188

Following the completion of the AFM imaging, further studies are to be carried out. Collaborators in Prof. V. Rotello's group at the University of Massachusetts Amherst will obtain small-angle X-ray scattering in order to further characterise the polymer and Prof. I. Samuel's group at the University of St. Andrew's will investigate the photovoltaic properties and photo physics of the polymer. Samples have been sent and results are pending.

4.3.2 Donor Block Polymers and Co-Polymers

First attempts to synthesise a donor block polymer began with an ATRP attempt of terthiophene monomer **184**. The polymerisation used Cu(I)Cl, Cu(II)Br_2, PMDETA and EBIB as the initiator (Scheme 66). However, after 48 hours the conversion was only 15% and after isolation only a few milligrams were recovered.

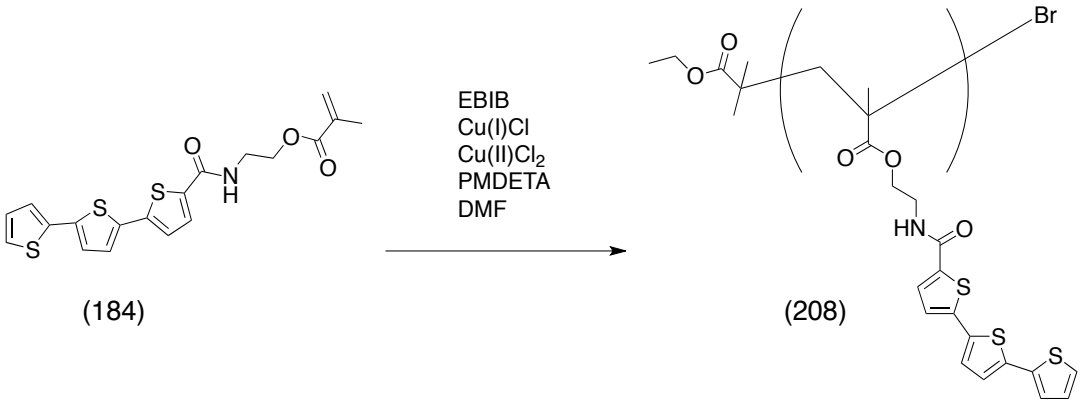

(184) (208)

Scheme 66 ATRP attempt with monomer 184

After the unsuccessful recovery from the ATRP reaction, the method was switched to RAFT polymerisation. The first attempt was to use AIBN as initiator and 2-cyano-2-propyl dodecyl trithiocarbonate as the RAFT agent (Scheme 67). GPC monitoring appeared to show the successful formation of a polymer with an M_n of 24365, however, the peak was very broad with a PDI of 1.63. Recovery after precipitation and soxhlet separations again proved very low with only around 40 mg recovery achieved.

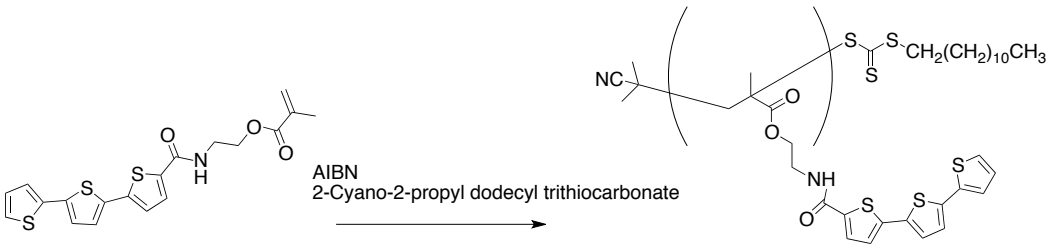

(184) (209)

Scheme 67 First attempt at RAFT polymerisation of monomer 184

With RAFT polymerisation showing to be the most viable option and the successful polymerisation of the NDI monomer **182** using 2-cyano-2-propyl benzothioate as a RAFT agent, these conditions were used with terthiophene monomer **184** (Scheme

68). The polymerisation occurred over 3 hours with a good recovery of polymer, however, GPC data showed a very large polymer with a M_n value of >100,000 and a very broad dispersion. Thin layer chromatography of the monomer showed a new product had appeared on the baseline and thus it was theorised that the monomer had self-polymerised. Although the reaction showed a skewed result, these conditions appear to be a good option for this monomer and further work should be carried out to investigate this.

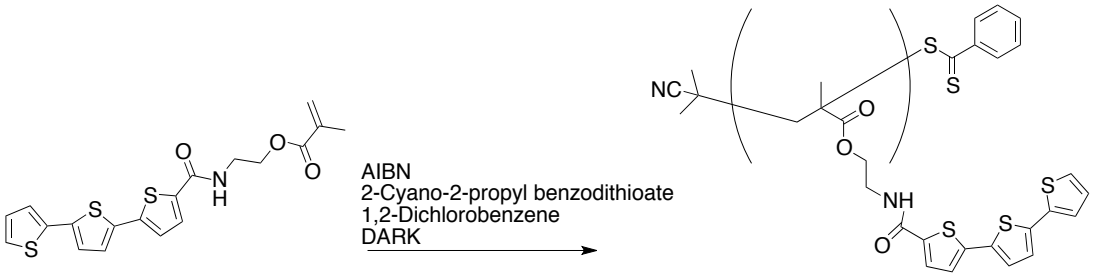

(184) (210)

Scheme 68 RAFT polymerisation of monomer 184

The final target for a non-conjugated polymer was to synthesise a block co-polymer with a tetrathiafulvalene moiety. This started with the synthesis of a tetrathiafulvalene monomer. Tetrathiafulvalene **189** was deprotonated using *n*-butyllithium followed by a reaction with 2-isocyanatoethyl methacrylate to yield compound **211**.

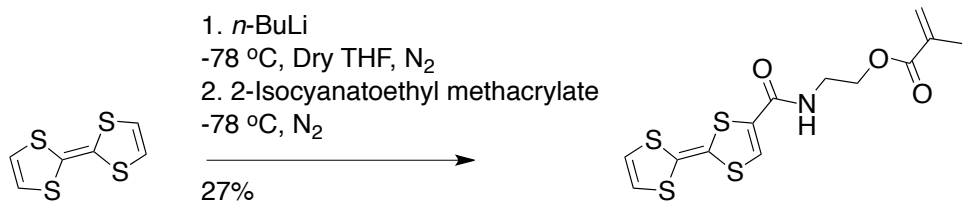

(189) (211)

Scheme 69 Synthesis of monomer 211

Following the synthesis of the monomer, the next stage was the ATRP with a second monomer. A variety of attempts were made using different monomers; NIPAM, styrene, benzyl methacrylate and the tetrathiafulvalene monomer alone. With the NIPAM and styrene reactions, the GPC showed that no polymerisation was occurring. The same problem arose with the polymerisation of tetrathiafulvalene monomer alone. The most promising second monomer proved to be benzyl methacrylate,

however, an issue arose when attempting to recover the polymer. Many purification methods were attempted including precipitation, column chromatography and centrifugation. However, the main issue was the separation of the polymer and the tetrathiafulvalene methacrylate. After many attempts, the target polymer was synthesised using benzyl methacrylate as co-polymer, and a combination of two precipitations, an extraction and column chromatography to separate the monomer and the polymer. Along with the successful recovery of polymer **190**, the unreacted tetrathiafulvalene monomer **211** was also recovered. Although the polymerisation was successful, further development is required to optimise the reaction.

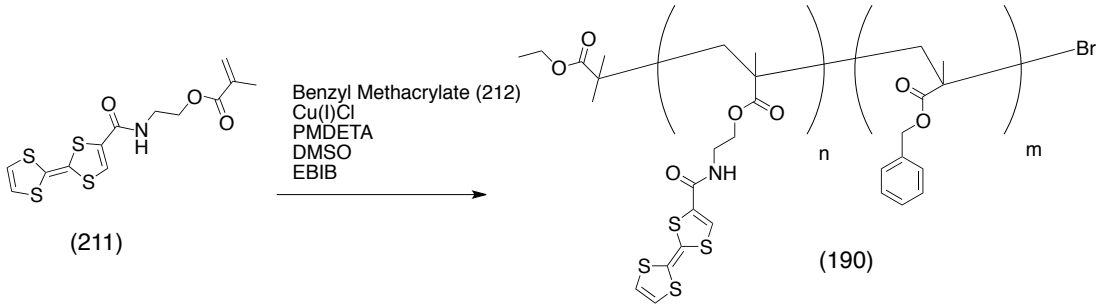

Scheme 70 ATRP of monomer 211 and monomer 212

4.3.2.1 UV/Vis and fluorescence spectroscopy

UV/Vis spectroscopy was performed at a concentration of 10^{-4}M in CH_2Cl_2. Figure 99 shows the UV/Vis spectrum of polymer **190**. It was observed that there are three broad absorbances at 236, 307 and 377 nm

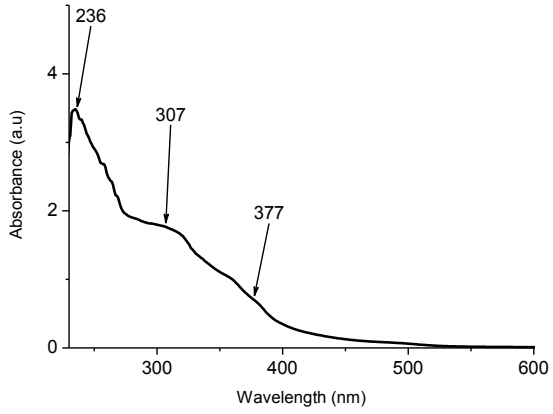

Figure 99 UV/Vis spectrum of polymer 190 recorded at a concentration of 1 x 10^{-4}M in CH_2Cl_2

4.3.2.2 Cyclic voltammetry and Square Wave voltammetry

CV and SWV were performed at 0.5 mM concentrations using 0.1 M TBA.PF_6 as the electrolyte. The LUMO level energy was calculated using the formula –[4.8 – $(E_{1/2})_{red}$], where $(E_{1/2})_{red}$ is the onset of the reduction wave seen for the compound. The HOMO level energy was calculated using the formula –[4.8 – $(E_{1/2})_{ox}$], where $(E_{1/2})_{ox}$ is the onset of the oxidation wave seen for the compound The CV analysis for compound **190** is shown in Figure 100. Two redox waves can be seen with $E_{1/2}$ values of -2.08 eV and -2.59 eV corresponding to two LUMO values of -2.72 eV and -2.21 eV respectively. The $E_{1/2}$ wave at 0.3 eV corresponded to a HOMO value of -5.10eV (Figure 101).

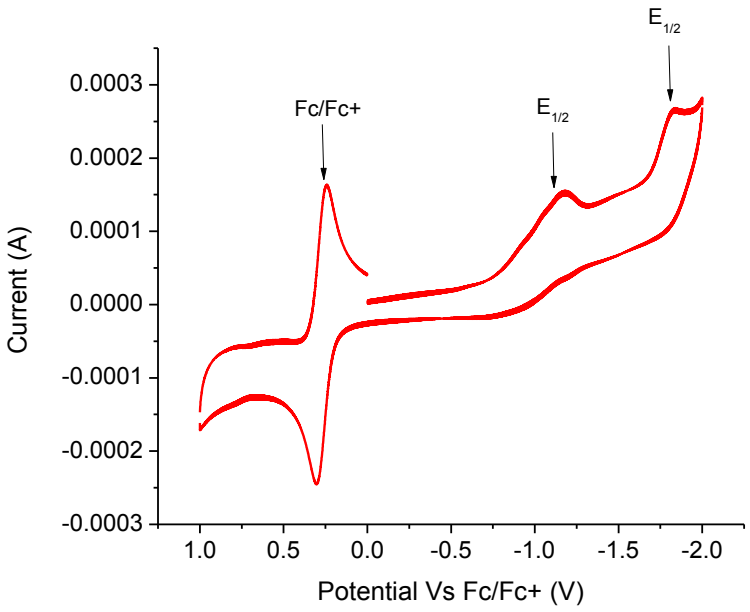

Figure 100 CV of compound 190 recorded at a concentration of 0.5 mM in CH_2Cl_2, (0.1 M TBA.PF_6, platinum working electrode, platinum wire counter electrode and silver reference electrode, reference to Fc/Fc^+ = 0.0 eV)

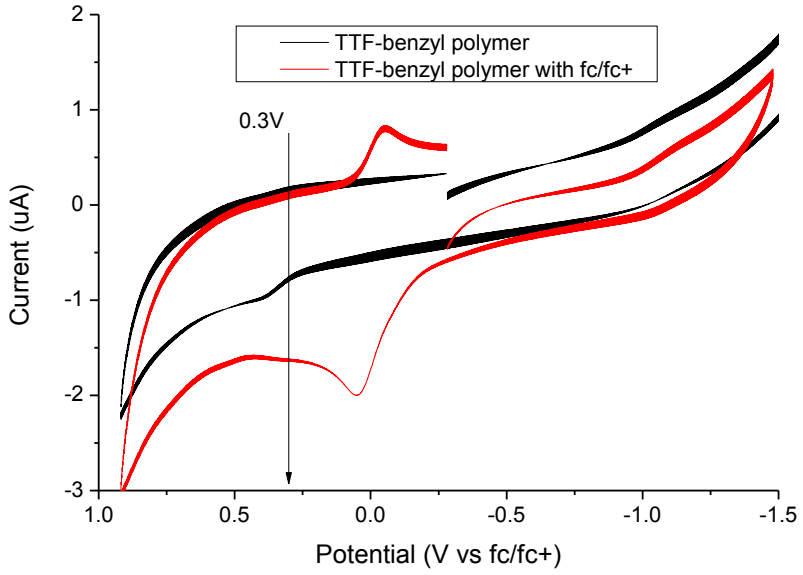

Figure 101 CV for compound 190 recorded at a concentration of 0.5 mM in CH_2Cl_2, (0.1 M TBA.PF_6, platinum working electrode, platinum wire counter electrode and silver reference electrode, reference to Fc/Fc^+ = 0.0 eV)

4.3.3 Conjugated polymers featuring recognition groups

The start of the project was to synthesise a monomer with a recognition group. The DAP moiety was chosen due to the possibility of 3-point hydrogen bonding.[114] The monomer **192** was synthesised from a coupling reaction between 2-thienyl ethanol (**213**) and 2-(Thiophen-3-yl)ethyl5-oxo-5-((6-propionamidopyridin-2-yl)amino) pentanoate **214** using standard esterification coupling reagents, EDCI and DMAP (Scheme 71).

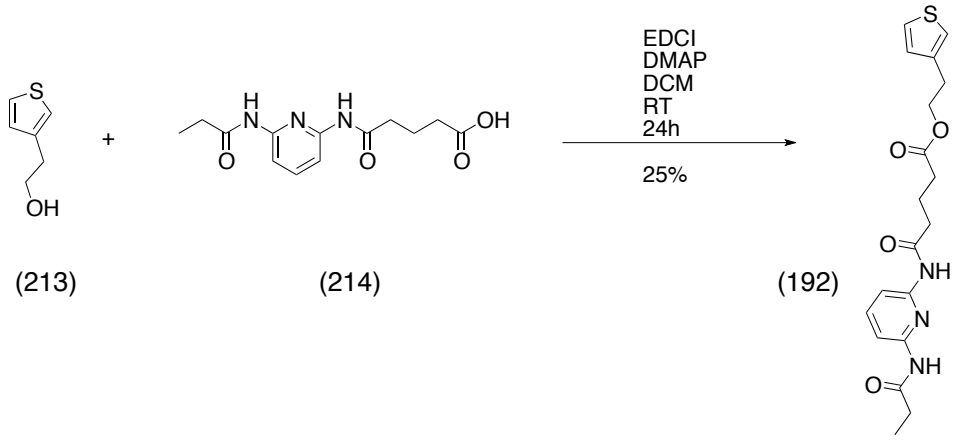

Scheme 71 Synthesis of monomer 192

With the monomer synthesised, the next step was oxidative polymerisation. The DAP monomer **192** and 3-hexylthiophene **191** were mixed together in a 20:80 mix with ferric chloride, carbon tetrachloride and nitromethane (Scheme 72). Following isolation after purification using soxhlet extractions, three separate polymers were recovered (Table 9) of varying M_n values and polydispersions typical of oxidative polymerisations. However, on examination of the ^1H NMR the ratio of monomers was at 7:1 rather than the 4:1 ratio expected. This is a very poor loading of the DAP monomer and a change in strategy was adopted.

Table 9 Data for three polymers obtained from oxidative polymerisation

Polymer	M_n	PDI
193a	33249	3.3
193b	38991	1.9
193c	43234	2.8

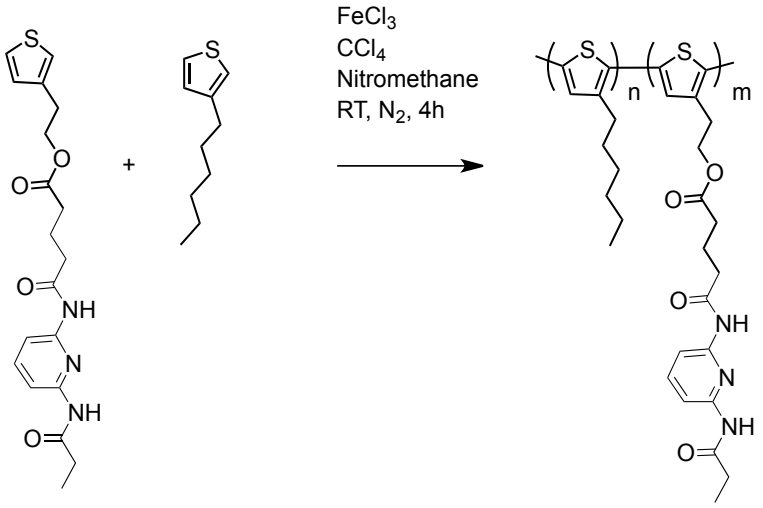

Scheme 72 Oxidative polymerisation of monomer 192 and 191

Following the poor loading from the oxidative polymerisation and the lack of compound **192**, a second monomer was synthesised **215**. The monomer **215** was synthesised using the same conditions as previously used (Scheme 73).

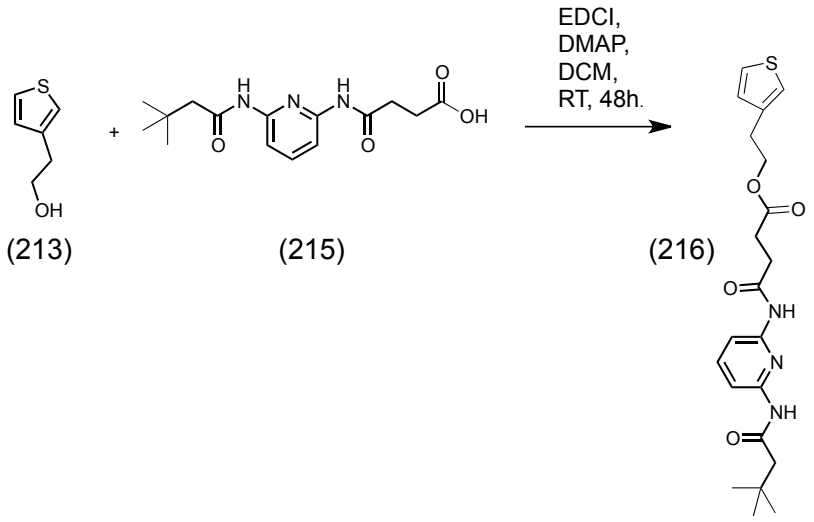

Scheme 73 Synthesis of monomer 216

Following the synthesis of the monomer a second oxidative polymerisation was attempted. Due to the poor loading previously seen, the reaction was performed using a 50:50 ratio of monomers (Scheme 74). After isolation from soxhlet extractions, a purple polymer **217** was recovered with an M_n of 24980 and a PDI = 2.4, however, due to the insolubility of the compound, further characterisation was not possible. Although there were issues with the two oxidative polymerisations, they indicate that a DAP incorporated polymer can be achieved with this type of polymerisation, however, further development is required.

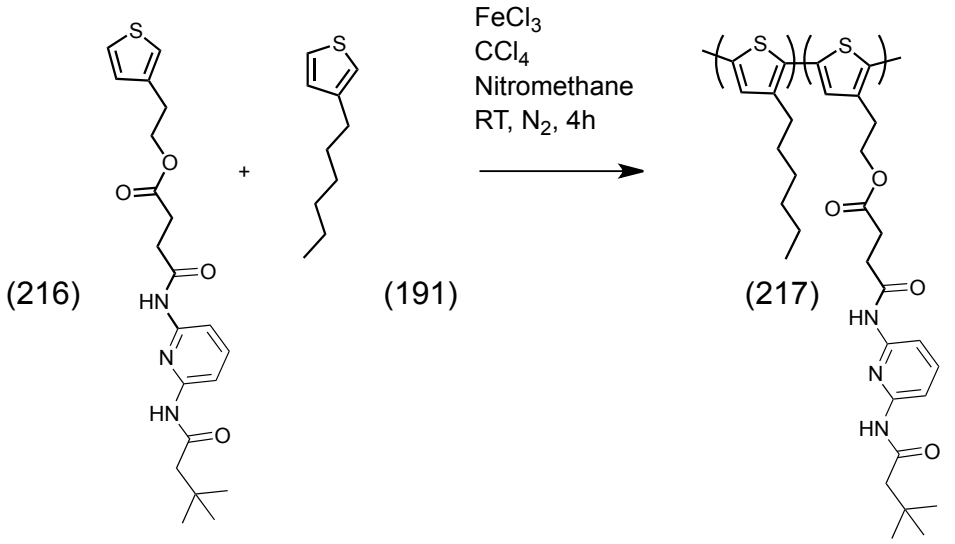

Scheme 74 Second oxidative polymerisation reaction with a 50:50 ratio of monomers

4.4 Conclusions and Future Work

A variety of methods were adopted in an attempt to synthesise a series of donor and acceptor block co-polymers, donor block co-polymers and conjugated polymers. The methodology was investigated to synthesise a novel NDI block co-polymer and results showed that RAFT polymerisation was the optimum method for this polymer. Along with the RAFT method, click methodology was also employed resulting in the synthesis of a novel NDI and P3HT block co-polymer. This compound has been sent to collaborators at the University of Massachusetts Amherst and the University of St Andrew's for further testing. A novel TTF incorporated block co-polymer was also successfully synthesised using ATRP. Further work is required to optimise this reaction and further testing required. Finally, two novel conjugated polymers were also synthesised incorporating a DAP moiety. Although the polymers were recovered, issues arose with the loading on the DAP monomer and also the solubility of the polymer. Further work is required to optimise this reaction and develop the recovery of the polymer and address the loading issues.

5.0 Synthesis of thiophene based star-shaped molecules and dye-sensitised solar cells

5.1 Introduction

5.1.1 Star-shaped structures

Thiophene-based structures are commonly used in organic electronics. Typically, polythiophenes are used in photovoltaics, transistors, batteries and as fluorescent and conductive materials in OLEDs.[115] However, the disadvantage of many polymers used in organic electronics is the low degree of crystallinity, which causes adverse affects in the film parameters, such as poor dispersion and poor morphology of the film.[116]

Star-shaped molecules have different electronic properties, morphologies and, unlike their linear counterparts, have the ability to organise into a supramolecular assembly.[117] The construction of these macromolecules, which due to the ability to self assemble, can form ordered structured films. They have proven a good alternative to the typical thiophene based organic electronics material.[118]

A study performed by Yevlampieva et al looked at star-shaped thiophene oligomers and dendrimers with a silicon atom centre, investigating the optical absorption and electro-optical molecular properties.[119] They synthesised a series of oligomers (Figure 102) and dendrimers (Figure 103), all with a silicon core and with a thiophene, bithiophene or terthiophene branched chain.

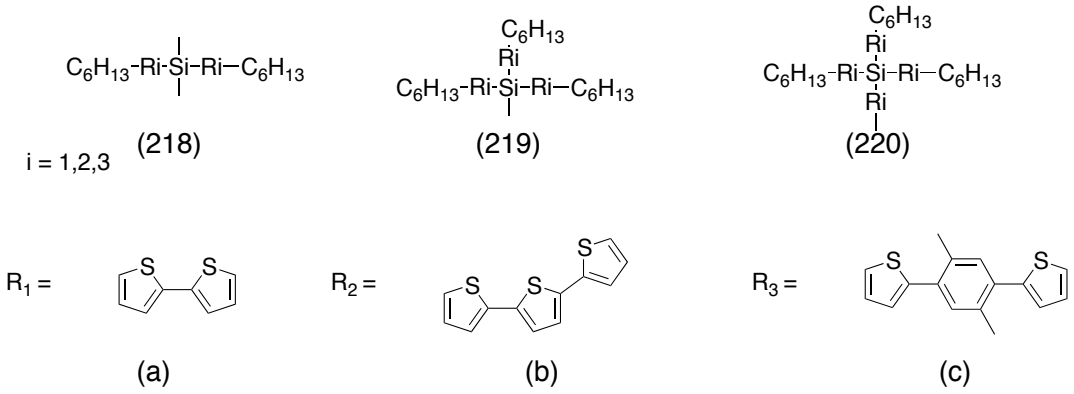

Figure 102 Thiophene based oligomers with silicon centres

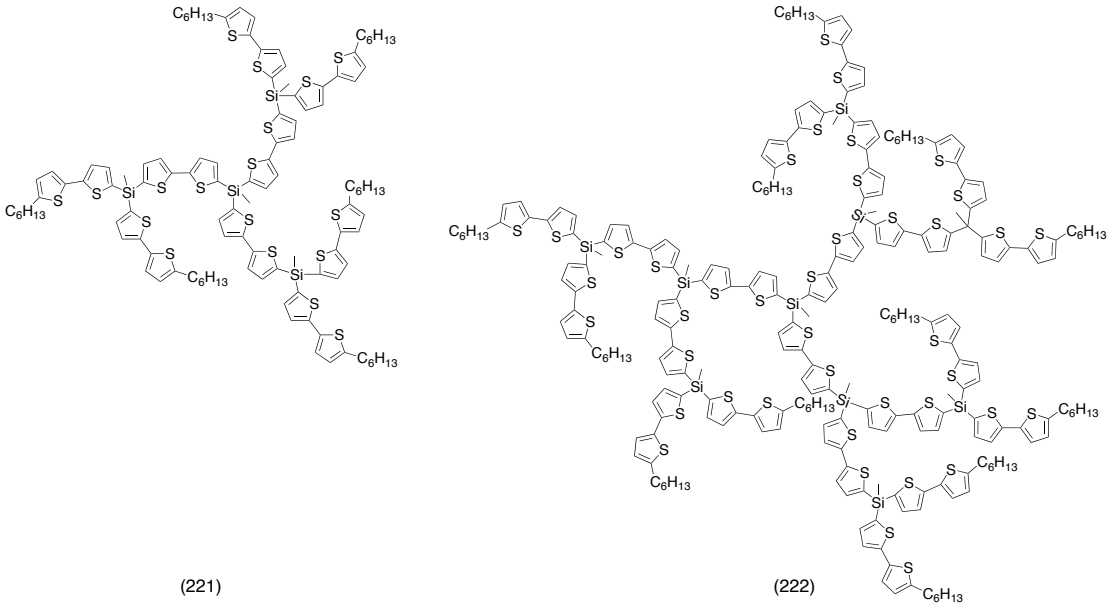

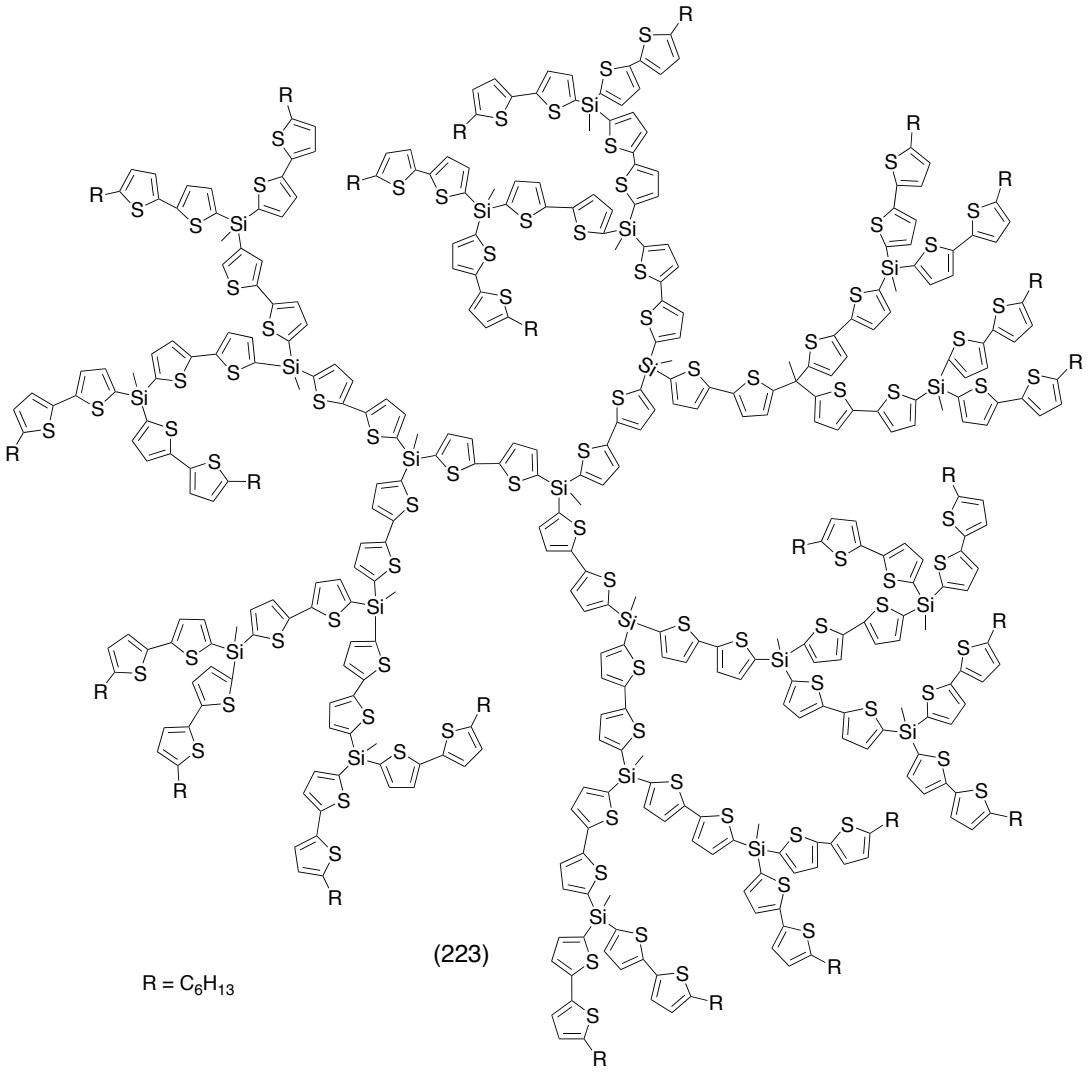

Figure 103 Star-shaped thiophene based dendrimers with a silicon centre[120]

In order to investigate the absorption and optical properties of these structures, two model chromophore compounds were also synthesised, 5-hexyl-2,2'-bithiophene (HB) and 5-hexyl-5'trimethylsilyl-2,2'-bithiophene (HTMSB). The structures of HB and HTMSB can be seen in Figure 104.

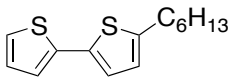

(HB)

(224)

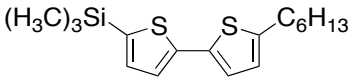

(HTMSB)

(225)

Figure 104 Structures of model structures 224 and 225

They noted that the absorption spectra of model compounds HTMSB and the thiophene oligomers shown in Figure 102 showed a slight shift of λ_{max} to longer wavelengths showing the effect of the introduction of silicon on the π-electron system on the nearest chromophore. Comparison of the dendrimers shown in Figure 103, and the oligomer containing two bithiophene units, showed that they had the same spectral characteristics and electro-optical properties. They showed from this study that the degree of substitution of silicon valence bonds by chromophores determined the properties of the molecule and unlike the oligomers, the also found that the dendrimers were kinetically flexible macromolecules.

Other core structures have also been investigated in the synthesis of these star-shaped macromolecules. One structure is that of triphenylamine (TPA). This TPA unit has a three-dimensional propeller structure, which provides good solubility. TPA-containing molecules have also been widely used in OLEDs as hole-injecting and transporting materials.[120] One such study looked at the use of a TPA-containing structure as charge transporting material in organic thin film transistors. Diallo et al synthesised a star-shaped molecule with TPA core and thiophene side arms shown in Figure 105, which they named VM5C9 **226**.[121]

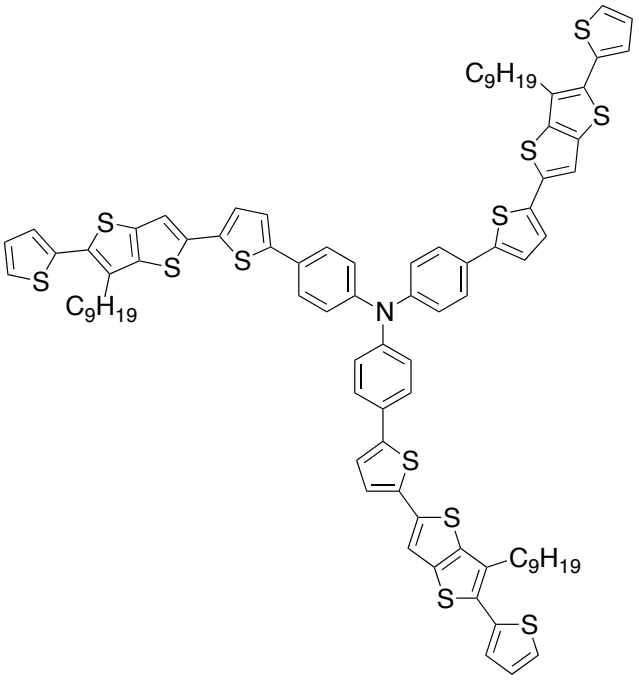

VM5C9

(226)

Figure 105 Structure of 226

They studied the electronic properties by UV/Vis spectroscopy and fluorescence spectroscopy in both the solution state and following the fabrication of spin-coated thin films. They saw a broad transition at around 420 nm from the absorption spectrum without vibronic shoulders, which suggested to them that there was a complete rotational disorder around the C-C bond. They also extrapolated the maximum of the absorption spectrum to determine the optical energy band gap, which gave a value of around 2.95 eV in all solvents. Following fabrication of thin films, they found that output characteristics confirmed closely with conventional transistor models. They found from this study that the TPA structure VM5C9 was a promising semiconductor in solution processed organic thin film transistors prepared from spin coating the active layer of VM5C9 on substrates. Further studies into the TPA structures as organic electronic materials have been performed, such as the study by Tang et al., where they synthesised a star-shaped molecule with TPA and diketopyrrolopyrrole (DPP) backbones with embedded thiophene for photovoltaics. Along with the good electron donating and charge transporting properties of TPA, they coupled this with DPP, which possesses good solubility and a strong ability to

harvest light.[122] They synthesised two molecules, one with a direct link between the TPA and DPP moieties (TPA-DPP) and a second with an embedded thiophene between the TPA and DPP units (TPA-T-DPP) in order to extend the conjugation. These can be seen in Figure 106.

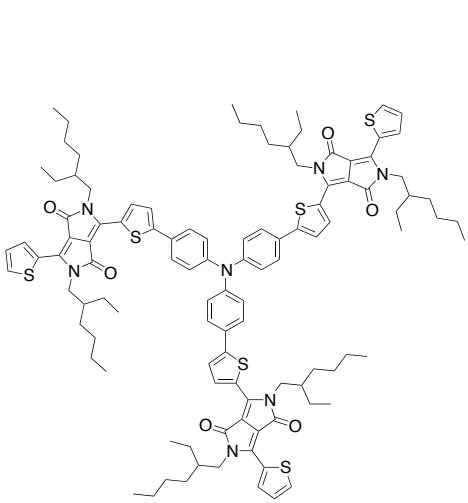

TPA-DPP

(227)

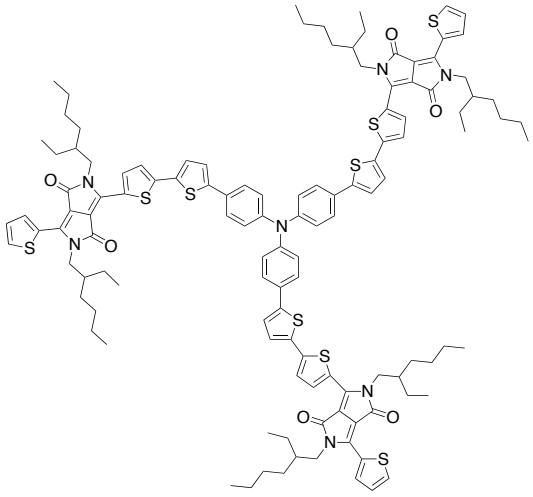

TPA-T-DPP

(228)

Figure 106 Structures of 227 and 228

UV/Vis spectra of the two compounds showed a broad absorption at 596 nm attributed to the photo-induced intermolecular charge transfer from the TPA to the DPP moiety. The thiophene bridge in the TPA-T-DPP could extend the delocalisation of the HOMO and increase the orbital overlapping of the HOMO and LUMO. This extended delocalisation was found to contribute to the enhanced absorption coefficient seen for this compound. They also found that embedding the thiophene within the structure caused enhanced light harvesting ability with the molar extinction coefficient increasing from 1.2 x 10^5 M^{-1} cm^{-1} for TPA-DPP to 1.7 x 10^5 M^{-1} cm^{-1} from TPA-T-DPP. They also found that incorporating this thiophene caused a narrowing of the optical band gap from 1.92 eV for TPA-DPP to 1.86 eV for TPA-T-DPP. They also looked at the cyclic voltammetry and calculated that the HOMO energies and LUMO energies were -5.18 eV and -3.25 eV for TPA-DPP and -5.13 eV and -3.32 eV for TPA-T-DPP, with the up-shifted HOMO level of TPA-T-DPP attributed to the extra electron rich thiophene in the backbone. These energy levels were found to be located in between those of $PC_{61}BM$, $PC_{71}BM$ and P3HT making

them good candidates for electron donor material to be blended with **6** or electron acceptor material blended with **11**.

Another interesting core molecule, which has attracted attention is the triindole molecule. Triindole is a planar conjugated aromatic structure with high electron donating ability that has previously been used as building block material in the construction of materials used in two photon absorption[123] and OLEDs[124]. Li et al. designed two triindole cored star-shaped molecules SM1 and SM2, that can be seen in Figure 107, for the use in organic solar cells. The molecules were designed so that, for SM1, there was a donor moiety at the end of the side arm in the TPA unit and an acceptor moiety in the centre of the arm in the benzothiadiazole unit. SM2 was designed with an acceptor moiety and the end of the side arm chain.[125]

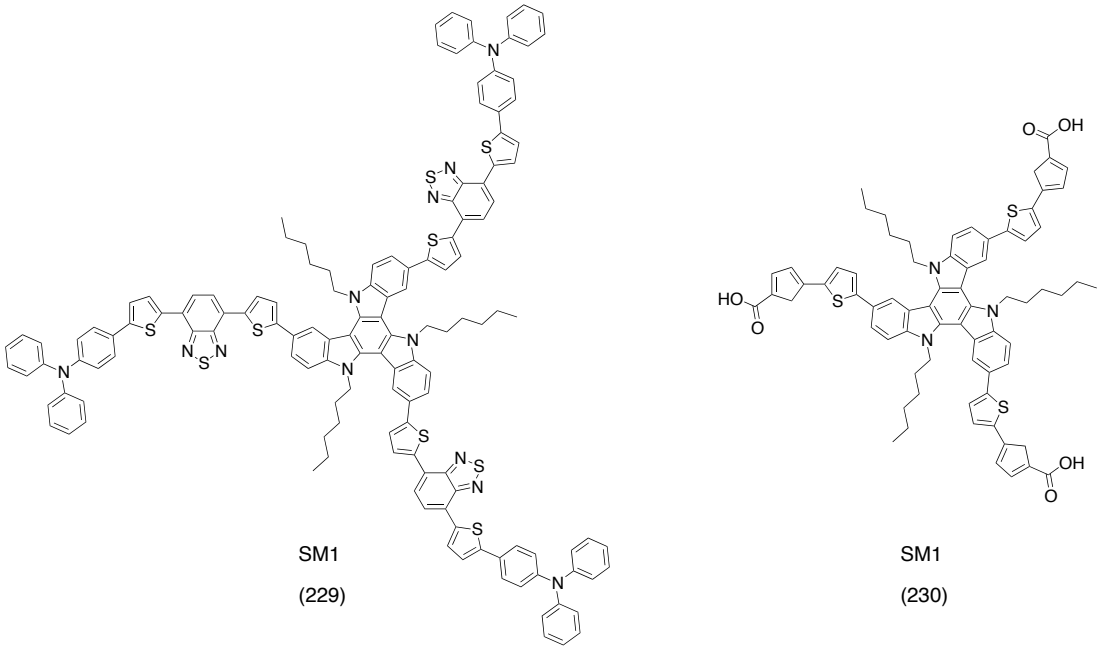

Figure 107 Structures of 229 and 230

They looked into the optical, electrochemical, thermal, transport and photovoltaic properties for these two compounds. They found that both exhibited a broad absorbance with the thin film absorptions becoming broader and red-shifting when going from solution to film. The film absorption onset was found to be 680 nm for SM1 and 598 nm for SM2 corresponding to an optical band gap of 1.82 eV and 2.07 eV for SM1 and SM2 respectively. Following investigations into the electrochemical properties of these structures, they calculated that the HOMO and LUMO levels were -5.12 eV and -3.00 eV for SM1 and -6.0 eV and -4.2 eV for SM2, which made them

compatible to be used a donor material with PCBM as acceptor material in the fabrication of organic solar cells. These star-shaped molecules also exhibited good thermal stability and relatively high hole mobility. Following the fabrication of bulk heterojunction solar cell devices blended with $PC_{71}BM$, they found that they gave a power conversion efficiency of 2.05% and 2.29%, which is promising for this early work into these structures.

A similar structure to triindole, truxene, has also been looked into as a potential compound for use in organic field effect transistors. In a study conducted by Sun et al they looked at a series of truxene-based molecules featuring oligothiophene units (Figure 108)[126]

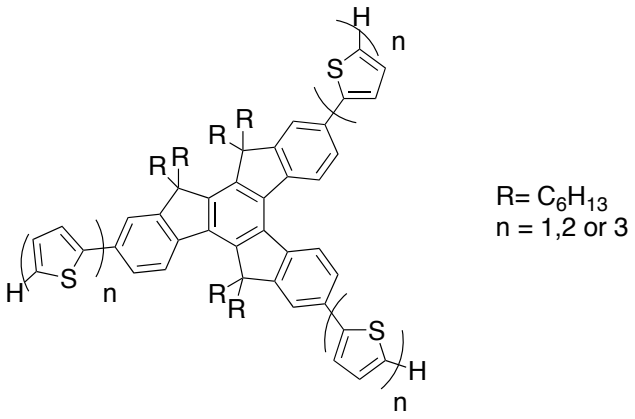

(231)

Figure 108 Structure of truxene star shaped molecules

They found that the increase of thiophene rings increases the stability of the compounds due to the extended conjugation. They also noted that the increase in conjugation also caused an increase in absorption maximum of the compounds from 343 nm for one thiophene to 413 nm for three thiophenes. This was also true for the fluorescence emission spectra of the compounds where, not only did the maximum increase from 381 nm to 527 nm with extended thiophenes, the emission spectrum also broadened. These results showed that by introducing the oligothiophene segments, the absorption and emission properties could be tuned. Following the fabrication of the OFETs they showed that there was a decrease in mobility when the thiophene chain was increased, however, they showed a high mobility with one thiophene of 1.03×10^{-3} $cm^2 V^{-1} s^{-1}$. This was attributed to the state of the compounds, which changed from polycrystalline to amorphous on the increase of the thiophenes.

This study demonstrated that it is possible to tune these types of molecules by increasing the thiophene chain, however, there should be a balance between the extent of conjugation and keeping the physical state of the structure.

Donor-acceptor, or push-pull systems, where an electron rich moiety is followed by an electron deficient moiety has become a promising way to produce molecules with higher absorption coefficients and broader absorption spectra to enhance power conversion efficiencies.[127] In a study conducted by Pelz et al., they looked at incorporating these systems into star-shaped structures synthesising structures with alternating donor-acceptor-donor segments with a central core.[128] They synthesised three different star-shaped structures S1-S3 seen in Figure 109, the donor segment is represented by a thiophene derivative and the acceptor portion is in the form of a benzothiadiazole unit. Hexyl side chains were also introduced in differing positions in order to influence the solubility and also the self assembly ability.

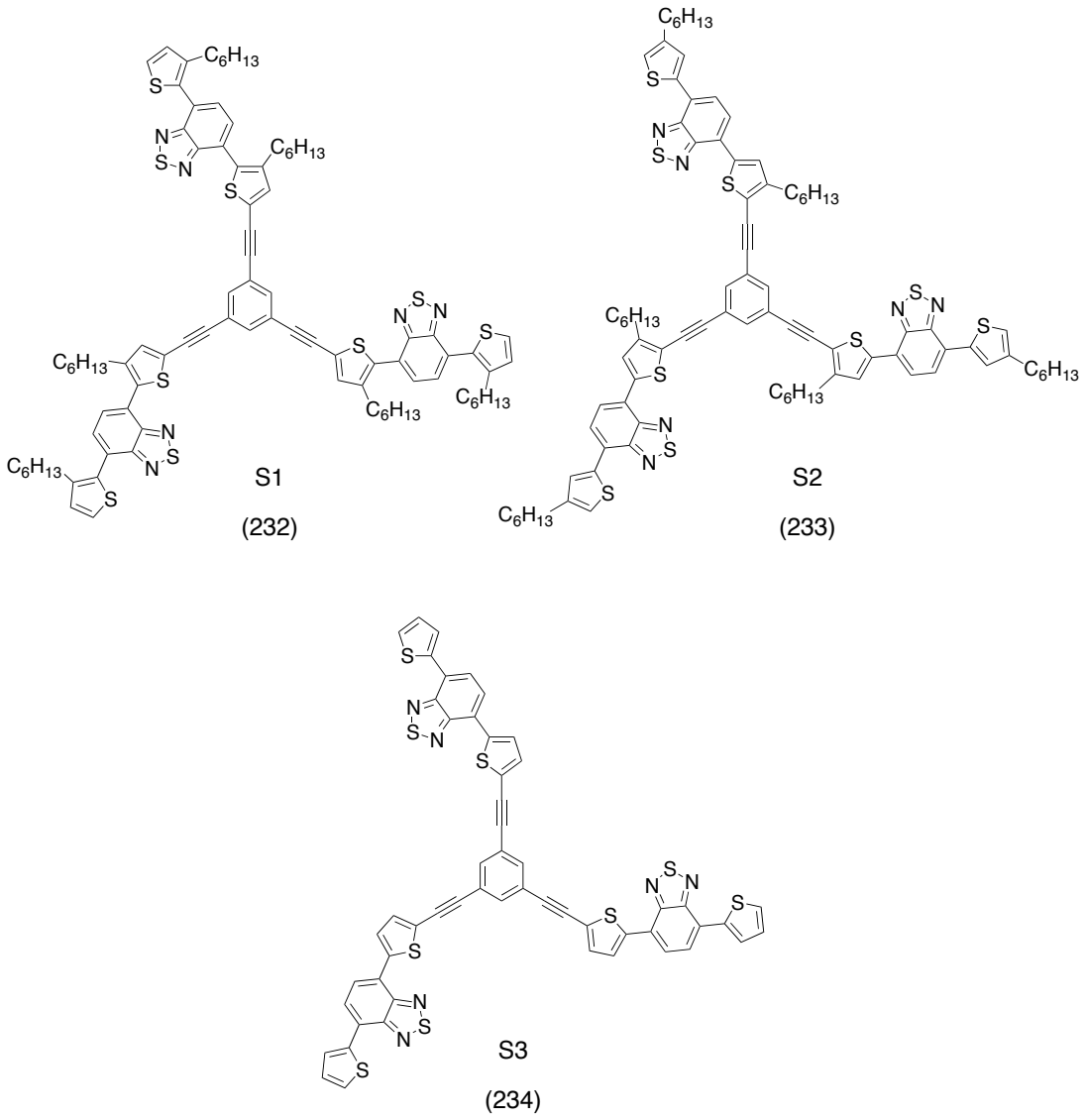

Figure 109 Structures of donor-acceptor-donor star shaped molecules 232, 233 and 234

Observing the absorption spectrum of each of these 3 star-shaped structures, it was noted that there was a red shift of around 25 nm when compared to their 'arm' precursors. It was also seen that the star-shaped structures showed an overlapping of absorption maxima due to the conjugation with the core. Compound S2 was shown to exhibit the largest bathochromic shift with a maximum at 485 nm compared with S1 at 423 nm. In addition, these compounds also displayed bright fluorescence under UV illumination. These results showed that the positions of the hexyl chains clearly had an influence on the absorption properties and therefore, the optical band gaps. This indicated that properties can be tuned in these molecules, which is a desirable trait in the design for new solar cells. Following the fabrication of thin films from

these structures, films of S3 blended with P3HT and PCBM gave promising results in terms of power conversion efficiencies.

5.1.2 Flavins as organic dyes for use in DSSCs

Dye-sensitised solar cells (DSSCs) have incurred a lot of interest for use as renewable energy systems.[129] Currently, photo-energy conversions of 11% can be achieved using ruthenium complexes, however these ruthenium dyes are not effective for photovoltaic systems due to the high cost of the ruthenium and the fact that they are environmentally unfriendly. Thus, investigations into metal–free organic dyes have attracted a lot of interest.

In a study conducted by Schmidt-Mende et al., they not only investigated the use of an organic dye as the semi-conducting material they also looked at the replacement of the liquid electrolyte with an organic hole transport material.[130] They utilised an indoline dye **235**, and 2,2',7,7'-tetrakis-(*N*,*N*-di-*p*-methoxyphenylamine)9,9'-spirobifluorene **236** as the organic hole transport material (Figure 110).

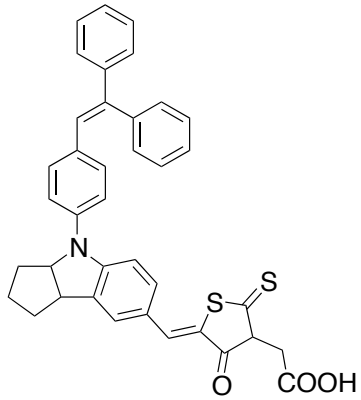

(235)

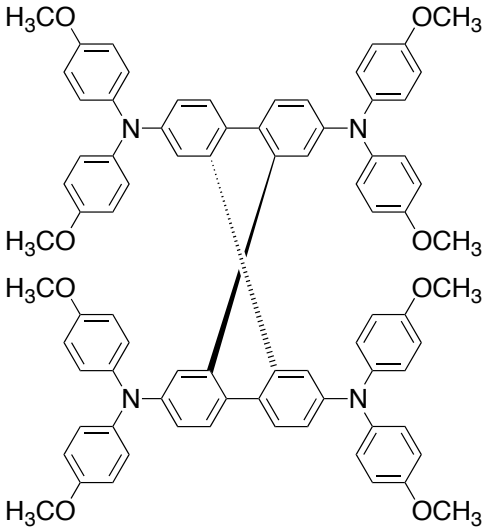

(236)

Figure 110 Structures of indoline dye 235 and spirobifluorene compound 236

Indoline dye **235** was of interest due to the high absorption co-efficicient of 55 800 L $mol^{-1}cm^{-1}$, which is four times stronger than the ruthenium counterparts. Figure 111 shows the absorption properties of the TiO_2 electrode sensitised with the dye and shows that the light harvesting properties of this organic dye is far superior to the

ruthenium dye **16**, absorbing more than 90% of the incident light over a wide range of the spectrum.

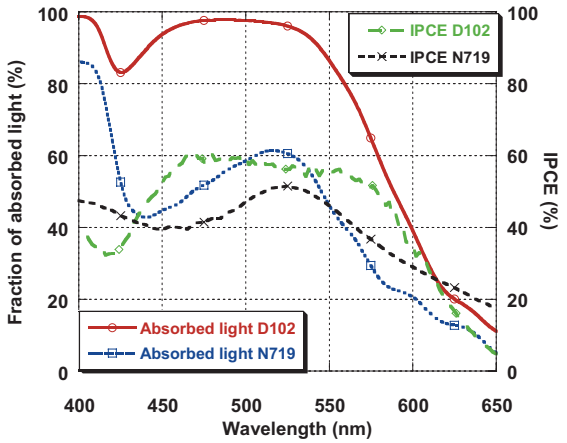

Figure 111 Absorption properties of the TIO_2 electrode doped with dye 235 and ruthenium dye 16[132]

Following construction of the DSSC, an overall efficiency of 4.1% was achieved. They concluded, however, that this result was highly promising and that with further optimisation, this dye could be a contender for a replacement to standard ruthenium dyes due to the easy and cheap synthesis.

In another study conducted by Hara et al., they investigated the use of coumarin-based dyes in DSSCs.[131] They had previously reported a coumarin based dye, NKX-2311 **237** (Figure 112) which gave an efficiency of 6.0%, however, they believed that extension of the π-conjugation would improve this efficiency. They therefore synthesised dyes NKX-2593 **238** and NKX-2677 **239** whereby thiophene moieties were introduced into the methine chain of **237** (Figure 113).

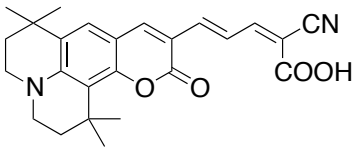

(237)

Figure 112 Structure of dye 237

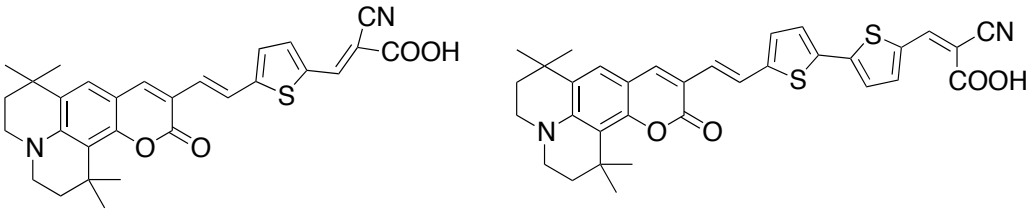

(238) (239)

Figure 113 Structures of dyes 238 and 239

They reported that introduction of the thiophenes showed no change in the absorption spectrum when in solution, with λ_{max} values of 507 nm, 507 nm and 510 nm observed. However, when absorbed onto the TiO_2 surface, the absorbance for NKX-2677 **239** had broadened. Alongside this, they also investigated the stability of the cell and noted that the introduction of the thiophenes appeared to stabilise the cell with no degradation observed when continuously irradiated with white light. The most promising indicator, however, was the increase in efficiency with a value of 7.7% observed using dye **239**. These results indicate how promising organic dyes are for DSSCs and in particular coumarin based dyes.

Although they have yet to feature in a DSSC, interest has been shown into developing flavin-based dyes. In 2008, Cooke and Rotello reported the synthesis of a donor-π-acceptor push-pull derivative 8-[[*p*-[bis(ethyl)amino]phenyl]azo]isobutylflavin (ABFL) **240** (Figure 114).[132] Their interest lay in the molecular recognition capabilities of this molecule and the ability to control the optical properties of the system.

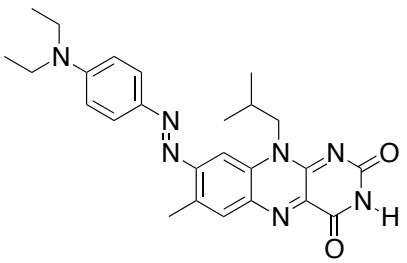

ABFL

(240)

Figure 114 Structure of 240

They utilised UV/Vis spectroscopy in order to monitor the influence of the molecular recognition on the optical properties. ABFL **240** initially displayed a strong absorption at 552 nm, which was attributed to an intramolecular charge transfer (ICT). They reported that on addition of DAP, there was a significant shift in the ICT, from 552 nm to 584 nm, and a colour change from purple to blue. They also noted that the π- π* transition observed at 335 nm decreased on addition of DAP. As a control, they used a methylated ABFL (MABFL) **241** in order to probe the molecular recognition process between ABFL and DAP. Due to the methyl group, the three-point H-bonding between ABFL and DAP would be blocked (Figure 115).

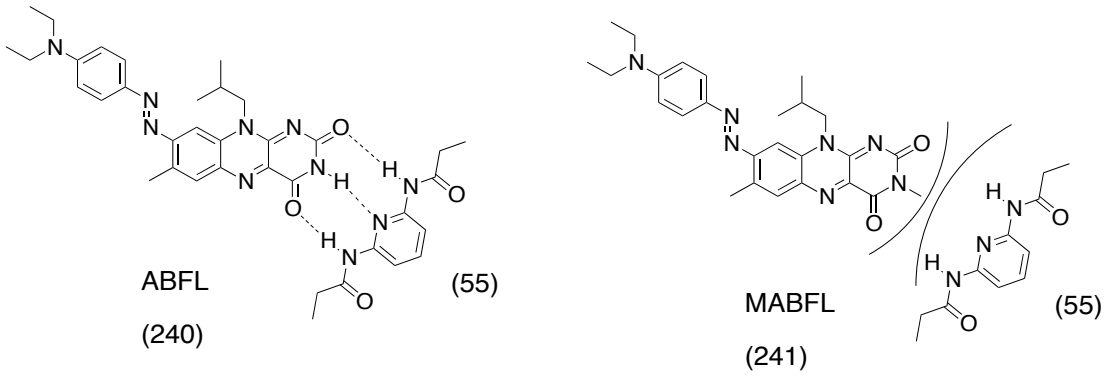

Figure 115 Molecular recognition between 240 and 55 and the blocking of H-Bonding with methyl

MABFL 240 displayed similar electronic behaviour as ABFL **241**, however, on addition of DAP no change was observed for the ICT or π- π* interaction indicating that the shift in absorbance for ABFL was a direct result of the molecular recognition. In 2013, Cooke, Rotello and Stanley investigated this system further in order to further understand the excited state properties of ABFL **240**.[133] They utilised Stark spectroscopy in order to study the charge redistribution of **240** upon vertical excitation from the ground state to the lowest excited state. They reported a dipole moment of 22.3, which agreed with their hypothesis that the lowest excited state is an intramolecular charge transfer and TD-DFT calculations showed that the charge transfer occurs from the diethylaniline donor to the flavin acceptor (Figure 116)

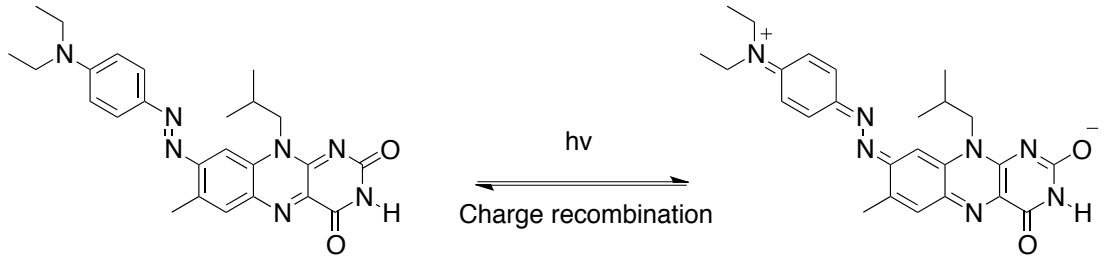

ABFL (240) ABFL (240)

Figure 116 Neutral (left) and charge separated (right) forms of 240

5.2 Project Outlines

5.2.1 Star-shaped molecules as electron transporting systems

The aim of this project was to synthesise a series of star-shaped molecules to be used as electron transporting systems in organic electronics such as photovoltaics. This would first involve taking the existing molecule, 1,3,5-tris(*N*-phenylbenzimidazol-2-yl)benzene, and functionalise it in order to adapt the properties for use in photovoltaics.

Due to the solubility problems associated with 1,3,5-tris(*N*-phenylbenzimidazol-2-yl) benzene, the aim would be to alkylate this molecule with simple alkyl groups in order to increase the solubility. The synthetic strategy involved introducing hexyl groups to the benzene ring of 1,3,5-tris(N-phenylbenzimidazol-2-yl) benzene to give compound **242**. This would follow a four-stage synthesis, as can be seen in Scheme 75. The first stage of the synthesis would be a substitution reaction to give the nitroaniline **245**, which would then be reduced to give the amine **246**. This would then be followed by a reaction with 1,3,5-benzenetricarbonyltrichloride **247** to give **248** and then the final condensation reaction to give compound **242**. A second target was also investigated utilising the electron donor properties of thiophenes and synthesising a star-like structures based on thiophene (Figure 117).

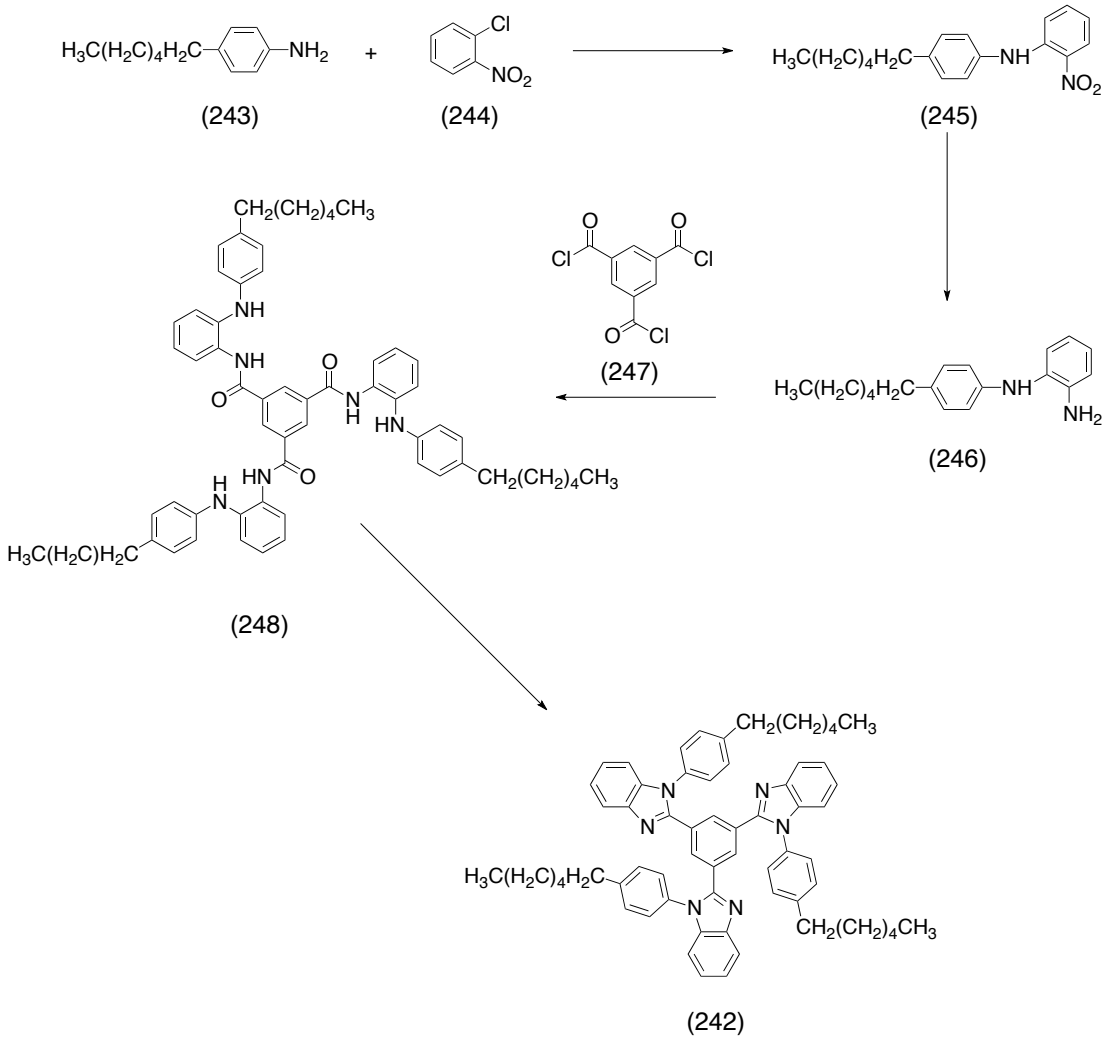

Scheme 75 Synthetic strategy for compound 242

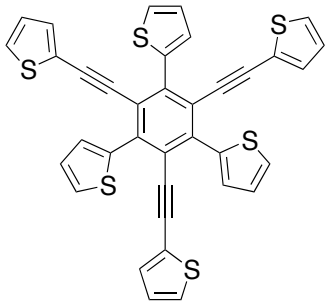

(249)

Figure 117 Structure of thiophene based star shaped target 249

5.2.2 Flavin based material for DSSCs

Flavin molecules are easily synthesised, stable molecules and have the advantage that the redox and optical properties can be tuned, which is a desirable quality for

developing DSSCs. As previously discussed, flavins have already been utilised in the formation of organic dyes. However, they have never been incorporated into a DSSC. With this in mind, the aim of this project was to take the flavin compound **57** and further functionalise it to give **250**, for use in DSSCs, Figure 118.

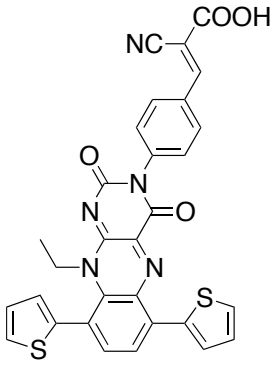

(250)

Figure 118 Structure of flavin dye 250

The proposed synthetic route for this compound was to start with flavin **57** and functionalise at the N(3) position to give the aldehyde **251** which would then undergo a Knovenagel condensation to give the target structure **250** (Scheme 76).

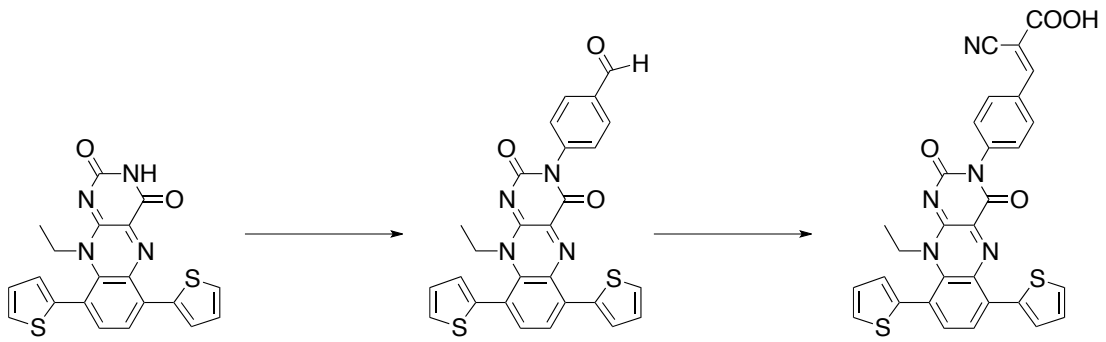

(57) (251) (250)

Scheme 76 Proposed synthetic route for compound 250

5.3 Results and Discussion

5.3.1 Functionalised 1,3,5-tris (N-phenylbenzimidazol-2-yl) benzene

The first stage of this synthesis was the substitution reaction between 4-hexylaniline **243** and 1-chloro-2nitrobenzene **244** to produce *N*-(4-hexylphenyl)-2-nitroaniline **245**.

This reaction was first attempted using THF as a solvent, and triethylamine as a base (Scheme 77), however, only starting material was recovered.

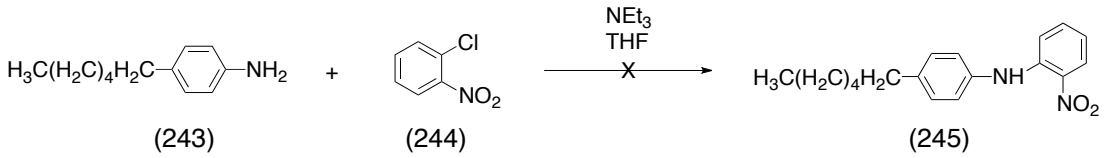

(243) (244) (245)

Scheme 77 First attempt at synthesis of 245

Following a literature search, a new method was adopted using DBU as base.[134] This method was first attempted using toluene as a solvent, however, after 3 days, thin layer chromatography indicated that the reaction was not proceeding and the reaction was tried as per the literature using DBU as both base and solvent. This proved more successful with the reaction proceeding, achieving compound **245** in a moderate yield of 27% (Scheme 78). This was then reduced using ammonium formate to give compound **246**, which was used without further purification (Scheme 78).

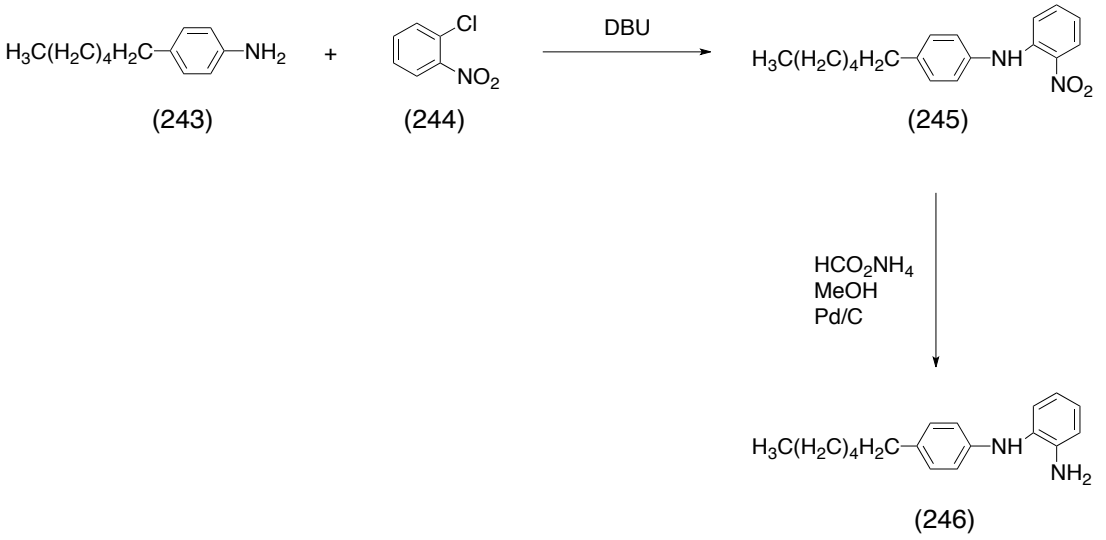

(243) (244) (245)

(246)

Scheme 78 Synthesis of 246

The final stage of the synthesis involved a reaction with 1,3,5-benzenetricarbonyltrichloride **247**. First attempts to synthesise compound **248** involved coupling the two compounds using just DCM as solvent (Scheme 79)

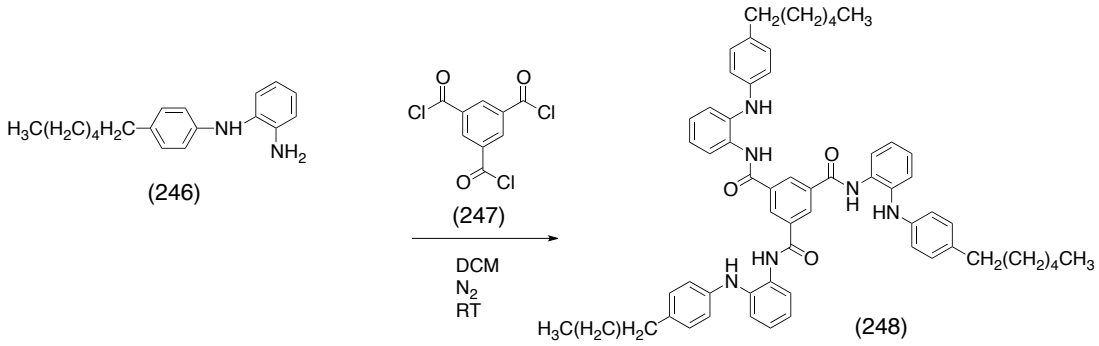

Scheme 79 First attempts at coupling reaction

^{1}H NMR data showed promise that the reaction had worked, however, purification of the compound was difficult with the impurities being very difficult to separate from the target compound. In order to achieve a 'cleaner' reaction, a new method was adopted. This involved a slight adjustment in conditions with triethylamine added to the reaction (Scheme 80)

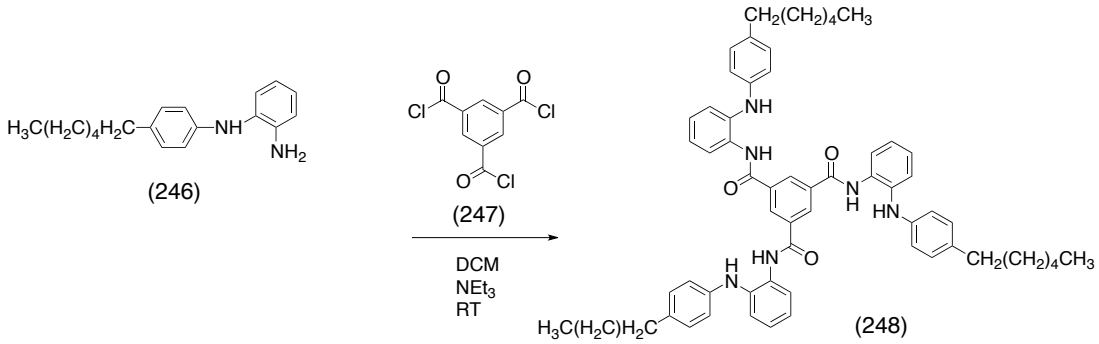

Scheme 80 Addition of triethylamine to the coupling reaction

^{1}H NMR data again showed promise, however, isolating the pure material was very difficult. Both ^{1}H NMR data and thin layer chromatography showed that there were a number of impurities and indicated that the amount of desired product was low. A lack of time meant that focus shifted to a new target.

5.3.2 Thiophene incorporated star shaped molecules

Synthesis of this target involved the reaction of a thiophene biacetylene compound which had previously been synthesised in the group[135] with cobalt octacarbonyl. The reaction took place in a glove box using 1,4-dioxane as solvent. The reaction proved successful yielding compound **249** as an off-white solid in a 15% yield (Scheme 81), typical for this reaction. Due to time constraints, this compound was passed to a colleague in the group for further analysis and characterisation.

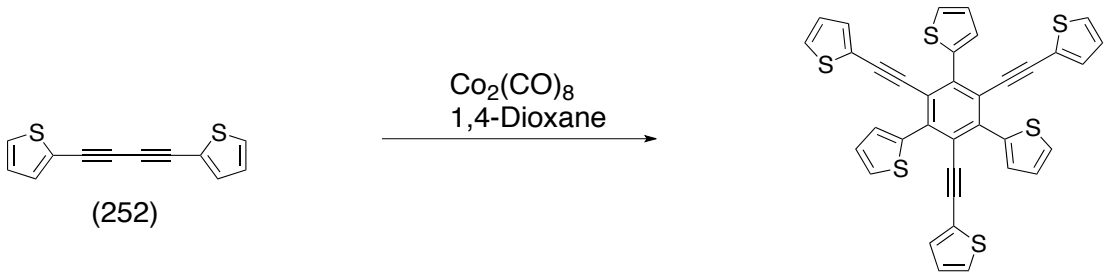

Scheme 81 Synthesis of star thiophene 249

5.3.3 Flavin incorporating material for DSSCs

Synthesis of this material started with a coupling reaction between flavin **57**, as previously discussed, with 4-formylphenylboronic acid at the N3 position with copper acetate and triethylamine in dichloromethane. The reaction was performed over 3 days and gave compound **251** in 15% yield (Scheme 82)

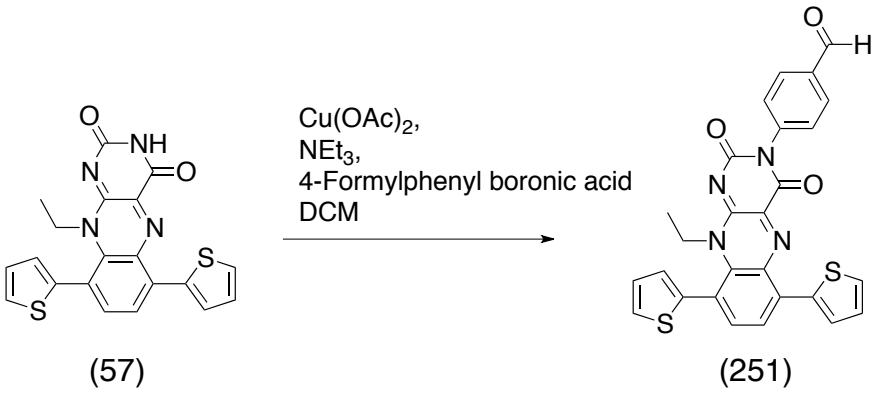

Scheme 82 Coupling reaction between flavin 57 and 4-formylphenyl boronic acid

Compound **251** was then reacted with cyanoacetic acid with pipiridine in dichloromethane to give the final compound **250** in 50% yield (Scheme 83). Due to time constraints, this compound was passed to a colleague in the group for further purification, analysis and characterisation.

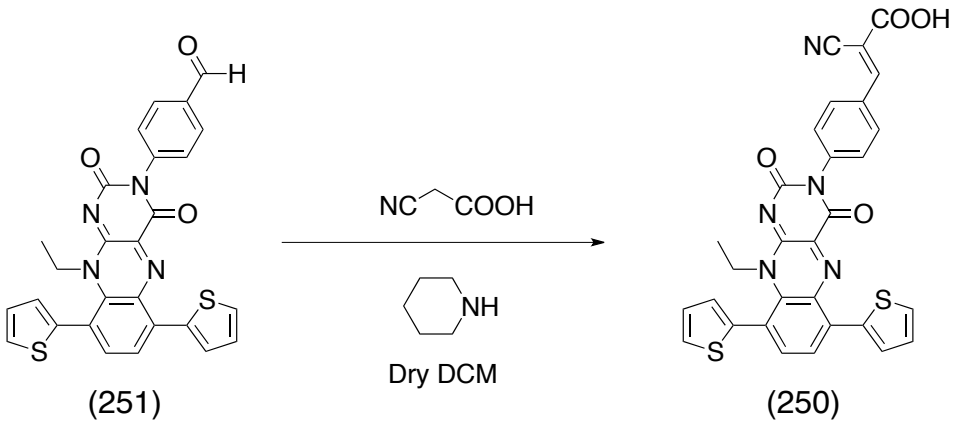

Scheme 83 Synthesis of flavin dye 250

5.4 Conclusions and Future Work

Investigations into the functionalisation of 1,3,5-tris(N-phenylbenzimidazol-2-yl) benzene proved promising, however, purification of this compound was very difficult and further development is required to optimise this reaction in order to achieve pure product in good yield. Synthesis of a thiophene-incorporated star molecule was successful and this compound was passed to a colleague for further analysis and characterisation before it could be sent to collaborators for testing.

Initial tests for synthesising flavin DSSC material also proved to be successful with one target successfully synthesised. Unfortunately, due to time restrictions this compound was also passed to a colleague to further analyse and characterise before it could be sent to collaborators.

6.0 Experimental

6.1 Apparatus

NMR spectra were recorded on a Bruker 400 MHz or Bruker DPX-500 MHz spectrometer (^{1}H NMR at 400 and 500 MHz respectively and ^{13}C NMR at 100 and 125 MHz respectively). Chemical shifts are reported in ppm. ^{1}H NMR spectra were recorded using $CDCl_3$, $(CD_3)_2SO$, CD_3CN calibrated using δ = 7.26, 2.50 and 1.94 as internal standards respectively. ^{13}C NMR spectra were calibrated relative to the central resonance of $CDCl_3$, $(CD_3)_2SO$, CD_3CN (δ = 77.16, 39.5 and 118.7 respectively). Signals in NMR spectra are described as singlet (s), doublet (d), triplet (t), quartet (q), quintet (quint) or multiplet (m), broad (br) or a combination of these, which refers to the spin-spin coupling pattern observed. DEPTQ and 2-dimensional (COSY, HSQC) NMR spectroscopy were used to assist in the assignment of signals. IR spectra were obtained using a Shimadzu FTIR-8400 instrument. UV/Vis and fluorescence analysis were obtained using a PerkinElmer Lambda 25 spectrometer and a RF-5301PC Shimadzu spectrofluorophotometer respectively. Cyclic Voltammetry was performed using a CH Instrument Electrochemical Workstation (CHI 440a), Austin, TX, USA. Samples were analysed at 10^{-4} M concentrations using 0.1M TBA.PF_6 as the electrolyte. High resolution mass spectra were recorded under FAB, CI, EI and ESI conditions by the analytical services at the University of Glasgow. Melting points were recorded with a Stuart Scientific SMP1 apparatus.

6.2 Chromatography

Column chromatography was performed using silica gel (Fluorochem LC60A, 35-70 micron) or aluminium oxide (Sigma Aldrich) as solid support and HPLC grade solvents as eluent. Reactions were monitored by thin layer chromatography (TLC) on Merck silica gel 60 covered aluminium plates and developed under UV-light.

6.3 Solvents and Reagents

All reagents were purchased from TCI, Sigma Aldrich and Fisher and used without further purification. Dry solvents were obtained from an Innovative Technology *inc.* Pure Solv 400-5-MD solvent purification system (activated alumina columns)

6.4 General Reaction Conditions

Reactions involving air sensitive reagents and dry solvents were performed in glassware dried in an oven prior to use and were carried out with the exclusion of air using a nitrogen atmosphere

6.5 Experimental Details

4,7-Dibromo-2,1,3-benzothiadiazole (60)[136]

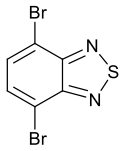

2,1,3-Benzothiadiazole **59** (10 g, 74 mmol) was stirred under reflux in HBr (150 mL). To this mixture was added Br_2 (11 mL, 205 mmol) in HBr (100 mL) slowly *via* dropping funnel. After full addition of the Br_2 the reaction was left to stir under reflux for 6h. The reaction was quenched with a saturated solution of $NaHSO_3$ and the orange precipitate removed *via* filtration and washed exhaustively with water and once with diethyl ether (100ml) before drying under high vacuum for ca. 20 hours to yield **60** as an off white solid (19 g, 86%) M.Pt = 185 – 187 ºC; ν_{max} (solid): 3154, 2981, 2253, 1794; ^{1}H NMR (500 MHz, $CDCl_3$) δ (ppm): 7.73 (2H, s, Ar C-H); ^{13}C NMR (125 MHz, $CDCl_3$) δ (ppm): 113.9 (quat-C), 132.4 (Ar C-H), 153.0 (quat-C); HRMS *m/z* (EI+) = 293.8288 ($C_6H_2N_2Br_2S$ requires 293.8285)

4,7-Dithienyl-2,1,3-benzothiadiazole 61[137]

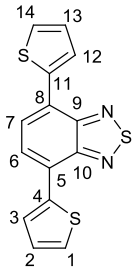

4,7-Dibromo-2,1,3-benzothiadiazole **60** (18 g, 62 mmol), $PdCl_2(PPh_3)_2$ (0.87 g, 2 mol %) and 2-(tributylstannyl-)thiophene (47 mL, 147 mmol) were stirred in dry THF (300 mL) at reflux, under N_2 for 3h. The mixture was concentrated *in vacuo* and the

product recrystallised from CH_2Cl_2/pet ether to yield **61** as a red solid (18 g, 99 %) M.Pt = 118 – 120 ºC; ν_{max} (solution): 3684, 3019, 2400, 1738; ^{1}H NMR (500 MHz, $CDCl_3$) δ (ppm): 7.22 (2H, dd, *J* = 5.1 & 3.7 Hz, C (3 & 12)H), 7.46 (2H, dd, *J* = 1.0 & 5.0 Hz, C (2 & 13)H), 7.89 (2H, s, C (6 & 7)H), 8.12 (2H, dd, *J* = 1.0 & 3.5 Hz, C (1 & 14)H); ^{13}C NMR (125 MHz, $CDCl_3$) δ (ppm): 125.8 (C (6 & 7)H), 126.0 (quat-C), 126.8 (C(3 & 12)H), 127.5 (C(1 & 14)H), 128.0 (C(2 & 13)H), 139.8 (quat-C), 152.7 (quat-C); HRMS *m/z* (EI+) = 299.9850 ($C_{14}H_8N_2S_3$ requires 299.9847)

10-Ethyl-6,9-di(thiophen-2-yl)benzo[*g*]pteridine-2,4(3*H*,10*H*)-dione 57

Method 1

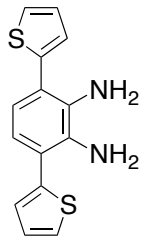

(62)

4,7-Dithienyl-2,1,3-benzothiadiazole **61** (3.3 g, 11 mmol) was stirred in THF (100 mL) at -10 °C, $LiAlH_4$ (1.6 g, 41 mmol) was added portion wise. The reaction was then stirred at room temperature for 1h and left stirring under reflux overnight. The reaction was then cooled to -10 °C and quenched with H_2O (10 mL) and 2M NaOH (10 mL). The crude product **62** was then extracted with CH_2Cl_2/H_2O and the organic extracts combined, dried over $MgSO_4$, which was removed *via* filtration, concentrated *in vacuo* and used without further purification.

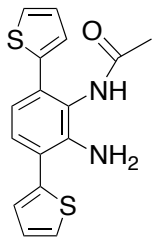

(63)

1,2-Diamino-3,6-dithien-2'-yl benzene **62** and NEt_3 (2.3 mL, 17 µmol) were stirred in THF (100 mL) at -10 °C. Acetyl chloride (0.78 mL, 11 µmol) was added dropwise

and the reaction stirred at -10 °C for 20m before stirring at room temperature overnight. The reaction mixture was concentrated *in vacuo* and the crude product **63** used without further purification.

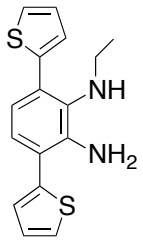

(64)

The acylated compound **63** was stirred in THF (100 mL) at -10 °C. $LiAlH_4$ (2.5 g, 66 mmol) was added dropwise. The reaction was left to stir at -10 °C for 30m before stirring at room temperature overnight. The mixture was quenched with H_2O (10 mL) and 2M NaOH (10 mL), extracted with CH_2Cl_2, dried over $MgSO_4$, which was removed *via* filtration, and concentrated. The crude product **64** used without further purification.

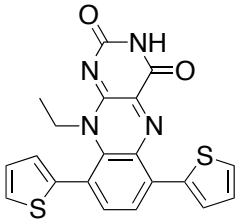

(57)

To this crude compound **64** was added alloxan monohydrate (1.7 g, 11 mmol) and boric anhydride (1.5 g, 22 mmol) and the mixture stirred in acetic acid (150 mL) at room temperature overnight. The mixture was then concentrated *in vacuo* and the product purified *via* column chromatography [SiO_2: CH_2Cl_2/acetone, 9/1] followed by crystallisation from ethanol to yield **57** as a purple solid (0.16 g, 4%) M.Pt = 269-270 ºC; ν_{max} (solid) 3615, 3491, 3086, 3032, 3001, 2820, 1705, 1659, 1597; ^{1}H NMR (500 MHz, $CDCl_3$) δ (ppm): 1.09 (3H, t, *J* = 7.0 Hz, C(16)H$_3$), 4.57 (2H, C(15)H$_2$), 7.15 (1H), 7.16 (1H), 7.21 (1H), 7.51 (1H), 7.66 (1H), 7.77 (1H), 7.93 (2H), 8.40 (1H, *br* s, N-H); ^{13}C NMR (125 MHz, $CDCl_3$) δ (ppm): 14.0 (C(16)H$_3$), 43.8 (C(15)H$_2$), 121.4 (quat-C), 123.6, 127.4, 127.7, 129.7, 132.5, 137.1 (quat-C), 139.7 (quat-C), 141.3,

155.2 (quat-C), 158.7 (C=O); HRMS *m/z* (FAB+) = 407.0636 ($C_{20}H_{15}O_2N_4S_2$ requires 407.0641)

Method 2

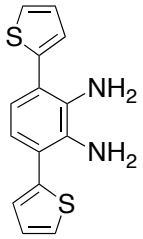

(62)

4,7-Dithienyl-2,1,3-benzothiadiazole **61** (3.0 g, 10 mmol), $NaBH_4$ (1.2 g, 30 mmol) and $CoCl_2$ (0.26 g, 2.0 mmol) were stirred in ethanol (300 mL) under reflux. After 30m a further equivalent of $NaBH_4$ was added and the reaction stirred for a further 1h. The mixture was then extracted with diethyl ether (2 × 200 mL) and washed with water (4 × 200 mL). The organic extracts were combined, dried over $MgSO_4$, which was removed *via* filtration, before the solvent was concentrated *in vacuo*. The crude product **62** was used without further purification.

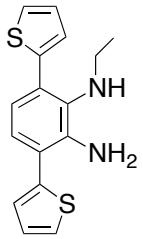

(64)

This crude product **62** was dissolved in dry diethyl ether (100 mL) with K_2CO_3 (2.1 g, 15 mmol) under N_2. To this was added ethyl trifluoromethane sulfonate (1.3 mL, 10 mmol) and the reaction stirred at room temperature. After 2h, a further 0.2 equivalents of ethyl trifluoromethane sulfonate (0.26 mL, 2.0 mmol) was added and the reaction stirred for a further hour. The mixture was then extracted with diethyl ether (1 × 100 mL) and washed with water (4 × 100 mL). The organic extracts were combined, dried over $MgSO_4$, which filtered and the solvent was removed *in vacuo*. The crude product **64** was used without further purification.

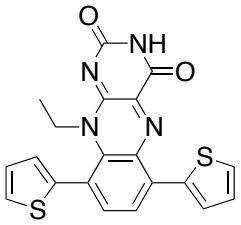

(57)

This crude product **64** was dissolved in acetic acid (100 mL) and cooled over ice. To this was added boric anhydride (1.4 g, 20 mmol) followed by alloxan monohydrate (1.6 g, 10 mmol) and the reaction stirred overnight. The mixture was then poured into water (500 mL) producing **57** as a deep purple precipitate (0.92 g, 23%), which was collected *via* filtration. M.Pt = 269-270 ºC; ν_{max} (solid): 3615, 3491, 3086, 3032, 3001, 2820, 1705, 1659, 1597; ^{1}H NMR (500 MHz, $CDCl_3$) δ (ppm): 1.11 (3H, t, *J* = 7.0 Hz, C(16)$\underline{H}_3$), 4.59 (2H, C(15)$\underline{H}_2$), 7.15 (1H, d), 7.18 (1H, dd), 7.23 (1H, dd), 7.54 (1H,dd), 7.68 (1H, d), 7.80 (1H, d), 7.95 (2H, dd), 8.42 (1H, *br* s, N-$\underline{H}$); ^{13}C NMR (125 MHz, $CDCl_3$) δ (ppm): 13.9 ($\underline{C}$(16)H_3), 43.8 ($\underline{C}$(15)H_2), 121.4 (quat-C), 123.6 (thiophene $\underline{C}$-H), 127.4 (thiophene $\underline{C}$-H), 127.7 (thiophene $\underline{C}$-H), 128.2 (thiophene $\underline{C}$-H), 129.8 (thiophene $\underline{C}$-H), 132.4 (thiophene $\underline{C}$-H), 137.1 (quat-C), 139.7 (quat-C), 141.3 (benzyl $\underline{C}$-H), 155.2 (C=O), 158.7 (C=O); HRMS *m/z* (FAB+) = 407.0636 ($C_{20}H_{15}O_2N_4S_2$ requires 407.0641)

10-Ethyl-3-heptyl-6,9-di(thiophen-2-yl)benzo[*g*]pteridine-2,4(3*H*,10*H*)-dione 67

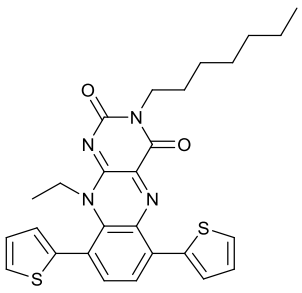

10-Ethyl-6,9-di(thiophen-2-yl)benzo[*g*]pteridine-2,4(3*H*,10*H*)-dione **57** (0.14 g, 0.35 mmol) was stirred under reflux at 35 °C in acetone (30 mL) with 1-iodoheptane (0.24 mL, 1.4 mmol) and K_2CO_3 (0.50 g, 3.6 mmol). The reaction was left to stir under reflux overnight. The reaction mixture was then concentrated *in vacuo* and the crude product purified *via* flash column chromatography [SiO_2: CH_2Cl_2] to yield **67** as a red

solid (0.03 g, 17%) M.Pt = 188-190 ºC; ν_{max} (solid): 3729, 3495, 3098, 2926, 2854, 2361, 1709, 1660, 1598; ^{1}H NMR (500 MHz, $CDCl_3$) δ (ppm): 0.86 (6H, t, *J* = 1.7 Hz, (2 x C<u>H</u>$_3$)), 1.21 – 1.41 (10H, m, (5 x C<u>H</u>$_2$)), 4.10 (2H, t, *J* = 7.7 Hz, (N-C<u>H</u>$_2$)), 4.54 (2H, *br* s, (N-C<u>H</u>$_2$)), 7.12 (1H, d, *J* = 1.0 Hz, (thiophene C-<u>H</u>), 7.14 (1H, t, *J* = 5.2 Hz, (thiophene C-<u>H</u>)), 7.19 (1H, t, *J* = 5.2 Hz, (thiophene C-<u>H</u>)), 7.50 (1H, dd, *J* = 1.2 & 5.2 Hz, (thiophene C-<u>H</u>)), 7.64 (1H, dd, *J* = 1.1 & 5.2 Hz (thiophene C-<u>H</u>)), 7.74 (1H, d, *J* = 8.2 Hz, (Ar C-<u>H</u>), 7.91 (1H, d, *J* = 8.2 Hz, (Ar C-<u>H</u>)), 7.94 (1H, dd, *J* = 1.2 & 4.0 Hz, (thiophene C-<u>H</u>)); ^{13}C NMR (125 MHz, $CDCl_3$) δ (ppm): 14.1 (2 x <u>C</u>H$_3$), 22.6 (<u>C</u>H$_2$), 27.8 (<u>C</u>H$_2$), 29.4 (<u>C</u>H$_2$), 30.2 (<u>C</u>H$_2$), 31.6 (<u>C</u>H$_2$), 42.3 (N-<u>C</u>H$_2$), 43.1 (N-<u>C</u>H$_2$), 121.3 (quat-<u>C</u>), 123.2 (Ar <u>C</u>-H), 127.2 (Ar <u>C</u>-H), 127.5 (Ar <u>C</u>-H), 128.1 (Ar <u>C</u>-H), 129.5 (Ar <u>C</u>-H), 129.7 (Ar <u>C</u>-H), 132.7 (Ar <u>C</u>-H), 133.4 (quat-<u>C</u>), 133.8 (quat-<u>C</u>), 135.4 (quat-<u>C</u>), 137.3 (quat-<u>C</u>), 138.0 (quat-<u>C</u>), 140.0 (quat-<u>C</u>), 140.7 (Ar <u>C</u>-H), 150.3 (quat-<u>C</u>), 155.8 (C=O), 159.4 (C=O); HRMS *m/z* (EI+) = 504.1654 ($C_{27}H_{28}O_2N_4S_2$ requires 504.1651)

6,9-Dibromo-10-ethylbenzo[*g*]pteridine-2,4(3*H*,10*H*)-dione 58

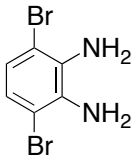

(65)

4,7-Dibromo-2,1,3-benzothiadiazole **60** (5.0 g, 17 mmol) was stirred in ethanol (100 mL) at 0 ºC under N_2. Sodium borohydride (12 g, 315 mmol) was added portionwise and the reaction stirred at room temperature overnight. The product was then extracted with ether (3 × 100 mL) and the aqueous extracted further with CH_2Cl_2 (1 × 100 mL). The organic extracts were then combined, dried over $MgSO_4$, which was removed *via* filtration, and the filtrate concentrated *in vacuo*. The crude product was used without further purification.

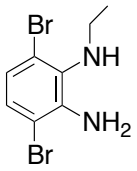

(66)

Crude 1,2-diamino-3,6-dibromobenzene **65** was dissolved in dry diethyl ether (100 mL) with K_2CO_3 (3.6 g, 26 mmol). To this was added ethyl trifluoromethane sulfonate (2.2 mL, 17 mmol) and the reaction was left to stir at room temperature overnight. The K_2CO_3 was removed *via* filtration and the reaction mixture washed with water (2 × 100 mL). The ether extracts were combined, dried over $MgSO_4$, which was removed *via* filtration, and the filtrate concentrated *in vacuo*. The crude product **66** was used without further purification.

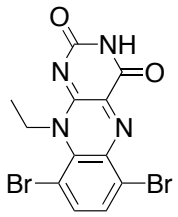

(58)

The crude product **66** was dissolved in acetic acid (100 mL) and cooled to -10 °C. To this was added alloxan monohydrate (2.7 g, 17 mmol) followed by boric anhydride (2.4 g, 34 mmol). The reaction stirred at -10 °C before warming to room temperature and stirred overnight. The mixture was poured into water (500 mL) precipitating **58** as a yellow solid (3.3 g, 48%) M.Pt > 300 ºC; ν_{max} (solution): 3584, 3154, 2982, 2359, 2340, 2253, 1793, 1728, 1602; ^{1}H NMR (500 MHz, $CDCl_3$) δ (ppm): 1.65 (3H, t, *J* = 6.9 Hz (alkyl C$\underline{H}_3$)), 5.20 (2H, q, *J* = 6.9 Hz (N-C$\underline{H}_2$), 7.73 (1H, d, *J* = 8.5 Hz, (Ar C-$\underline{H}$)), 7.98 (1H, d, *J* = 8.5 Hz, (Ar C-$\underline{H}$)), 8.42 (1H, s, (N-H)); ^{13}C NMR (125 MHz, $CDCl_3$) δ (ppm): 15.0 ($\underline{C}H_3$), 45.2 (N-$\underline{C}H_2$), 122.0 (Ar quat-C), 125.6 (Ar quat-C), 130.8 (Ar quat-C), 131.0 (Ar $\underline{C}$-H), 132.4 (Ar $\underline{C}$-H), 138.5 (Ar quat-C), 141.9 (Ar quat-C), 147.3 (Ar quat-C), 150.2 (C=0), 157.7 (C=0); HRMS *m/z* (ESI (Na + M)$^+$) = 420.8901 ($C_{12}H_8O_2N_4{}^{79}Br_2Na$ requires 420.8906)

6,9-Dibromo-3,10-bis(2-ethylhexyl)benzo[*g*]pteridine-2,4(3*H*,10*H*)-dione 69

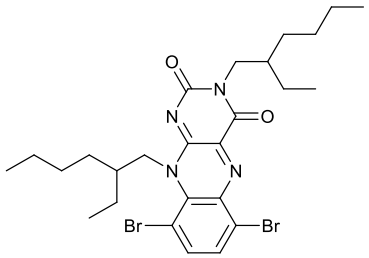

6,9-Dibromo-10-ethylbenzo[*g*]pteridine-2,4(3*H*,10*H*)-dione **58** (0.51 g, 1.3 mmol) was stirred in DMF (15 mL) with Na_2CO_3 (0.54 g, 5.1 mmol). To this was added 2-ethylhexylbromide (0.90 mL, 5.1 mmol) and the reaction was left to stir at room temperature. After 5d, the mixture was extracted with ethyl acetate (1 × 50 mL) and washed with water (2 × 50 mL). The organic extracts were combined, dried over $MgSO_4$, filtered, and concentrated *in vacuo* before purification *via* column chromatography [SiO_2: ether] followed by recrystallisation from pet ether to yield **69** as a yellow solid (0.34 g, 44%) M.Pt = 159-161 ºC; ν_{max} (solution): 3684, 3019, 2963, 2400, 1725, 1681; ^{1}H NMR (500 MHz, $CDCl_3$) δ (ppm): 0.85 (12H, m, 4 × C$\underline{H}_3$), 1.26 – 1.42 (16H, m, 8 × C$\underline{H}_2$), 1.97 (1H, quint., *J* = 6.6 Hz, alkyl C-$\underline{H}$), 2.14 (1H, quint., *J* = 6.1 Hz, alkyl C-$\underline{H}$), 4.12 (2H, m, N-C$\underline{H}_2$), 4.45 (2H, m, N-C$\underline{H}_2$), 7.90 (1H, d, *J* = 8.1 Hz, Ar C-$\underline{H}$), 8.02 (1H, d, *J* = 8.1 Hz, Ar C-$\underline{H}$); ^{13}C NMR (125 MHz, $CDCl_3$) δ (ppm): 10.7 (C$\underline{H}_3$), 14.1 (C$\underline{H}_3$), 22.6 (C$\underline{H}_3$), 23.0 (C$\underline{H}_2$), 23.1 (C$\underline{H}_2$), 23.8 (C$\underline{H}_2$), 27.7 (C$\underline{H}_3$), 28.6 (C$\underline{H}_2$), 29.1 (C$\underline{H}_2$), 30.5 (C$\underline{H}_2$), 30.7 (C$\underline{H}_2$), 37.1 (alkyl $\underline{C}$-H (^{1}H at 2.14)), 37.6 (alkyl $\underline{C}$-H (^{1}H at 1.97)), 41.4 (C$\underline{H}_2$), 46.6 (N-$\underline{C}$H$_2$ (^{1}H at 4.12)), 47.3 (N-$\underline{C}$H$_2$ (^{1}H at 4.45)), 121.8 (Ar quat-$\underline{C}$), 125.4 (Ar quat-$\underline{C}$), 130.6 (Ar quat-$\underline{C}$), 132.3 (Ar $\underline{C}$-H), 136.6 (Ar $\underline{C}$-H), 138.2 (Ar quat-$\underline{C}$), 141.8 (Ar quat-$\underline{C}$), 146.3 (Ar quat-$\underline{C}$), 150.7 (C=0), 158.7 (C=0); HRMS *m/z* (EI+) 596.1188 ($C_{26}H_{36}O_2N_4Br_2$ requires 596.1187)

6,9-Dibromo-10-(2-ethylhexyl)benzo[*g*]pteridine-2,4(3*H*,10*H*)-dione 70

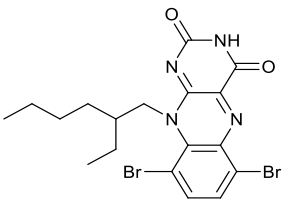

6,9-Dibromo-10-ethylbenzo[*g*]pteridine-2,4(3*H*,10*H*)-dione **58** (0.31 g, 0.76 mmol) was stirred in DMF (10 mL) with Na_2CO_3 (0.33 g, 3.1 mmol). To this was added 2-ethylhexylbromide (0.53 mL, 3.0 mmol) and the reaction was left to stir at room temperature. After 2d, the mixture was extracted with ethyl acetate (1 × 50 mL) and washed with water (1 × 50 mL) and brine (2 × 50 mL). The organic extracts were combined, dried over $MgSO_4$, filtered, and concentrated *in vacuo* before purification *via* column chromatography [SiO_2: ether] followed by recrystallisation with pet ether to yield **70** as a yellow solid (0.11 g, 34%) M.Pt = 188-190 ºC; ν_{max} (solution): 3582, 3160, 2981, 2351, 2339, 2256, 1791, 1727, 1601; ^{1}H NMR (500 MHz, $CDCl_3$) δ (ppm): 0.89 (3H, t, *J* = 7.0 Hz (alkyl C$\underline{H}_3$)), 0.98 (3H, t, *J* = 7.5 Hz (Alkyl C$\underline{H}_3$), 1.30 (8H, m, (4 x C$\underline{H}_2$)), 2.17 (1H, m, (C$\underline{H}$)), 4.42 (2H, t, *J* = 6.5 Hz, (N-C$\underline{H}_2$)), 7.97 (1H, d, *J* = 8.0 Hz, (Ar C-$\underline{H}$)), 8.08 (1H, d, *J* = 8.0 Hz, (Ar C-$\underline{H}$)), 8.61 (1H, s, (N-$\underline{H}$)); ^{13}C NMR (125 MHz, $CDCl_3$) δ (ppm): 10.6 ($\underline{C}H_3$), 14.1 ($\underline{C}H_3$), 23.1 (CH_2), 23.7 (CH_2), 28.6 (CH_2), 30.5 (CH_2), 37.1 ($\underline{C}H$), 47.0 (N-$\underline{C}H_2$), 122.2 (Ar quat-$\underline{C}$), 126.1 (Ar quat-$\underline{C}$), 131.0 (Ar quat-$\underline{C}$), 132.7 (Ar $\underline{C}$-H), 137.0 (Ar $\underline{C}$-H), 138.4 (Ar quat-$\underline{C}$), 141.4 (Ar quat-$\underline{C}$), 147.8 (Ar quat-$\underline{C}$), 157.6 (2 x C=O); HRMS *m/z* (ESI (Na + M)$^+$) = 420.8901 ($C_{12}H_8O_2N_4{}^{79}Br_2Na$ requires 420.8906)

6,9-Dibromo-10-methylbenzo[g]pteridine-2,4(3H,10H)-dione 72

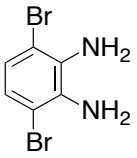

(62)

4,7-Dibromo-2,1,3-benzothiadiazole **60** (5.0 g, 17 mmol) was dissolved in ethanol (100 mL) and cooled to 0 ºC under N_2. To this was added $NaBH_4$ (12 g, 316. mmol) portion wise. The reaction was stirred overnight at room temperature. The mixture

was extracted with diethyl ether (1 × 100 mL) and washed with water (4 × 400 mL). The organic extracts were combined, dried over $MgSO_4$, filtered and the solvent removed *in vacuo*. The crude product **62** was used without further purification.

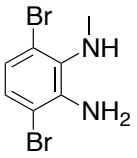

(71)

Crude 1,2-diamino-3,6-dibromo benzene **62** was dissolved in dry diethyl ether (100 mL) with K_2CO_3 (3.5 g, 25 mmol) under N_2. To this was added methyl trifluoromethane sulfonate (1.9 mL, 17 mmol) and the reaction stirred at room temperature overnight. The mixture was then extracted with diethyl ether (1 × 100 mL) and washed with water (2 × 100 mL). The organic extracts were combined, dried over $MgSO_4$, filtered and the solvent removed *in vacuo*. The crude product **71** was used without further purification.

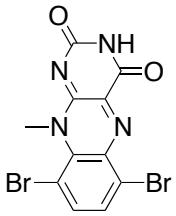

(72)

The crude product **71** was dissolved in acetic acid (100 mL) and cooled to 0 ºC. To this was added boric anhydride (2.4 g, 34 mmol) followed by alloxan monohydrate (2.7 g, 17 mmol). The reaction was left to stir overnight. The mixture was poured into water (500 mL) producing a yellow precipitate which was collected *via* filtration, washed with pet ether and dried under high vacuum giving product **72** as a yellow solid (4.0 g, 61%). M.Pt > 300 ºC; ν_{max} (solid): 3683, 3019, 2434, 2399, 1883, 1725, 1711, 1692; ^{1}H NMR (500 MHz, $CDCl_3$) δ (ppm): 4.38 (1H, s, N-C<u>H</u>$_3$), 7.78 (1H, d, *J* =8.0 Hz, Ar C-<u>H</u>), 7.97 (1H, d, *J* = 8.0 Hz, Ar C-<u>H</u>), 8.49 (1H, s, N<u>H</u>); ^{13}C NMR (125 MHz, $CDCl_3$) δ (ppm): 41.1(N-<u>C</u>H$_3$), 107.4 (quat <u>C</u>), 113.9 (quat <u>C</u>), 129.5 (quat <u>C</u>), 131.2 (Ar <u>C</u>-H), 132.5 (Ar <u>C</u>-H), 142.1 (C=O); HRMS ESI (M+ Na)$^+$ = 406.8752 ($C_{11}H_6O_2N_4Br_2Na$ requires 406.8750)

6,9-Dibromo-3,10-dimethylbenzo[g]pteridine-2,4(3H,10H)-dione 75

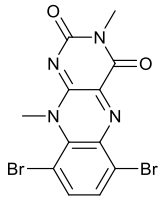

6,9-Dibromo-10-methylbenzo[g]pteridine-2,4(3H,10H)-dione **72** (1.0 g, 2.6 mmol) was dissolved in dry DMF (20 mL) with Na_2CO_3 (1.1g, 10 mmol). To this was added methyl iodide (0.65 mL, 10 mmol) and the reaction stirred at room temperature for 4d. The mixture was then extracted with ethyl acetate and washed with brine (3 × 100 mL). The organic extracts were combined and dried over $MgSO_4$, filtered and the solvent was removed *in vacuo*. The crude product was purified *via* column chromatography [SiO_2: CH_2Cl_2] to yield **75** as a yellow solid (0.31 g, 30%) M.Pt = 199 – 201 ºC; ν_{max} (solid): 3683, 3016, 2430, 2401, 1880, 1726, 1714, 1694; ^{1}H NMR (500 MHz, $CDCl_3$) δ (ppm): 3.55 (3H, s, N-C$\underline{H}_3$), 4.38 (3H, s, N-C$\underline{H}_3$), 7.76 (1H, d, *J* = 8.5 Hz, Ar C-$\underline{H}$), 7.94 (1H, d, *J* = 8.5 Hz, Ar C-$\underline{H}$); ^{13}C NMR (125 MHz, $CDCl_3$) δ (ppm): 30.9 (N-$\underline{C}H_3$), 40.6 (N-$\underline{C}H_3$), 107.26 (quat-$\underline{C}$), 131.0 (Ar $\underline{C}$-H), 137.3 (quat-$\underline{C}$), 141.8 (Ar $\underline{C}$-H), 155.5 (C=O); HRMS ESI (M+ Na)$^+$ 420.8906 ($C_{12}H_8N_4O_2Br_2Na$ requires 420.8908)

6,9-Dibromo-3,10-dihexylbenzo[g]pteridine-2,4(3H,10H)-dione 73

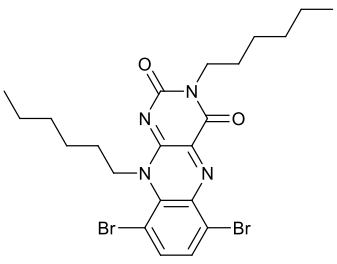

6,9-Dibromo-10-ethylbenzo[g]pteridine-2,4(3H,10H)-dione **58** (0.20 g, 0.52 mmol) was dissolved in dry DMF (5 mL) with Na_2CO_3 (0.22 g, 2.1 mmol). To this was added 1-bromohexane (0.29 mL, 2.1 mmol) and the reaction stirred at room temperature for 4d. The mixture was extracted with ethyl acetate (1 × 100 mL) and washed with brine (3 × 100 mL). The organic extracts were combined and dried over $MgSO_4$, filtered and the solvent was removed *in vacuo*. The crude product was

purified *via* column chromatography [SiO_2: ether] to yield **73** as a yellow solid (0.13 g, 25%) M.Pt = 164 - 166 ºC; ν_{max} (solution): 3864, 2960, 3019, 2931, 2860, 1726, 1682; ^{1}H NMR (500 MHz, $CDCl_3$) δ (ppm): 0.92 (3H, t, *J* = 7.8 Hz, (2 C$\underline{H}_3$)), 1.39 (12H, m, (6×C$\underline{H}_2$)), 1.79 (2H, quint. *J* = 7.8 Hz, (CH_2)), 1.90 (2H, quint. *J* = 7.8 Hz (C$\underline{H}_2$)), 4.20 (2H, t, *J* = 7.8 Hz, (N-C$\underline{H}_2$)), 4.51 (2H, t, *J* = 7.8 Hz, (N-C$\underline{H}_2$)), 7.93 (1H, d, *J* = 8.0 Hz, (Ar C-$\underline{H}$)), 8.05 (1H, d, *J* = 8.0 Hz, (Ar C-$\underline{H}$)); ^{13}C NMR (125 MHz, $CDCl_3$) δ (ppm): 14.0 (2 x $\underline{C}H_3$), 22.5 (2 x $\underline{C}H_2$), 22.6 ($\underline{C}H_2$), 26.6 ($\underline{C}H_2$), 26.6 ($\underline{C}H_2$), 27.2 ($\underline{C}H_2$), 27.7 ($\underline{C}H_2$), 31.4 ($\underline{C}H_2$), 42.9 (N-$\underline{C}H_2$), 43.6 (N-$\underline{C}H_2$), 121.9 (quat-$\underline{C}$), 125.7 (quat-$\underline{C}$), 130.9 (quat-$\underline{C}$), 132.3 (Ar $\underline{C}$-H), 136.0 (quat-$\underline{C}$), 136.6 (Ar $\underline{C}$-H), 138.6 (quat-$\underline{C}$), 146.0 (quat-$\underline{C}$), 150.2 (C=O), 158.4 (C=O); HRMS ESI (M+ Na)$^+$ 561.0460 ($C_{22}H_{28}N_4O_2Br_2Na$ requires 561.0471)

6,9-Dibromo-3,10-dibenzylbenzo[g]pteridine-2,4(3H,10H)-dione 74

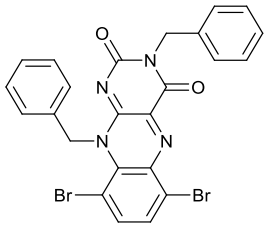

6,9-Dibromo-10-ethylbenzo[g]pteridine-2,4(3H,10H)-dione **58** (0.20 g, 0.52 mmol) was dissolved in dry DMF (5 mL) with Na_2CO_3 (0.22 g, 2.1 mmol). To this was added benzyl bromide (0.25 mL, 2.1 mmol) and the reaction stirred at room temperature for 4d. The mixture was extracted with ethyl acetate (1 × 100 mL) and washed with brine (3 × 100 mL). The organic extracts were combined and dried over $MgSO_4$, filtered and the solvent was removed *in vacuo*. The crude product was purified *via* column chromatography [SiO_2: ether] to yield **74** as a yellow solid (0.09 g, 31%). M.Pt = 230 - 232 ºC; ν_{max} (solution): 3684, 3019, 2931, 2400, 1970, 1728, 1711, 1685; ^{1}H NMR (500 MHz, $CDCl_3$) δ (ppm): 5.40 (2H, s, (N-C$\underline{H}_2$)), 5.70 (2H, s, (N-C$\underline{H}_2$)), 7.34 (6H, m, (Ar C-$\underline{H}$)), 7.63 (2H, d, *J* = 8.2 Hz, (2 x (Ar C-$\underline{H}$)), 7.80 (2H, d, *J* = 8.2 Hz, (2 x Ar C-$\underline{H}$)), 7.93 (1H, d, *J* = 8.0 Hz, (Ar C-$\underline{H}$)), 8.10 (1H, d, *J* = 8.0 Hz, (Ar C-$\underline{H}$)); ^{13}C NMR (125 MHz, $CDCl_3$) δ (ppm): 46.0 (N-$\underline{C}H_2$), 46.3 (N-$\underline{C}H_2$), 121.8 (quat-$\underline{C}$), 125.4 (quat-$\underline{C}$), 128.1 (Ar $\underline{C}$-H), 128.2 (Ar $\underline{C}$-H), 128.5 (Ar $\underline{C}$-H), 128.6 (Ar $\underline{C}$-H), 129.6 (Ar $\underline{C}$-H), 129.8 (Ar $\underline{C}$-H), 130.7 (quat-$\underline{C}$), 132.5 (Ar $\underline{C}$-H), 135.8 (Ar $\underline{C}$-H), 135.9 (quat-$\underline{C}$), 136.8 (Ar $\underline{C}$-H), 138.4 (quat-$\underline{C}$), 145.7 (quat-$\underline{C}$),

150.4 (C=O), 158.2 (C=O); HRMS ESI (M+ Na)$^+$ 572.9521 ($C_{24}H_{16}N_4O_2Br_2Na$ requires 572.9532)

Poly(3,10-bis(2-ethylhexyl)benzo[*g*]pteridine-2,4(3*H*,10*H*)-dione)-(9,9-dioctylfluorene) 78

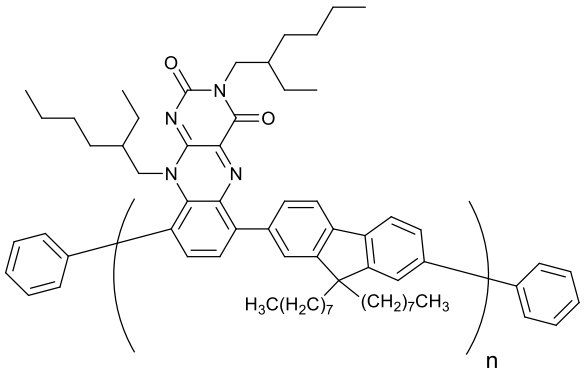

Reaction 1

6,9-Dibromo-3,10-bis(2-ethylhexyl)benzo[*g*]pteridine-2,4(3*H*,10*H*)-dione **69** (0.30 g, 0.50 mmol), 9,9-dioctylfluorene-2, 7-diboronic acid bis(1,3-propanediol) ester **77** (0.28 g, 0.50 mmol), aq K_2CO_3 (0.35 g, 2.5 mmol) and $Pd(PPh_3)_4$ (17 mg, 0.015 mmol) were dissolved in toluene (10 mL) and degassed. The reaction then stirred at 85 °C for 48h under N_2 in the dark. To this was added phenyl boronic acid (12 mg, 0.10 mmol) and the reaction stirred for another 15h. Bromobenzene (0.1 mL, 0.95 mmol) was added and the reaction stirred for a further 12h. The reaction mixture was then precipitated into methanol (300 mL). The precipitate was collected *via* filtration and purified *via* soxhlet with petroleum ether to yield a polymer **78** as an orange solid (80 mg) GPC: (THF, 30°C at 1mL/min): M_n = 1864, M_w = 2600, PDI = 1.4

Reaction 2

6,9-Dibromo-3, 10-bis(2-ethylhexyl)benzo[*g*]pteridine-2,4(3*H*,10*H*)-dione **69** (0.29 g, 0.49 mmol), 9,9-dioctylfluorene-2, 7-diboronic acid bis(1,3-propanediol) ester **77** (0.27 g, 0.49 mmol), aq K_2CO_3 (0.35 g, 2.5 mmol) and $Pd(PPh_3)_4$ (18 mg, 0.016 mmol) were dissolved in toluene (10 mL) and degassed. The reaction then stirred at 85 °C for 48 h under N_2 in the dark. Bromobenzene (10 µL, 0.097 mmol) was added and the reaction stirred for 1 h. Phenyl boronic acid (12 mg, 0.10 mmol) was then added and the reaction stirred for another 15 h. The reaction mixture was then

precipitated into diethyl ether (200 mL) and pet ether (200 mL). Precipitate and filtrate were extracted with CH_2Cl_2 (3 x 300 mL) and the organic extracts were combined, dried over $MgSO_4$, which was removed by filtration, and concentrated *in vacuo* to yield an orange polymer **78** (90 mg) GPC: (THF, 30°C at 1mL/min) M_n = 3433, M_w = 5192, PDI = 1.5

^{1}H NMR (500 MHz, $CDCl_3$) δ (ppm): 0.6-1.4 (*br*, *m*, alkyls), 1.8-2.1 (*br*, *m*, alkyls), 4.02 (*br*, m, N-C$\underline{H}_2$), 4.44 (*br*, m, N-CH_2), 7.49-8.05 (*br*, m, aromatics),

3,10-Diheptyl-6,9-di(thiophen-2-yl)benzo[g]pteridine-2,4(3H,10H)-dione 80

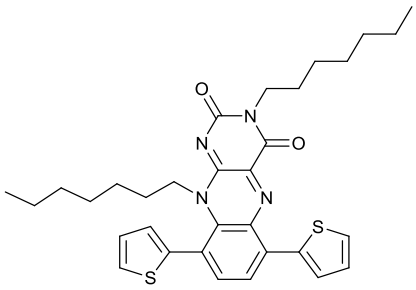

10-Ethyl-6,9-di(thiophen-2-yl)benzo[*g*]pteridine-2,4(3*H*,10*H*)-dione **57** (0.50 g, 1.2 mmol) was dissolved in dry DMF (10 mL) with Na_2CO_3 (0.52 g, 4.9 mmol). To this was added 1-iodoheptane (0.81 mL, 4.9 mmol) and the reaction stirred at room temperature for 4d. The mixture was extracted with ethyl acetate (1 × 100 mL) and washed with brine (3 × 100 mL). The organic extracts were combined and dried over $MgSO_4$, filtered and the solvent was removed *in vacuo*. The crude product was purified *via* column chromatography [SiO_2: diethyl ether] to yield **80** as a red/purple solid (0.184 g, 27 %) M.Pt = 148 – 150 ºC; ν_{max} (solution): 3774, 3683, 3583, 3019, 2961, 2930, 2858, 1711, 1677; ^{1}H NMR (500 MHz, $CDCl_3$) δ (ppm): 0.90 (6H, t, *J* = 7.0 Hz, (2 x C$\underline{H}_3$)), 1.33 (16H, m, (8 x C$\underline{H}_2$)), 1.85 (4H, m, (2 x C$\underline{H}_2$)), 4.21 (2H, t, *J* = 8.0 Hz, (N-C$\underline{H}_2$)), 4.58 (2H, t, *J* = 8.0 Hz, (N-C$\underline{H}_2$)), 7.32 (2H, t, *J* = 5.5 Hz, (2 x thiophene C-$\underline{H}$)), 7.58 (2H, dd, *J* = 5.0 Hz, (2 x thiophene C-$\underline{H}$)), 7.78 (1H, d, *J* = 8.0 Hz, (Ar C-$\underline{H}$)), 8.08 (1H, d, *J* = 5.0 Hz, (Ar C-$\underline{H}$)), 8.14 (1H, d, *J* = 8.0 Hz, (thiophene C-$\underline{H}$)), 8.29 (1H, d, *J* = 8.0 Hz, (thiophene C-$\underline{H}$)); ^{13}C NMR (125 MHz, $CDCl_3$) δ (ppm): 14.1 (2 x $\underline{C}H_3$), 22.6 (2 x $\underline{C}H_2$), 27.0 ($\underline{C}H_2$), 27.1 ($\underline{C}H_2$), 27.5 ($\underline{C}H_2$), 27.8 ($\underline{C}H_2$), 29.0 ($\underline{C}H_2$), 29.1 ($\underline{C}H_2$), 31.8 ($\underline{C}H_2$), 31.9 ($\underline{C}H_2$), 42.8 (N-$\underline{C}H_2$), 43.7 (N-$\underline{C}H_2$), 125.6 (Ar $\underline{C}$-H), 126.2 (Ar $\underline{C}$-H), 126.8 (Ar $\underline{C}$-H), 127.2 (Ar $\underline{C}$-H), 128.0 (Ar $\underline{C}$-H),

128.2 (Ar C-H), 128.4 (quat C), 129.5 (quat C), 130.0 (Ar C-H), 130.9 (Ar C-H), 133.1 (quat C), 136.5 (quat C), 137.8 (quat C), 138.1 (quat C), 139.5 (quat C), 144.2 (quat C), 150.2 (C=O), 159.2 (C=O); HRMS ESI (M+ Na)$^+$ 597.2306 ($C_{32}H_{38}N_4O_2S_2Na$ requires 597.2328)

3,10-bis(2-ethylhexyl)-6,9-di(thiophen-2-yl)benzo[*g*]pteridine-2,4(3*H*,10*H*)-dione 81

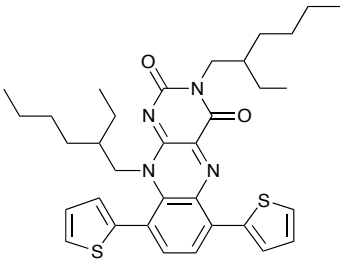

Flavin **57** (0.20 g, 0.50 mmols), was dissolved in dry DMF (10 mL) with Na2CO3 (0.21 g, 1.97 mmols). To this was added 2-ethylhexylbromide (0.34 mL, 1.97 mmols) and the reaction stirred at room temperature for 4d. The mixture was extracted with ethyl acetate (1 × 100 mL) and washed with water (1 x 100 mL) and brine (3 × 100 mL). The organic extracts were combined and dried over $MgSO_4$, filtered and the solvent was removed *in vacuo*. The crude product was purified *via* column chromatography [SiO_2: diethyl ether] to yield **81** as a red/purple solid (0.088 g, 29 %) M.Pt = 183-185 ºC; ν_{max} (solution): 3864, 2960, 3019, 2931, 2860, 1726, 1682; ^{1}H NMR (500 MHz, $CDCl_3$) δ (ppm): 0.95 (12H, m, (4 x C$\underline{H}_3$)), 1.34 (16H, m, (8 × C$\underline{H}_2$)), 2.05 (1H, m, (C$\underline{H}$)), 2.18 (1H, m, (C$\underline{H}$)), 4.15 (2H, m, (N-C$\underline{H}_2$)), 4.56 (2H, m, (N-C$\underline{H}_2$)), 7.53 (1H, dd, *J* =, (thiophene C-$\underline{H}$)), 7.22 (2H, dt, *J* = 5.1 & 3.8 Hz, (thiophene C-$\underline{H}$)) 7.59 (1H, dd, *J* = 5.1 & 1.1 Hz, (thiophene C-$\underline{H}$)), 7.76 (1H, dd, *J* = 3.7 & 1.1 Hz, (thiophene C-$\underline{H}$)), 8.06 (1H, dd, *J* = 3.7 & 1.0 Hz,(thiophene C-$\underline{H}$)), 8.11 (1H, d, *J* = 8.0 Hz, (Ar C-$\underline{H}$)), 8.22 (1H, d, *J* = 8.0 Hz, (Ar C-$\underline{H}$)); ^{13}C NMR (125 MHz, $CDCl_3$) δ (ppm): 10.6 (C$\underline{H}_3$), 14.1 (C$\underline{H}_3$), 23.1 (C$\underline{H}_2$), 23.2 (C$\underline{H}_2$), 23.5 (C$\underline{H}_2$), 23.9 (C$\underline{H}_2$), 28.5 (C$\underline{H}_2$), 28.7 (C$\underline{H}_2$), 30.2 (C$\underline{H}_2$), 30.6 (C$\underline{H}_2$), 36.8 (C$\underline{H}$), 37.6 (C$\underline{H}$), 46.6 (N-C$\underline{H}_2$), 47.2 (N-C$\underline{H}_2$), 125.8 (Ar C-H), 126.9 (Ar C-H), 127.3 (Ar C-H), 127.5 (Ar C-H), 127.9 (Ar C-H), 128.1 (Ar C-H), 128.42 (quat-C), 129.8 (quat-C), 129.9 (Ar C-H), 131.6 (Ar C-H), 133.4 (quat-C), 136.7 (quat-C), 137.9 (quat-C), 138.2 (quat-C), 139.8 (quat-C), 144.9 (quat-C), 151.0 (C=O), 159.6 (C=O); HRMS (EI$^+$) 602.2749 ($C_{34}H_{42}N_4O_2S_2$ requires 602.2747)

1,1'-Dibenzyl-4,4'-bipyridilium dibromide 106

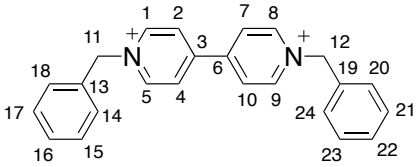

4,4'-Bipyridine **100** (1.0 g, 6.5 mmol) and benzyl bromide **107** (1.5 mL, 13 mmol) were stirred under reflux for 6h in dry acetonitrile (50 mL). The mixture was left to cool overnight. After cooling the precipitate was filtered to give **106** as a bright yellow solid (2.6 g, quant.). 250 ˚C dec; ν_{max}/cm^{-1} (solid state) 3988, 3377 (*br)*, 3040, 2987, 2949, 2364; ^{1}H NMR (400 MHz, D_2O) δ (ppm): 5.89 (4H, s, C (11 & 12)H), 7.47 (10H, s, C(14, 15, 16, 17, 18, 20, 21, 22, 23 & 24)H), 8.46 (4H, d, *J* = 7.1 Hz, C(2, 4, 7 & 10)H), 9.10 (4H, d, *J* = 7.1 Hz, C(1, 5, 8 & 9)H); ^{13}C NMR (100 MHz, $CDCl_3$) δ (ppm): 68.8 C(11 & 12)H_2, 127.1 C(2, 4, 7 & 10)H, 129.3 & 129.7 C(14, 18, 20, 24 & 15, 17, 21, 23)H, 130.2 C(16 & 22)H, 132.2 C(13 & 19), 145.5 C(1, 5, 8 & 9)H, 150.3 C(3 & 6); HRMS *m/z* (FAB+) 338.1783 ($C_{24}H_{22}N_2$ requires 338.1781)

3,5-Bis(benzyloxy)benzyl chloride 117

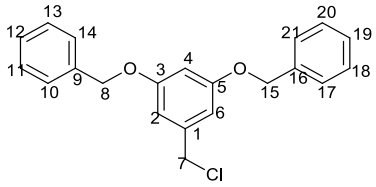

Thionyl chloride (0.55 mL, 7.5 mmol) was added dropwise to a stirred solution of 3,5-bis(benzyloxy)phenyl)methanol **116** (1.6 g, 5.0 mmol), triethylamine (0.80 mL, 5.3 mmol) and dry toluene (35 mL) at 0˚C. The resulting solution was allowed to warm to room temperature. After 3h the reaction was cooled to 0˚C and washed successively with water (3 × 20 mL), 10% 2N HCl, saturated aqueous $NaHCO_3$ (30 mL), water (20 mL). The organics were combined and dried over sodium sulphate, filtered and concentrated *in vacuo*. The product was purified using flash column chromatography, [gradient 80:20 pet ether : diethyl ether to 70:30 pet ether : diethyl ether] to give the title compound **117** as an off white solid (0.45 g, 25%). M.Pt. = 75-77 ˚C; ν_{max}/cm^{-1} (evaporated film) 3063, 3032, 2922, 2870-2851; ^{1}H NMR: (500 MHz, $CDCl_3$) δH (ppm): 4.51 (2H, s, C(7)H_2), 5.03 (4H, s, C(8 & 15)H_2), 6.57 (1H, t, *J* = 2.3 Hz,

C(4)H), 6.64 (2H, d, *J* = 2.3 Hz, C(2 & 6)H), 7.30-7.42 (10H, m, C(9, 10, 11, 12, 13, 14, 16, 17, 18, 19, 20 & 21)H); ^{13}C NMR: (125 MHz, $CDCl_3$) δC (ppm): 46.3 C(7)H_2, 70.2 C(8 & 15)H_2, 102.1 C(4)H, 107.7 C(2 & 6), 127.6 C(10, 11, 13 & 14 or 17, 18, 20 & 21)H, 128.1 C(12 & 19)H, 128.7 C(10, 11, 13 & 14 or 17, 18, 20 & 21)H, 136.6 (quat-C), 139.6 (quat-C), 160.1 (quat-C); HRMS *m/z* (EI +) 338.1074 ($C_{21}H_{19}O_2Cl$ requires 338.1065).

3,5-Bis(benzyloxy)benzyl methanesulfonate 118

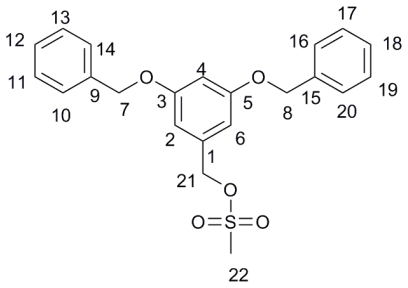

3,5-Bis(benzyloxy)phenyl)methanol **116** (1.0 g, 3.2 mmol) dissolved in CH_2Cl_2 (35 mL) was stirred with triethylamine (0.46 mL, 3.3 mmol). Methane sulphonyl chloride (0.36 mL, 4.7 mmol) was added and the mixture was left to stir for 2 h. The mixture was washed with water (20 mL) and aqueous brine (20 mL). The organics were combined and dried over sodium sulphate, filtered and concentrated *in vacuo* to give the title compound **118** as a clear liquid (1.0 g, 80%); ν_{max}/cm^{-1} (solution) 3140, 3024, 2924, 2338, 2029, 1967; ^{1}H NMR: (400 MHz, $CDCl_3$) δH (ppm): 2.85 (3H, s, C(22)H_3), 3.64 (2H, s, C(21)H_2), 5.06 (4H, s, C(7 & 8)H_2), 6.67 (3H, C(2, 4 & 6)H), 7.44 (10H, m, C(10H, m, C(9, 10, 11, 12, 13, 14, 16, 17, 18, 19, 20 & 21)H). ^{13}C NMR: (125MHz) δC (ppm): 38.4 (C(22)H_3), 52.4 (C(21)H_2), 70.1 (C(7 & 8)H_2) 103.2 (Ar C-H), 107.6 (Ar C-H), 127.5 (Ar C-H), 128.1 (Ar C-H), 128.7 (Ar C-H), 135.3 (2 × quat-C), 136.7 (2 × quat-C), 139.5 (quat-C). HRMS *m/z* (EI +) 398.1188 ($C_{22}H_{22}O_5S$ requires 398.1187)

1,1''-1,4-Phenylene-bis(methylene) bis-4,4'-bipyridinium 92

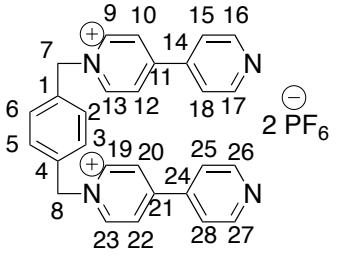

1,4-Bisbromomethylbenzene **93** (1.5 g, 5.7 mmol) in acetonitrile (100 mL) was added dropwise over an hour period to a refluxing solution of 4,4'-bipyridine **100** (5.0 g, 32 mmol) in acetonitrile (40 mL) and left to stir overnight. The crude product was collected by filtration and dissolved in water (30 mL) and heated. This solution was then pipetted slowly into an aqueous solution of NH_4PF_6 (9.0 g in 30 mL water) to precipitate a white solid, the powder was collected *via* filtration to give title compound **92** as a white powder (5.2 g, 98%); M.Pt = 200 ˚C dec.; ν_{max}/cm^{-1} (solid state) 3140, 3024, 2924, 2338, 2029, 1967, 1643; ^{1}H NMR: (400 MHz, $(CD)_3SO$) δH (ppm): 5.91 (4H, s, C(7 & 8)H), 7.70 (4H, s, C(2, 3, 5 & 6)H), 8.04 (4H, dd, *J* = 1.57 & 4.32 Hz, C(15, 18, 25 & 28)H), 8.67 (4H, d, *J* = 7.0 Hz, C(10, 12, 20 & 22)H), 8.90 (4H, dd, *J* = 1.57 & 4.32 Hz, C(16, 17, 26 & 27)H), 9.40 (4H, d, *J* =.7.0 Hz, C(9, 13, 19 & 23)H ; ^{13}C NMR: (100 MHz, $(CD)_3SO$) δC (ppm): 63.5 C(7 & 8)H_2 , 123.0 C(15, 18, 25 & 28)H, 126.9 C(10, 12, 20 & 22)H, 128.2 C(1, 2, 3, 6, 7 & 8), 130.7 C(4, 5, 9 & 10)H, 130.8 C(11, 12, 13 & 14), 136.3 (quat-C), 146.4 C(9, 13, 19 & 23)H, 146.78 (quat-C), 150.3 (quat-C), 152.0 C(16, 17, 26 & 27)H, 154.0 (quat-C); HRMS *m/z* (ESI +) 561.1624 ($C_{28}H_{24}N_4PF_6$ requires 561.1637)

1,5-Bis (2-(2'-(2''-ethanol)ethoxy)ethoxy) naphthalene 102

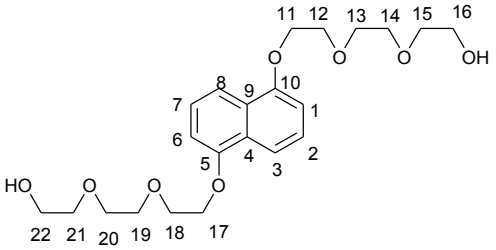

1,5 - Dihydroxynaphthalene **101** (10 g, 62 mmol) and K_2CO_3 (35 g, 251 mmol) were heated under reflux, under N_2 in dry acetonitrile (250 mL) for 10 min. To this mixture

was added 2-(2'-(2"-chloroethoxy)ethoxy) ethanol (20 mL) 138 mmol) dropwise. The reaction was stirred under reflux, under N_2 for 7d. The solvent was removed *in vacuo* and the residue partitioned between CH_2Cl_2 (100 mL) and water (100 mL). The organic layer was separated, washed with water (1 × 100 mL), 1M HCl (1 × 100 mL) and water (1 × 100 mL) respectively, dried over $MgSO_4$, filtered, and concentrated *in vacuo* before final purification *via* flash column chromatography [SiO_2: CH_2Cl_2/MeOH, 95/5] to yield **102** as a brown solid (16.6 g, 62%). M.Pt = 68-69 °C; ν_{max} (evaporated film) = 3497 (*br*), 3019, 2876, 1594; ^{1}H NMR (500 MHz, $CDCl_3$) δ (ppm): 2.94 (2H, *br* s, 2 × O<u>H</u>), 3.56 (4H, m, C(<u>H</u>$_2$), 3.66 (8H, m, C(13,14,19 & 20)<u>H</u>$_2$), 3.75 (4H, m, 2 × C<u>H</u>$_2$), 3.94 (4H, t, *J* = 4.5 Hz, 2 × C(11 & 17)<u>H</u>$_2$), 4.24 (4H, t, *J* = 4.8 Hz, C(16 & 22)<u>H</u>$_2$), 6.78 (2H, d, *J* = 7.7 Hz, C(1 & 6)<u>H</u>), 7.30 (2H, t, *J* = 7.8 Hz, (C(2 & 7)<u>H</u>), 7.83 (2H, d, *J* = 8.5 Hz, C(3 & 8)<u>H</u>); ^{13}C NMR (125 MHz, $CDCl_3$) δ (ppm): 61.7, 69.8 (<u>C</u> (16 & 22)H_2), 70.3, 70.5, 71.0, 72.6, 106.1, 114.9, 125.4, 127.0 (quat-<u>C</u>), 154.6 (quat-<u>C</u>) HRMS *m/z* (EI+) = 424.2096 ($C_{22}H_{32}O_8$ requires 424.2097)

1,5-Bis-(2-{2-[2-(triisopropylsilyloxy)ethoxy]ethoxy}ethoxy)naphthalene 109[75]

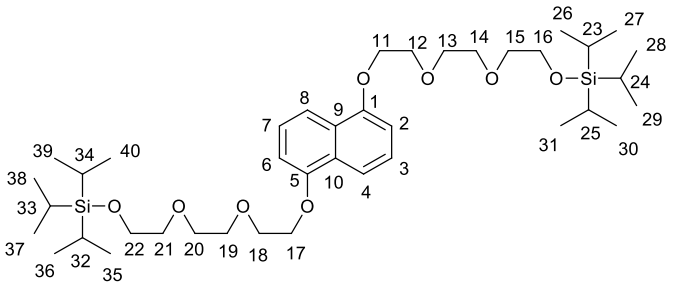

Triisopropylsilyl trifluoromethane sulfonate (1.6 mL, 5.9 mmol) and 2,6-dimethylpyridine (0.68 mL, 5.9 mmol) were added to a stirring solution of 1,5-bis (2-(2'-(2"-ethanol)ethoxy)ethoxy) naphthalene **102** (1.0 g, 2.4 mmol) in dry CH_2Cl_2 (30 mL) and left to stir at room temperature for 1h. The organic layer was then washed with water (20mL) and dried over $MgSO_4$, filtered and the solvent was removed *in vacuo* to yield **109** as an oil (1.6 g, 95 %). The observed data was in accordance with literature data.[75]

[2]-Rotaxane 103[75]

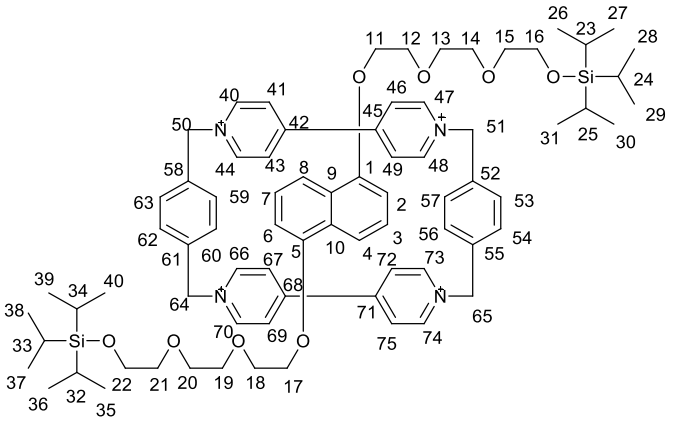

A solution of 1,1''-1,4-phenylene-bis(methylene) bis-4,4'-bipyridinium **92** (4.3 g, 6.1 mmol), 1,4-bis (bromomethyl) benzene **93** (1.6 g, 6.0 mmol) and 1,5-Bis-(2-{2-[2-(triisopropylsilyloxy)ethoxy]ethoxy}ethoxy)naphthalene **109** (1.6 g, 2.2 mmol) in dry acetonitrile (70 mL) was stirred at room temperature for 3w. The solvent was then removed *in vacuo* and the residue washed with diethyl ether and dissolved in acetone. Following filtration the solvent was removed *in vacuo* and the residue purified by column chromatography [SiO_2: MeOH / 2 M $NH_4Cl_{(aq)}$ / $MeNO_2$ (7:2:1)] to yield a purple solid which was dissolved in water and added dropwise to an aqueous solution of NH_4PF_6 to give rotaxane **103** (0.44 g, 11%). M.Pt >300˚C; ν_{max}/cm^{-1} (solid state) 3638, 3626, 3329, 3063, 3026, 1738, 1726; ^{1}H NMR (400MHz, CD_3CN) δ (ppm): 1.01 (42H, s, C (23, 24, 25, 26, 27, 28, 29, 30, 31, 32, 33, 34, 35, 36, 37, 38, 39 & 40)H & H_3), 2.46 (2H, d, C (4 & 8)H), 3.53 & 3.63 (4H, m, C (12 & 18)H_2), 3.70 (4H, m, C (13 & 19)H_2), 3.77 & 3.82 (4H, m, C (11 & 17)H_2), 3.98 (4H, m, C (16 & 22)H_2), 4.05 & 4.23 (4H, m, C (14 & 20)H_2), 4.32 (4H, m, C (15 & 21)H_2), 5.88 (8H, m, C (50, 51, 64 & 65)H_2) 6.01 (2H, t, C (3 & 7)H), 6.30 (2H, d, C (2 & 6)H), 7.26 (4H, s, C (40, 47, 70 & 74)H), 7.42 (4H,s, C (44, 48, 66 & 73)H), 8.0 (8H, d, C (53, 54, 56, 57, 59, 60, 62 & 63)H), 8.68 (4H, s, C (41, 46, 69 & 75)H), 9.05 (4H, s, C (43, 49, 67 & 72)H) ^{13}C NMR (100 MHz, CD_3CN) δ (ppm): 12.6 (C (23, 24, 25, 32, 33 & 34)H), 18.3 (C (26, 27, 28, 29, 30, 31, 35, 36, 37, 38,39 & 40)H_3), 63.6 (C (13 & 19)H_2), 66.0 (C (51, 52, 65 & 66)H_2), 69.3 (C (15 & 21)H_2), 70.7 (C (14 & 20)H_2), 71.8 (C (11 & 17)H_2), 72.1 (C (16 & 22)H_2), 73.6 (C (12 & 18)H_2), 105.2 (C (2 & 6)H) & C (3 & 7)H), 109.2 (C (4 & 8)H), 125.3 & 125.7 (C (44, 48, 66 & 73)H) , 127.2 (C (41, 46, 69 & 75)H), 129.1, 130.8 (C (53, 54, 56, 57, 59, 60, 62 & 63)H),

137.5 (C (1 & 5)), 145.0 (C (40, 47, 70 & 74)H), 146.1 (C (42, 45, 68 & 71)), 152.0 (C (52, 55, 58 & 61)

1,5-Bis(2-(2-(2-bromoethoxy)ethoxy)ethoxy)naphthalene 110

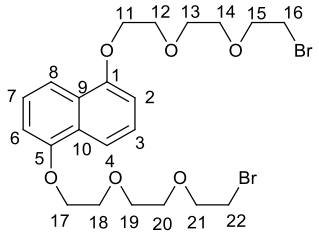

Triphenylphosphine (2.5 g, 9.5 mmol), carbon tetrabromide (3.1 g, 9.5 mmol) and 1,5-bis (2-(2'-(2''-ethanol)ethoxy)ethoxy) naphthalene **102** (2.0 g, 4.8 mmol) in dry acetonitrile (200 mL) were stirred at room temperature under N_2 for 24h. The solvent was removed *in vacuo* to afford the crude product which was purified *via* flash column chromatography [SiO_2: CH_2Cl_2/ethyl acetate (3:1)] to yield **110** as a dark brown oil (1.8 g, 67%) ν_{max}/cm^{-1} (evaporated film) 2920, 2872, 1738, 1728; ^{1}H NMR (500 MHz, $CDCl_3$) δ = 7.86 (2H, d, *J= 8.6 Hz,* C (4 & 8)H), 7.35 (2H, t, *J*= 8 Hz, C (3 & 7)H), 6.84 (2H, d, *J*=7.7Hz, C (2 & 6)H), 4.30 (4H, t, *J* =4.8 Hz, C (11 & 17)H_2), 4.0, (4H, t, *J*= 4.8Hz, C (12 & 18)H_2), 3.81 (8H, m, C (14, 15, 20 & 21)H_2), 3.72 (4H, m, C (13 & 19)H_2), 3.46 (4H, t, *J*= 6.3 Hz, C (16 & 22)H_2); ^{13}C NMR (125 MHz, $CDCl_3$) δ = 154.5 (C (1 & 5)H), 126.9 (C (9 & 10)H), 125.2 (C (3 & 7)H), 114.8 (C (4 & 8)H), 105.8 (C (2 & 6)H), 71.4, 71.1 (C (13 & 19)H_2) 70.8 (C (14, 15, 20 & 21)H_2), 70.0 (C (12 & 18)H_2), 68.1 (C (11 & 17)H_2), 30.5 (C (16 & 22)H_2); HRMS *m/z* (EI +) 550.0388 ($C_{22}H_{30}O_6Br_2$ requires 550.0390)

3,6 –Di-*tert*-butyl- 9*H*-carbazole[138] 112

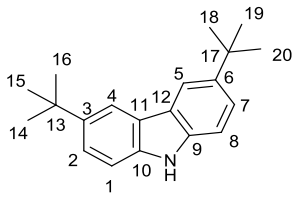

Carbazole **111** (5.1 g, 3.0 mmol) and anhydrous $AlCl_3$ (4.0 g, 3.0 mmol) were dissolved in CH_2Cl_2 (100 mL). The mixture was then cooled to 0 ˚C and a solution of *tert*-butyl chloride (6.6 mL, 6.0 mmol) in CH_2Cl_2 (20 mL) was added. The ice-bath

was removed and the mixture was stirred at room temperature for 24h. The mixture was then poured into water, extracted into CH_2Cl_2 (2 x 100 mL), dried over $MgSO_4$, and filtered. The solvent was removed *in vacuo* to afford the crude product, which was re-crystallised from pet ether to produce **112** as an off-white solid (3.5 g, 41%). M.Pt = 212-215 ˚C; ν_{max}/cm^{-1} (evaporated film) 3408, 3390, 2950, 2932, 2924, 2889, 2851, 2358, 2344, 2326; ^{1}H NMR (400 MHz, $CDCl_3$) δ = 1.44 (18H, s, C (14, 15, 16, 18, 19 & 20)H), 7.34 (2H, d, *J*=8.5Hz, C (1&8)H) , 7.46 (2H, dd, *J*=8.5Hz & 1.8Hz C (2&7)H), 7.86 (1H, s, N-H), 8.07 (2H, d, *J*= 1.8 Hz, C (4&5)H); ^{13}C NMR (100 Hz, $CDCl_3$) δ= 32.1 C (14, 15, 16, 18, 19&20)H_3, 34.8 C (13&17), 110.1 C (1&8)H, 116.3 C (4&5)H, 123.4 C (11&12), 123.6 C (2&7)H, 138.1 C (9&10), 142.3 C (3&6); HRMS *m/z* (EI +) 280.2065 ($C_{20}H_{25}N$ requires 280.2061)

1,5-Bis(triethoxy-*tert*-butyl carbazole) naphthalene 113

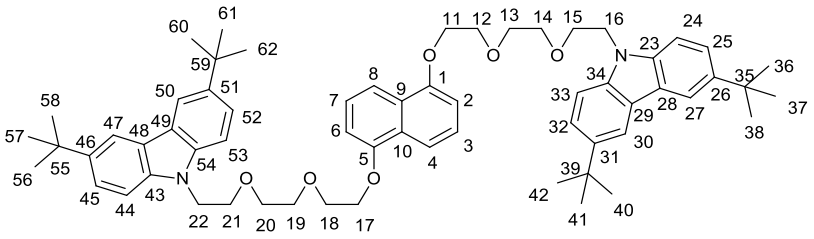

3,6–Di-*tert*-butyl- 9*H*-carbazole **112** (1.3 g, 4.5 mmol), 1,5-Bis(2-(2-(2-bromoethoxy)ethoxy)ethoxy)naphthalene **110** (1.0 g, 1.8 mmol), potassium hydroxide (2.3 g, 41.5 mmol) and sodium iodide (1.4 g, 9.2 mmol) were stirred in acetone (50 mL) at room temperature for 48h. The solvent was then removed *in vacuo* and the product purified *via* flash column chromatography [SiO_2: CH_2Cl_2 100% - CH_2Cl_2 96%/acetone 4%] to yield **113** as a brown oil (0.69 g, 39%). ν_{max}/cm^{-1} (evaporated film) 2955, 2909, 2870, 2361, 1983, 1713, 1659, 1597; ^{1}H NMR (500 MHz $CDCl_3$) δ (ppm): 1.43 (36H, s, C (36, 37, 38, 40, 41, 42, 56, 57, 58, 60, 61 & 62)H), 3.60 - 4.50 (24H, m, C (11, 12, 13, 14, 15, 16, 17, 18, 19, 20, 21 & 22)H_2), 6.81 (4H, m (carbazole Ar C-H)), 7.33 (4H, m (naphthalene Ar-C-H)), 7.47 (2H, m, (naphthalene Ar C-H)), 7.84 (4H, dd, *J* = 16.1 & 22.4 Hz (carbazole Ar-C-H)), 8.07 (4H, d, *J* = 1.5 Hz, (carbazole Ar C-H)); ^{13}C NMR (125 MHz $CDCl_3$) δ (ppm): 31.1, 32.2 & 34.8 (C (11, 12, 13, 14, 15, 16, 17, 18, 19, 20, 21 & 22)H_2), 43.3 (C (35, 39, 55 & 59)quart), 68.0, 68.1, 69.6, 69.9, 70.0 & 70.6 (C (11, 12, 13, 14, 15, 16, 17, 18, 19, 20, 21 & 22)H_2), 105.8 (Ar C-H), 106.0 (Ar C-H), 108.4 (Ar C-H), 116.3 (Ar C-H), 122.9 (Ar

quat-C), 123.4 (Ar C-H), 125.2 (Ar C-H), 126.9 (Ar quat-C), 139.2 (Ar quat-C), 141.9 (Ar quat-C), 154.5 (Ar quat-C),

[2]-Rotaxane 104

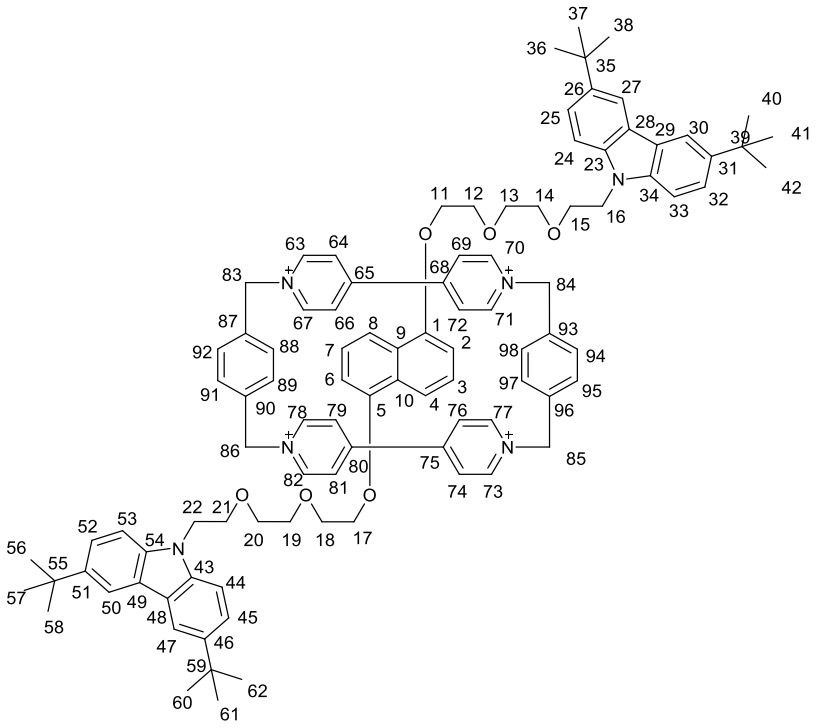

1,1''-1,4-Phenylene-bis(methylene) bis-4,4'-bipyridinium **92** (1.2 g, 1.7 mmol), 1,4-bis (bromomethyl) benzene **93** (0.45 g, 1.7 mmol) and 1,5-bis (triethoxy- *tert*-butyl carbazole) naphthalene **113** (0.58 g, 1.6 mmol) in dry acetonitrile (50 mL) were stirred at room temperature for 10d. The solvent was removed *in vacuo* and the residue was washed with diethyl ether and dissolved in acetone. Following filtration the solvent was reduced *in vacuo* and the residue was purified by flash column chromatography [SiO_2: MeOH: 2 M NH_4Cl: $MeNO_2$ (7:2:1)] to afford **104** as a purple solid (0.59 g, 20%). M.Pt > 300˚C; ν_{max}/cm^{-1} (solid state) 3750, 3634, 2415, 2284, 2238, 2183, 1736; ^1H NMR (500 MHz, CD_3CN) δ= 1.62 (36H, d, *J*= 5.2 Hz, C (36, 37, 38, 40, 41, 42, 56, 57, 58, 60, 61 & 62) H_3), 2.26 (2H, m, C (4 & 8) H), 4.25 - 4.46 (20H, m, C (11, 12, 13, 14, 15, 17, 18, 19, 20 & 21)H_2), 4.71 (4H, m, C (16 & 22)H_2), 5.33 - 5.54 (8H, m, C (83, 84, 85 & 86) H_2), 5.97 - 6.02 (2H, m, C (3 & 7)H), 6.33 (2H, t, *J*= 9.7 Hz C(2 & 6)H), 6.9 - 7.3 (8H, m, C (63, 67, 70, 71, 73, 77, 78 & 82)H), 7.6 - 7.7 (8H, m, 88, 89, 91, 92, 94, 95, 97 & 98)H), 8.05 (12H, m, 24, 25, 27,

30, 32, 33, 44, 45, 47, 50, 52 & 53)H), 8.52, (4H, d, *J*=10.5 Hz, C (64, 69, 74 & 81)H), 8.8 (4H, m, 66, 72, 76 & 79)H); ^{13}C NMR (125 MHz $CDCl_3$) δ (ppm): 30.9, 31.1 & 33.9 (C (11, 12, 13, 14, 15, 16, 17, 18, 19, 20, 21 & 22)H_2), 43.0 (C (35, 39, 55 & 59)quart), 64.2 C(7 & 8)H_2, 67.6, 68.1, 69.3, 69.9, 70.5& 70.6 (C (11, 12, 13, 14, 15, 16, 17, 18, 19, 20, 21 & 22)H_2), 105.8 (Ar C-H), 106.0 (Ar C-H), 108.5 (Ar C-H), 116.3 (Ar C-H), 122.9 (Ar quat-C), 123.3 C (15, 18, 25 & 28)H, 123.4 (Ar C-H), 125.2 (Ar C-H), 126.9 (Ar quat-C), 128.3 (Ar C-H), 130.5 (Ar C-H), 136.3, 139.2 (Ar quat-C), 141.9 (Ar quat-C), 146.4 C (9, 13, 19 & 23)H, 154.5 (Ar quat-C),

1,5-Bis(2-{2-[2-(4,4'-[(2,2'-bithienyl)-N-pyrrolyl]-3-(carboxybenzene) ethoxy] ethoxy} ethoxy) naphthalene 115

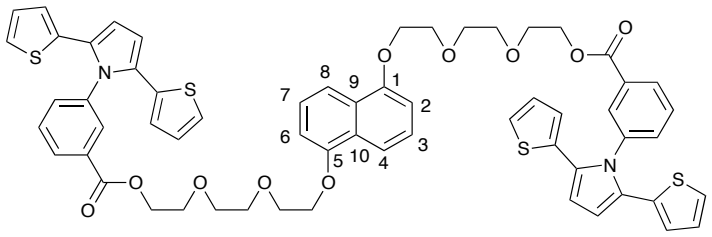

Bis-4,4'-[(2,2'-bithienyl)-*N*-pyrroyl]-3-carboxybenzene **114** (0.37 g, 1.1 mmol), 1,5-bis (2-(2'-(2''-ethanol)ethoxy)ethoxy) naphthalene **102** (0.21 g, 0.49 mmol), DMAP (0.14 g, 1.2 mmol), and DIC (0.17 mL, 1.1 mmol) were stirred in CH_2Cl_2 (100 mL) at room temperature for 6d. The crude product was then purified using flash column chromatography [SiO_2: CH_2Cl_2] to yield **115** as a brown oil (0.29 g, 56%). ν_{max} (evaporated film) 3338, 3104, 2967, 2873; ^{1}H NMR (500 MHz, $CDCl_3$) δ (ppm): 3.71 (4H, m), 3.76 - 4.44 (24H, m, (12 × CH_2)), 6.51 (4H, dd, *J* = 1.1 & 3.6 Hz), 6.53 (4H, s, (pyrrole C-H)), 6.80 (4H, m, (Ar C-H)), 7.23 (2H, m, Ar (C-H)), 7.32 (4H, m, (Ar C-H)), 7.47 (4H, m, (Ar C-H)), 7.60 (2H, m, (Ar C-H)), 7.84 (2H, m, (Ar C-H)), 8.01 (2H, s, (Ar C-H)), 8.15 (2H, dt, *J* = 1.9 & 7.1 Hz, (Ar C-H)); ^{13}C NMR (125 MHz, $CDCl_3$) δ (ppm): 64.4, 68.0, 69.3, 70.6, 71.2 & 72.6 (CH_2), 105.8 (Ar C-H), 110.3 (Ar C-H), 114.7 (Ar C-H), 124.6 (Ar C-H), 126.9 (Ar quat-C), 130.3 (Ar quat-C), 131.4 (Ar C-H), 134.6 (Ar C-H), 138.9 (Ar quat-C), 154.4 (Ar quat-C), 165.6 (Ar quat-C), 207.2 (C=O); HRMS *m/z* (ESI + Na)$^+$ =1113.2567 ($C_{60}H_{54}N_2O_{10}S_4Na$ requires 1113.2553)

[2]-Rotaxane 105

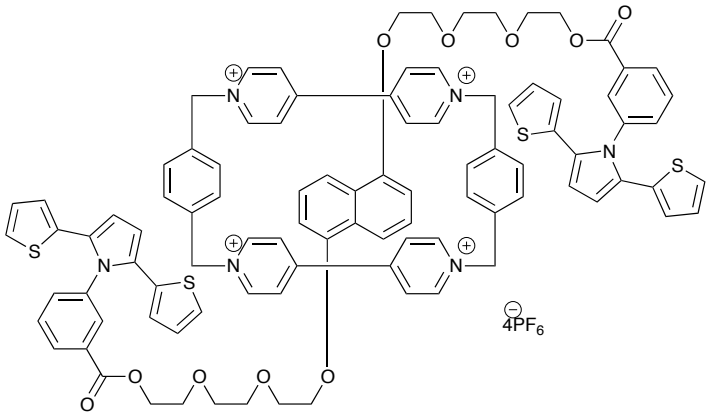

1,5-Bis(2-{2-[2-(4,4'-[(2,2'-bithienyl)-N-pyrrolyl]-3-carboxybenzene)ethoxy] ethoxy}ethoxy) naphthalene **115** (0.27 g, 0.25 mmol), α,α'-1,4-phenylene-bis-methylene bis-4,4'-bipyridinium **92** and (0.49 g, 0.69 mmol) and 1,4-bis(bromomethyl)benzene **93** (0.19 g, 0.71 mmol) were stirred in dry acetonitrile (30 mL) at room temperature for 10d. The solvent was then removed and the residue washed with diethyl ether and dissolved in acetone. The mixture was filtered and the solvent was again removed to give the crude product. The product was purified *via* flash column chromatography [SiO_2: MeOH/2M NH_4Cl (*aq*)/ nitromethane 7:2:1] to yield a purple solid. The solid was dissolved in water and added slowly to a saturated solution of NH_4PF_6 (*aq*) and the purple precipitate was collected *via* filtration to give the final rotaxane **105** as the PF_6 salt (0.16 g, 28%) M.Pt >300 °C; ν_{max} (evaporated film) 2359, 1715; ^{1}H NMR (500 MHz, CD_3CN) δ (ppm): 3.91 (4H, m), 3.95 (4H, m), 4.02 (4H, m), 4.20 (4H, m), 4.29 (4H, m), 4.43 (4H, m), 5.68 (12H, s), 5.96 (8H, t, *J* = 8.1 Hz), 6.25 (8H, d, *J* = 7.9 Hz), 6.54 (4H, s), 6.58 (4H, dd, *J* = 1.1 & 3.6 Hz), 6.86 (4H, dd, *J* = 1.5 & 8.8 Hz), 7.19 (4H, dd, *J* = 1.1 & 5.2 Hz), 7.49 (4H, m), 7.71 (2H, m), 8.04 (4H, m), 8.59 (4H, s), 8.97 (4H,s); ^{13}C NMR (125 MHz, CD_3CN) δ (ppm): 29.6, 64.0, 64.8, 68.7, 70.4, 70.7, 104.0, 110.0, 124.7, 124.7, 127.0, 129.7, 130.1, 130.94, 133.86, 136.1, 144.7, 164.9

***N* - (Propanol)- *N′* -(octyl) naphthalene diimide 194**

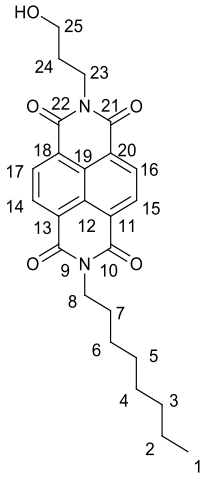

1,4,5,8-Naphthalene tetracarboxylic dianhydride **160** (15 g, 56 mmol) was stirred in dry DMF (150 mL) under N_2. To this mixture was added octylamine (9.3 mL, 56 mmol) and the reaction stirred at reflux, under N_2 for 24h. 3-Amino-1-propanol (4.3 mL, 56 mmol) was added and the reaction stirred for a further 24h. The mixture was partitioned between CH_2Cl_2 and water and the organic layers collected, dried over $MgSO_4$, filtered, and concentrated before purification *via* column chromatography [SiO_2: CH_2Cl_2/acetone, 9/1] to yield **194** as a pale pink/brown solid (0.99 g, 4%) M.Pt = 197-199 °C; ν_{max} (solid state): 3356, 3086, 2924, 2851, 1701, 1655, 1578; ^{1}H NMR (500 MHz, $CDCl_3$) δ (ppm): 0.87 (3H, t, *J* =7.7 Hz, C(1)$\underline{H}_3$), 1.34 (12H, m, C(2, 3, 4, 5, 6 & 7)$\underline{H}_2$), 1.74 (4H, quint, *J* = 15.1 Hz, C(8 & 23)$\underline{H}_2$-N), 4.18 (4H, t, *J* = 7.7 Hz, C(24 & 25)$\underline{H}_2$-O) 8.76 (4H,s, C(14, 15, 16 & 17)$\underline{H}$); ^{13}C NMR (125 MHz, $CDCl_3$) δ (ppm): 14.1 (C(1)$\underline{H}_3$), 22.6, 27.1, 28.1, 29.3 & 31.8 (C(2, 3, 4, 5, 6 & 7)$\underline{H}_2$), 29.2 $\underline{C}$(8 & 23)H_2-N), 41.0 ($\underline{C}$(24 & 25)H_2-O), 126.7 (quat-$\underline{C}$), 126.7 (quat-$\underline{C}$), 130.9 ($\underline{C}$(14, 15, 16 & 17)H), 162.8 (C=O); HRMS *m/z* (EI+) = 437.2076 ($C_{25}H_{28}O_5N_2$ requires 437.2072)

***N*-(Octyl)-*N′*-(propyl methacrylate) naphthalene diimide 182**

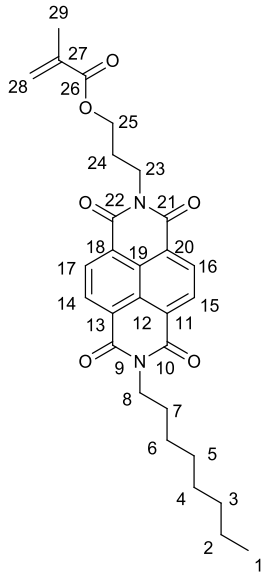

N-(Propanol)-*N′*-(octyl) naphthalene diimide **194** (0.69 g, 1.6 mmol) was stirred in dry THF (20 mL). NEt_3 (0.44 mL, 3.2 mmol) followed by methacryolyl chloride (0.31 mL, 3.2 mmol) was added and the reaction stirred at room temperature overnight. The solvent was removed *in vacuo* and the product purified *via* recrystallisation from pet ether to yield **182** as a cream solid (0.60 g, 76%). M.Pt = 141 – 143 °C; ν_{max} (evaporated film): 3432, 3356, 3089, 2957, 2926, 2855, 1964, 1721, 1703, 1660, 1603, 1579; ^{1}H NMR (500 MHz, $CDCl_3$) δ (ppm): 0.88 (3H, C(1)$\underline{H}_3$), 1.41 (10H, m, C(2, 3, 4, 5 & 6)$\underline{H}_2$), 1.74 (2H, C(7)$\underline{H}_2$), 2.17 (2H, C(24)$\underline{H}_2$), 3.10 (3H, C(29)$\underline{H}_3$), 4.19 (2H, C(8)$\underline{H}_2$), 4.28 (2H, C(23 or 25)$\underline{H}_2$), 4.36 (2H, C(23 or 25)$\underline{H}_2$), 5.51 (1H, C(28)$\underline{H}$), 6.10 (1H, C(28)$\underline{H}$), 8.76 (4H, s, C(14, 15, 16 & 17)$\underline{H}$); ^{13}C NMR (125 MHz, $CDCl_3$) δ (ppm): 14.1 ($\underline{C}$(1)H_3), 8.6, 28.1, 29.2, 29.3 & 31.8 ($\underline{C}$(2, 3, 4, 5 & 6)H_2), 22.6 ($\underline{C}$(24)H_2), 27.1 ($\underline{C}$(7)H_2), 41.0 ($\underline{C}$(8)H_2), 45.8 ($\underline{C}$29)H_3), 62.4 ($\underline{C}$(23 or 25)H_2), 130.9, 131.1, 162.9 (C=O); HRMS *m/z* (CI+) = 505.2340 ($C_{29}H_{33}O_6N_2$ requires 505.2339)

Poly(*N*-(Octyl)-*N′*-(propyl methacrylate) naphthalene diimide) 196

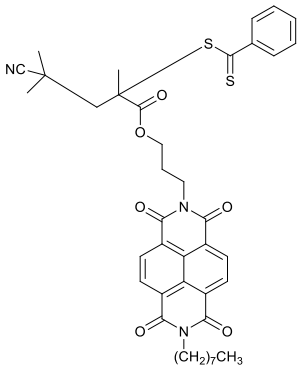

N-(Octyl)-*N′*-(propyl methacrylate) naphthalene diimide **182** (0.66 g, 1.3 mmol), AIBN (2.0 mg, 0.012 mmol) and 2-cyano-2-propyl benzodithioate (10.0 mg, 0.045 mmol) were dissolved in 1,2-dichlorobenzene (3 mL) and subjected to freeze-pump-thaw degassing before transfer to a preheated oil bath at 60 ºC. The reaction was monitored by GPC and terminated after 3h by precipitation into MeOH (300 mL). The precipitate was collected *via* filtration and subjected to purification *via* soxhlet extraction using pet ether followed by $CHCl_3$ producing polymer **196** as a white solid (40 mg) GPC: (THF, 30°C at 1mL/min) M_n = 4634, M_w = 5375, PDI 1.2

Poly(3-hexylthiophene)-ethynyl (205)

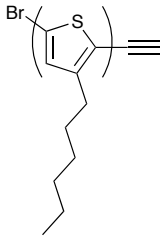

2,5-Dibromo-3-hexyl-thiophene **204** (0.87 mL, 4.2 mmol) was stirred in dry THF (50 mL) under N_2. To this was added isopropylmagnesium chloride (2.1 mL of 2.0 M solution in THF) and the reaction stirred for 2h. Ni(dppp)Cl_2 (0.055 g, 0.102 mmol) was then added and the solution turned orange. After 10m of stirring ethynyl magnesium bromide (2.5 mL of a 0.5 M solution in THF) was added and the reaction stirred for a further 5m. The mixture was then precipitated into MeOH (300 mL) producing a purple precipitate. The solid was collected *via* filtration and purified by a series of soxhlet extractions, acetone, diethyl ether, pet ether, CH_2Cl_2. The final

CH_2Cl_2 soxhlet extraction was concentrated *in vacuo* to yield polymer **205** as a purple polymer (180 mg) GPC: (THF, 30°C at 1mL/min) M_n = 6021, M_w = 8642, PDI 1.3

Poly(*N*-(Octyl)-*N′*-(propyl methacrylate) naphthalene diimide)- 3-azido-1-propanol ester 206

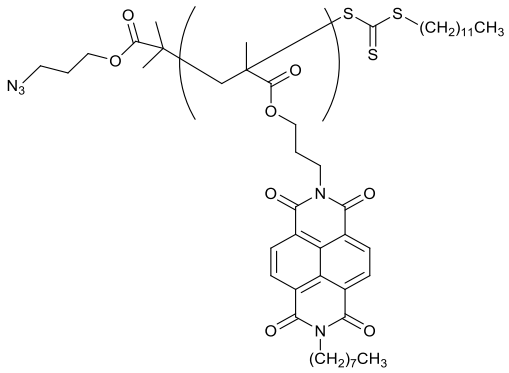

Reaction 1

N-(Octyl)-*N′*-(propyl methacrylate) naphthalene diimide **182** (0.57 g, 1.1 mmol), AIBN (2 mg, 0.0098 mmol) and 2-(dodecylthiocarbonothioylthio)-2-methylpropionic acid 3-azido-1-propanol ester **207** (0.017 g, 0.038 mmol) were dissolved in 1,2-dichlorobenzene (3 mL) and subjected to freeze-pump-thaw degassing before transfer to a preheated oil bath at 70 ºC. The reaction was monitored *via* GPC and terminated after 2.5h by precipitation into MeOH (300 mL). The solid was purified *via* soxhlet extraction with diethyl ether to give polymer **206a** as a white solid (0.17 g) GPC: (THF, 30°C at 1mL/min) M_n = 21135, M_w = 28059, PDI 1.3

Reaction 2

N-(Octyl)-*N′*-(propyl methacrylate) naphthalene diimide **182** (0.35 g, 0.70 mmol), AIBN (1.0 mg, 0.0061 mmol) and 2-(dodecylthiocarbonothioylthio)-2-methylpropionic acid 3-azido-1-propanol ester **207** (0.011 g, 0.023 mmol) were dissolved in 1,2-dichlorobenzene (3 mL) and subjected to freeze-pump-thaw degassing before transfer to a preheated oil bath at 70 ºC. The reaction was monitored *via* GPC and terminated after 1.5h by precipitation into MeOH (300 mL). The solid was purified *via* column chromatography [Al_2O_3: CH_2Cl_2] to give polymer **206b** as a white solid (0.18 g) GPC: (THF, 30°C at 1mL/min) M_n = 59503, M_w = 86623, PDI 1.4

Poly(3-hexylthiophene)-(*N*-(Octyl)-*N′*-(propyl methacrylate) naphthalene diimide) 188

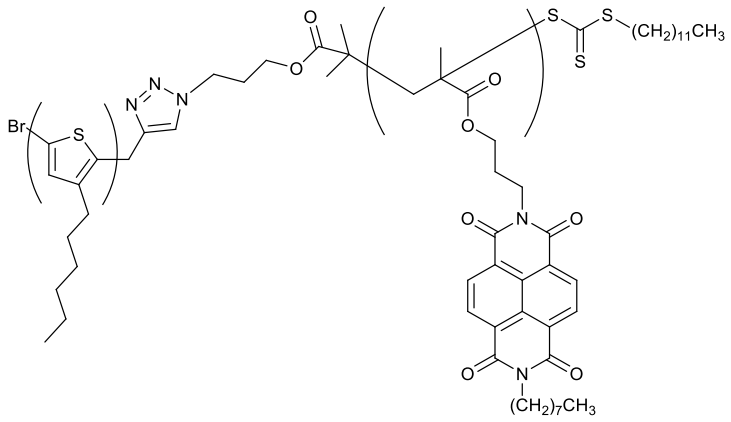

Reaction 1

Polymer **205** (72.0 mg, 8.5 μmol), polymer **206** (150 mg, 7.1 μmol), Cu(I)Br (5.5 mg, 0.038 mmol) and PMDETA (8.0 μL, 0.038 mmol) were dissolved in dry THF (20 mL). The mixture was degassed for 5m before stirring at 55 ºC for 3d. The polymerisation was terminated by precipitation into MeOH (300 mL) and the solid purified *via* column chromatography [Al_2O_3: $CHCl_3$ then THF] to yield a purple polymer **188** (108 mg) GPC: (THF, 30°C at 1mL/min) M_n=24029 g/mol, M_w=30100 g/mol, PDI=1.2

Reaction 2

Polymer **205** (15 mg, 1.7 μmol), polymer **206** (120 mg, 2.0 μmol), Cu(I)Br (1.7 mg, 0.012 mmol) and PMDETA (2.0 μL, 0.0089 mmol) were dissolved in dry THF (20 mL). The mixture was degassed for 5m before stirring at 55 ºC for 2d. The polymerisation was terminated by precipitation into MeOH (300 mL) and the solid purified *via* column chromatography [Al_2O_3: $CHCl_3$ then THF] to yield a purple polymer **188** (80 mg) GPC: (THF, 30°C at 1mL/min) M_n = 79828, M_w = 104469, PDI = 1.3

^{1}H NMR (500 MHz, $CDCl_3$) δ (ppm) 0.80-0.99 (*br*, m, alkyls), 1.11-1.20 (*br*, m, alkyls), 1.21-1.47 (*br*, m, alkyls) 1.51-1.53 (*br*, m, alkyls), 2.01-2.19 (*br*, m, alkyls), 3.98-4.29 (*br*, m, O/N-CH_2), 8.15-8.49 (*br*, m, aromatics)

2-([2,2':5',2''-Terthiophene]-5-carboxamido)ethyl methacrylate 184

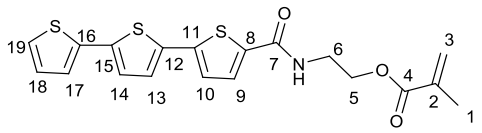

2,2':5',2''-Terthiophene **197** (1.1 g, 4.3 mmol) was stirred in dry DMF (200 mL) at -78 °C under N_2. To this solution was added *n*-BuLi (2.8 mL, 4.4 mmol) and the reaction left to stir at -78°C under N_2 for 1h. 2-Isocyanatoethyl methacrylate (0.63 mL, 4.4 mmol) was then added and the reaction left to stir for a further 1h at -78 °C under N_2. The reaction was allowed to warm to room temperature and the solvent was removed *in vacuo* and the crude product was dissolved in CH_2Cl_2 (100 mL) and washed with water (3 × 100 mL) before purification *via* flash column chromatography [SiO_2: chloroform/acetone, 98/2] to yield **184** as a yellow solid (0.37 g, 21%) M.Pt = 97-99 ºC; ν_{max} (solid state) = 2361, 1707; ^{1}H NMR (500 MHz, $CDCl_3$) δ (ppm): 1.97 (3H, s, C (1)H$_3$), 3.76 (2H, q, *J* = 5.5 Hz, C (6)H$_2$), 4.38 (2H, t, *J* = 5.2 Hz, C (5)H$_2$), 5.63 (1H, quin, *J* = 1.6 Hz, C (3)H), 6.16 (1H, t, *J* = 1.1 Hz, C (3)H), 6.36 (1H, *br* s, N-H), 7.04 (1H, dd, *J* = 3.7 Hz, C (18)H), 7.11 (2H, dd, *J* = 3.8 Hz, C(10 & 13)H), 7.16 (1H, d, *J* = 3.8 Hz, C (14)H), 7.20 (1H, dd, *J* = 1.1 & 3.6 Hz, C (19)H), 7.25 (1H, d, *J* = 1.1 Hz, C (17)H), 7.38 (1H, d, *J* = 3.9 Hz, C (9)H); ^{13}C NMR (125 MHz, $CDCl_3$) δ (ppm): 18.3 (C(1)H$_3$), 39.7 (C(6)H$_2$), 63.5 (C(5)H$_2$), 123.7 (C(10)H), 124.2 (C(19)H), 124.5 (C(13)H), 125.0 (C(17)H), 125.7 (C(14)H), 126.4 (C(3)H$_2$), 128.0 (C(18)H), 128.9 (C(9)H), 135.0 (thiophene quat-C), 135.9 (thiophene quat-C), 136.5 (thiophene quat-C), 136.7 (thiophene quat-C), 141.8 (thiophene quat-C), 161.6 (C=O); HRMS *m/z* (EI+) = 403.0371 ($C_{19}H_{17}O_3NS_3$ requires 403.0373)

***N*-(Nitrophenyl)-3,6-*tert*-butyl-9*H*- carbazole 198**

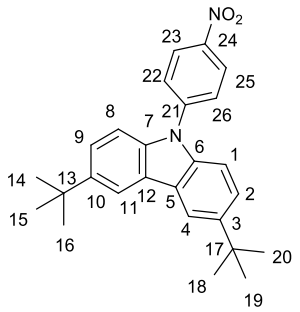

3,6-*Tert*-butyl-9*H*- carbazole **112** (1.0 g, 3.7 mmol), 1-iodo-4-nitrobenzene **199** (0.98 g, 3.9 mmol), palladium(II)acetate (8.8 mg, 3.9 μmol) and rubidium carbonate (2.5 g, 11 mmol) were stirred in xylene (50 mL) under N_2 at room temperature. To this mixture was added, carefully, tri-*tert*-butyl phosphine (30 μL, 0.012 mmol) under a N_2 atmosphere. The mixture was left to stir at 120 ˚C for 5h. The solvent was removed *in vacuo* and the product purified *via* flash column chromatography [Al_2O_3 : pet ether /ethyl acetate , 80/20] to yield **198** as a yellow solid (1.5 g, 98%) M.Pt = 112-115 °C; ν_{max} (solid state): 3411, 3345, 2955, 2905, 2862; ^{1}H NMR (500 MHz, $CDCl_3$) δ (ppm): 1.46 (18H, s C (14, 15, 16, 18, 19 & 20)H$_3$) 7.34 (2H, d, *J* = 8.5 Hz, C(1 & 8)H), 7.46 (2H, dd, *J* = 1.9 & 8.5 Hz C(22 & 26)H), 7.93 (2H, m, C(2 & 9)H), 8.07 (2H, d, *J* =1.7 Hz, C(23 & 25)H); ^{13}C NMR (125 MHz, $CDCl_3$) δ (ppm): 32.2 C(14, 15, 16, 18, 19 & 20)H$_3$, 34.8 C(13 & 17),110.1 & 116.3 C(1 & 8)H, 123.6 & 123.4 C(22 & 26)H, 125.0, 138.1 & 138.8 C(2 & 9)H, 142.3; HRMS *m/z* (EI+) = 400.2146 ($C_{26}H_{28}O_2N_2$ requires 400.2151)

***N*-(Aniline)-3,6-*tert*-butyl-9*H*-carbazole 200**

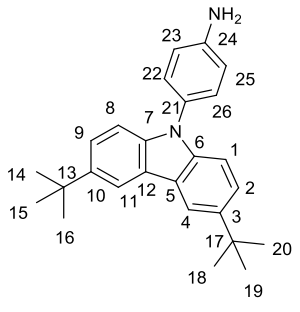

N-(Nitrophenyl)-3.6-*tert*-butyl-9*H*-carbazole **198** (0.82 g, 2.0 mmol), ammonium formate (1.6 g, 26 mmol) and 10% Pd/C (0.28 g, 0.26 mmol) were stirred in methanol

(20 mL) at room temperature. After 24h, 2 drops of acetic acid were added and the reaction mixture was left to stir for a further 3d at room temperature. The Pd/C was removed *via* filtration through 1 cm celite and the mixture was extracted with ethyl acetate (2 × 100 mL). The organic extracts were combined, washed with water (2 × 100 mL), dried over $MgSO_4$, filtered and concentrated *in vacuo* to yield **200** as a brown solid (0.40 g, 53%) ^{1}H NMR (500 MHz, $CDCl_3$) δ (ppm): 1.45 (18H, s C (14, 15, 16, 18, 19 & 20)H$_3$) 7.34 (2H, d, *J* =8.5 Hz, C(1 & 8)H), 7.46 (2H, dd, *J* =1.9 & 8.5 Hz C(22 & 26)H), 7.92 (2H, m, C(2 & 9)H), 8.07 (2H, d, *J* =1.7, C(23 & 25)H); ^{13}C NMR (125 MHz, $CDCl_3$) δ (ppm): 31.8 C(14, 15, 16, 18, 19 & 20)H$_3$, 34.7 C(13 & 17), 110.0 & 110.5 C(1 & 8)H, 116.2 C(23 & 25)H, 123.4 C(22 & 26)H, 123.5, 124.9 C(2 & 9)H, 138.0, 138.7, 142.2

2-([2,2'-(Tetrathiafulvalene)]carboxamido)ethyl methacrylate 211

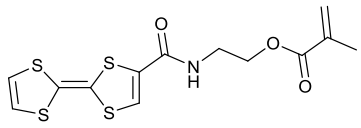

Tetrathiafulvalene **189** (1.0 g, 5.0 mmol) was dissolved in dry diethyl ether (200 mL) and cooled to -78 °C under N_2. *N*-BuLi (3.5 mL of 1.6M solution in hexane) was then added slowly and the reaction stirred for 1h. 2-Isocyanatoethyl methacrylate (0.77 mL, 5.4 mmol) was then added at -78 °C and the reaction stirred until the solution warmed to room temperature. The reaction mixture was washed with water (3 × 100 mL) and the organic extracts combined, dried over $MgSO_4$, filtered and the solvent concentrated in vacuo. The product was purified via column chromatography [SiO_2: CH_2Cl_2] to yield **211** as an orange solid (0.47 g, 27%) M.Pt = 110-112 ºC; ν_{max} (solid state): 3684, 3019, 2400, 1716, 1660, 1601; ^{1}H NMR (500 MHz, $CDCl_3$) δ (ppm): 1.99 (3H, s, (CH$_3$)), 3.68 (2H, q, *J* = 5.5 Hz, (N-CH$_2$), 4.34 (2H, t, *J* = 5.5 Hz, (O-CH$_2$)), 5.64 (1H, quint. *J* = 1.5 Hz, (alkene C-H)), 5.99 (1H, s, (N-H)), 6.16 (1H, t, *J* = 1.5 Hz, (alkene C-H)), 6.34 (2H, *br* s, (thiophene C-H)), 7.07 (1H, *br* s, (thiophene C-H)); ^{13}C NMR (125 MHz, $CDCl_3$) δ (ppm): 18.4 (CH$_3$), 39.8 (CH$_2$), 63.2 (CH$_2$), 119.1 (3 x thiophene C-H), 126.6 (2 x alkene C-H), 135.8 (quat C), 167.7 (2 x C=O); HRMS *m/z* (EI+) = 358.9775 ($C_{13}H_{13}O_3NS_4$ requires 358.9778)

Poly(2-([2,2'-(tetrathiafulvalene)]carboxamido)ethylmethacrylate)-(benzyl methacrylate) 190

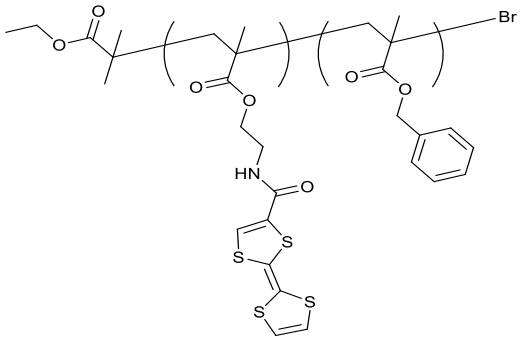

2-([2,2'-(Tetrathiafulvalene)]carboxamido)ethylmethacrylate **211** (0.28 g, 0.77 mmol), benzyl methacrylate **212** (0.52 mL, 3.1 mmol), Cu(I)Cl (0.039 g, 0.0038 mmol) and PMDETA (0.0080 mL, 0.039 mmol) was dissolved in DMSO (3 mL) and subjected to freeze-pump-thaw degassing before transferring to a preheated oil bath at 70 ºC. EBIB (0.0057 mL, 0.039 mmol) was then added and the reaction left to stir under N_2. The reaction was monitored *via* GPC and terminated after 2.5h by precipitation into a mixture of MeOH (300 mL), pet ether (100 mL) and water (100 mL). The solid was collected *via* filtration. The filtrate was extracted with CH_2Cl_2 (3 x 300 mL). The organic extracts were combined, dried over $MgSO_4$, filtered, and concentrated *in vacuo*. This was then re-precipitated into pet ether and the solid collected *via* filtration. The collected solids were then purified via column chromatography [AlO_2: pet ether] to yield **190** as a yellow solid (80 mg). GPC: (THF, 30°C at 1mL/min): M_n = 4258, M_w = 5072, PDI = 1.2; ^{1}H NMR (500 MHz, $CDCl_3$) δ (ppm): 0.74 (alkyl C-H), 0.94 (alkyl C-H), 1.28 (alkyl C-H), 1.88 (alkyl C-H), 3.59 (N-CH_2), 4.12 (O-CH_2), 4.98 (benzyl CH_2), 6.24 (thiophene C-H), 7.32 (benzyl C-H)

2-(Thiophen-3-yl)ethyl-5-oxo-5-((6-propionamidopyridin-2-yl)amino)pentanoate 192

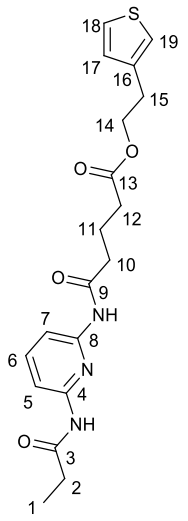

3-Thiophene ethanol **213** (0.42 mL, 3.7 mmol), 5-oxo-5-((6-propionamidopyridin-2-yl)amino)pentanoic acid **214** (0.56 g, 2.0 mmol) and EDCI (0.43 g, 2.2 mmol) were stirred in CH_2Cl_2 (50 mL). To this mixture was added DMAP (23 mg, 0.19 mmol) and the reaction was left to stir at room temperature overnight. The solvent was removed *in vacuo* and the product purified *via* flash column chromatography [SiO_2: ether] to yield **192** as a white solid (0.19 g, 25%). M.Pt = 100-103 °C; ν_{max} (evaporated film): 3683, 3420, 3019, 2400, 1727, 1699; ^{1}H NMR (500 MHz, $CDCl_3$) δ (ppm): 1.25 (3H, t, *J* =7.5 Hz, C (1)$\underline{H}_3$), 2.02 (2H, quin, *J* = 7.2 Hz, C (2)$\underline{H}_2$), 2.42 (6H, m, C (10, 11 & 12)$\underline{H}_2$), 2.98 (2H, t, *J* = 6.9 Hz, C (15)$\underline{H}_2$), 4.32 (2H, t, *J* = 6.9 Hz, C (14)$\underline{H}_2$), 6.98 (1H, dd, *J* = 1.3 & 4.9 Hz,(thiophene C-$\underline{H}$), 7.03, (1H, d, *J* =1.4 Hz, (thiophene C-$\underline{H}$), 7.28 (1H, m, (thiophene C-$\underline{H}$), 7.5-7.6 (2H, *br* s, N-H), 7.70, (1H, t, *J* = 8.0 Hz, C (6)$\underline{H}$), 7.90 (2H, d, *J* = 8.0 Hz, C (5 & 7)$\underline{H}$); ^{13}C NMR (125 MHz, $CDCl_3$) δ (ppm): 9.3 ($\underline{C}$(1)H_3), 20.4 ($\underline{C}$(2)H_2), 29.6 ($\underline{C}$(15)H_2), 30.8, 33.1 & 36.3 ($\underline{C}$(10, 11 & 12)H_2), 64.3 ($\underline{C}$(14)H_2), 109.3 & 109.4 ($\underline{C}$(5 & 7)H), 121.7 ($\underline{C}$(6)H), 125.7 (thiophene $\underline{C}$-H), 128.6 (thiophene $\underline{C}$-H); HRMS *m/z* (EI+) = 389.1409 ($C_{19}H_{23}O_4N_3S$ requires 389.1410)

Poly(3-hexylthiophene)-(2-(thiophen-3-yl)ethyl-5-oxo-5-((6-propionamidopyridin-2-yl)amino)pentanoate 193

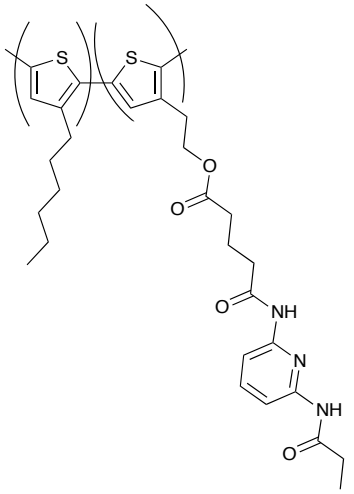

3-Hexylthiophene **191** (1.4 mL, 7.7 mmol) and 2-(thiophen-3-yl)ethyl 5-oxo-5-((6-propionamidopyridin-2-yl)amino)pentanoate **192** (0.75 g, 1.9 mmol) were mixed together under a stream of N_2. Nitromethane (45 mL) was added and the reaction stirred under N_2. $FeCl_3$ (6.3 g, 39 mmol) was then added and the reaction stirred for 1h. CCl_4 (180 mL) was finally added and the reaction stirred for 3h. The polymerisation was then terminated by precipitation into MeOH (900 mL) with 5% HCl. The precipitate was collected *via* filtration and the residue washed with MeOH until no iron detected through the NH_4SCN test. Purification by soxhlet extractions with MeOH (a) and $CHCl_3$ and re-precipitation with MeOH (b) and again with diethyl ether (c) gave three solids of different polymer sizes (**193a,b,c**). GPC: (THF, 30°C at 1mL/min) a) M_n = 33249 and PDI = 3.3 (125 mg), b) M_n = 38991 and PDI = 1.9 (182 mg), c) M_n = 43234 and PDI = 2.8 (337 mg)

2-(Thiophen-3-yl)ethyl-3-(3-(3,3-dimethylbutanamido)phenylcarbamoyl) propanoate 216

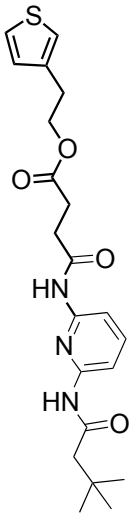

2-(3-Thienyl)-ethanol **213** (0.35 mL, 3.1 mmol) and 3-(6-(3,3-dimethylbutanamido) pyridin-2-ylcarbamoyl)propanoic acid **215** (0.79 g, 2.6 mmol) were stirred in CH_2Cl_2 (50 mL). To this was added EDCI (1.2 g, 6.2 mmol) and DMAP (76 mg, 0.62 mmol) and the reaction stirred at room temperature for 48h. The solvent was removed *in vacuo* and the product was purified *via* column chromatography [SiO_2: diethyl ether /pet ether 50/50) to yield **216** as a colourless oil. ν_{max} (evaporated film): 3680, 3420, 3015, 1728, 1698; ^{1}H NMR (500 MHz, $CDCl_3$) δ (ppm): 1.09 (9H, s, (3 x C$\underline{H}_3$)), 2.22 (2H, s, (C$\underline{H}_2$)), 2.73 (4H, m, (2 x C$\underline{H}_2$)), 2.97 (2H, t, *J* = 6.9 Hz, (C$\underline{H}_2$)), 4.32 (2H, t, *J* = 6.9 Hz, (O-C$\underline{H}_2$)), 6.95 (1H, dd, *J* = 1.28 & 5.0 Hz, (thiophene C-$\underline{H}$)), 7.01 (1H, m, (thiophene C-$\underline{H}$)), 7.24 (1H, dd, *J* = 3.0 & 5.0 Hz, (thiophene C-$\underline{H}$)), 7.6 (1H, *br* s, (N-$\underline{H}$)), 7.66 (1H, t, *J* = 8.0 Hz, (pyridine C-$\underline{H}$)), 7.82 (1H, *br* s, (N-$\underline{H}$)), 7.89 (2H, d, *J* = 8.0 Hz, (2 x pyridine C-$\underline{H}$)); ^{13}C NMR (125 MHz, $CDCl_3$) δ (ppm): 29.9 ($\underline{C}H_2$), 30.9 ($\underline{C}H_2$), 31.3 (2 x $\underline{C}H_3$), 32.1 ($\underline{C}H_3$), 36.0 (quat-$\underline{C}$), 40.1 ($\underline{C}H_2$), 51.7 ($\underline{C}H_2$), 64.8 ($\underline{C}H_2$), 109.4 (pyridine $\underline{C}$-H), 109.8 (pyridine $\underline{C}$-H), 121.6 (thiophene $\underline{C}$-H), 125.7 (thiophene $\underline{C}$-H), 128.2 (thiophene $\underline{C}$-H), 137.8 (quat $\underline{C}$), 140.7 (pyridine $\underline{C}$-H), 149.3 (quat $\underline{C}$), 149.5 (quat $\underline{C}$), 170.0 (C=O), 173.0 (C=O), 207.0 (C=O); HRMS ESI (M -) 416.1641 ($C_{21}H_{26}N_3O_4S$ requires 416.1650)

Poly(3-hexylthiophene)-(2-(thiophen-3-yl)ethyl 3-(3-(3,3-dimethylbutanamido) phenylcarbamoyl)propanoate 217

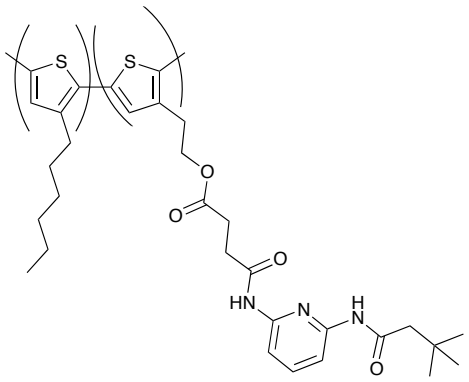

3-Hexylthiophene **191** (0.14 mL, 0.82 mmol) and 2-(thiophen-3-yl) ethyl 3-(3-(3,3-dimethylbutanamido) phenylcarbamoyl) propanoate **216** (0.34 g, 0.82 mmol) were mixed together under a stream of N_2. Nitromethane (20 mL) was added and the reaction stirred under N_2. $FeCl_3$ (2.7 g, 17 mmol) was then added and the reaction stirred for 1h. CCl_4 (90 mL) was added and the reaction stirred for 3h. The polymerisation was then terminated by precipitation into MeOH (500 mL) with 5% HCl. The precipitate was collected *via* filtration and the residue washed with MeOH until no iron detected through the NH_4SCN test. Purification by soxhlet extractions with MeOH and $CHCl_3$ and re-precipitation with MeOH gave the polymer **217** as a purple solid (250 mg) GPC: (THF, 30°C at 1mL/min) M_n = 24980, M_w = 59914 and PDI = 2.4

***N*-Parahexylphenyl-2-nitroaniline 245**

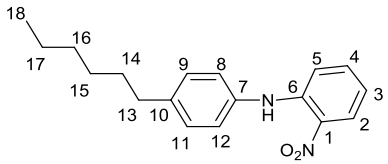

4-Hexylaniline **243** (5.4 mL, 29 mmol), 1-chloro-2-nitrobenzene **244** (4.6 g, 29 mmol) and DBU (8.7 mL, 58 mmol) were stirred under reflux for 2d. The crude product was extracted with CH_2Cl_2, washed with water (1 × 100 mL) and brine (1 × 100 mL) and the organic layer was collected, dried over $MgSO_4$, filtered and the solvent was removed *in vacuo.* The residue was purified *via* column chromatography [SiO_2: CH_2Cl_2: pet ether 40:60] to yield **245** as an orange oil (5.9 g, 67%), ν_{max}/cm^{-1}

(evaporated film) 3096, 2955, 2928, 2859; ^{1}H NMR (500 MHz, $CDCl_3$) δ (ppm): 0.88 (3H, m, C (18)$\underline{H_3}$), 1.33 (6H, m, C (15, 16 & 17)$\underline{H_2}$) 1.62 (2H, m, C (14)$\underline{H_2}$), 2.62 (2H, t, *J* = 7.7 Hz, C (13)$\underline{H_2}$), 6.60 (1H, d, *J* = 1.1 Hz, C (5)$\underline{H}$), 6.75 (1H, t, *J* = 7.5 Hz, C (4)$\underline{H}$), 7.34 (1H, t, *J* = 5.4 Hz, C (3)$\underline{H}$), 7.42 (1H, t, *J* = 5.8 Hz, C (8)$\underline{H}$), 7.52 (2H, m, C (9 & 11)$\underline{H}$), 7.87 (1H, d, *J* = 1.5 Hz, C (12)$\underline{H}$), 8.20 (1H, d, *J* = 1.5 Hz, C (2)$\underline{H}$), 9.46 (1H, s, N-H); ^{13}C NMR (125MHz, $CDCl_3$) δ (ppm): 14.1 ($\underline{C}$ (18)H_3), 22.6, 29.0 & 31.5 ($\underline{C}$ (15, 16 & 17)H_2), 35.5 ($\underline{C}$ (14)H_2), 44.0 ($\underline{C}$ (13)H_2), 112.69 ($\underline{C}$ (5)H), 116.0 ($\underline{C}$ (4)H), 117.1 ($\underline{C}$ (9)H), 117.8 ($\underline{C}$ (11)H), 124.7 ($\underline{C}$ (8)H), 125.6 ($\underline{C}$ (2)H), 129.3 ($\underline{C}$ (12)H), 133.2, 136.1, 140.8 & 143.7 ($\underline{C}$ (1, 6, 7 & 10); HRMS *m/z* (EI +) 299.1760 ($C_{18}H_{22}N_2O_2$ requires 299.1761)

2,2',2''-((2,4,6-Tri(thiophen-2-yl)benzene-1,3,5-triyl)tris(ethyne-2,1-diyl))trithiophene 249

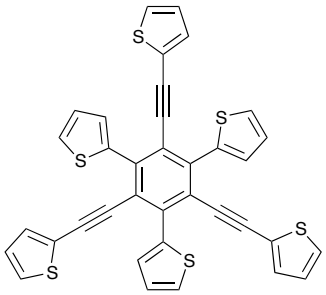

1,4-Di(thiophen-2-yl)buta-1,3-diyne **252** (0.30 g, 1.4 mmol), and $Co_2(CO)_8$ (44 mg, 0.14 mmol) were added to a dry flask in a glove box. 1,4-Dioxane (5 mL) was then added and the reaction stirred at 110 ºC overnight. The reaction mixture was then extracted with CH_2Cl_2 (3 x 100 mL) and washed with water (3 x 100 mL). The organic extracts were combined, dried over $MgSO_4$, filtered and concentrated *in vacuo*. The product was then purified *via* column chromatography [SiO_2: toluene/pet ether, 50/50] to yield **249** as an off-white solid (10 mg, 15%) M.Pt = 237 - 239°C; ν_{max} (evaporated film): 3100, 2208, 1518, 1390; ^{1}H NMR (500 MHz, $CDCl_3$) δ (ppm): 6.79 (3H, dd, *J* = 5.0 & 1.1 Hz, (3 x thiophene C-$\underline{H}$)), 7.12 (3H, dd, *J* = 3.0 & 1.1 Hz, (3 x thiophene C-$\underline{H}$)), 7.22 (3H, m, (3 x thiophene C-$\underline{H}$)), 7.43 (3H, dd, *J* = 5.0 & 3.0 Hz, 7.49 (3H, m, (3 x thiophene C-$\underline{H}$)), 7.68 (3H, dd, *J* = 3.0 & 1.3 Hz, (3 x thiophene C-$\underline{H}$)); ^{13}C NMR (125 MHz, $CDCl_3$) δ (ppm): 91.6 (alkyne-$\underline{C}$), 93.0 (alkyne-$\underline{C}$), 123.0 (quat-$\underline{C}$), 124.8 (quat-$\underline{C}$), 126.4 ($\underline{C}$-H), 127.0 ($\underline{C}$-H), 127.9 ($\underline{C}$-H), 129.3 ($\underline{C}$-H), 132.4

(C-H), 138.0 (quat-C), 139.2 (quat-C); HRMS *m/z* (ESI + Na)$^+$ =664.9566 ($C_{36}H_{18}S_6Na$ requires 664.9570)

4-(10-Ethyl-2,4-dioxo-6,9-di(thiophen-2-yl)benzo[*g*]pteridin-3(2*H*,4*H*,10*H*)-yl) benzaldehyde 251

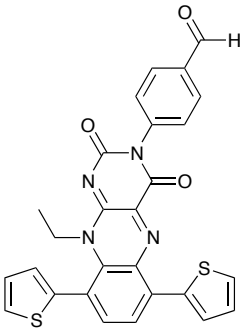

10-Ethyl-6,9-di(thiophen-2-yl)benzo[*g*]pteridine-2,4(3*H*,10*H*)-dione **57** (0.51 g, 1.2 mmol), 4-formyl phenyl boronic acid (0.36 g, 2.4 mmol), copper acetate (0.13 g, 0.74 mmol) and NEt_3 (1.7 mL, 12.0 mmol) were dissolved in CH_2Cl_2 (10 mL). The reaction was stirred at room temperature for 3d. The solvent was removed *in vacuo* and the residue subjected to purification *via* column chromatography [SiO_2: CH_2Cl_2] to yield **251** as a red solid (50 mg, 8.0 %) M.Pt = 269-270 ºC; ν_{max} (evaporated film): 3712, 3648, 3101, 2924, 2850, 2736, 2246, 1716, 1699, 1666, 1597, 1574. ^{1}H NMR (500 MHz, $CDCl_3$) δ (ppm): 1.05 (3H, t, *J* = 7.0 Hz, (C$\underline{H}_3$)), 4.54 (2H, *br* s, (N-C$\underline{H}_2$), 6.86 (2H, d, *J* = 7.0 Hz, (Ar C-$\underline{H}$)), 7.09 (2H, m, (Ar C-$\underline{H}$)), 7.46 (2H, m, (Ar C-$\underline{H}$)), 7.70 (2H, dd, *J* = 2.0 & 8.0 Hz (Ar C-$\underline{H}$)), 7.88 (2H, d, *J* = 8.0 Hz, (Ar C-$\underline{H}$)), 7.98 (2H, d, *J* = 8.0 Hz, (Ar C-$\underline{H}$)), 10.01 (1H, s, aldehyde-$\underline{H}$); ^{13}C NMR (125 MHz, $CDCl_3$) δ (ppm): 14.1 (C$\underline{H}_3$), 43.6 (N-C$\underline{H}_2$), 116.0 (Ar $\underline{C}$-H), 121.4 (quat $\underline{C}$), 123.6 (Ar $\underline{C}$-H), 126.7 (Ar $\underline{C}$-H), 127.3 (Ar $\underline{C}$-H), 127.7 (Ar $\underline{C}$-H), 127.8 (Ar $\underline{C}$-H), 127.9 (Ar C-H), 128.2 (Ar $\underline{C}$-H), 129.3 (Ar $\underline{C}$-H), 129.8 (Ar $\underline{C}$-H), 130.6 (Ar $\underline{C}$-H), 132.3 (Ar $\underline{C}$-H), 132.8 (quat $\underline{C}$), 133.7 (quat $\underline{C}$), 135.1 (quat $\underline{C}$), 136.2 (quat $\underline{C}$), 137.0 (quat $\underline{C}$), 138.4 (quat $\underline{C}$), 139.6 (quat $\underline{C}$), 140.7 (quat $\underline{C}$), 141.6 (Ar $\underline{C}$-H), 150.7 (quat $\underline{C}$), 155.2 (C=O), 159.2 (C=O), 191.4 (aldehyde $\underline{C}$); HRMS ESI (M+ Na)$^+$ 533.0709 ($C_{27}H_{18}N_4O_3S_2Na$ requires 533.0713).

7.0 References

[1] http://www.eia.gov/forecasts/ieo/ - Accessed on 21.7.14

[2] Renewables 2013, Global Status Report

[3] Key world energy statistics 2013, International Energy Agency

[4] Bp Statistical Review of World Energy, June 2014, bp.com/statisticalreview

[5] Armaruli N., Balzani V., *Angew. Chem. Int. Ed*, **2007**, *46*, 52

[6] Goetzberger A., Hebling C., Schock H-W., *Materials Science and Engineering*, **2003**, *R40*, 1

[7] http://solarcellcentral.com/limits_page.html - Accessed on 19.8.14

[8] http://en.wikipedia.org/wiki/File:Solar_Spectrum.png - Accessed on 20/08/2014

[9] Chapin D. M., Fuller C. S., Pearson G.L., *J. Appl. Phys*., **1954**, *25*, 676

[10] http://www.nrel.gov/ncpv/images/efficiency_chart.jpg - Accessed 22.7.14

[11] A: Tang C. W., *Appl. Phys. Lett.*, **1986**, *48*, 183; B: Tang C. W., VanSlyke S. A., *Appl. Phys. Lett.* **1987**, *51*, 913; C: Tsumura A., Koezuka H., Ando T., *Appl. Phys. Lett.*, **1986**, *49*, 1210.

[12] Braga D., Horowitz G., *Adv. Mater.*, **2009**, *21*, 1473.

[13] Tsumura A., Koezuka H., Ando T, *Appl. Phys. Lett.*, **1986**, *49*, 1210.

[14] Paloheimo J., Kuivalainen P., Stubb H., Vuorimaa E., Lahti P. Y., *Appl. Phys. Lett.*, **1990**, *56*, 157.

[15] Bao Z., Dodabalapur A., Lovinger A. J., *Appl. Phys. Lett.*, **1996**, *69*, 4108.

[16] Delgado J. L., Bouit P. A., Filipone S., Herranz M-A., Martin N., *Chem. Commun.*, **2010**, *46*, 4853.

[17] Li Y., Zou Y., *Adv. Mater*, **2008**, *20*, 2952

[18] Aernouts T., Aleksandrov T., Girotto C., Genoe J., Poortmans J., *Appl. Phys. Lett.*, **2008**, *92*, 033306

[19] Kim S. S., Na S. I., Kang S. J., Kim D. Y., *Sol. Energ. Mater.*, **2010**, *94*, 171.

[20] Krebs F. C., Gevorgyan S. A., Alstrup J., *J. Mater. Chem.*, **2009**, *19*, 5442.

[21] Cheng Y-J., Yang S-H., Hsu C-S., *Chem. Rev.,* **2009,** *109,* 5868

[22] Qi B., Wang J., *Phys. Chem. Chem. Phys.,* **2013**, *15*, 8972

[23] Lin Y., Lia Y., Zhan X., *Chem*. *Soc*. *Rev*., **2012**, *41*, 4245

[24] Xue J., Rand B. P., Uchida S., Forrest S. R., *Adv. Mater.*, **2005**, *17*, 66

[25] Sharma G. D., Suresh P., Mikroyannidis J. A., Stylianakis M. M., *J. Mater. Chem*., **2010**, *20*, 561

[26] Shu Y., Lim Y-F., Li Z., Purishothaman B., Hallani R., Kim J. E., Parkin S. R., Malliarvas G. G., Anthony J. E., *Chem*. *Sci.*, **2011**, *2*, 363

[27] Sonar P., Ng G-M., Lin T. T., Dodabalapur A., Chen Z-K., *J. Mater. Chem*., **2010** *20*, 3626

[28] Li Z., He G., Wan X., Liu Y., Zhou J., Long G., Zuo Y., Zhang M., Chen Y., *Adv. Energ. Mater.,***2012**, *1*, 74

[29] Kyaw A. K., Wang D. H., Vinay G., Zhang J., Chand S., Bazan G. C., Heeger A. J., *Adv*. *Mater*., **2013**, *25*, 2397

[30] Zhou J., Zuo Y., Wan X., Long G., Zhang Q., Ni W., Liu Y., Li Z., He G., Li C., Kan B., Li M., Chen Y., *J. Am*. *Chem*. *Soc*., **2013**, *135*, 8434

[31] Li Y., Zou Y., *Adv. Mater*, **2008**, *20*, 2952.

[32] Dou L., You J., Yang J., Chen C-C., He Y., Murase S., Moriarty T., Emery K., Li G, Yang Y., *Nature Photonics*, **2012**, *6*, 180

[33] You D., Dou L., Yoshimura K., Kato T., Ohya K., Moriarty T., Emery K., Chen C-C., Gao J., Li G., Yang Y., *Nature Commun*., **2013**, DOI: 10.1038/ncomms2411

[34] Xie Z., Midya A., Loh K. P., Adams S., Blackwood D. J., Wang J., Zhang X., Chen Z., *Prog. Photovol: Res. Appl.*, **2010**, *18*, 573

[35] Grätzel M., *J. Photochem. Photobio*. *A*, **2004***, 164*, 3

[36] O'Regan B., Grätzel M., *Nature*, **1991**, *353*, 737

[37] Hwang S., Lee J. H., Park C., Lee H., Kim C., Park C., Lee M-H., Lee W., Park J., Kim K., Park N-G., Kim C., *Chem*. *Commun*., **2007**, 4887

[38] Chiba Y., Islam A., Watanabe Y., Komiya R., Koide N., Han L., *Jpn*. *J. Appl*. *Phys*., **2006**, *45*, L638

[39] Nazeeruddin Md. K., De Angelis F., Fantacci S., Selloni A., Viscardi G., Liska P., Ito S., Takeru B., Grätzel M., *J. Am*. *Chem*. *Soc*., **2005**, *127*, 16835

[40] Mathew S., Yella A., Gao P., Humphrey-Baker R., Curchod B. F. E., Ashari-Astani N., Tavernelli I., Rothlisberger U., Nazeeruddin Md. K., Grätzel M., *Nature*, **2014**, *6*, 242

[41] Song S., Kim J., Shim J. Y., Kim G., Lee B. H., Jin Y., Park S. H., Kim I., Lee K., Suh H., *Synth. Met.*, **2012**, *162*, 988

[42] Nantalaksakul A., Mueller A., Klaikherd A., Bardeen C. J., Thayumanavan S., *J. Am. Chem. Soc.*, **2009**, *131*, 2727

[43] Deng Z., Chen L., Wu F., Chen Y., *J. Phys. Chem. C,* **2014**, *118*, 6038

[44] O'Regan B., Grätzel M., *Nature*, **1991**, *353*, 757

[45] Ito S., Miura H., Uchida S., Takata M., Sumioka K., Liska P., Comte P., Péchy P., Grätzel M., *Chem. Comm.*, **2008**, 5194

[46] Heelis. P. F., *Chem. Soc. Rev.*, **1982**, *11*, 15

[47] Massey V., *Biochem. Soc. Trans.*, **2000**, *28,* 283

[48] Kozial L., Kumar N., Wong S.E., Lightstone F.C., *J. Phys. Chem. A.,* **2013**, *117*, 12946

[49] Walsh C. T., Wencewicz T. A., *Nat. Prod. Rep.*, **2013**, *30*, 1

[50] Mansoorabadi S. O., Thibodeaux C. J., Liu. H-W., *J. Org. Chem.*, **2007**, *72*, 6329

[51] Ghisla S., Massey V., *Eur. J. Biochem.*, **1989**, *181*, 1

[52] Choy N., Russell K. C., Alvarez J. C., Fider A., *Tet. Lett.*, **2000**, *41*, 1515

[53] Breinlinger E. C., Keenan C. J., and Rotello V. M., *J. Am. Chem. Soc.* 1**998**, *120,* 8606

[54] Nandwana V., Samuel I., Cooke G., Rotello V. M., *Acc. Chem. Res.*, **2013**, *46*, 1000

[55] Carroll J. B., Jordan B. J., Xu H., Erdogan B., Lee L., Cheng L., Tiernan C., Cooke G., Rotello. V. M., *Org. Lett.*, **2005**, *7*, 2551

[56] Cerda J. F., Koder R. L., Lichtenstein B. R., Moser C. M., Miller A-F., Dutton P. L., *Org. Biomol. Chem.*, **2008**, *6*, 2204

[57] Legrand Y-M., Gray M., Cooke G., Rotello V. M., *J. Am. Chem. Soc.*, **2003**, *125*, 15789

[58] Gray M., Goodman A. J., Carroll J. B., Bardon K., Markey M., Cooke G., Rotello V. M., *Org. Lett*., **2004**, *3*, 385

[59] Caldwell S. T., Cooke G., Hewage S. G., Mabruk S., Rabani G, Rotello V. M., Smith B. O., Subramani C., Woisel P., *Chem. Comm.*, **2008**, 4126

[60] Long D., Cronin Research Group, University of Glasgow

[61] Mei Q.,Wang L.,Tian B.,Tong B.,Weng J.,Zhang B., Jiang Y., Huang W., *Dyes Pigments*, **2013,** *97*, 43

[62] Zhang. X., Cooke Research Group, University of Glasgow

[63] Schill G., Zollenkopf H., *Justus Liebigs Ann. Chem.*, **1969**, *721*, 53

[64] Furusho Y., Oku T., Rajikumar G. A., Takata T., *Chem. Letters.*, **2004**, *33,* 52

[65] Aprahamian I., Milijanić O. Š., Dichtel W. R., Isoda K., Yasuda T., Kato T., Stoddart J. F., *Bull. Chem. Soc. Jpn.*, **2007**, *80*, 1856-1869

[66] Annelli P-L., Spencer N., Stoddart J. F., *J. Am. Chem. Soc.*, **1991**, *113*, 5131

[67] Sauvage J-P., *Acc. Chem. Res*. **1998**, *31*, 611

[68] Funk and Wagnalls Standard Dictionary of the English language 1963

[69] Balzani., Credi., Venturi., Molecular Devices and Machines, 2nd Edition, 2008

[70] Cacialli F., Wilson J. S., Michels J. J., Daniel C., Silva C., Friend R. H., Severin N., Samorì P., Rabe J. P., O'Connell M. J., Taylor P. N and Anderson H. L., *Nature*, **2002**, *1*, 160

[71] Bissell R. A., Córdova E., Kaifer A. E., Stoddart J. F., *Nature*, **1994**, *369*, 133

[72] Laursen B. W., Nygaard S., Jeppesen J. O., Stoddart J. F., *Org. Lett*. **2004**, *6*, 4167

[73] Badjić J. D., Balzani V., Credi A., Silvi S., Stoddart J. F., *Science*, **2004**, *303*, 1845

[74] Collins J. P., Dietrich-Buchecker C., Gaviña A. P., Jimenez-Molero H. C., Sauvage J. P., *Acc.Chem.Res*. **2001**, *34*, 477

[75] Bravo J. A., Raymo F. M., Stoddart J. F., White A. J. P., Williams D. J., *Eur. J. Org. Chem.* **1998**, *45*, 2565

[76] Monk P. M. S., *The Viologens*, **1998**

[77] Michaelis L., *Chem. Rev.*, **1935**, *16*, 243

[78] Kamogawa H., Suzuki T., *Bull. Chem. Soc. Jpn.* **1987**, *60*, 794

[79] Gunter M. J., Hockless D. C. R., Johnston M. R., Skelton B. W., White A. H., *J. Am. Chem. Soc*., **1994**, *116*, 4810

[80] Geuder W., Hünig S., Suchy A., *Tetrahedron.* **1986**, *42*, 1665

[81] Lu T., Lu R., Liu X., Zheng X., Qiu X., Zhao Y., *Org. Lett*. **2007**, *9*, 797

[82] Li W., Li H., Li Y., Hou Z., *Angew. Chem. Int. Ed*. **2006**, *45*, 7609

[83] Rao A. V. R., Gurjar M. K., Kaiwar V., Khare V. B., *Tet. Lett*. **1993**, *34*, 1661

[84] Zainalaabdeen. N., Cooke Research Group, University of Glasgow

[85] Ashton P. R., Glink P. J., Stoddart J. F., Tasker P. A., White A. J. P., Williams D. J., *Eur. Chem. J.*, **1996**, *2*, 729

[86] Yang S. K., Ambade. A. V., Weck M., Chem. Soc. Rev., **2011**, *40*, 129

[87] Ciferri A., *Macromol. Rapid. Commun.*, **2002**, *23*, 511

[88] Sivakova S., Wu J., Campo C. J., Mather P. T., Rowan S. J., *Chem. Eur. J.,* **2006**, *12*, 446

[89] Moad G., Rizzardo E. Thang S. H., *Aust. J. Chem.*, **2005**, *58*, 379

[90] Haridharan N., Dhamodharan R., *J. Polym. Sci. Part A: Polym. Chem.*, **2011**, *49*,

[91] Zhao K., Cheng Z., Zhang Z., Zhu J., Zhu X., *Polym. Bull.*, **2009**, *63*, 355

[92] Jin Z., Xu Q., Li N., Lu J., Xia X., Yan F., Wang L., *Eur. Polym. J.*, **2008**, *44*, 1752

[93] Appel E. A., Barrio J. D., Loh X. J., Dyson J., Scherman O. A., *J. Polym. Sci. A*., **2012**, *50*, 181

[94] Ifuku S., Miwa T., Morimoto M., Saimoto H., *Int. J., Bio. Macro.*, **2013**, *52*, 14

[95] Pugh C., Tang C.N., Paz-Pazos M., Samtani O., Dao A. H., *Macromolecules*, **2007**, *40*, 8178

[96] Pickett P. D., Radzinski S. C., Tillman E. S., *J. Polym. Sci. Part A: Polym. Chem.,* **2012**, *50*, 156

[97] Moad G., Chong Y. K., Postma A., Rizzardo E., Thang S. H., *Polymer*, **2005**, *46*,

8458

[98] Kumar S., Roy S. G., De P., *Polym. Chem*., **2012**, *3*, 1239

[99] Stenzel M. H., *Chem. Commun*., **2008**, 3486

[100] Chen M., Häussler M., Moad G., Rizzardo E., *Org. Biomol. Chem.,* **2011**, *9*, 6111

[101] Bhosale S. V., Jani C. H., Langford S. J., *Chem. Soc. Rev.*, **2008**, *37*, 351

[102] Würthner F., Ahmed S., Thalacker C., Debaerdemocker T., *Chem. Eur. J*. **2002**, *8*, 4742

[103] Kolb H. C., Finn M. G., Sharpless K. B., *Angew. Chem. Int. Ed.* **2001**, *40*, 2004

[104] Evans R. A., *Aust. J. Chem.* **2007**, *60*, 384

[105] Banishoeib F., Fourier S., Cleij T. J., Lutsen L., Vanderzande D., *Eur. Phys. J. Appl. Phys.*, **2007**, *37*, 237

[106] Lee J-Y., Lin C-J., Lo C-T., Tsai J-C., *Macromolecules*.**, 2013**, *46*, 3005

[107] Tang W., Kietzke T., Vemulamada P., Chen Z-K., *Journal of Polymer Science. A*., **2007**, *45*, 5266

[108] Sang G., Zou Y., Li Y., *J. Phys. Chem. C.*, **2008**, *112*, 12058

[109] Chujo Y., *Conjugated Polymer Synthesis*, **2010,** Wiley-VCH Verlag GmbH & Co. KGaA

[110] Fraleoni-Morgera A., Della-Casa C., Costa-Bizzarri P., Lanzi M., Missiroli A., *Macromolecules*, **2005**, *38*, 3170

[111] Zhang Z-G., Fan H., Min J., Zhang S., Zhang J., Zhang M., Guo X., Zhan X., Li Y., *Polym. Chem.,* **2011**, *2*, 1678

[112] Naden. A, Materials and Condensed Matter Physics Group, University of Glasgow

[113] García R., Pérez R., *Surface Science Reports,* **2002**, *47*, 197-301

[114] Beijer F. H., Sijbesma R. P., Vekemans J. A. J. M., Meijer E. W., Kooijman H., Spek A. L., *J. Org. Chem.*, **1996**, *61*, 6371

[115] Klauk H., Organic Electronics: Materials Manufacturing and Applications, **2006**

[116] Zhau K., Xue L., Liu J., *Langmuir*, **2010**, *26*, 471

[117] Detert H., Lehmann M., Meier H., *Materials*, **2010**, *3*, 3218

[118] Gittins P. J., Twyann L. J., *Supramol. Chem*, **2003**, *15*, 5

[119] Yevlampieva N. P., Khurchak A. P., Luponosov Y. N., Kleimyuk E. A., Ponomarenko S. A., Ryumtsev E. I., *Russ. Jour. Appl. Chem.*, **2013**, *86*, 747

[120] ShirotaY., *J. Mater. Chem.*, **2005**, *15*, 75

[121] Diallo A. K., Metri N., Brunel F., Sallenave X., Goubard F., Margeat O., Ackermann J., Videlot-Ackermann C., *Synth. Met.*, **2013**, *184*, 35

[122] Tang A., Li L., Lu Z., Huang J., Jia H., Zhan C., Tan Z., Li Y., Yao J., *J. Mater. Chem. A.*, **2013**, *1*, 5747

[123] Shao J. J., Guan Z. P., Yan Y. L., Jiao C. J., Xu Q. H., Chi C. Y., *J. Org. Chem.*, **2011**, *76*, 780

[124] Lai W. Y., He Q. Y., Zhu R., Chen Q. Q., Huang W., *Adv. Funct. Mater.*, **2008**, *18*, 265

[125]Lu Z., Li C., Fang T., Li G., Bo Z., *J. Mater. Chem. A.*, **2013**, *1*, 7657

[126] Sun Y., Xiao K., Liu Y., Wang J., Pei J., Yu G., Zhu D., *Adv. Funct. Mater.*, **2005**, *15*, 818

[127] Bouderoult P. T., Najari A., Leclerc M., *Chem. Mater.*, **2011**, *23*, 456

[128] Pelz S., Zhang J., Kanelidis I., Klink D., Hyzak L., Wulf V., Schmitz O. J., Gasse J-C., Frahm R., Pütz A., Colsmann A., Lemmer U., Holder E., *Eur. J. Org. Chem.*, **2013**, 4761

[129] O'Regan B., Grätzel M., *Nature*, **1991**, *353*, 757

[130] Schmidt-Mende L., Bach U., Humphry-Baker R., Horiuchi T., Miura H., Ito S., Uchida S., Grätzel M., *Adv. Mater.*, **2005**, *17*, 813

[131] Hara K., Kurashige M., Dan-oh Y., Kasada C., Shinpo A., Suga S., Sayama K., Arakawa H., *New. J. Chem.*, **2003**, *27*, 783

[132] Jordan B. J., Pollier M. A., Ofir Y., Joubanian S., Mehtala J. G., Sinkel C., Caldwell S. T., Kennedy A., Rabani G., Cooke G., Rotello V. M., *Chem. Comm.*, **2008**, 1653

[133] Pauszek R. F., Kodali G., Caldwell S. T., Fitzpatrick B., Zainalabdeen N. Y., Cooke G., Rotello V. M., Stanley R. J., *J. Phys. Chem. B.*, **2013**, *117*, 15684

[134] Chauhan S. M. S., Singh R., *Synth. Comm.*, **2003**, 2899

[135] PhD Thesis, Manal El Eid, Cooke Research Group, University of Glasgow

[136] Neto B. A. D., Lopes A. S., Ebeling G., Gonçalves R. S., Costa V. E. U, Quina F. H., Dupont J.*Tetrahedron*., **2005**, *61*, 10975

[137] Kim J-J., Choi H., Lee J-W., Kang M-S., Song K., Kang S. O., Ko J., *J. Mater. Chem*., **2008**, *18*, 5223

[138] Xu T., Lu R., Liu X., Zheng X., Qiu X., Zhao Y., *Org. Lett*., **2007**, *9*, 797

8.0 Appendices

Appendix 1: ^{1}H NMR of compound 69 showing the two alkyl C-H peaks

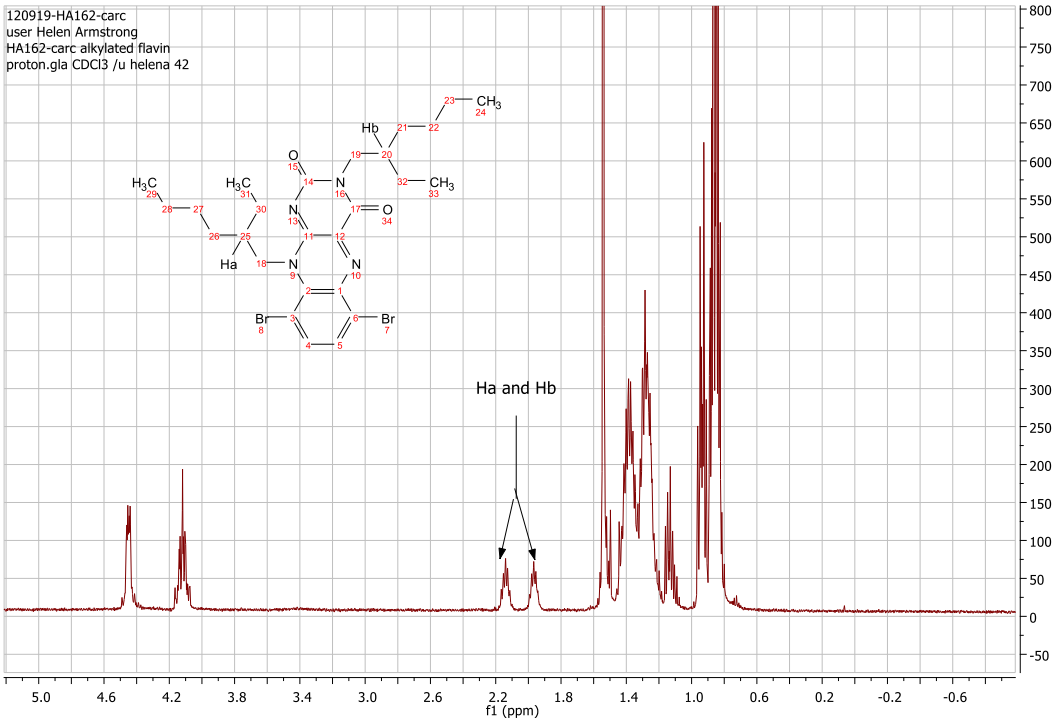

Appendix 2. X-Ray data for compound 75

Identification code	gcha2311a
Empirical formula	C12 H8 Br2 N4 O2
Formula weight	400.04
Temperature	150(2) K
Wavelength	0.71073 A
Crystal system, space group	Monoclinic, P2(1)/n
Unit cell dimensions	a = 8.5490(4) A alpha = 90 deg.
	b = 11.4214(4) A beta = 98.186(3) deg.
	c = 13.0051(4) A gamma = 90 deg.
Volume	1256.90(8) A^3
Z, Calculated density	4, 2.114 Mg/m^3

Absorption coefficient	6.456 mm^-1
F(000)	776
Crystal size	0.18 x 0.13 x 0.05 mm
Theta range for data collection	3.00 to 26.00 deg.
Limiting indices	-10<=h<=10, -14<=k<=13, -15<=l<=16
Reflections collected / unique	10418 / 2466 [R(int) = 0.0329]
Completeness to theta = 26.00	99.8 %
Max. and min. transmission	0.7384 and 0.3895
Refinement method	Full-matrix least-squares on F^2
Data / restraints / parameters	2466 / 0 / 173
Goodness-of-fit on F^2	1.046
Final R indices [I>2sigma(I)]	R1 = 0.0249, wR2 = 0.0545
R indices (all data)	R1 = 0.0320, wR2 = 0.0575
Largest diff. peak and hole	0.528 and -0.441 e.A^-3

Table 2. Atomic coordinates (x 10^4) and equivalent isotropic displacement parameters (A^2 x 10^3) for gcha2311a. U(eq) is defined as one third of the trace of the orthogonalized Uij tensor.

	x	y	z	U(eq)
C(1)	**1532(3)**	**2127(2)**	**5586(2)**	**20(1)**
C(2)	**2218(3)**	**1797(2)**	**4745(2)**	**21(1)**
C(3)	**2873(3)**	**2649(2)**	**4143(2)**	**21(1)**

C(4)	**2819(3)**	**3806(2)**	**4389(2)**	**18(1)**
C(5)	**2106(3)**	**4183(2)**	**5258(2)**	**18(1)**
C(6)	**1457(3)**	**3325(2)**	**5868(2)**	**17(1)**
C(7)	**1385(3)**	**5621(2)**	**6295(2)**	**16(1)**
C(8)	**764(3)**	**4768(2)**	**6920(2)**	**17(1)**
C(9)	**57(3)**	**5145(2)**	**7845(2)**	**20(1)**
C(10)	**521(3)**	**7196(2)**	**7333(2)**	**19(1)**
C(11)	**-978(4)**	**6768(3)**	**8756(2)**	**28(1)**
C(12)	**2104(4)**	**7650(3)**	**5959(2)**	**23(1)**
N(1)	**789(3)**	**3646(2)**	**6714(2)**	**19(1)**
N(2)	**2053(3)**	**5338(2)**	**5479(2)**	**18(1)**
N(3)	**-110(3)**	**6347(2)**	**7933(2)**	**20(1)**
N(4)	**1290(3)**	**6797(2)**	**6536(2)**	**19(1)**
O(1)	**-368(3)**	**4474(2)**	**8470(2)**	**28(1)**
O(2)	**396(2)**	**8229(2)**	**7511(2)**	**25(1)**
Br(1)	**694(1)**	**975(1)**	**6398(1)**	**26(1)**
Br(2)	**3712(1)**	**4942(1)**	**3594(1)**	**22(1)**

Table 3. Bond lengths [A] and angles [deg] for gcha2311a.

C(1)-C(2)	**1.366(4)**
C(1)-C(6)	**1.421(4)**
C(1)-Br(1)	**1.890(3)**
C(2)-C(3)	**1.413(4)**

C(3)-C(4)	**1.363(4)**
C(4)-C(5)	**1.424(4)**
C(4)-Br(2)	**1.886(3)**
C(5)-N(2)	**1.352(3)**
C(5)-C(6)	**1.423(4)**
C(6)-N(1)	**1.360(3)**
C(7)-N(2)	**1.315(3)**
C(7)-N(4)	**1.384(3)**
C(7)-C(8)	**1.420(4)**
C(8)-N(1)	**1.310(4)**
C(8)-C(9)	**1.485(4)**
C(9)-O(1)	**1.210(3)**
C(9)-N(3)	**1.387(4)**
C(10)-O(2)	**1.210(3)**
C(10)-N(4)	**1.381(3)**
C(10)-N(3)	**1.400(4)**
C(11)-N(3)	**1.469(4)**
C(12)-N(4)	**1.466(4)**

C(2)-C(1)-C(6)	**120.9(3)**
C(2)-C(1)-Br(1)	**119.7(2)**
C(6)-C(1)-Br(1)	**119.4(2)**
C(1)-C(2)-C(3)	**120.2(3)**
C(4)-C(3)-C(2)	**120.6(3)**
C(3)-C(4)-C(5)	**120.8(3)**
C(3)-C(4)-Br(2)	**120.6(2)**

C(5)-C(4)-Br(2)	**118.6(2)**
N(2)-C(5)-C(6)	**121.7(2)**
N(2)-C(5)-C(4)	**119.7(2)**
C(6)-C(5)-C(4)	**118.6(2)**
N(1)-C(6)-C(1)	**120.5(2)**
N(1)-C(6)-C(5)	**120.5(2)**
C(1)-C(6)-C(5)	**118.9(2)**
N(2)-C(7)-N(4)	**117.9(2)**
N(2)-C(7)-C(8)	**122.3(2)**
N(4)-C(7)-C(8)	**119.8(2)**
N(1)-C(8)-C(7)	**122.4(2)**
N(1)-C(8)-C(9)	**118.0(2)**
C(7)-C(8)-C(9)	**119.6(2)**
O(1)-C(9)-N(3)	**121.9(3)**
O(1)-C(9)-C(8)	**123.8(3)**
N(3)-C(9)-C(8)	**114.3(2)**
O(2)-C(10)-N(4)	**122.0(3)**
O(2)-C(10)-N(3)	**121.1(3)**
N(4)-C(10)-N(3)	**116.8(2)**
C(8)-N(1)-C(6)	**116.7(2)**
C(7)-N(2)-C(5)	**116.3(2)**
C(9)-N(3)-C(10)	**126.0(2)**
C(9)-N(3)-C(11)	**116.9(2)**
C(10)-N(3)-C(11)	**117.1(2)**
C(10)-N(4)-C(7)	**122.7(2)**
C(10)-N(4)-C(12)	**118.4(2)**

C(7)-N(4)-C(12)	**118.8(2)**

Symmetry transformations used to generate equivalent atoms**:**

Table 4. Anisotropic displacement parameters (A^2 x 10^3) for gcha2311a.

The anisotropic displacement factor exponent takes the form:

-2 pi^2 [h^2 a*^2 U11 + ... + 2 h k a* b* U12]

	U11	**U22**	**U33**	**U23**	**U13**	**U12**
C(1)	**18(2)**	**19(1)**	**22(1)**	**2(1)**	**1(1)**	**-1(1)**
C(2)	**22(2)**	**17(1)**	**25(2)**	**-4(1)**	**3(1)**	**1(1)**
C(3)	**20(2)**	**24(2)**	**20(1)**	**-4(1)**	**6(1)**	**5(1)**
C(4)	**14(1)**	**21(1)**	**19(1)**	**1(1)**	**6(1)**	**0(1)**
C(5)	**14(2)**	**19(1)**	**19(1)**	**-1(1)**	**1(1)**	**1(1)**
C(6)	**15(2)**	**21(1)**	**16(1)**	**0(1)**	**1(1)**	**1(1)**
C(7)	**13(1)**	**17(1)**	**18(1)**	**-2(1)**	**2(1)**	**1(1)**
C(8)	**14(2)**	**20(1)**	**18(1)**	**1(1)**	**5(1)**	**1(1)**
C(9)	**19(2)**	**22(2)**	**21(1)**	**1(1)**	**5(1)**	**0(1)**
C(10)	**16(2)**	**23(2)**	**18(1)**	**-4(1)**	**2(1)**	**-2(1)**
N(1)	**17(1)**	**21(1)**	**20(1)**	**0(1)**	**4(1)**	**1(1)**
N(2)	**17(1)**	**18(1)**	**18(1)**	**1(1)**	**4(1)**	**1(1)**
N(3)	**23(1)**	**19(1)**	**20(1)**	**-3(1)**	**10(1)**	**-1(1)**

N(4)	**20(1)**	**17(1)**	**22(1)**	**-1(1)**	**8(1)**	**-1(1)**
O(1)	**36(1)**	**24(1)**	**28(1)**	**2(1)**	**18(1)**	**-2(1)**
O(2)	**30(1)**	**18(1)**	**29(1)**	**-6(1)**	**13(1)**	**-1(1)**
Br(1)	**31(1)**	**18(1)**	**29(1)**	**3(1)**	**8(1)**	**-3(1)**
Br(2)	**25(1)**	**22(1)**	**21(1)**	**0(1)**	**11(1)**	**-2(1)**

—

Appendix 3. X-Ray data for compound 76

Identification code	gcha2312b
Empirical formula	C12 H8 Br2 N4 O2
Formula weight	400.04
Temperature	150(2) K
Wavelength	0.71073 A
Crystal system, space group	Triclinic, P-1
Unit cell dimensions	a = 7.2099(11) A alpha = 103.671(8) deg.
	b = 13.064(2) A beta = 91.926(8) deg.
	c = 13.7929(19) A gamma = 96.630(9) deg.
Volume	1251.4(3) A^3
Z, Calculated density	4, 2.123 Mg/m^3
Absorption coefficient	6.484 mm^-1
F(000)	776
Crystal size	0.08 x 0.07 x 0.02 mm
Theta range for data collection	1.52 to 25.99 deg.
Limiting indices	-8<=h<=8, -15<=k<=16, -16<=l<=17
Reflections collected / unique	16044 / 4830 [R(int) = 0.0435]
Completeness to theta = 25.99	98.6 %

Max. and min. transmission	0.8813 and 0.6250
Refinement method	Full-matrix least-squares on F^2
Data / restraints / parameters	4830 / 0 / 365
Goodness-of-fit on F^2	1.069
Final R indices [I>2sigma(I)]	R1 = 0.0410, wR2 = 0.0909
R indices (all data)	R1 = 0.0566, wR2 = 0.1031
Largest diff. peak and hole	1.819 and -1.556 e.A^-3

Table 2. Atomic coordinates (x 10^4) and equivalent isotropic displacement parameters (A^2 x 10^3) for gcha2312b. U(eq) is defined as one third of the trace of the orthogonalized Uij tensor.

	x	y	z	U(eq)
C(1)	**2638(7)**	**1467(4)**	**2695(4)**	**17(1)**
C(2)	**3371(7)**	**1963(4)**	**3647(4)**	**21(1)**
C(3)	**4114(7)**	**3029(4)**	**3910(4)**	**21(1)**
C(4)	**4013(7)**	**3625(4)**	**3213(4)**	**18(1)**
C(5)	**3270(7)**	**3150(4)**	**2231(4)**	**18(1)**
C(6)	**2704(7)**	**2039(4)**	**1936(4)**	**18(1)**
C(7)	**2429(7)**	**468(4)**	**466(4)**	**21(1)**
C(8)	**1920(7)**	**2231(4)**	**292(4)**	**19(1)**
C(9)	**2368(7)**	**3362(4)**	**701(4)**	**20(1)**

C(10)	2109(8)	4073(4)	10(4)	27(1)
C(11)	1392(9)	4185(4)	-1693(4)	33(1)
C(12)	1158(8)	2425(4)	-1290(4)	21(1)
C(13)	9058(7)	2806(4)	4221(4)	23(1)
C(14)	9356(8)	3579(4)	3692(4)	26(1)
C(15)	8778(7)	3402(4)	2694(4)	24(1)
C(16)	7898(7)	2422(4)	2212(4)	22(1)
C(17)	7571(7)	1603(4)	2717(4)	18(1)
C(18)	8155(7)	1779(4)	3749(4)	18(1)
C(19)	8288(13)	1011(5)	5255(5)	59(2)
C(20)	6908(7)	-36(4)	3656(4)	19(1)
C(21)	6346(7)	-106(4)	2622(4)	18(1)
C(22)	5294(7)	-1149(4)	2041(4)	19(1)
C(23)	3923(8)	-2930(4)	2063(4)	30(1)
C(24)	5689(8)	-1788(4)	3564(4)	26(1)
N(1)	2231(6)	1594(3)	928(3)	17(1)
N(2)	3083(6)	3797(3)	1591(3)	21(1)
N(3)	1320(6)	1792(3)	-633(3)	19(1)
N(4)	1560(7)	3543(3)	-957(3)	25(1)
N(5)	7775(6)	929(3)	4192(3)	21(1)
N(6)	6653(6)	646(3)	2180(3)	20(1)
N(7)	6620(6)	-827(3)	4098(3)	24(1)
N(8)	4989(6)	-1910(3)	2577(3)	22(1)
O(1)	666(5)	2051(3)	-2166(3)	27(1)
O(2)	2353(7)	5032(3)	281(3)	41(1)
O(3)	5441(6)	-2536(3)	3951(3)	39(1)

O(4)	**4751(5)**	**-1286(3)**	**1181(3)**	**24(1)**
Br(1)	**1364(1)**	**73(1)**	**2516(1)**	**19(1)**
Br(2)	**4811(1)**	**5091(1)**	**3561(1)**	**30(1)**
Br(3)	**10059(1)**	**3272(1)**	**5564(1)**	**53(1)**
Br(4)	**7129(1)**	**2167(1)**	**845(1)**	**23(1)**

Table 3. Bond lengths [A] and angles [deg] for gcha2312b.

C(1)-C(2)	**1.376(7)**
C(1)-C(6)	**1.422(7)**
C(1)-Br(1)	**1.899(5)**
C(2)-C(3)	**1.392(7)**
C(3)-C(4)	**1.377(7)**
C(4)-C(5)	**1.408(7)**
C(4)-Br(2)	**1.877(5)**
C(5)-N(2)	**1.372(6)**
C(5)-C(6)	**1.419(7)**
C(6)-N(1)	**1.387(6)**
C(7)-N(1)	**1.485(6)**
C(8)-N(3)	**1.306(6)**
C(8)-N(1)	**1.374(6)**
C(8)-C(9)	**1.445(7)**
C(9)-N(2)	**1.286(6)**
C(9)-C(10)	**1.501(7)**

C(10)-O(2)	**1.210(7)**
C(10)-N(4)	**1.371(7)**
C(11)-N(4)	**1.471(6)**
C(12)-O(1)	**1.215(6)**
C(12)-N(3)	**1.373(6)**
C(12)-N(4)	**1.416(7)**
C(13)-C(14)	**1.381(8)**
C(13)-C(18)	**1.416(7)**
C(13)-Br(3)	**1.896(5)**
C(14)-C(15)	**1.382(8)**
C(15)-C(16)	**1.366(7)**
C(16)-C(17)	**1.412(7)**
C(16)-Br(4)	**1.887(5)**
C(17)-N(6)	**1.374(6)**
C(17)-C(18)	**1.428(7)**
C(18)-N(5)	**1.394(6)**
C(19)-N(5)	**1.476(7)**
C(20)-N(7)	**1.319(6)**
C(20)-N(5)	**1.368(7)**
C(20)-C(21)	**1.448(7)**
C(21)-N(6)	**1.276(6)**
C(21)-C(22)	**1.509(7)**
C(22)-O(4)	**1.203(6)**
C(22)-N(8)	**1.375(6)**
C(23)-N(8)	**1.466(7)**
C(24)-O(3)	**1.218(6)**

C(24)-N(7)	**1.380(7)**
C(24)-N(8)	**1.402(6)**

C(2)-C(1)-C(6)	**119.7(5)**
C(2)-C(1)-Br(1)	**116.4(4)**
C(6)-C(1)-Br(1)	**123.6(4)**
C(1)-C(2)-C(3)	**122.1(5)**
C(4)-C(3)-C(2)	**118.9(5)**
C(3)-C(4)-C(5)	**120.7(5)**
C(3)-C(4)-Br(2)	**120.7(4)**
C(5)-C(4)-Br(2)	**118.7(4)**
N(2)-C(5)-C(4)	**117.9(4)**
N(2)-C(5)-C(6)	**122.0(4)**
C(4)-C(5)-C(6)	**120.1(4)**
N(1)-C(6)-C(5)	**117.4(4)**
N(1)-C(6)-C(1)	**124.9(4)**
C(5)-C(6)-C(1)	**117.6(4)**
N(3)-C(8)-N(1)	**119.2(4)**
N(3)-C(8)-C(9)	**124.5(4)**
N(1)-C(8)-C(9)	**116.2(4)**
N(2)-C(9)-C(8)	**124.9(5)**
N(2)-C(9)-C(10)	**117.7(5)**
C(8)-C(9)-C(10)	**117.2(4)**
O(2)-C(10)-N(4)	**122.7(5)**
O(2)-C(10)-C(9)	**123.0(5)**
N(4)-C(10)-C(9)	**114.3(5)**

O(1)-C(12)-N(3)	**121.7(5)**
O(1)-C(12)-N(4)	**117.9(4)**
N(3)-C(12)-N(4)	**120.4(4)**
C(14)-C(13)-C(18)	**120.7(5)**
C(14)-C(13)-Br(3)	**112.8(4)**
C(18)-C(13)-Br(3)	**126.5(4)**
C(13)-C(14)-C(15)	**122.4(5)**
C(16)-C(15)-C(14)	**118.7(5)**
C(15)-C(16)-C(17)	**121.1(5)**
C(15)-C(16)-Br(4)	**119.0(4)**
C(17)-C(16)-Br(4)	**119.9(4)**
N(6)-C(17)-C(16)	**117.3(4)**
N(6)-C(17)-C(18)	**122.0(5)**
C(16)-C(17)-C(18)	**120.7(5)**
N(5)-C(18)-C(13)	**126.5(4)**
N(5)-C(18)-C(17)	**117.0(4)**
C(13)-C(18)-C(17)	**116.4(5)**
N(7)-C(20)-N(5)	**119.3(4)**
N(7)-C(20)-C(21)	**124.4(5)**
N(5)-C(20)-C(21)	**116.3(4)**
N(6)-C(21)-C(20)	**124.9(5)**
N(6)-C(21)-C(22)	**118.4(4)**
C(20)-C(21)-C(22)	**116.6(4)**
O(4)-C(22)-N(8)	**123.3(5)**
O(4)-C(22)-C(21)	**121.8(5)**
N(8)-C(22)-C(21)	**114.8(4)**

O(3)-C(24)-N(7)	**120.3(5)**
O(3)-C(24)-N(8)	**119.3(5)**
N(7)-C(24)-N(8)	**120.5(5)**
C(8)-N(1)-C(6)	**120.3(4)**
C(8)-N(1)-C(7)	**117.1(4)**
C(6)-N(1)-C(7)	**121.3(4)**
C(9)-N(2)-C(5)	**117.6(4)**
C(8)-N(3)-C(12)	**119.2(4)**
C(10)-N(4)-C(12)	**124.3(4)**
C(10)-N(4)-C(11)	**117.4(4)**
C(12)-N(4)-C(11)	**118.3(4)**
C(20)-N(5)-C(18)	**121.4(4)**
C(20)-N(5)-C(19)	**116.3(4)**
C(18)-N(5)-C(19)	**122.4(4)**
C(21)-N(6)-C(17)	**118.3(4)**
C(20)-N(7)-C(24)	**119.2(4)**
C(22)-N(8)-C(24)	**124.3(4)**
C(22)-N(8)-C(23)	**117.5(4)**
C(24)-N(8)-C(23)	**118.1(4)**

Symmetry transformations used to generate equivalent atoms:

Table 4. Anisotropic displacement parameters (A^2 x 10^3) for gcha2312b.

The anisotropic displacement factor exponent takes the form:

-2 pi^2 [h^2 a*^2 U11 + ... + 2 h k a* b* U12]

	U11	U22	U33	U23	U13	U12
C(1)	22(3)	9(2)	22(3)	4(2)	1(2)	2(2)
C(2)	23(3)	21(3)	19(3)	7(2)	0(2)	2(2)
C(3)	25(3)	19(3)	17(3)	0(2)	2(2)	-1(2)
C(4)	23(3)	10(2)	21(3)	1(2)	1(2)	0(2)
C(5)	19(3)	16(3)	20(3)	7(2)	2(2)	2(2)
C(6)	20(3)	16(3)	18(3)	4(2)	1(2)	4(2)
C(7)	26(3)	15(3)	20(3)	4(2)	2(2)	2(2)
C(8)	19(3)	14(3)	23(3)	4(2)	0(2)	4(2)
C(9)	27(3)	13(3)	19(3)	2(2)	2(2)	3(2)
C(10)	38(3)	19(3)	25(3)	8(2)	0(2)	2(2)
C(11)	56(4)	19(3)	25(3)	11(2)	-9(3)	-2(3)
C(12)	28(3)	15(3)	20(3)	4(2)	2(2)	5(2)
C(13)	23(3)	19(3)	23(3)	0(2)	0(2)	4(2)
C(14)	24(3)	19(3)	32(3)	3(2)	-4(2)	0(2)
C(15)	20(3)	17(3)	36(3)	10(2)	0(2)	1(2)
C(16)	21(3)	22(3)	23(3)	7(2)	-1(2)	4(2)
C(17)	13(3)	19(3)	21(3)	5(2)	2(2)	6(2)
C(18)	21(3)	17(3)	16(2)	2(2)	2(2)	5(2)
C(19)	113(7)	28(4)	27(3)	13(3)	-24(4)	-30(4)

C(20)	22(3)	16(3)	22(3)	6(2)	0(2)	6(2)
C(21)	21(3)	13(3)	17(2)	0(2)	0(2)	3(2)
C(22)	18(3)	16(3)	21(3)	5(2)	0(2)	3(2)
C(23)	30(3)	21(3)	36(3)	7(3)	-9(3)	-4(2)
C(24)	34(3)	23(3)	21(3)	7(2)	-3(2)	3(2)
N(1)	20(2)	15(2)	16(2)	5(2)	0(2)	2(2)
N(2)	30(3)	14(2)	18(2)	3(2)	1(2)	1(2)
N(3)	22(2)	16(2)	18(2)	5(2)	0(2)	3(2)
N(4)	36(3)	19(2)	19(2)	6(2)	-3(2)	1(2)
N(5)	26(2)	18(2)	18(2)	6(2)	-3(2)	1(2)
N(6)	17(2)	19(2)	21(2)	2(2)	-1(2)	3(2)
N(7)	32(3)	17(2)	21(2)	6(2)	-5(2)	-1(2)
N(8)	29(3)	14(2)	22(2)	7(2)	-7(2)	-4(2)
O(1)	39(2)	24(2)	17(2)	5(2)	-2(2)	1(2)
O(2)	76(3)	15(2)	30(2)	8(2)	-12(2)	0(2)
O(3)	64(3)	19(2)	32(2)	13(2)	-14(2)	-6(2)
O(4)	30(2)	22(2)	20(2)	8(2)	-3(2)	0(2)
Br(1)	23(1)	14(1)	20(1)	5(1)	1(1)	0(1)
Br(2)	51(1)	15(1)	21(1)	2(1)	-3(1)	-6(1)
Br(3)	88(1)	31(1)	30(1)	5(1)	-24(1)	-16(1)
Br(4)	27(1)	22(1)	22(1)	10(1)	1(1)	3(1)

Appendix 4: CV analysis for compound 79

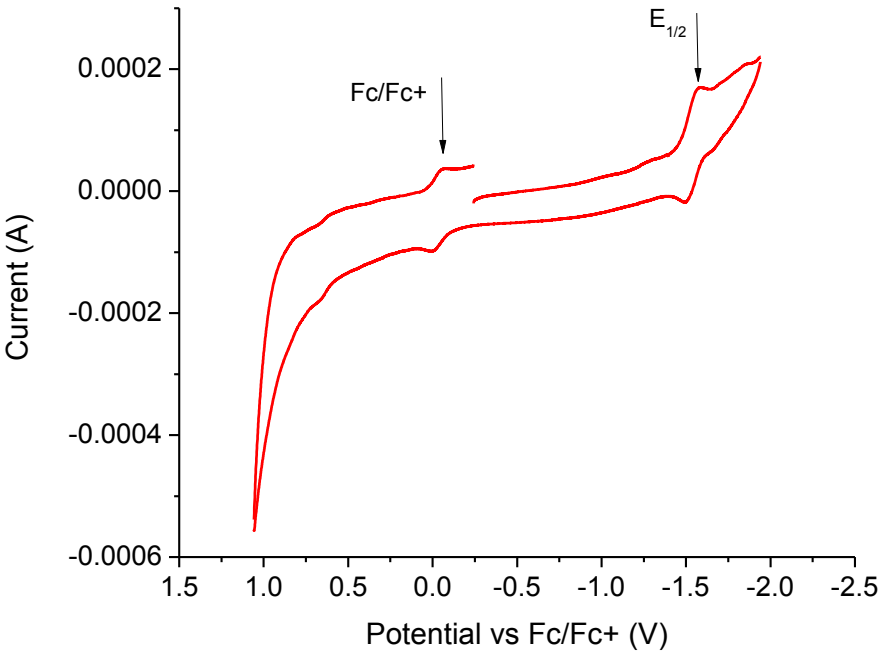

CV analysis of polymer 79 recorded at a concentration of 0.5 mM in CH_2Cl_2, (0.1 M TBA.PF_6, platinum working electrode, platinum wire counter electrode and silver reference electrode, reference to Fc/Fc^+ = 0.0eV)